

Electronic Thesis and Dissertation Repository

2-14-2014 12:00 AM

Control of Cooperative Haptics-Enabled Teleoperation Systems with Application to Minimally Invasive Surgery

Amir Takhmar, *The University of Western Ontario*

Supervisor: Dr. Ilia Polushin, *The University of Western Ontario*

Joint Supervisor: Dr. Rajni Patel, *The University of Western Ontario*

A thesis submitted in partial fulfillment of the requirements for the Doctor of Philosophy degree in Electrical and Computer Engineering

© Amir Takhmar 2014

Follow this and additional works at: <https://ir.lib.uwo.ca/etd>



Part of the [Biomedical Commons](#), and the [Controls and Control Theory Commons](#)

Recommended Citation

Takhmar, Amir, "Control of Cooperative Haptics-Enabled Teleoperation Systems with Application to Minimally Invasive Surgery" (2014). *Electronic Thesis and Dissertation Repository*. 1899.
<https://ir.lib.uwo.ca/etd/1899>

This Dissertation/Thesis is brought to you for free and open access by Scholarship@Western. It has been accepted for inclusion in Electronic Thesis and Dissertation Repository by an authorized administrator of Scholarship@Western. For more information, please contact wlsadmin@uwo.ca.

CONTROL OF COOPERATIVE HAPTICS-ENABLED TELEOPERATION
SYSTEMS WITH APPLICATION TO MINIMALLY INVASIVE SURGERY
(Thesis format: Integrated Article)

by

Amir Takhmar

Graduate Program in Electrical and Computer Engineering

A thesis submitted in partial fulfillment
of the requirements for the degree of
Doctor of Philosophy

The School of Graduate and Postdoctoral Studies
The University of Western Ontario
London, Ontario, Canada

© Amir Takhmar 2014

Abstract

Robot-Assisted Minimally Invasive Surgical (RAMIS) systems frequently have a structure of cooperative teleoperator systems where multiple master-slave pairs are used to collaboratively execute a task. Although multiple studies indicate that haptic feedback improves the realism of tool-tissue interaction to the surgeon and leads to better performance for surgical procedures, current telesurgical systems typically do not provide force feedback, mainly because of the inherent stability issues. The research presented in this thesis is directed towards the development of control algorithms for force reflecting cooperative surgical teleoperator systems with improved stability and transparency characteristics.

In the case of cooperative force reflecting teleoperation over networks, conventional passivity-based approaches may have limited applicability due to potentially nonpassive slave-slave interactions and irregular communication delays imposed by the network. In this thesis, an alternative small gain framework for the design of cooperative network-based force reflecting teleoperator systems is developed. Using the small gain framework, control algorithms for cooperative force-reflecting teleoperator systems are designed that guarantee stability in the presence of multiple network-induced communication constraints. Furthermore, the design conservatism typically associated with the small-gain approach is eliminated by using the Projection-Based Force Reflection (PBFR) algorithms. Stability results are established for networked cooperative teleoperator systems under different types of force reflection algorithms in the presence of irregular communication delays. The proposed control approach is consequently implemented on a dual-arm (two masters/two slaves) robotic MIS testbed. The testbed consists of two Haptic Wand devices as masters and two PA10-7C robots as the slave manipulators equipped with da Vinci laparoscopic surgical instruments. The performance of the proposed control approach is evaluated in three different cooperative surgical tasks, which are knot tightening, pegboard transfer, and object manipulation. The experimental results obtained indicate that the PBFR algorithms demonstrate statistically significant performance improvement in comparison with the conventional direct force reflection algorithms.

One possible shortcoming of using PBFR algorithms is that implementation of these algorithms may lead to attenuation of the high-frequency component of the contact force which is important, in particular, for haptic perception of stiff surfaces. In this thesis, a solution to this problem is proposed which is based on the idea of separating the different frequency bands in the force reflection signal and consequently applying the projection-based principle to the low-frequency component, while reflecting the high-frequency component directly. The experimental results demonstrate that substantial improvement in transient fidelity of the force feedback is achieved using the proposed method without negative effects on the stability of the system.

Keywords: Cooperative Teleoperation, Haptic, Small-gain Design, Projection-Based Force Reflection, Robot-Assisted Minimally Invasive Surgery

Co-Authorship Statement

The work presented in Chapter 2 involves collaboration with Dr. Sergey Dashkovskiy who contributed to theoretical developments. The work presented in Chapters 2 – 5 involves collaboration with my supervisor Dr. Ilya Polushin who contributed to theoretical developments, writing, and reviewing several drafts of the manuscript. The work presented in Chapters 2 – 5 involves collaboration with my supervisor Dr. Rajni Patel who reviewed and corrected several drafts of the manuscript. The work presented in Chapter 5 involves collaboration with Dr. Ali Talasaz who developed the dual-Arm MIS setup and provided me with information and the Simulink program of the setup.

Dedication

To my parents for their love, inspiration, and guidance.

Acknowledgements

I would like to express my sincerest thanks to my supervisors, Professor Rajni Patel, and Dr. Ilia Polushin for their inspiring advices, supports, and encouragements throughout my study. I would particularly like to thank Dr. Polushin for his continuous help and guidance during all stages of research.

I would like to extend my thanks to my lab-mates in the Robotics and Control Laboratory and CSTAR for their help throughout the time I worked on my research.

I would like to thank my friends in Western University, which made the time of my study fun and enjoyable.

I would like to express my deepest and sincerest thanks to my family in Iran for their love, support, and encouragement throughout my life.

I would also like to acknowledge the financial support from the NSERC Collaborative Research and Training Experience (CREATE) program in "Computer-Assisted Medical Interventions".

Contents

Abstract	ii
Co-Authorship Statement	iii
Dedication	iv
Acknowledgements	v
List of Figures	ix
List of Tables	xiii
Nomenclature	xiv
1 Introduction	1
1.1 Previous Works	2
1.1.1 Stability of Teleoperation Systems	2
Passivity approach	3
Small gain approach	5
1.1.2 Cooperative Teleoperation Systems	7
1.1.3 RAMIS Application	9
1.2 Contributions	12
1.3 Thesis Outline	13
2 A Small Gain Framework for Networked Cooperative Force-Reflecting Teleoperation	21
2.1 Introduction	21
2.2 Small Gain Theorem for Network-Based Interconnections	24
2.2.1 Preliminaries	24
2.2.2 The Small-Gain Theorem	26
2.2.3 Proof of Theorem 1	29
2.3 Design of a networked cooperative force-reflecting teleoperator	33
2.3.1 Masters and slaves manipulators	33
2.3.2 Communication process	34
2.3.3 Control algorithms	36
2.3.4 Environmental model and slave-environment interconnections	37
2.3.5 Small gain analysis	37

2.4	Experimental Results	40
2.5	Conclusions	45
3	Small Gain Design of Cooperative Teleoperator Systems with PBFR	51
3.1	Introduction	51
3.2	Notation and Definitions	54
3.3	Small gain analysis of networked cooperative teleoperators	57
3.4	Dynamics of the human operators and stability of the cooperative teleoperator system	62
3.5	Stability of cooperative teleoperator system with projection-based force reflection	70
3.6	Experimental results	74
3.7	Conclusions	81
4	Experimental Evaluation of PBFR Algorithm on MIS Setup	86
4.1	Introduction	86
4.2	Experimental Setup	88
4.2.1	Haptic Wand devices	89
4.2.2	PA10-7C Robots	90
4.2.3	daVinci Tools	90
4.3	Mathematical Models and Controller Design	91
4.3.1	Master Subsystems	93
4.3.2	Slave Subsystems	95
4.4	Force Reflection Algorithms	97
4.5	Stability Analysis	98
4.6	Experimental Results	102
	Experiment A: Knot Tightening	102
	Experiment B: Pegboard Transfer	102
	Experiment C: Object Manipulation	103
4.6.1	Results of the Knot Tightening Experiment	105
4.6.2	Results of the Pegboard Transfer Experiment	110
4.6.3	Results of the Object Manipulation Experiment	115
4.6.4	Discussion	119
4.7	Conclusions	122
	Appendix A. Stability analysis of the dual-arm MIS teleoperator system with projection-based force reflection	126
5	Projection-Based Force Reflection Algorithms with Frequency Separation	131
5.1	Introduction	131
5.2	Teleoperator system and human dynamics	134
5.3	Projection-based force reflection algorithms with frequency separation	137
5.4	Theoretical Results	140
5.5	Experimental Results	143
5.6	Conclusions	152
	Appendix: Proof of Theorems and related materials	155

6	Conclusions and Future Work	162
6.1	Conclusions	162
6.2	Future Work	164
A	Reprint Permissions	167
	Curriculum Vitae	173

List of Figures

2.1	Cooperative network-based teleoperator system	23
2.2	Experimental setup scheme	41
2.3	Implementation of the object in virtual environment	42
2.4	Case of negligible communication delays (RTT delay ≈ 0): x -trajectories of the masters, slaves, and the object (left); Interaction x -forces (right)	43
2.5	Case of sufficiently large constant communication delays (RTT delay ≈ 1 s): x -trajectories of the masters, slaves, and the object (left); Interaction x -forces (right)	44
2.6	Case of time-varying communication delays with random packet dropouts: x -trajectories of the masters, slaves, and the object (left); Interaction x -forces (right)	44
2.7	Examples of time-varying communication delays for experiments in Figure 2.6: Network 1 (left); Network 2 (right)	45
3.1	Cooperative network-based teleoperator system [12]	57
3.2	Gain structure of the cooperative teleoperator systems	61
3.3	Dynamics of the human operator	66
3.4	Experimental setup scheme	75
3.5	Example of communication delay	76
3.6	Experiment I, irregular communication delays, direct force reflection ($\alpha = 1$). Contact X-Force experienced by Slave 1 and X-Force reflected to Master 1 (top); contact X-Force experienced by Slave 2 and X-Force reflected to Master 2 (middle); X-Trajectories of masters, slaves and object (bottom)	78
3.7	Experiment I, irregular communication delays, projection-based force reflection ($\alpha = 0.7$). Contact X-Force experienced by Slave 1 and X-Force reflected to Master 1 (top); contact X-Force experienced by Slave 2 and X-Force reflected to Master 2 (middle); X-Trajectories of masters, slaves and object (bottom)	79
3.8	Experiment I, irregular communication delays, projection-based force reflection ($\alpha = 0.3$). Contact X-Force experienced by Slave 1 and X-Force reflected to Master 1 (top); contact X-Force experienced by Slave 2 and X-Force reflected to Master 2 (middle); X-Trajectories of masters, slaves and object (bottom)	80
3.9	Experiment II: A pulse of interaction forces between slaves, operator releases the master. Left: Contact force and reflected forces for different $\alpha \in (0, 1]$; Right: the corresponding induced master motions	81

3.10	Experiment III: A pulse of interaction forces between slaves, operator holds the master. Left: Contact force vs. reflected force for $\alpha = 0.7$; Right: contact force vs. reflected force for $\alpha = 0.3$	81
4.1	Experimental MIS setup: the master subsystem (top); the slave subsystem (bottom).	89
4.2	(a) Task space coordinates of the Haptic Wand device [23]; (b) Structure of the Mitsubishi PA10-7C manipulator [11].	91
4.3	The structure of the teleoperation system	92
4.4	Block diagram of each master/slave system	92
4.5	Experimental setup for the Knot Tightening task	103
4.6	Experimental Setup for the Pegboard Transfer task	103
4.7	Experimental Setup for the Object Manipulation task	104
4.8	Knot Tightening experiment: mean values and SDs of magnitudes of the pulling forces applied by the slaves to the thread for RTT Delays ≈ 0 s and ≈ 0.5 s; DFR (red bars) vs. PBFR (blue bars). Left plot: Slave 1; right plot: Slave 2. . .	107
4.9	Knot Tightening experiment: mean values and SDs of magnitudes of the Masters' accelerations for RTT Delays ≈ 0 s and ≈ 0.5 s; DFR (red bars) vs. PBFR (blue bars). Left plot: Master 1; right plot: Master 2.	107
4.10	Samples of Knot Tightening experiment, RTT delay ≈ 0.5 s. Left column: DFR ($\alpha = 1$). Right column: PBFR ($\alpha = 0.3$). Top plots: contact forces, human forces, and reflected forces of the Master 1. Bottom plots: contact forces, human forces, and reflected forces of the Master 2.	109
4.11	Samples of Knot Tightening experiment, RTT delay ≈ 0.5 s. Magnified view of the induced acceleration of the Master 1 during the knot tightening phase. Left plot: DFR ($\alpha = 1$), Right plot: PBFR ($\alpha = 0.3$).	110
4.12	Peg Transfer experiment: mean values and corresponding SDs of the slaves' forces in x- and z-directions, DFR (red bars) vs. PBFR (blue bars). Top plots: x-forces; bottom plots: z-forces. Left plots: Slave 1; right plots: Slave 2. . . .	112
4.13	Peg Transfer experiment: mean values and corresponding SDs of the Masters' accelerations in x- and z-directions, DFR (red bars) vs. PBFR (blue bars). Top plots: x-accelerations; bottom plots: z-accelerations. Left plots: Master 1; right plots: Master 2.	113
4.14	Samples of Peg Transfer experiment, RTT delay ≈ 0.5 s. Left column: DFR ($\alpha = 1$). Right column: PBFR algorithm ($\alpha = 0.3$). Top plots: contact forces, human forces, and reflected forces of the Master 1 in x direction. Bottom plots: contact forces, human forces, and reflected forces of the Master 2 in x direction.	114
4.15	Samples of Peg Transfer experiment, RTT delay ≈ 0.5 s. Magnified view of the induced accelerations of the Master 1 in x direction during the initial phase of the experiment. Left plot: DFR ($\alpha = 1$). Right plot: PBFR algorithm ($\alpha = 0.3$).	115
4.16	Samples of Peg Transfer experiment, RTT delay ≈ 0.5 s. Left column: Slave 1 and induced Master 1 position with DFR ($\alpha = 1$). Right column: Slave 1 and induced Master 1 position with PBFR ($\alpha = 0.3$)	115
4.17	Object Manipulation experiment, Success rate of the object manipulation for RTT ≈ 0 s and ≈ 0.5 s.	116

4.18	Object Manipulation experiment: mean values and corresponding standard deviations of the forces and Master's acceleration for RTT delays ≈ 0 s. Left diagram: master/slave 1; Right diagram: master/slave 2. DFR (red bars) vs. PBFR (blue bars).	118
4.19	Samples of Object Manipulation experiment, RTT delay ≈ 0 s. Left column: DFR ($\alpha = 1$). Right column: PBFR algorithm ($\alpha = 0.3$). Top plots: contact forces, human forces, and reflected forces of the Master 1 in x direction. Bottom plots: contact forces, human forces, and reflected forces of the Master 2 in x direction.	120
4.20	Samples of Object Manipulation experiment, RTT delay ≈ 0.5 s. Left column: DFR ($\alpha = 1$). Right column: PBFR algorithm ($\alpha = 0.3$). Top plots: contact forces, human forces, and reflected forces of the Master 1 in x direction. Bottom plots: contact forces, human forces, and reflected forces of the Master 2 in x direction.	121
4.21	Samples of Object Manipulation experiment. Left plot: force histogram of master 1 in x direction, RTT delay ≈ 0 s. Right plot: force histogram of master 1 in x direction, RTT delay ≈ 0.5 s	122
5.1	General structure of the teleoperator system with projection-based force reflection and frequency separation. Acronyms: PBFR - projection-based force reflection algorithm; M/E - measurement/estimation of the human force.	140
5.2	Experimental Setup	144
5.3	Tracking performance of the teleoperator system during free motion test: X-trajectories of the master and slave vs. time (left); Z-trajectories of the master and slave vs. time (right).	145
5.4	Examples of (one directional) communication delays: delay with minimum RTT= 400 ms used in the experiments shown in Figures 5.5-5.9 (left plot); delay with minimum RTT= 1000 ms used in the experiments shown in Figures 5.10-5.12 (right plot)	147
5.5	Response of the teleoperator system, min RTT= 400 ms, PBFR without FS (5.11), (5.12), $\alpha = 0.1$: X-trajectories of the master and slave (top plot); contact X-forces as received on the master site vs. reflected X-forces (bottom plot).	147
5.6	Response of the teleoperator system, min RTT= 400 ms, PBFR FS (5.15), (5.16), (5.17), (5.18), $\alpha = 0.1$, $\omega_c = 30$ Hz: X-trajectories of the master and the slave (top plot); contact X-forces as received on the master site vs. reflected X-forces (bottom plot).	148
5.7	Response of the teleoperator system, min RTT= 400 ms, PBFR FS (5.15), (5.16), (5.17), (5.18), $\alpha = 0.1$, $\omega_c = 20$ Hz: X-trajectories of the master and the slave (top plot); contact X-forces as received on the master site vs. reflected X-forces (bottom plot).	148
5.8	Response of the teleoperator system, min RTT= 400 ms, PBFR FS (5.15), (5.16), (5.17), (5.18), $\alpha = 0.1$, $\omega_c = 10$ Hz: X-trajectories of the master and the slave (top plot); contact X-forces as received on the master site vs. reflected X-forces (bottom plot).	149

5.9	Magnified plot of the force responses during the initial phase of the contact, min RTT= 400 ms: PBFR without FS, $\alpha = 0.1$ (top plot); PBFR FS, $\alpha = 0.1$, $\omega_c = 10$ Hz (bottom plot).	149
5.10	Response of the teleoperator system, min RTT= 1000 ms, PBFR without FS (5.11), (5.12), $\alpha = 0.1$: X-trajectories of the master and slave (top plot); contact X-forces as received on the master site vs. reflected X-forces (bottom plot).	150
5.11	Response of the teleoperator system, min RTT= 1000 ms, PBFR FS (5.15), (5.16), (5.17), (5.18), $\alpha = 0.1$, $\omega_c = 10$ Hz: X-trajectories of the master and the slave (top plot); contact X-forces as received on the master site vs. reflected X-forces (bottom plot).	150
5.12	Magnified plot of the force responses during the initial phase of the contact, min RTT= 1000 ms: PBFR without FS, $\alpha = 0.1$ (top plot); PBFR FS, $\alpha = 0.1$, $\omega_c = 10$ Hz (bottom plot).	151
5.13	Stability test: a pulse of contact force is simulated in VE, the operator releases the haptic device; the corresponding induced master motions for different $\alpha \in [0, 1]$ and $\omega_c > 0$ are shown.	151
5.14	Structure of the master interconnection. Acronyms: PBFR - projection-based force reflection; Passive HR - passive reaction of the human operator hand to movement of the master device.	158
5.15	Transformed structure of the master interconnection.	158

List of Tables

4.1	Knot Tightening experiment: mean values and SDs of magnitudes of the pulling forces applied by the slaves to the thread	106
4.2	Knot Tightening experiment: mean values and SDs of magnitudes of the induced masters' accelerations	106
4.3	Knot Tightening experiment: statistical significance (p-values) of the differences (mean forces and mean accelerations) between PBFR and DFR.	106
4.4	Peg Transfer experiment: mean values and SDs of the slaves' forces in x-direction	111
4.5	Peg Transfer experiment: mean values and SDs of the slaves' forces in z-direction	111
4.6	Peg Transfer experiment: mean values and SDs of the Masters' accelerations in x-direction	111
4.7	Peg Transfer experiment: mean values and SDs of the Masters' accelerations in z-direction	112
4.8	Peg Transfer experiment: statistical significance (p-values) of the average forces and the average accelerations between PBFR and DFR algorithms	113
4.9	Object Manipulation experiment, mean values and corresponding standard deviations of the forces applied by slaves in x and z direction, with zero delay . .	117
4.10	Object Manipulation experiment, mean values and corresponding standard deviations of Master's acceleration in x and z direction, with zero delay	117
4.11	Object Manipulation experiment, statistical significance (p-values) of forces and accelerations between PBFR and DFR algorithms in zero delay	117

Nomenclature

DDE Delayed Differential Equation

FDE Functional Differential Equation

IOS Input-to-Output Stable

ISS Input-to-State Stable

MIS Minimally Invasive Surgery

ODE Ordinary Differential Equations

RAMIS Robot-Assisted Minimally Invasive Surgery

WIOPS Weak Input-to-Output Practical Stability

Chapter 1

Introduction

Teleoperation systems have recently found important applications in several areas of health care technology such as telesurgery, minimally invasive surgery (MIS), and surgical training. MIS (also known as "endoscopic" or "laparoscopic" surgery) avoids large incisions by using a small endoscopic camera and several thin, long instruments that enter the body through small incisions about 1 cm wide. MIS has a number of advantages over the traditional open surgery which include less pain, less trauma to the tissue, faster recovery, and shorter hospital stays. However, downsides of MIS include restricted mobility and vision, difficult hand-eye coordination, as well as reduced haptic perception [11, 52]. Robot-assisted minimally invasive surgery (RAMIS) is a specialized form of MIS which aims to provide surgeons with improved vision, maneuverability, and control in comparison with conventional laparoscopy.

Frequently, robot-assisted surgical systems have a structure of a teleoperator system [49, 48]. Teleoperator systems enable the human operator to perform a task on a remote environment. A conventional teleoperator system consists of two manipulators, called the master and the slave. A human operator manipulates the master, which is connected through a communication channel to the remotely located slave. The slave manipulator follows the master motion and executes the task on the environment. If the slave manipulator interacts with the environment, the interaction forces can be transmitted back to the master manipulator. If the master position is transmitted to the slave site, but no information regarding the interaction force from the task environment is sent back to the operator, the teleoperation system is called unilateral. In bilateral teleoperation, the interaction forces between the slave and the environment are re-

flected back to the master manipulator, which allows the human operator to feel the interaction. Although there have been some experimental research that indicates that the presence of tactile or haptic force feedback improves the realism of the tool-tissue interaction to the surgeon and leads to higher performance for surgical procedures [37, 53], current commercial telesurgical MIS systems such as da Vinci (Intuitive Surgical Inc.) do not provide force feedback, mainly because of the inherent stability issues.

On the other hand, in some typical surgical tasks such as suturing and tissue cutting, surgeon frequently needs to use both hands to perform the task. This requires a dual arm master-slave teleoperation system. Performing tasks cooperatively using multiple robot manipulators has significant advantages over single robot manipulation in terms of better handling capabilities, greater dexterity and shorter task completion time. Despite the significant potential of cooperative force-reflecting teleoperation systems for surgical applications, there has been very little research done on this topic.

In the following section, a brief overview of some results related to stability and transparency of teleoperation systems, cooperative teleoperation, and robot-assisted minimally invasive surgery systems is given.

1.1 Previous Works

1.1.1 Stability of Teleoperation Systems

One of the main challenges in the design of teleoperation system is to achieve transparency while maintaining stability of the closed loop teleoperation system. A teleoperator is called transparent if the human operator feels the same forces and velocities at the master device as if he/she was directly interacting with the environment. Although the force reflection can improve the transparency in bilateral teleoperation systems, Ferrel [7] has shown that it may also cause instability in the presence of time delays in the communication channel. Therefore, the design of bilateral teleoperation systems in the presence of communication delays always involves a trade off between the conflicting goals of stability and transparency.

During the past few decades, a significant amount of research has been done with the aim to

overcome the instability of bilateral teleoperation system caused by communication delay. The following paragraphs present a brief literature review of two main control approaches which have been used for this purpose.

Passivity approach

One of the most widely accepted approaches is the passivity-based approach, which has been introduced in different forms, such as scattering transformations [2] and wave variables [21], among others. A system is called passive if it does not have an inner source of energy; in other words, the energy produced by the system over any time interval does not exceed the energy absorbed by the system over the same interval in addition to the energy initially stored in the system. Using electric network analogy [10], a bilateral teleoperation system can be represented as an interconnection of one-port networks (*i.e.*, the human operator and the environment) and two-port networks (*i.e.*, master, slave, and communication medium) that exchange effort (force) and flow (velocity) variables. One of the most important features of passivity is that a cascade interconnection of passive networks is passive. It has been shown that the apparent behaviour of the human operator interacting with an environment is typically passive [12]. Therefore, if the environment is passive, then passivity of the teleoperator system guarantees that the overall system is passive and therefore stable.

Anderson *et al.* [2] have shown that the instability of the teleoperator system with communication delay is a result of non-passivity of the communication channel. To overcome the delay-induced instability, the authors of [2] have proposed a scattering-based method which renders the communication channel with constant time delay passive (more precisely, lossless); as a result, stability of the teleoperator system is ensured. Although scattering-based criterion is easy to apply, it results in more conservative stability conditions in comparison with the absolute stability criterion [1]. The other well-known passivity-based approach that guarantees stability of teleoperator systems in the presence of constant communication delays is the wave variables based approach [21, 22], which is conceptually similar to the scattering. In this approach, instead of transmitting the power variables (*i.e.*, velocity of master and environment force), the wave variables are transmitted over communication channel. Although stability is achieved, the performance may be low as a result of wave reflection phenomenon and/or posi-

tion drift during free motion [22]. A number of works aims at improving performance of the wave variables approach. Among these, Tanner *et al.* [46, 47] have proposed to eliminate the wave reflection phenomenon by either appropriate tuning of the control parameters (impedance matching) or by sending the wave signal through a low-pass filter. Chopra *et al.* [5] have proposed to transmit, in addition to the force/velocity signals, the master/slave position signals and to use a proportional controller in order to eliminate the position drift between the master and slave in steady state. Aziminejad *et al.* [3] have extended the wave variable approach to four-channel teleoperator systems, which leads to improved transparency of the system.

There also exists a number of passivity-based approaches that do not use scattering transformation and/or wave variables. Hannaford *et al.* [9] have proposed time-domain passivity approach to the design of stable haptic systems, where a Passivity Observer and a Passivity Controller are used to monitor the passivity of the system and dissipate excessive energy. Ryu *et al.* [35, 36] have extended the time domain passivity approach to the case of bilateral teleoperation systems. Nuno *et al.* [23] have shown that, under passivity assumptions imposed on the human and the environment, a simple PD-like controller ensures stability of the overall system.

Most of the previous approaches address the stability problem of teleoperator systems in the presence of constant time delays. One problem related to these approaches became clear by the time when Internet started to be actively used as a communication medium. Communication over the Internet is characterized by random time-varying delays which distort the signals transmitted across the channel; the latter, in turn, may result in instability. It has been shown in [17] that the passivity condition is typically violated in the presence of time varying communication delays. To overcome this problem, it was proposed in [17] to add a time varying gain in the transmission path to recover passivity. This approach imposes some restrictive assumptions on the communication delays which, in particular, include differentiability as well as the requirement that the time derivative of the delay function must be less than or equal to one.

A more comprehensive survey of the passivity based approaches to the design of teleoperation systems can be found in the works of Nuno *et al.* [24] and Hokayem *et al.* [13].

Small gain approach

An alternative method to analyze closed-loop stability of the teleoperation system is the small-gain approach. The small-gain approach gives sufficient conditions for stability of the interconnection in terms of gains of its subsystems. One appropriate definition of the subsystem's gain is based on the notions of the input-to-state stability (ISS) [40] and the input-to-output stability (IOS) [43]. The input-to-state stability provides an extension of the notion of the global asymptotic stability to the case of nonzero input. This notion means that the state of the system remains bounded for bounded input, and the ultimate bound of the state is a function of the input norm [41]. Such a function is called the nonlinear ISS gain of the system. The IOS gain is defined analogously. Most of the results on the ISS (IOS) reported in the literature deal with systems described by ordinary differential equations (ODE) [42, 41]. However, teleoperation systems frequently contain delays in the communication channel and, therefore, cannot be described in terms of ODEs. An appropriate mathematical object to describe a teleoperator system with communication delay is the Delayed Differential Equations (DDEs). The DDEs is a special case of Functional Differential Equations (FDEs) where the right-hand side depend on the previous values of the system's state and possibly the input. The standard notion of input-to-output (input-to-state) stability for ODE is, therefore, not directly applicable for teleoperation systems with communication delays. Teel [50] has extended the notion of input-to-state stability to the case of FDEs.

The application of the ISS notion to the design of teleoperator systems was used first in Polushin *et al.* [27], where a control scheme was proposed which makes both master and slave subsystem ISS separately. By using the ISS property for DDE [50], it was shown that the network interconnection of the subsystems is ISS for constant delays in the communication channels. Moreover the stability is proven for the case of digitally implemented control system. In [29], the IOS small gain theorem for interconnections with constant communication delays is introduced and consequently applied to the teleoperation problem in the presence of parametric uncertainty. A partial extension of these results to the case of time-varying communication delay was proposed in [28], where the dirty-derivative filter was used to generate the reference trajectory for the slave manipulator. The filter has two important roles in this scheme.

In the case there is no packet loss in the communication channel and the input is continuous the filter works as an observer and gives the estimate of the velocity and acceleration. On the other hand, if there exist packet loss in the communication, the filter provides a smooth approximation of the discontinuous input. A more general version of the IOS small gain theorem for systems with communication delays was established in [32]. In the above cited work, instead of considering a maximum gain for each subsystem over all channels, a set of gain functions was introduced for a multi-input multi-output IOS system where a separate gain function describes the gain of for each input-output pair. This approach results in less conservative conditions in comparison with the more traditional approaches where a maximal gain over all channels is used to derive the stability conditions. Using an extension of this small gain condition to the case of DDEs, the stability of the teleoperation system in presence of the multiple communication channel with time-varying delays is proposed. The assumption on the delays used in this work is less restrictive in comparison with the results of [28]. This assumption requires the existence of an upper bound function for time delays that is not growing faster than the time itself. Practically, this assumption can be satisfied by using techniques such as time-stamping or sequence-numbering.

To satisfy the small gain stability conditions of the teleoperation system, the gain of the master manipulator or reflected force should be assigned sufficiently small. Practically, this could be achieved by increasing the stiffness/damping of the master manipulator or by decreasing the magnitude of the force reflecting signal. However, these methods deteriorate transparency of the system [6]. For instance, increasing the damping of the master device makes the system sluggish especially in free motion, and may result in operator's fatigue. To resolve this contradiction, Polushin *et al.* [30, 31, 33] have proposed a new force reflection algorithm. This new algorithm, which is called the projection-based force reflection (PBFR) algorithm, shapes the environment force reflected back to the master side based on the force applied by human operator to the master device. Using the ISS small-gain approach, it was shown that implementation of the PBFR algorithm guarantees the stability of the system even for a high force reflection gain and low damping of the master device.

1.1.2 Cooperative Teleoperation Systems

Performing daily tasks using human hands can be categorized into two groups: the unimanual tasks where a single hand is used alone, and the bimanual tasks where two hands are needed to perform the task. Majority of the daily living tasks is performed bimanually using two hands; examples include picking up a heavy object and transferring an object from one hand to another. Although in bimanual tasks, both hands cooperate to achieve a common goal, however, in most of the tasks the hands have different functions. The non-dominant hand typically plays a stabilizing role while the dominant hand performs the object manipulation task [16]. Opening a bottle is an example of the bimanual action, where one hand holds the bottle and the other hand opens the cap.

In cooperative teleoperation systems, multiple operators interact with each other via the master and slave manipulators to perform tasks on a common shared environment. Cooperative teleoperators enable collaboration between spatially separated operators and may lead to significant improvement in handling capabilities, dexterity, and task completion time. The cooperative teleoperation systems can be categorized into three major groups based on the configuration of the master and slave manipulators.

1. Single-Master-Multiple-Slave (SMMS) teleoperator systems, where a human operator simultaneously controls multiple slave manipulators. Such systems have typically found applications in situations where the manipulation dexterity, mechanical strength and safety cannot be achieved by using a single slave manipulator and where the human intelligence is necessary for successful execution of the given tasks, however, it is impossible or dangerous to send humans on the site. One simple example of such a task is manipulating a load which is heavier than the capacity of a single manipulator. In these situations, the load can be distributed between the multiple slave manipulators, while the human operator controls the object position.
2. Multiple-Master-Single-Slave (MMSS) teleoperator systems, where multiple human operators control a single slave manipulator [8]. These systems, in particular, have found applications in training and rehabilitation systems. Typically, in these systems, one of the human operators (trainer, therapist) has the major role in commanding the slave ma-

nipulator while, at the same time, the sensory information such as haptic is sent back to the other operators (trainees/patients). For example, Malysz *et al.* [20] introduced the idea of projective force mapping in MMSS teleoperation system. In this approach, the position control of the single slave manipulator is divided between multiple master robots. The needle insertion task is an example of the application of this approach where the position/orientation of the needle is controlled by one master and the depth of it by another master. Khademian *et al.* [15] have proposed a design method for four channel, two-master-one-slave teleoperator system. In this approach, the communication is performed not only between the master and the slave in each master-slave pair, but also between the masters.

3. The third and the most important group of cooperative teleoperation systems is Multiple-Masters-Multiple-Slaves (MMMS) teleoperator systems. Depending on the task, these systems can be controlled in centralized or decentralized manner. In the decentralized control architecture, the system consists of separate single-master-single-slave teleoperation systems without any information exchange between them. In the centralized control architecture, on the other hand, communication of information between the operators is performed.

Although the multi-master/multi-slave teleoperation systems can potentially be used in significant number of applications, a few control architectures have been proposed for these systems. Sirouspour [38] has used μ -synthesis to design four-channel control architecture for a system with multiple slaves holding a common tool for manipulating a common environment. The closed kinematic chain formed by the slave robots and the tool imposes constraints on the motion of the slaves. In [39], a two-channel multilateral position-position adaptive controller has been introduced and studied for the delay-free case. Bacocco *et al.* [4] have proposed a method for control design of cooperative teleoperation system in the presence of constant communication delays. Their control algorithm consists of local PD position controllers whose gains were tuned using optimal LQ synthesis.

Specific features that makes the cooperative teleoperation systems difficult for analysis and control design include multiple networked communication channels between the masters and

the corresponding slaves, and the possibility of non-passive slave-slave interactions through the common environment. These features make it problematic to apply conventional passivity-based approaches for the design of such systems. For example, when the slave manipulators are different in size and mass, scaled passivity approach could not be applied directly as the scaled passivity condition can be violated during direct mechanical slave-slave interaction. In this thesis, the application of the small-gain approach to design of the cooperative teleoperation system will be addressed.

1.1.3 RAMIS Application

Robot-assisted surgery is a specialized form of MIS which aims to provide surgeons with better vision, maneuverability and control in comparison with conventional laparoscopy. Typically, robot-assisted minimally invasive surgery (RAMIS) systems have a structure of a teleoperation system. Application of haptic technology to RAMIS have recently received substantial attention of the research community. The purpose of haptic feedback is to provide the surgeon with the increased feel of presence by displaying him/her, in addition to the visual feedback, the interaction forces at the patient side. Although experimental data indicates that the presence of haptic feedback improves the realism of the tool-tissue interaction to the surgeon and leads to higher performance of surgical procedures, current commercial surgical MIS systems do not provide force feedback, mainly because of the inherent stability issues. The instability may arise because of different factors such as the existence of time delays in the communication between master (surgeon) and slave (patient) sites, or inability of the control system to compensate the dynamics of the master or slave robots (for example, due to modelling uncertainties). To avoid the instability while, at the same time, providing the surgeon with the force information, sensory substitution force feedback such as graphical force displays is used in many applications.

Yip *et al.* [54] have addressed the effect of delayed force feedback on users' task performance. Their experiments consisted of performing the peg-in-hole task in the presence of different delays and three different feedback scenarios which are unilateral, bilateral, and graphical force feedback. They demonstrated experimentally that, regardless of the delay, the

task completion time of the unilateral teleoperation is the lowest in comparison with the other two scenarios, while the interaction force is the highest. It has also been shown that, regardless of the delay, the haptic force feedback decreases the average and the peak interaction forces, while the graphical force feedback attenuates the peak force if the delay is low. To ensure stability of the teleoperation system, the wave variable approach was chosen.

Mahvash *et. al.*, [19] have experimentally compared the performance of the following four force feedback scenarios: direct force feedback, graphical force feedback, graphical plus direct force feedback, and no force feedback. The force feedback was implemented by introducing the virtual coupling between the master and the slave, as explained in [18]. The experiments consisted of palpation of a phantom heart and a prostate model with a needle driver tool, and localization of a hidden stiff objects inside the phantom. The experimental results showed that, in the case of heart model, the direct force feedback results in more accurate localization of the hidden object in comparison with the other scenarios. However, in the case of prostate model, no differences have been found between the direct force feedback and the other scenarios. The main reason of this outcome is the fact that the virtual coupling results in transparency deterioration in the case of stiff environments (such as the prostate model).

Wagner *et. al.*, [53] have studied the effect of the force feedback on the performance during the blunt dissection task. The results have shown that the force feedback reduces the force applied to the tissue during the task and, as a result, reduces the tissue trauma.

Talasaz *et. al.*, [45] have compared the performance of the knot-tightening task between three different force feedback scenarios, which include visual force feedback, direct force feedback, and augmented direct/visual force feedback. The experimental results showed that the visual force feedback leads to better quality of the knots and better consistency of the the tightening force, while the direct force feedback results in less collisions between the two instruments and and between the instrument and the tissue.

Trejos *et. al.*, [51] have proposed to use a tactile sensing instrument under robotic control to locate tumors inside the tissue. In their work, the area of palpation is defined during the preoperative stage by the user and, consequently, the robotic-palpation is performed autonomously using the augmented hybrid impedance controller. Talasaz *et. al.* [44] have proposed a semi-autonomous palpation of the tissue using master-slave teleoperation system. They have used

the Jacobian transpose hybrid impedance controller developed in [26] on the slave side. In this approach, first the user at the master side moves the TSI at the slave side to the area of palpation. Then, the user switches from position control to force control in the direction of palpation by using a manual switch on the master device. This approach not only helps the user to locate the position of the tumor but also to avoid applying excessive forces that may damage the tissue or deteriorate the tactile measurement. A comprehensive survey of haptic in RAMIS systems can be found in [25].

As of today, significant number of publications are available that deal with performance comparison of MIS teleoperator systems with direct force feedback and other scenarios such as no force feedback or graphical force feedback, for different MIS tasks. However, only a few works evaluate the effect of the control scheme on the performance of the MIS task. For example, Kazi [14] evaluated the performance of a telesurgical system during some surgical tasks using the following three stabilization methods: scaling down the motion of the slave, increasing the compliance at the slave, and increasing the motion resistance at the master arm. The experimental results have shown that the effect of these schemes on the performance substantially depends on the particular task. It was also suggested in the above work that transparency level can be increased without negative effect on the stability if the damping of the operator's hand is high enough. Therefore, the work [14] proposes to implement an on-line identification of the human arm damping and use this estimate to adjust the the damping of the controller. The experimental results, however, demonstrated that this approach does not lead to noticeable performance improvement.

The work of Preusche, *et. al.*, [34] proposes two different control algorithms for a force reflecting teleoperator MIS system. The first proposed control algorithm uses a three-channel teleoperation system, where the slave follows the master position and the force feedback to the master side is calculated as a combination of the sensed force at the slave side and a scaled error between master and slave position. The other proposed approach is a force-force teleoperation scenario, where the operator's force applied to the master device serves as a reference input to the slave force controller. The work [34] also suggested to adapt the position error scaling gain as a function of the estimated environment stiffness in order to reduce the effect of position coupling in free motion while increasing the stability during contact phase. Theoretical stability

and transparency analysis, however, is not performed in [34] and the experimental results are limited to the case of contact with a soft environment.

The use of force sensors at the patient side is limited in the currently available MIS teleoperation system, mainly because of the sterilization issue. To avoid using force sensors, Mahvash *et al.* [18] have proposed a position-position scheme for haptic-enabled MIS teleoperation systems. The proposed approach uses a virtual coupling network placed between the end-effectors of the master and the slave devices in combination with the feed-forward cancellation of the master and the slave dynamics. Stability analysis is carried out based on the assumptions that the master and the slave devices are linear and no delay exist in the communication channel. It has been demonstrated that the proposed control approach provides perfect transparency for the contact with soft environment if the dynamics of the master and the slave robots are cancelled completely and the gain of the virtual coupling is chosen sufficiently high. To ensure the stability of the system, the gain of the virtual coupling is derived using Llewellyn's absolute stability criteria. Although this approach works well in the case of interaction with soft environments, the performance deteriorates in the case of contact with stiff environments (such as the prostate model) [19]. The other shortcoming of this approach is that, in practice, the dynamics of the master and the slave robots cannot be cancelled completely due to modelling uncertainties, and this may have a negative effect on the performance.

1.2 Contributions

One of the main issues in the design of haptics-enabled cooperative teleoperation for MIS application is the potential instability of the closed-loop system. Currently, the most accepted approach to control design for conventional single-master/single-slave teleoperation systems is based on the passivity framework and its extensions, such as the scattering transformations and the wave variables. Using this framework, the stability of the teleoperation system can be guaranteed based on the passivity properties of the parts of the teleoperation system. However, in cooperative teleoperation, the passivity condition does not necessarily hold. In particular, slave-slave interactions may lead to energy exchange between parts of cooperative teleoperation systems, which may result in violation of the passivity condition. A simple example of

this situation is a collision between tools that might happen during surgical procedures. Thus, the application of passivity-based techniques in the design of cooperative surgical teleoperation systems may encounter significant difficulties.

The main contributions of this work can be summarized as follows:

1. Development of an alternative small-gain approach to the design of stable and transparent force-reflecting cooperative teleoperator systems in the presence of time-varying communication delays and interaction between the slave manipulators.
2. Improvement of the transparency of the system and reducing the conservatism of the small-gain design by incorporating the projection-based force reflection (PBFR) algorithms into cooperative teleoperator system.
3. Improvement of the transient fidelity of the the PBFR algorithms using a frequency separation method.
4. Evaluating the effect of the proposed control design on some basic surgical tasks using a dual-arm MIS setup.

1.3 Thesis Outline

The remainder of this thesis is organized as follows:

- Chapter 2 presents a small gain framework for the design of force reflecting cooperative teleoperation systems in the presence of the multiple time-varying communication delays. Consequently, a control algorithm for cooperative force reflecting teleoperation system is presented, and stability conditions are formulated based on the proposed small gain framework. The design is experimentally evaluated on a testbed that consists of a two-master/two-slave cooperative force reflection teleoperation system, where two PHANTOM Omni devices are used as master manipulators, while the slaves are represented by two simulated models of PHANTOM Premium 1.5A devices implemented in virtual environment.

- In Chapter 3, the PBFR algorithms are incorporated into the small gain design of the cooperative teleoperation system to overcome the conservatism of the small gain design. The effect of the human dynamic and different force reflection algorithms on the stability of the teleoperation system is described. It is demonstrated that, using the PBFR algorithm, the stability of the system can be guaranteed regardless of the dynamic properties of the human hand(s). The theoretical results are experimentally evaluated on the same setup as that used in Chapter 2.
- In Chapter 4, the performance of the proposed PBFR algorithms is experimentally evaluated and compared with that of the DFR algorithms on the dual-arm MIS setup in three simple surgical tasks: knot tightening, pegboard transfer, and object manipulation. Nine subjects participated in the experiments. All the experiments have been performed for both the DFR and PBFR algorithms and in the presence of negligible as well as substantial communication delays. The experimental results are presented and the effect of different force reflection algorithms on the performance of the system is discussed.
- In Chapter 5, a new type of the PBFR algorithms is introduced that aims to improve the transient fidelity of the force response. The new type of PBFR algorithms is based on the separation of different frequency bands in the force reflection signal and on applying the projection-based algorithm only for low frequencies while reflecting the high frequency forces directly. The theoretical and experimental results are presented to show the improvement of the transient fidelity of the system without negative effects on stability.
- In Chapter 6, a summary of the thesis results, conclusions, and future research directions are presented.

Bibliography

- [1] Richard J. Adams and Blake Hannaford. Stable haptic interaction with virtual environment. *IEEE Transactions on Robotics and Automation*, 15(3):465–474, 1999.

- [2] Robert J. Anderson and Mark W. Spong. Bilateral control of teleoperators with time delay. *IEEE Transactions on Automatic Control*, 34(5):494–501, 1989.
- [3] Arash Aziminejad, Mahdi Tavakoli, Rajni V. Patel, and Mehrdad Moallem. Transparent time-delayed bilateral teleoperation using wave variables. *IEEE Transactions on Control Systems Technology*, 16(3):548–555, 2008.
- [4] Rita Bacocco and Claudio Melchiorri. Lq control design of cooperative teleoperation systems. In *Proceedings of the 2009 International Conference on Advanced Robotics*, pages 1–6. IEEE, 2009.
- [5] Nikhil Chopra and Mark W. Spong. Passivity-based control of multi-agent systems. In *Advances in Robot Control*, pages 107–134. Springer, 2006.
- [6] RW Daniel and PR McAree. Fundamental limits of performance for force reflecting teleoperation. *The International Journal of Robotics Research*, 17(8):811–830, 1998.
- [7] William R. Ferrell. Delayed force feedback. *Human Factors: The Journal of the Human Factors and Ergonomics Society*, 8(5):449–455, 1966.
- [8] Daniela Feth, Binh An Tran, Raphaela Groten, Angelika Peer, and Martin Buss. Shared-control paradigms in multi-operator-single-robot teleoperation. In *Human Centered Robot Systems*, pages 53–62. Springer, 2009.
- [9] Blake Hannaford and Jee-Hwan Ryu. Time-domain passivity control of haptic interfaces. *IEEE Transactions on Robotics and Automation*, 18(1):1–10, 2002.
- [10] Simon S. Haykin. *Active network theory*. Addison-Wesley, 1970.
- [11] Sandra Hirche, Manuel Ferre, Jordi Barrio, Claudio Melchiorri, and Martin Buss. Bilateral control architectures for telerobotics. *Advances in Telerobotics*, pages 163–176, 2007.
- [12] Neville Hogan. The mechanics of multi-joint posture and movement control. *Biological Cybernetics*, 52(5):315–331, 1985.

- [13] Peter F. Hokayem and Mark W. Spong. Bilateral teleoperation: An historical survey. *Automatica*, 42(12):2035–2057, 2006.
- [14] Arif Kazi. Operator performance in surgical telemanipulation. *Presence: Teleoperators and Virtual Environments*, 10(5):495–510, 2001.
- [15] Behzad Khademian and Keyvan Hashtrudi-Zaad. A four-channel multilateral shared control architecture for dual-user teleoperation systems. In *Proceedings of the 2007 IEEE/RSJ International Conference on Intelligent Robots and Systems*, pages 2660–2666. IEEE, 2007.
- [16] Marliese Kimmerle, Lynda Mainwaring, and Marlene Borenstein. The functional repertoire of the hand and its application to assessment. *The American Journal of Occupational Therapy*, 57(5):489–498, 2003.
- [17] Rogelio Lozano, Nikhil Chopra, and Mark W. Spong. Passivation of force reflecting bilateral teleoperators with time varying delay. *Mechatronics*, 2:24–26, 2002.
- [18] Mohsen Mahvash and Allison M. Okamura. Enhancing transparency of a position-exchange teleoperator. In *Proceedings of the 2007 EuroHaptics Conference, and Symposium on Haptic Interfaces for Virtual Environment and Teleoperator Systems*, pages 470–475, 2007.
- [19] Mohsen Mahvash, Jim Gwilliam, Rahul Agarwal, Balazs Vagvolgyi, Li-Ming Su, DD Yuh, and Allison M. Okamura. Force-feedback surgical teleoperator: Controller design and palpation experiments. In *Proceedings of the 2008 symposium on Haptic Interfaces for Virtual Environment and Teleoperator Systems*, pages 465–471. IEEE, 2008.
- [20] Pawel Malysz and Shahin Sirouspour. Cooperative teleoperation control with projective force mappings. In *Proceedings of the 2010 IEEE Haptics Symposium*, pages 301–308. IEEE, 2010.
- [21] Günter Niemeyer and Jean-Jacques E. Slotine. Stable adaptive teleoperation. *IEEE Journal of Oceanic Engineering*, 16(1):152–162, 1991.

- [22] Gunter Niemeyer and Jean-Jacques E. Slotine. Telem Manipulation with time delays. *International Journal of Robotics Research*, 23(9):873–890, September 2004.
- [23] Emmanuel Nuno, Romeo Ortega, Nikita Barabanov, and Luis Basanez. A globally stable pd controller for bilateral teleoperators. *IEEE Transactions on Robotics*, 24(3):753–758, 2008.
- [24] Emmanuel Nuño, Luis Basañez, and Romeo Ortega. Passivity-based control for bilateral teleoperation: A tutorial. *Automatica*, 47(3):485–495, 2011.
- [25] Allison M. Okamura. Haptic feedback in robot-assisted minimally invasive surgery. *Current opinion in urology*, 19(1):102, 2009.
- [26] Rajni V. Patel, Heidar A. Talebi, Jagadeesan Jayender, and Farshid Shadpey. A robust position and force control strategy for 7-dof redundant manipulators. *IEEE/ASME Transactions on Mechatronics*, 14(5):575–589, 2009.
- [27] Ilija G. Polushin and Horacio J. Marquez. Stabilization of bilaterally controlled teleoperators with communication delay: An iss approach. *International Journal of Control*, 76(8):858–870, 2003.
- [28] Ilija G. Polushin, Peter Xiaoping Liu, and Chung-Horng Lung. A control scheme for stable force-reflecting teleoperation over ip networks. *IEEE Transactions on Systems, Man, and Cybernetics, Part B: Cybernetics*, 36(4):930–939, 2006.
- [29] Ilija G. Polushin, Abdelhamid Tayebi, and Horacio J. Marquez. Control schemes for stable teleoperation with communication delay based on {IOS} small gain theorem. *Automatica*, 42(6):905 – 915, 2006.
- [30] Ilija G. Polushin, Peter Xiaoping Liu, and Chung-Horng Lung. A force-reflection algorithm for improved transparency in bilateral teleoperation with communication delay. *IEEE/ASME Transactions on Mechatronics*, 12(3):361–374, 2007.
- [31] Ilija G. Polushin, Peter Xiaoping Liu, and Chung-Horng Lung. Projection-based force reflection algorithm for stable bilateral teleoperation over networks. *IEEE Transactions on Instrumentation and Measurement*, 57(9):1854–1865, 2008.

- [32] Ilia G. Polushin, Horacio J. Marquez, Abdelhamid Tayebi, and Peter Xiaoping Liu. A multichannel ios small gain theorem for systems with multiple time-varying communication delays. *IEEE Transactions on Automatic Control*, 54(2):404–409, 2009.
- [33] Ilia G. Polushin, Xiaoping P. Liu, and Chung-Horng Lung. Stability of bilateral teleoperators with generalized projection-based force reflection algorithms. *Automatica*, 48(6): 1005 – 1016, 2012.
- [34] Carsten Preusche, Tobias Ortmaier, and Gerd Hirzinger. Teleoperation concepts in minimal invasive surgery. *Control Engineering Practice*, 10(11):1245–1250, 2002.
- [35] Jee-Hwan Ryu, Dong-Soo Kwon, and Blake Hannaford. Stable teleoperation with time-domain passivity control. *IEEE Transactions on Robotics and Automation*, 20(2):365–373, 2004.
- [36] Jee-Hwan Ryu, Jordi Artigas, and Carsten Preusche. A passive bilateral control scheme for a teleoperator with time-varying communication delay. *Mechatronics*, 20(7):812–823, 2010.
- [37] Karun B. Shimoga. A survey of perceptual feedback issues in dexterous telemanipulation. ii. finger touch feedback. In *Proceedings of the 1993 IEEE Virtual Reality Annual International Symposium*, pages 271–279. IEEE, 1993.
- [38] Shahin Sirouspour. Modeling and control of cooperative teleoperation systems. *IEEE Transactions on Robotics*, 21(6):1220–1225, 2005.
- [39] Shahin Sirouspour and Peyman Setoodeh. Multi-operator/multi-robot teleoperation: an adaptive nonlinear control approach. In *Proceedings of the 2005 IEEE/RSJ International Conference on Intelligent Robots and Systems*, pages 1576–1581. IEEE, 2005.
- [40] Eduardo D. Sontag. Smooth stabilization implies coprime factorization. *IEEE Transactions on Automatic Control*, 34(4):435–443, 1989.
- [41] Eduardo D. Sontag. Input to state stability: Basic concepts and results. In *Nonlinear and Optimal Control Theory*, pages 163–220. Springer, 2006.

- [42] Eduardo D. Sontag and Yuan Wang. On characterizations of the input-to-state stability property. *Systems & Control Letters*, 24(5):351–359, 1995.
- [43] Eduardo D. Sontag and Yuan Wang. Notions of input-to-output stability. *Systems & Control Letters*, 38:235–248, 1999.
- [44] Ali Talasaz and Rajni V. Patel. Integration of force reflection with tactile sensing for minimally invasive robotics-assisted tumor localization. *IEEE Transactions on Haptics*, 6(2):217–228, 2013. ISSN 1939-1412.
- [45] Ali Talasaz, Ana Luisa Trejos, and Rajni V. Patel. Effect of force feedback on performance of robotics-assisted suturing. In *Proceedings of the 2012 IEEE RAS & EMBS International Conference on Biomedical Robotics and Biomechatronics*, pages 823–828. IEEE, 2012.
- [46] Neal A. Tanner and Günter Niemeyer. Improving perception in time-delayed telerobotics. *The International Journal of Robotics Research*, 24(8):631–644, 2005.
- [47] Neal A. Tanner and Günter Niemeyer. High-frequency acceleration feedback in wave variable telerobotics. *IEEE/ASME Transactions on Mechatronics*, 11(2):119–127, 2006.
- [48] Mahdi Tavakoli, Rajni V. Patel, and Mehrdad Moallem. A force reflective master-slave system for minimally invasive surgery. In *Proceedings of the 2003 IEEE/RSJ International Conference on Intelligent Robots and Systems*, volume 4, pages 3077–3082. IEEE, 2003.
- [49] Mahdi Tavakoli, Rajni V. Patel, Mehrdad Moallem, and Arash Aziminejad. Haptics-based systems for robot-assisted surgery and telesurgery: Design, control, and experimentation, 2008.
- [50] Andrew R. Teel. Connections between razumikhin-type theorems and the iss nonlinear small gain theorem. *IEEE Transactions on Automatic Control*, 43(7):960–964, 1998.
- [51] Ana Luisa Trejos, Jagadeesan Jayender, Melissa T Perri, Michael D. Naish, Rajni V. Patel, and Richard A. Malthaner. Robot-assisted tactile sensing for minimally invasive tumor localization. *The International Journal of Robotics Research*, 28(9):1118–1133, 2009.

- [52] Ana Luisa Trejos, Rajni V. Patel, and Michael D. Naish. Force sensing and its application in minimally invasive surgery and therapy: a survey. *Proceedings of the Institution of Mechanical Engineers, Part C: Journal of Mechanical Engineering Science*, 224(7): 1435–1454, 2010.
- [53] Christopher R Wagner, Nicholas Stylopoulos, and Robert D. Howe. The role of force feedback in surgery: Analysis of blunt dissection. In *Symposium on Haptic Interfaces for Virtual Environment and Teleoperator Systems*, pages 73–79. Citeseer, 2002.
- [54] Michael C. Yip, Mahdi Tavakoli, and Robert D. Howe. Performance analysis of a haptic telemanipulation task under time delay. *Advanced Robotics*, 25(5):651–673, 2011.

Chapter 2

A Small Gain Framework for Networked Cooperative Force-Reflecting Teleoperation

The material presented in this chapter is published in *Automatica*, vol., 49,2013, pp. 338 – 348. A part of this work has also been published in the *Proceeding of the IEEE International Conference of Robotics and Automation (ICRA)*, pp. 892 – 897, Shanghai, 2011.

2.1 Introduction

Teleoperation over communication networks has recently attracted significant attention due to its high flexibility, accessibility, and relatively low cost [10]. The primary purpose of teleoperator systems is to make it possible for a human operator to execute a manipulation task remotely. A typical networked teleoperator system consists of two (or more) manipulators, called master(s) and slave(s), that are connected through a communication network. The master manipulator is manually controlled by the human operator, while the slave executes the task by following the motion of the master. In order to let the human operator feel the interaction with the task, the haptic data (slave positions/velocities as well as the interaction forces between the slave and the environment) can be transmitted back to the master site and dis-

played to the human operator through some sort of haptic interface. The theory and design of networked master-slave teleoperator system has become increasingly active research area in recent years, with a large and growing number of applications including telemedicine, telesurgery and collaborative surgery, telemaintenance, teleassistance for disabled, applications to education, entertainment, and many others. For an excellent account of the recent developments, please refer to the survey papers [12, 19], where the former gives an overview of some recent contributions put in historical perspective, while the latter presents a number of teleoperation control schemes within a unifying passivity-based framework. For information on the theory and applications of the networked (in particular, Internet-based) teleoperators, the reader is referred to [10, 9]; see also [12, Section 3.7].

In cooperative teleoperator systems, multiple teleoperators perform tasks on the same environment [26, 32]. Cooperative teleoperation enables collaboration between human operators that are geographically separated, and may lead to drastic improvement in handling capabilities, dexterity, as well as task completion time. Typical examples of applications include different assembly tasks, handling of toxic/radioactive materials and collaborative telesurgery. A structure of cooperative network-based teleoperator system is shown in Figure 2.1. Specific features that makes such a system difficult for analysis and control design include multiple networked communication channels between the masters and the corresponding slaves, and the possibility of the slave-slave interactions through the common environment which may become non-passive if the slaves have different size. These features limit the applicability of the conventional passivity-based approaches (that typically involve different forms of scattering transformations or wave variables [1, 18, 16]) for the design of such systems. In fact, there exists only a few works that deal with stability analysis of cooperative force reflecting teleoperator systems with communication constraints. Recent works on this topic include [25, 4]. In [25], the stability analysis is intrinsically linear, the communication delays are assumed to be constant and known, and the communication errors are not permitted; moreover, apparently the approach of [25] can not be extended to the case of nonlinear systems or irregular unknown communication delays and communication errors. In [4], the passivity & wave variables approach is employed; however, this work does not contain rigorous stability analysis, the communication delay are assumed to be constant, and no communication errors are admitted.

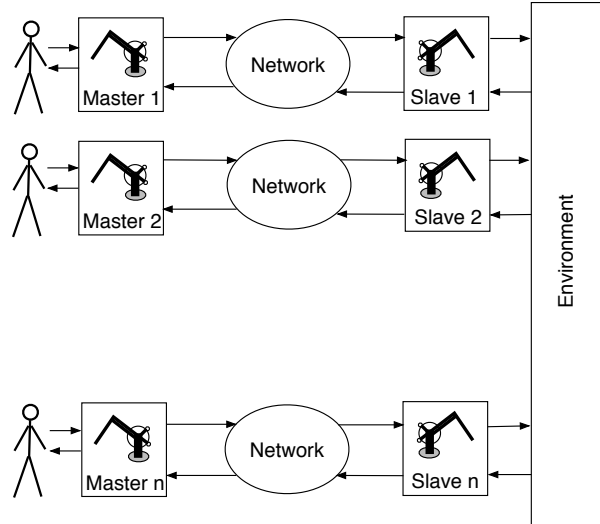


Figure 2.1: Cooperative network-based teleoperator system

In this paper, we develop a framework for the design of bilateral cooperative teleoperators with network-induced communication constraints that is based on the small-gain arguments. Along with passivity theorems [11, 3], the small-gain theorems are among the most powerful tools in analysis and control of interconnected nonlinear systems [13]. However, the small-gain ideas have not yet been applied to the design of cooperative network-based teleoperator systems, which can probably be attributed to a number of difficulties associated with such an application. First, a cooperative teleoperator system can consist of multiple master-slave pairs that interact through environment, which generally results in an interconnection structure more complex than simple feedback interconnections to which the small-gain arguments are traditionally applied. Second, communication over networks imposes communication constraints that include time-varying discontinuous possibly unbounded communication delays and possible packet losses. Also, in robotic systems, stability with prescribed gains usually cannot be achieved globally, which implies that an appropriate version of the small-gain theorem must admit stability properties of subsystems to be satisfied within a compact subset of the state space and a compact range of inputs rather than globally (which corresponds to stability with finite restrictions as well as a bounded domain of small-gain conditions). Although a number of nonlinear small-gain theorems presented in the literature addressed some of the above mentioned issues (see, for example, [6, 14, 31, 7] for small gain conditions for interconnection of

multiple subsystems, [31] for the case of bounded communication delays, [22, 23] for the case of discontinuous time-varying unbounded communication delays, and [29, 22, 23] for the case of finite restrictions), no small-gain results exist that would directly fit the specific requirements of the networked cooperative bilateral teleoperator systems. In this work, we first formulate and prove a new version of the weak input-to-output practical stability (WIOPS) small gain theorem that is applicable to stability analysis of large-scale network-based interconnections where the subsystems are assumed to satisfy the WIOPS property. Based on this result, we present a design of a cooperative networked force-reflecting teleoperator system with a typical interconnection structure. More specifically, using the developed multi-channel small-gain approach, we design a cooperative force-reflecting teleoperator system which is guaranteed to be stable in the presence of multiple network-induced communication constraints by appropriate adjustment of local control gains and/or force-reflection gains. Theoretical developments presented in this paper are supported by experiments. To the best of our knowledge, this is the first work where the small gain approach is applied to analyze stability of a networked cooperative force reflecting teleoperator system.

The organization of this paper is as follows. In Section 2.2, we formulate and prove a new version of the WIOPS small gain theorem that meets the specific requirements of networked force-reflecting cooperative teleoperator systems. In Section 2.3, we design a force-reflecting cooperative teleoperator system using the small-gain framework, and show that the system is stable in the presence of irregular communications. Experimental results are discussed in Section 2.4, and concluding remarks are given in Section 2.5.

2.2 Small Gain Theorem for Network-Based Interconnections

2.2.1 Preliminaries

Throughout the paper, the following standard notation is used. Let \mathbb{R}_+ be the set of nonnegative real numbers, $\mathbb{R}_+ := [0, +\infty)$. A continuous function $\gamma: \mathbb{R}_+ \rightarrow \mathbb{R}_+$ is said to belong to class \mathcal{G} ($\gamma \in \mathcal{G}$) if it is strictly increasing; a function $\gamma \in \mathcal{G}$ belongs to class \mathcal{K} ($\gamma \in \mathcal{K}$) if it satisfies

$\gamma(0) = 0$; a function $\gamma \in \mathcal{K}$ belongs to class \mathcal{K}_∞ if $\gamma(s) \rightarrow \infty$ as $s \rightarrow \infty$. Also, we will occasionally use the notation \mathcal{K}_{lin} to denote a subclass of \mathcal{K}_∞ which consists of linear functions of the form $\gamma(s) := g \cdot s$, where $g > 0$. Finally, let us formally introduce a class of zero functions \mathcal{O} which consists of a single element, *i.e.*, $\gamma \in \mathcal{O}$ if $\gamma(s) \equiv 0$ for all $s \in \mathbb{R}_+$.

When analyzing stability of cooperative teleoperator systems, one deals with Multiple Inputs - Multiple Outputs (MIMO) systems where each input-output pair has a specific gain function associated with it. For simplicity of notation in the MIMO case, it is convenient to use multivariable extensions of the classes \mathcal{G} , \mathcal{K} , \mathcal{K}_∞ , \mathcal{K}_{lin} , defined as follows. Let \mathbb{R}_+^n be the positive orthant in \mathbb{R}^n , *i.e.*, $\mathbb{R}_+^n := \{x \in \mathbb{R}^n, x_i \geq 0 \text{ for all } i = 1, \dots, n\}$. Given a set $\Gamma_{ij}: \mathbb{R}_+ \rightarrow \mathbb{R}_+$, $i \in \{1, \dots, n\}$, $j \in \{1, \dots, m\}$, consider an associated map $\Gamma: \mathbb{R}_+^m \rightarrow \mathbb{R}_+^n$ defined according to the formula $\Gamma(s) = [(\Gamma(s))_1, \dots, (\Gamma(s))_n]$, where

$$(\Gamma(s))_i := \max_{j \in \{1, \dots, m\}} \Gamma_{ij}(s_j).$$

A map $\Gamma: \mathbb{R}_+^m \rightarrow \mathbb{R}_+^n$ is said to belong to class $\mathcal{G}^{n \times m}$ if and only if it can be associated with a set $\{\Gamma_{ij}\}$, $i \in \{1, \dots, n\}$, $j \in \{1, \dots, m\}$, where all $\Gamma_{ij} \in \{\mathcal{G} \cup \mathcal{O}\}$. Classes $\mathcal{K}^{n \times m}$, $\mathcal{K}_\infty^{n \times m}$, and $\mathcal{K}_{lin}^{n \times m}$ are defined analogously.

Further notation that we use in the paper is as follows. Given two maps Γ_1, Γ_2 of appropriate dimensions, their composition is denoted by $\Gamma_1 \circ \Gamma_2$ (*i.e.*, $\Gamma_1 \circ \Gamma_2(s) := \Gamma_1(\Gamma_2(s))$). Given a map $\Gamma \in \mathcal{G}^{n \times n}$ and a number $i \in \mathbb{N} := \{0, 1, \dots\}$, denote

$$\Gamma^i := \underbrace{\Gamma \circ \Gamma \circ \dots \circ \Gamma}_{i \text{ times}}.$$

In particular, Γ^i for $i = 0$ is the identity map, $\Gamma^0(s) := s$. Further, given $x, y \in \mathbb{R}_+^n$, we write $x \geq y$ iff $x_i \geq y_i$ for all $i \in \{1, \dots, n\}$, and $x \not\geq y$ otherwise. Relations $>$ and $\not>$ are defined analogously. The maximum of two or more vectors is calculated componentwise. For a finite set X , the number of its elements is denoted by $\#X$. Given $I \subset \{1, \dots, n\}$, $I \neq \emptyset$, and $y \in \mathbb{R}_+^n$, denote $y_I := \{y_i\}_{i \in I}$. Thus, $y_I \in \mathbb{R}^{\#I}$ is the projection of $y \in \mathbb{R}^n$ onto the subspace of \mathbb{R}^n spanned by the basis vectors $\{e_i\}$, $i \in I$. The projection operator $y \rightarrow y_I$ is denoted by \mathbb{P}_I ; thus, $y_I := \mathbb{P}_I(y)$.

2.2.2 The Small-Gain Theorem

Below, we use the following notation borrowed from [30]. Given functions $f: \mathbb{R} \rightarrow \mathbb{R}^n$, $t_d: \mathbb{R} \rightarrow \mathbb{R}_+$, by $f_d(t)$ we denote the restriction of f on the interval $[t - t_d(t); t]$, *i.e.*, $f_d(t) = \{f(s), s \in [t - t_d(t); t]\}$. Consider a system described by functional differential equations (FDEs) of the form

$$\begin{aligned} \dot{x} &= f(x_d, u_{1d}, \dots, u_{md}, w_{1d}, \dots, w_{qd}), \\ y_1 &= g_1(x_d, u_{1d}, \dots, u_{md}, w_{1d}, \dots, w_{qd}), \\ &\vdots \\ &\vdots \\ y_p &= g_p(x_d, u_{1d}, \dots, u_{md}, w_{1d}, \dots, w_{qd}). \end{aligned} \quad (2.1)$$

Here, x_d is a state, $x_d(t) := \{x(s), s \in [t - t_d(t); t]\}$, $x \in \mathbb{R}^n$, u_1, \dots, u_m are finite-dimensional control inputs, y_1, \dots, y_p are finite-dimensional outputs, and w_1, \dots, w_q are finite-dimensional disturbance inputs. According to the notation introduced above, the right-hand side of (2.1) depends on state and input trajectories restricted on the interval $[t - t_d(t); t]$ for some $t_d: \mathbb{R} \rightarrow \mathbb{R}_+$. For regularity purposes, it is assumed that f, g_1, \dots, g_p are Lipschitz continuous operators; also, $t_d(t)$ does not grow faster than time t ; more precisely, the inequality $t_d(t_2) - t_d(t_1) \leq t_2 - t_1$ holds for all $t_1, t_2 \in \mathbb{R}$, $t_2 \geq t_1$; also, $t - t_d(t) \rightarrow +\infty$ as $t \rightarrow +\infty$. Denote $|y| := (|y_1|, \dots, |y_p|)^T \in \mathbb{R}_+^p$; $|u| \in \mathbb{R}_+^m$, $|w| \in \mathbb{R}_+^q$ are defined analogously. It is assumed that system (2.1) satisfies the following local version of the input-to-output stability property [27].

Assumption 1. The system (2.1) is weakly input-to-output practically stable (**WIOPS**) with restrictions $\Delta_x \in \mathbb{R}_+$, $\Delta_u \in \mathbb{R}_+^m$, $\Delta_w \in \mathbb{R}_+^q$, *i.e.*, there exist $\beta \in \mathcal{K}_\infty^{p \times 1}$, $\Gamma_u \in \mathcal{G}^{p \times m}$, $\Gamma_w \in \mathcal{G}^{p \times q}$, such that the conditions $|x_d(0)| \leq \Delta_x$, $\sup_{t \geq 0} |u_d(t)| \leq \Delta_u$, $\sup_{t \geq 0} |w_d(t)| \leq \Delta_w$ imply that the solutions of (2.1) are well defined for $t \in [0, +\infty)$, and the following inequalities hold

$$\sup_{t \geq 0} |y(t)| \leq \max \left\{ \begin{array}{l} \beta(|x_d(0)|), \\ \Gamma_u(\sup_{t \geq 0} |u_d(t)|), \\ \Gamma_w(\sup_{t \geq 0} |w_d(t)|) \end{array} \right\}, \quad (2.2)$$

$$\limsup_{t \rightarrow +\infty} |y(t)| \leq \max \left\{ \begin{array}{l} \Gamma_u(\limsup_{t \rightarrow +\infty} |u_d(t)|), \\ \Gamma_w(\limsup_{t \rightarrow +\infty} |w_d(t)|) \end{array} \right\}. \quad (2.3)$$

The WIOPS property described in Assumption 1 is closely related to a well-known property of the IOS ([27, p. 192]). In the case of single-input-single-output time-invariant systems of

ODEs, however, WIOPS is strictly weaker than IOS. Indeed, IOS implies properties similar to (2.2) and (2.3), however, the converse is generally not true. One particular difference is that IOS assumes existence of a uniform decaying estimate for the system's output which is not necessarily guaranteed by WIOPS. This fact can be illustrated by a counterexample from [27, p. 194], which is also applicable to our situation. The other difference between IOS and WIOPS is that the latter admits gain functions from class \mathcal{G} . See also [8], where another non-global version of IOS-like property is used.

In this work, we address the situation where different input and output channels of the system (2.1) are pairwise interconnected through a communication network. The existence of a communication network may impose significant communication constraints such as time-varying discontinuous possibly unbounded communication delays as well as perturbations due to transmission errors, information losses and quantization. The communication constraints imposed on j -th input, where $j \in \{1, \dots, m\}$, are described according to the formula

$$|u_j(t)| \leq \max_{i \in \{1, \dots, p\}} \left\{ \mathcal{M}_i^j \left(|y_i^*(t - \tau_i^j(t))| \right) \right\}, \quad (2.4)$$

where $y_i^*(t) = y_i(t)$ for $t \geq 0$ and $y_i^*(t) = 0$ for $t < 0$ (which implies that the connection is initiated at $t = 0$), $\tau_i^j(t)$ is the communication delay induced by the network between i -th output and j -th input, and $\mathcal{M}_i^j \in \mathcal{G}$ is the corresponding ‘‘gain’’ function which, in particular, gives a room for possible amplification and/or distortion of the signal transmitted; it also provides an upper bound for errors due to quantization and information losses. All the communication delays satisfy the following assumption.

Assumption 2. The communication delays $\tau_i^j: \mathbb{R}_+ \rightarrow \mathbb{R}_+$, $i \in \{1, \dots, p\}$, $j \in \{1, \dots, m\}$ are Lebesgue measurable functions with the following properties:

i) there exists a piecewise continuous function $\tau^*: \mathbb{R}_+ \rightarrow \mathbb{R}_+$ satisfying $\tau^*(t_2) - \tau^*(t_1) \leq t_2 - t_1$, such that the following inequalities hold for all $t \geq 0$

$$\max_{\substack{i \in \{1, \dots, p\} \\ j \in \{1, \dots, m\}}} \tau_i^j(t) \leq \tau^*(t); \quad (2.5)$$

ii)

$$t - \max_{\substack{i \in \{1, \dots, p\} \\ j \in \{1, \dots, m\}}} \tau_i^j(t) \rightarrow +\infty \quad \text{as} \quad t \rightarrow +\infty. \quad (2.6)$$

Assumption 2 is a relaxed version of similar assumptions used in [22]. As shown in [22], it does not impose any restrictions on the characteristics of the communication channel, and can always be satisfied in real-life networks unless the communication is totally lost on a semi-infinite time interval.

Now, let us denote $\Gamma := \Gamma_u \circ \mathcal{M} \in \mathcal{G}^{p \times p}$, where

$$\mathcal{M} := \begin{bmatrix} \mathcal{M}_1^1 & \dots & \mathcal{M}_p^1 \\ \vdots & \ddots & \vdots \\ \mathcal{M}_1^m & \dots & \mathcal{M}_p^m \end{bmatrix} \in \mathcal{G}^{m \times p}.$$

The following theorem gives small-gain conditions for WIOPS of system (2.1), (2.4).

Theorem 1. Consider an interconnected system (2.1), (2.4). Suppose Assumptions 1, 2 hold. Suppose also there exist $\delta, \Delta \in \mathbb{R}_+^p$, satisfying $\Gamma^{i-1}(\delta) < \Delta$ for all $i \in \{1, \dots, p\}$, and $\mathcal{M}(\Delta) \leq \Delta_u$, such that the following conditions hold

$$\Gamma(s) \not\leq s \quad \text{for all } s \in \mathbb{R}_+^p, s \leq \Delta, s \not\leq \delta. \quad (2.7)$$

Then the interconnection (2.1), (2.4) is WIOPS with restrictions Δ_x^* , Δ_w^* , where

$$\Delta_x^* := \max \left\{ \begin{array}{l} s \in \mathbb{R}_+ : s \leq \Delta_x, \\ \max_{i \in \{1, \dots, p\}} \Gamma^{i-1} \circ \beta(s) \leq \Delta \end{array} \right\}, \quad (2.8)$$

$$\Delta_w^* := \max \left\{ \begin{array}{l} s \in \mathbb{R}_+^q : s \leq \Delta_w, \\ \max_{i \in \{1, \dots, p\}} \Gamma^{i-1} \circ \Gamma_w(s) \leq \Delta \end{array} \right\}. \quad (2.9)$$

More precisely, the conditions $|x_d(0)| \leq \Delta_x^*$,

$\sup_{t \geq 0} |w_d(t)| \leq \Delta_w^*$ imply that the following inequalities

$$\sup_{t \geq 0} |y(t)| \leq \max_{i \in \{1, \dots, p\}} \Gamma^{i-1} \left(\max \left\{ \begin{array}{l} \beta(|x_d(0)|), \\ \Gamma_w(\sup_{t \geq 0} |w_d(t)|), \delta \end{array} \right\} \right), \quad (2.10)$$

$$\limsup_{t \rightarrow +\infty} |y(t)| \leq \max_{i \in \{1, \dots, p\}} \Gamma^{i-1} \left(\max \left\{ \Gamma_w(\limsup_{t \rightarrow +\infty} |w_d(t)|), \delta \right\} \right). \quad (2.11)$$

hold along the trajectories of (2.1), (2.4).

It is worth mentioning that, for sufficiently large p , the small gain condition (2.7) may be hard to check. In this case, one can use sufficient conditions for (2.7) provided by Lemma 2.2.1

below. Let $I_1, \dots, I_k \subset \{1, \dots, q\}$, $k \in \{1, q\}$, be nonempty index sets such that $(I_1, \dots, I_k) = (1, \dots, q)$. Consider the following partition of Γ ,

$$\Gamma = \begin{bmatrix} \Gamma_{I_1 I_1} & \cdots & \Gamma_{I_1 I_k} \\ \vdots & \ddots & \vdots \\ \Gamma_{I_k I_1} & \cdots & \Gamma_{I_k I_k} \end{bmatrix}. \quad (2.12)$$

A function of the form

$$\Gamma_{I_{k_1} I_{k_2}} \circ \dots \circ \Gamma_{I_{k_p} I_{k_1}} \in \mathcal{G}^{\#I_{k_1} \times \#I_{k_1}} \quad (2.13)$$

where $k_1, \dots, k_p \in \{1, \dots, k\}$ are pairwise different, is said to be a minimal cycle of the (partitioned) matrix-function $\Gamma \in \mathcal{G}^{p \times p}$. The following lemma provides sufficient conditions for (2.7).

Lemma 2.2.1 *The small gain condition (2.7) holds if there exists a partition of $\Gamma \in \mathcal{G}^{p \times p}$ of the form (2.12) such that for each $k_1 \in \{1, \dots, k\}$, each minimal cycle of (2.12) satisfies*

$$\Gamma_{I_{k_1} I_{k_2}} \circ \dots \circ \Gamma_{I_{k_p} I_{k_1}}(s) < s \quad \text{for all } s \in [\delta_{k_1}, \bar{\Delta}_{k_1}], \quad (2.14)$$

where $\delta_{k_1} := \mathbb{P}_{I_{k_1}}(\delta)$, $\bar{\Delta}_{k_1} := \mathbb{P}_{I_{k_1}}(\bar{\Delta})$, and $\bar{\Delta} := \max_{i \in \{1, \dots, p\}} \Gamma^{i-1}(\Delta)$.

Proof. Assume the converse, i.e., there exists $s \in \mathbb{R}_+^p$, $s \leq \Delta$, $s \not\leq \delta$ such that $\Gamma(s) \geq s$. The last inequality can be rewritten as follows

$$s_{I_j} \leq \max_{r \in \{1, \dots, k\} \setminus j} \{\Gamma_{I_j I_r}(s_{I_r})\}, \quad j \in \{1, \dots, k\}. \quad (2.15)$$

Combining inequalities (2.15), one arrives at contradiction with (2.14).

2.2.3 Proof of Theorem 1

The proof makes use of the following two lemmas.

Lemma 2.2.2 *Suppose $\Gamma \in \mathcal{G}^{p \times p}$ satisfies (2.7) for some $\delta, \Delta \in \mathbb{R}_+^p$ such that $\Gamma^{i-1}(\delta) < \Delta$ for all $i \in \{1, \dots, p\}$. Let $I \subset \{1, \dots, p\}$ be an arbitrary nonempty index set, and $I^c := \{1, \dots, p\} \setminus I$. Then*

$$\Gamma_{II}(s) \not\leq s \quad \text{for all } s \in \mathbb{R}_+^I, \quad s \leq \Delta_I, \quad s \not\leq \delta_I. \quad (2.16)$$

Proof Pick an arbitrary $s_0 \in \mathbb{R}_+^{\#I}$ such that $s_0 \leq \Delta_I$ and $s_0 \not\leq \delta_I$. Let $s \in \mathbb{R}_+^p$ be such that $s_I = s_0$ and $s_{I^c} = 0$. Clearly, $s \leq \Delta$, and $s \not\leq \delta$. Condition (2.7) then implies that

$$\begin{bmatrix} s_I \\ 0_{I^c} \end{bmatrix} \not\leq \begin{bmatrix} \Gamma_{II} & \Gamma_{II^c} \\ \Gamma_{I^c I} & \Gamma_{I^c I^c} \end{bmatrix} \begin{bmatrix} s_I \\ 0_{I^c} \end{bmatrix}.$$

where 0_{I^c} is the representation of the zero vector in the coordinate system $\{e_i\}$, $i \in I^c$. Clearly, $0 \leq \max\{\Gamma_{I^c I}(s_I), \Gamma_{I^c I^c}(0)\}$, therefore

$$s_I \not\leq \max\{\Gamma_{II}(s_I), \Gamma_{I^c I^c}(0)\} \geq \Gamma_{II}(s_I).$$

The statement follows due to arbitrary choice of $s_0 = s_I$.

Lemma 2.2.3 *Suppose (2.7) holds. Then for any $y \in \mathbb{R}_+^p$, $y \leq \Delta$, and any $v \in \mathbb{R}_+^p$ satisfying $\Gamma^{i-1}(v) < \Delta$ for all $i \in \{1, \dots, p\}$, the condition*

$$y \leq \max\{\Gamma(y), v\} \tag{2.17}$$

implies

$$y \leq \phi := \max_{i \in \{1, \dots, p\}} \left\{ \Gamma^{i-1}(\max\{v, \delta\}) \right\}. \tag{2.18}$$

Proof Let $y \leq \Delta$. First, we claim that under the assumptions of Lemma 2.2.3,

$$y \not\leq \max\{\delta, v\}. \tag{2.19}$$

Indeed, assume the converse, *i.e.*,

$$y > \max\{\delta, v\}. \tag{2.20}$$

Taking into account (2.17), this implies $y \leq \Gamma(y)$. On the other hand, (2.20) also implies that $y \in (\delta, \Delta]$, where $(\delta, \Delta]$ denotes the set of all vectors $y \in \mathbb{R}_+^p$ with $\delta < y \leq \Delta$, and therefore (2.7) implies $y \not\leq \Gamma(y)$. This contradiction proves (2.19).

Now, inequality (2.19) implies that there exists a (possibly empty) index set $I_1 \subset \{1, \dots, p\}$ such that $I_1^c := \{1, \dots, p\} \setminus I_1 \neq \emptyset$, and $y_{I_1^c} \leq \max\{\delta_{I_1^c}, v_{I_1^c}\} \leq \phi_{I_1^c}$. If $I_1 = \emptyset$, then (2.18) is proven. Otherwise, taking into account the last inequality, it follows from (2.17) that

$$y_{I_1} \leq \max\left\{ \Gamma_{I_1 I_1}(y_{I_1}), \Gamma_{I_1 I_1^c}(\delta_{I_1^c}), \Gamma_{I_1 I_1^c}(v_{I_1^c}), v_{I_1} \right\}.$$

Now, taking into account Lemma 2.2.2, and using exactly the same line of reasoning as above, one can show that

$$y_{I_1} \not\leq \max\{\delta_{I_1}, \Gamma_{I_1 I_1^c}(\delta_{I_1^c}), \Gamma_{I_1 I_1^c}(v_{I_1^c}), v_{I_1}\}.$$

The last inequality precisely means that there exists a (possibly empty) index set $I_2 \subset I_1$, $I_2 \neq I_1$, such that $y_{I_2} \leq \phi_{I_2}$. Continuing this line of reasoning, after at most $p - 1$ steps, we get (2.18). This completes the proof of Lemma 2.2.3.

Now, consider the system (2.1), (2.4). Suppose

$$|x_d(0)| \leq \Delta_x^*, \quad \sup_{t \geq 0} |w_d(t)| \leq \Delta_w^*. \quad (2.21)$$

Denote $\Delta^* := \max\{\beta(\Delta_x^*), \Gamma_w(\Delta_w^*), \delta\}$. First, let us prove that

$$\sup_{t \geq 0} |y(t)| \leq \Delta := \max_{i \in \{1, \dots, p\}} \Gamma^{i-1}(\Delta^*). \quad (2.22)$$

Note that, due to finite restriction Δ_u as well as bounded domain of the small-gain condition, the above inequality cannot be proven by applying small-gain arguments directly. Instead, let us consider the system (2.1) where the following interconnection constraints are imposed on each input u_j , $j \in \{1, \dots, m\}$,

$$|u_j(t)| \leq \epsilon \cdot \max_{i \in \{1, \dots, p\}} \left\{ \mathcal{M}_i^j \left(|y_i^*(t - \tau_i^j(t))| \right) \right\}, \quad (2.23)$$

where $\epsilon \in [0, 1]$. Using homotopy-like arguments similar to the ones used in the Appendix of [29], we will show that (2.22) holds for all $\epsilon \in [0, 1]$. First, for $\epsilon = 0$, inequality (2.22) follows directly from Assumption 1. Fix an arbitrary $T \in (0, +\infty)$, and let $\nu \in \mathbb{R}_+^p$, $\nu > 0$ be a vector with sufficiently small norm. Due to regularity (Lipschitz continuity) of the right-hand sides of system (2.1), the upper bound on trajectories of (2.1), (2.4) for $t \in [0, T]$ depends continuously on parameter ϵ ; more precisely, there exists $\epsilon^* > 0$ such that the inequality

$$\sup_{t \in [0, T]} |y(t)| \leq \Delta + \nu, \quad (2.24)$$

holds as long as ϵ in (2.23) satisfies $\epsilon \in [0, \epsilon^*]$. Since $\epsilon^* < 1$, for sufficiently small $\nu > 0$ one has $\epsilon^* \cdot \mathcal{M}(\Delta + \nu) \leq \mathcal{M}(\Delta) \leq \Delta_u$. Combining this with (2.23), (2.24), we see that

$$\sup_{t \in [-t_d(0), T]} |u(t)| \leq \Delta_u, \quad (2.25)$$

i.e., the restriction on u is met for all $t \in [0, T]$. Now, using (2.2), one gets

$$\sup_{t \in [0, T]} |y(t)| \leq \max \left\{ \Delta^*, \Gamma_u \circ (\epsilon^* \cdot \mathcal{M}) \left(\sup_{t \in [0, T]} |y(t)| \right) \right\}, \quad (2.26)$$

as long as ϵ in (2.23) satisfies $\epsilon \in [0, \epsilon^*]$. Furthermore, since $0 < \epsilon^* < 1$ and $\Gamma_u(\cdot)$ is non-decreasing, it is easy to see that, for sufficiently small $\nu > 0$, condition (2.7) implies that $\Gamma_u \circ (\epsilon^* \cdot \mathcal{M})(s) \not\leq s$ holds for all $s \in \mathbb{R}_+^p$, such that $s \leq \Delta + \nu$ and $s \not\leq \delta$. Applying Lemma 2.2.3, we see that

$$\sup_{t \in [0, T]} |y(t)| \leq \Delta \quad (2.27)$$

holds as long as $\epsilon \in [0, \epsilon^*]$. Now, let $\epsilon_{max} \in (0, 1]$ be the maximal number such that (2.27) holds for all $\epsilon \in [0, \epsilon_{max}]$. We claim that $\epsilon_{max} = 1$. Indeed, assume the converse, *i.e.*, $\epsilon_{max} < 1$. Then, for sufficiently small $\nu > 0$, it follows by continuity of trajectories that there exists $\epsilon^{**} \in (\epsilon_{max}, 1)$ such that (2.24) holds for all $\epsilon \in [0, \epsilon^{**}]$. Using exactly the same line of reasoning as above, one can see that in this case (2.27) holds for all $\epsilon \in [0, \epsilon^{**}]$, which contradicts the definition of ϵ_{max} . Thus, $\epsilon_{max} = 1$. Due to the arbitrary choice of $T \in (0, +\infty)$, this implies (2.22); also, (2.25) holds for all $T > 0$, which means that the restriction on u is met. Thus, (2.2) holds along the trajectories of (2.1), (2.4).

Now, combining (2.2), (2.4), we get

$$\sup_{t \geq 0} |y(t)| \leq \max \left\{ \beta(|x_d(0)|), \Gamma(\sup_{t \geq 0} |y(t)|), \Gamma_w(\sup_{t \geq 0} |w_d(t)|) \right\}.$$

Taking into account (2.7), (2.22), and applying Lemma 2.2.3, we see that (2.10) holds. To prove (2.11), note that due to Assumption 2, part ii), we have

$$\limsup_{t \rightarrow +\infty} |y_i^*(t - \tau_i^j(t))| = \limsup_{t \rightarrow +\infty} |y_i^*(t)|$$

holds for each $i \in \{1, \dots, p\}$, $j \in \{1, \dots, m\}$. Taking into account (2.4) as well as the definition of $y^*(\cdot)$, we see that

$$\limsup_{t \rightarrow +\infty} |u_d(t)| \leq \mathcal{M} \left(\limsup_{t \rightarrow +\infty} |y(t)| \right).$$

Combining the above inequality with (2.3), taking into account the small-gain condition (2.7) as well as (2.22), and applying Lemma 2.2.3, we get (2.11). The proof of Theorem 1 is now complete.

Theorem 1 and Lemma 2.2.1 are applicable to stability analysis of a very general class of large-scale network-based interconnections where the communication between subsystems are subject to constraints typical for communication networks such as the Internet. Below, these results are utilized to derive conditions for stability of a cooperative networked force-reflecting teleoperator system.

2.3 Design of a networked cooperative force-reflecting teleoperator

In this section, Theorem 1 and Lemma 2.2.1 are applied to the design of a networked cooperative teleoperator system shown schematically in Figure 2.1.

2.3.1 Masters and slaves manipulators

The cooperative teleoperator system under consideration consists of $2N$ manipulators, N masters and N slaves. The manipulator dynamics are described by Euler-Lagrange equations of the form

$$H_{mi}(q_{mi})\ddot{q}_{mi} + C_{mi}(q_{mi}, \dot{q}_{mi})\dot{q}_{mi} + G_{mi}(q_{mi}) = u_{mi} + J_{mi}^T(q_{mi})(f_{hi} - f_{ri}), \quad (2.28)$$

$$H_{si}(q_{si})\ddot{q}_{si} + C_{si}(q_{si}, \dot{q}_{si})\dot{q}_{si} + G_{si}(q_{si}) = u_{si} - J_{si}^T(q_{si})f_{ei}, \quad (2.29)$$

where $i \in \{1, \dots, N\}$. Here, q_{mi} , q_{si} represent joint positions of the i -th master and the i -th slave manipulator, $H_{mi}(q_{mi})$, $H_{si}(q_{si})$ are inertia matrices, $C_{mi}(q_{mi}, \dot{q}_{mi})$, $C_{si}(q_{si}, \dot{q}_{si})$ are matrices of Coriolis/centrifugal forces, $G_{mi}(q_{mi})$, $G_{si}(q_{si})$ are vectors of potential forces, and $J_{mi}(q_{mi})$, $J_{si}(q_{si})$ are Jacobians of the i -th master and i -th slave manipulator, respectively. Also, f_{hi} is the force (torque) applied by the human operator to i -th master, f_{ei} is the environmental force (torque) applied to i -th slave, f_{ri} is the force reflected to i -th master, and u_{mi} , u_{si} are the control inputs of i -th master and i -th slave, respectively. The dynamics of all the manipulators involved are assumed to satisfy the set of standard properties described, for example, in [28, Section 2.1]. For simplicity of presentation, it is assumed that all the manipulators involve either rotational

or translational motions with finite translational joints; in particular, this implies that all the manipulators have compact configuration spaces.

2.3.2 Communication process

For each $i \in \{1, \dots, N\}$, the i -th master is connected with the i -th slave over a networked communication channel. This interconnection is described as follows. First, the spatial coordinates (position and orientation) of the end-effector of i -th master are calculated according to the formula

$$x_{mi} = T_{mi}(q_{mi}), \quad (2.30)$$

where $T_{mi}: \mathbb{R}^{n_i} \rightarrow \mathbb{R}^6$ are forward kinematics of the i -th master manipulator. These coordinates are then transmitted over the communication channel to the i -th slave with communication delay $\tau_{fi}: \mathbb{R} \rightarrow \mathbb{R}_+$ and communication error σ_{fi} , according to the formula

$$\hat{x}_{mi}(t) := x_{mi}(t - \tau_{fi}(t)) + \sigma_{fi}(t). \quad (2.31)$$

The communication error in the i -th forward channel is assumed to be uniformly essentially bounded by the (sufficiently small) bound $\sigma_{fi}^* \geq 0$,

$$\sup_{t \in [0, +\infty)} |\sigma_{fi}(t)| \leq \sigma_{fi}^*.$$

On the slave's side, the reference joint space trajectory \hat{q}_{mi} is obtained from \hat{x}_{mi} according to the formula

$$\hat{q}_{mi} := T_{si}^{-1}(\hat{x}_{mi}), \quad (2.32)$$

where $T_{si}^{-1}: \mathbb{R}^6 \rightarrow \mathbb{R}^{n_{si}}$ is the inverse kinematics map for i -th slave manipulator. For simplicity of presentation, we assume that inverse kinematics maps $T_{si}^{-1}(\cdot)$ are well-defined and continuous for all possible trajectories $\hat{x}_{mi}(\cdot)$. Additionally, it is assumed that

$$|T_{si}^{-1} \circ T_{mi}(q_{mi})| \leq \gamma_i^{\tau_{fi}}(|q_{mi}|) \quad (2.33)$$

holds for some $\gamma_i^{\tau_{fi}} \in \mathcal{G}$, $i \in \{1, \dots, N\}$.

Remark 1. Generally speaking, the existence of well-defined and continuous inverse kinematic maps $T_{si}^{-1}(\cdot)$ imposes significant restrictions on the kinematic structure of the manipulators. Our primary motivation for transmitting the master trajectories in the task space

coordinates was to increase the generality of the design by allowing the master-slave pairs with dissimilar kinematics. Indeed, for the master-slave pairs with identical kinematics, the master trajectories can be transferred to the slave side directly in joint space; in this case, we can formally set $T_{si}^{-1} \circ T_{mi} = Id$, and therefore, all $\gamma_i^{\tau f}$ can be chosen to be identity functions. In the case of the master-slave pairs with dissimilar kinematics, however, the problem becomes more complicated; in particular, it must be guaranteed that any possible master trajectory in the task space can be executed by a kinematically dissimilar slave. This is a nontrivial problem, and its solution strongly depends on the particular choice of the master and the slave kinematic structures. Our assumption of the existence of well-defined and continuous inverse kinematic maps $T_{si}^{-1}(\cdot)$ is a simple way to guarantee that a solution to the above mentioned problem exists and is known. It is also worth mention that non-identity functions $\gamma_i^{\tau f}(\cdot)$ in (2.33) allow to consider scaling of the trajectories between the master(s) and the slave(s) sides. •

Now, let f_{ei} , $i \in \{1, \dots, N\}$ be the interaction forces between the environment and the i -th slave. These forces are transmitted over a communication channel to the corresponding master site, according to the formula

$$\hat{f}_{ei}(t) := f_{ei}(t - \tau_{bi}(t)) + \sigma_{bi}(t), \quad (2.34)$$

where $\tau_{bi}: \mathbb{R}_+ \rightarrow \mathbb{R}_+$ is the communication delay in the i -th backward channel, and $\sigma_{bi}(\cdot)$ is the corresponding measurement/estimation/quantization/transmission error which is assumed to be uniformly essentially bounded by the (sufficiently small) bound $\sigma_{bi}^* \geq 0$,

$$\sup_{t \in [0, +\infty)} |\sigma_{bi}(t)| \leq \sigma_{bi}^*.$$

On the master side, the force reflection term f_{ri} is generated based on force signal \hat{f}_{ei} received from the corresponding slave manipulator. We address a simple case where f_{ri} is equal to \hat{f}_{ei} amplified (attenuated) with certain gain function $\gamma_{fi} \in \mathcal{G}$, *i.e.*,

$$f_{ri} := \gamma_{fi}(|\hat{f}_{ei}|) \frac{\hat{f}_{ei}}{|\hat{f}_{ei}|}.$$

2.3.3 Control algorithms

The control law for the i -th master device ($i = 1, \dots, N$) is “PD plus gravity compensation” of the form

$$u_{mi} = G_{mi}(q_{mi}) - K_{mi}(\Lambda_{mi}q_{mi} + \dot{q}_{mi}), \quad (2.35)$$

where K_{mi}, Λ_{mi} are symmetric positive definite matrices. As shown in [2], this control law guarantees the input-to-state stability of each master device with respect to joint force/torque input. Taking into account the uniform boundedness of all $J_{mi}(\cdot)$, we see that the master subsystems are ISS with respect to spatial force (torque) inputs $f_{hi} - f_{ri}$; considering f_{hi}, f_{ri} as separate inputs, the corresponding ISS gains are denoted by $\gamma_{mi} \in \mathcal{G}$.

For each slave subsystem, the control law has the following form [20],

$$\dot{\xi}_{1i} = \xi_{2i} - g_i \alpha_{1i} \tilde{\xi}_{1i}, \quad (2.36)$$

$$\dot{\xi}_{2i} = -g_i^2 \alpha_{0i} \tilde{\xi}_{1i}, \quad (2.37)$$

$$\begin{aligned} u_{si} = & -H_{si}(q_{si}) \left(g_i^2 \alpha_{0i} \tilde{\xi}_{1i} + \Lambda_{si} \left(g_i \alpha_{1i} \tilde{\xi}_{1i} + \tilde{q}_{si} \right) \right) \\ & + C_{si}(q_{si}, \dot{q}_{si}) (\xi_{2i} - \Lambda_{si} \tilde{q}_{si}) + G_{si}(q_{si}) \\ & - K_{si} \left(\tilde{q}_{si} + \Lambda_{si} \tilde{q}_{si} \right), \end{aligned} \quad (2.38)$$

where, for each $i \in \{1, \dots, N\}$, we denote $\tilde{\xi}_{1i} := \xi_{1i} - \hat{q}_{mi}$, $\tilde{q}_{si} := \xi_{1i} - q_{si}$, $\tilde{\xi}_{2i} := \xi_{2i} - \dot{q}_{si}$, and where $K_{si} \in \mathbb{R}^{n \times n}$, $\Lambda_{si} \in \mathbb{R}^{n \times n}$ are symmetric positive-definite matrices; α_{0i}, α_{1i} are positive constants such that the roots of $p_i(s) = s^2 + \alpha_{1i}s + \alpha_{0i}$ have negative real parts; and $g_i > 0$ is a constant. The control law (2.36)-(2.38) consists of a filter (2.36), (2.37), which provides a smooth approximation of a possibly discontinuous delayed master trajectory \hat{q}_{mi} , and passivity-based tracking control algorithm (2.38). For any fixed $g > 0$, the filter (2.36), (2.37) is stable; due to its linearity it is also ISS with respect to input \hat{q}_{mi} . The ISS gain of the i -th filter is denoted by $\gamma_{qi}^f \in \mathcal{K}_{lin}$. On the other hand, the control law (2.38) guarantees that, in the absence of external forces, the i -th slave subsystem tracks the output of the i -th filter. More precisely, the closed-loop i -th slave subsystem with state $\chi_{si} := \left(\tilde{q}_{si}^T, \tilde{\xi}_{2i}^T \right)^T$ and inputs \hat{q}_{mi} , ξ_{1i} , and f_{ei} is ISS; the corresponding ISS gains are denoted by $\gamma_{qi}^s \in \mathcal{G}$, $\gamma_{\xi i}^s \in \mathcal{G}$, $\gamma_{fi}^s \in \mathcal{G}$, respectively. For our analysis, it is important that the gains γ_{fi}^s can in fact be assigned to be arbitrary functions from \mathcal{K}_{lin} , by an appropriate choice of matrices K_{si}, Λ_{si} (see [20]).

2.3.4 Environmental model and slave-environment interconnections

All the slave manipulators interact with the same environment. The environment is described by a model of the form

$$\begin{aligned}
 \dot{x}_e &= f_e(x_e, u_1^e, \dots, u_N^e, f_{ext}), \\
 f_{e1} &= g_{e1}(x_e, u_1^e, \dots, u_N^e, f_{ext}), \\
 &\vdots \\
 f_{eN} &= g_{eN}(x_e, u_1^e, \dots, u_N^e, f_{ext}).
 \end{aligned} \tag{2.39}$$

Here, x_e is the state of the environment, u_{ei} is the input from the i -th slave, $i \in \{1, \dots, N\}$, and f_{ext} is an external force acting on the environment. The inputs u_{ei} are spatial motion variables (positions and velocities) of the slave devices,

$$u_{ei} := \begin{pmatrix} x_{si}^T \\ \dot{x}_{si}^T \end{pmatrix}^T, \quad i \in \{1, \dots, N\},$$

i.e., $x_{si} = T_{si}(q_{si})$, $\dot{x}_{si} := J_{si}(q_{si})\dot{q}_{si}$, where $T_{si}(\cdot)$ are the forward kinematics and $J_{si}(\cdot)$ is the Jacobian of the i -th slave robot. The environmental dynamics are assumed to be WIOPS with respect to inputs u_{ei} , $i \in \{1, \dots, N\}$, and f_{ext} . The corresponding WIOPS gain matrices are denoted by $\Gamma_e \in \mathcal{G}^{N \times N}$, $\Gamma_{ef} \in \mathcal{G}^{N \times 1}$. It is straightforward to show that the inputs u_{ei} , $i \in \{1, \dots, N\}$ of the environment (2.39) satisfy the inequalities

$$|u_{ei}| \leq \gamma_i^{ue} \left(\left| \begin{pmatrix} q_{si}^T \\ \dot{q}_{si}^T \end{pmatrix} \right| \right) \leq \gamma_i^{ue} (|\chi_{si}| + |\xi_{si}|) \leq \gamma_i^{ue} (2 \max \{|\chi_{si}|, |\xi_{si}|\})$$

for some $\gamma_i^{ue} \in \mathcal{G}$, $i \in \{1, \dots, N\}$. One can combine the above gains γ_i^{ue} into a matrix gain function $\Gamma^{ue} \in \mathcal{G}^{N \times N}$ according to the formula $\Gamma^{ue} := \text{diag} \{ \gamma_1^{ue}(2 \cdot), \dots, \gamma_N^{ue}(2 \cdot) \}$. Each f_{ei} , $i \in \{1, \dots, N\}$, represents the interaction force between the environment and the i -th slave; it is applied to the corresponding slave input. These signals are also transmitted over a communication channel to the corresponding master site, according to the formula (2.34).

2.3.5 Small gain analysis

To perform the small gain stability analysis of the closed-loop teleoperator system described above, we need to rewrite its equations in the form of (2.1), and represent the interconnections in the form (2.4). Consider first the teleoperator system without interconnections. This system

consists of N closed-loop master subsystems (2.28,2.35), N filters (2.36,2.37), N closed-loop slave subsystems (2.29,2.38), and the environment (2.39). Simple analysis shows that this system has $5N$ control inputs $f_{r1}, \dots, f_{rN}, \hat{q}_{m1}, \dots, \hat{q}_{mN}, \xi_1, \dots, \xi_N, f_{e1}, \dots, f_{eN}, u_1^e, \dots, u_N^e$, as well as $N + 1$ external (disturbance) inputs $f_{h1}, \dots, f_{hN}, f_{ext}$. For our purposes, it is convenient to write the $5N$ control inputs in the following order: for each $i = 1, \dots, N$ we have $u_i := f_{ri}, u_{N+i} := \hat{q}_{mi}, u_{2N+i} := \xi_i, u_{3N+i} := f_{ei}$, and $u_{4N+i} := u_i^e$. The system also has $4N$ outputs, their order can be chosen as follows: for each $i = 1, \dots, N$, we have $y_i := (q_{mi}^T, \dot{q}_{mi}^T)^T$, $y_{N+i} := \xi_i$, $y_{2N+i} := \chi_{si}$, and $y_{3N+i} := f_{ei}$. Denote $\Gamma_m := \text{diag}\{\gamma_{m1}, \dots, \gamma_{mN}\} \in \mathcal{G}^{N \times N}$, $\Gamma_q^f := \text{diag}\{\gamma_{q1}^f, \dots, \gamma_{qN}^f\} \in \mathcal{G}^{N \times N}$, $\Gamma_q^s := \text{diag}\{\gamma_{q1}^s, \dots, \gamma_{qN}^s\} \in \mathcal{G}^{N \times N}$, $\Gamma_\xi^s := \text{diag}\{\gamma_{\xi1}^s, \dots, \gamma_{\xi N}^s\} \in \mathcal{G}^{N \times N}$, $\Gamma_f^s := \text{diag}\{\gamma_{f1}^s, \dots, \gamma_{fN}^s\} \in \mathcal{G}^{N \times N}$. The corresponding gain matrix $\Gamma_u \in \mathcal{G}^{4N \times 5N}$ has the form

$$\Gamma_u = \begin{bmatrix} \Gamma_m & \mathbb{O} & \mathbb{O} & \mathbb{O} & \mathbb{O} \\ \mathbb{O} & \Gamma_q^f & \mathbb{O} & \mathbb{O} & \mathbb{O} \\ \mathbb{O} & \Gamma_q^s & \Gamma_\xi^s & \Gamma_f^s & \mathbb{O} \\ \mathbb{O} & \mathbb{O} & \mathbb{O} & \mathbb{O} & \Gamma_e \end{bmatrix},$$

where \mathbb{O} is zero function of the corresponding dimension.

Our next task is to determine the gain functions that correspond to interconnections between the masters, the slaves, and the environment, and write them in the form of the interconnection gain matrix \mathcal{M} . First, consider the forward communication channels (2.30) - (2.32). Taking into account the continuity of $T_{si}^{-1}(\cdot)$ as well as the fact that all the manipulators involved have compact configuration spaces, one can derive the following:

$$|\hat{q}_{mi}(t)| \leq \gamma_i^{\tau f} \left(|q_{mi}(t - \tau_{fi}(t))| \right) + \bar{\sigma}_{fi}^* := \gamma_i^{\tau f*} \left(|q_{mi}(t - \tau_{fi}(t))| \right),$$

where $\bar{\sigma}_{fi}^* \geq 0$ depends on T_{si}^{-1} and σ_{fi}^* , and $\gamma_i^{\tau f*}(\cdot) := \gamma_i^{\tau f}(\cdot) + \bar{\sigma}_{fi}^* \in \mathcal{G}$. Consequently, let us denote by $\Gamma^{\tau f}$ the matrix gain function that corresponds to forward communication channels, $\Gamma^{\tau f} := \text{diag}\{\gamma_1^{\tau f*}, \dots, \gamma_N^{\tau f*}\} \in \mathcal{G}^{N \times N}$. Similarly, the matrix gain function corresponding to backward communication channels can be derived, according to the formula $\Gamma^{\tau b} := \text{diag}\{\gamma_1^{\tau b*}, \dots, \gamma_N^{\tau b*}\} \in \mathcal{G}^{N \times N}$, where $\gamma_i^{\tau b*}(\cdot) := \gamma_i^{\tau b}(\cdot + \sigma_{bi}^*) \in \mathcal{G}$. Using the above notation, the

interconnection gain matrix \mathcal{M} can be derived as follows,

$$\mathcal{M} = \begin{bmatrix} \mathbb{O} & \mathbb{O} & \mathbb{O} & \Gamma^{\tau b} \\ \Gamma^{\tau f} & \mathbb{O} & \mathbb{O} & \mathbb{O} \\ \mathbb{O} & \mathbb{I} & \mathbb{O} & \mathbb{O} \\ \mathbb{O} & \mathbb{O} & \mathbb{O} & \mathbb{I} \\ \mathbb{O} & \Gamma^{ue} & \Gamma^{ue} & \mathbb{O} \end{bmatrix},$$

where \mathbb{I} is the identity function of the corresponding dimension. Now, the system gain matrix $\Gamma := \Gamma_u \circ \mathcal{M}$ has the form

$$\Gamma = \begin{bmatrix} \mathbb{O} & \mathbb{O} & \mathbb{O} & \Gamma_m \circ \Gamma^{\tau b} \\ \Gamma_q^f \circ \Gamma^{\tau f} & \mathbb{O} & \mathbb{O} & \mathbb{O} \\ \Gamma_q^s \circ \Gamma^{\tau f} & \Gamma_\xi^s & \mathbb{O} & \Gamma_f^s \\ \mathbb{O} & \Gamma_e \circ \Gamma^{ue} & \Gamma_e \circ \Gamma^{ue} & \mathbb{O} \end{bmatrix}.$$

Applying the small-gain theorem (Theorem 1), one can conclude that the cooperative teleoperator system is stable (more specifically, input-to-output stable with arbitrary prescribed restrictions) if the small gain condition

$$\Gamma(s) \not\geq s \quad \forall s \in \mathbb{R}_+^N, s \leq \Delta, s \not\leq \delta, \quad (2.40)$$

holds for sufficiently small $\delta \in \mathbb{R}_+^N$, $\delta > 0$ and sufficiently large $\Delta \in \mathbb{R}_+^N$. Taking into account the structure of the matrix Γ and using Lemma 2.2.1, one sees that the last condition can be guaranteed if the following cycle conditions

$$\Gamma_m \circ \Gamma^{\tau b} \circ \Gamma_e \circ \Gamma^{ue} \circ \Gamma_\xi^s \circ \Gamma_q^f \circ \Gamma^{\tau f}(s) < s, \quad (2.41)$$

$$\Gamma_m \circ \Gamma^{\tau b} \circ \Gamma_e \circ \Gamma^{ue} \circ \Gamma_q^f \circ \Gamma^{\tau f}(s) < s, \quad (2.42)$$

$$\Gamma_m \circ \Gamma^{\tau b} \circ \Gamma_e \circ \Gamma^{ue} \circ \Gamma_q^s \circ \Gamma^{\tau f}(s) < s, \quad (2.43)$$

$$\Gamma_f^s \circ \Gamma_e \circ \Gamma^{ue}(s) < s, \quad (2.44)$$

hold for all $s \in [\delta^*, \Delta^*]$, where $\delta^* \in \mathbb{R}_+^N$, $\delta^* > 0$ is sufficiently small and $\Delta^* \in \mathbb{R}_+^N$ is sufficiently large. However, condition (2.44) can always be satisfied by an appropriate choice of linear gain function Γ_f^s (as mentioned above, the latter can in turn be assigned arbitrarily by an appropriate choice of slave's feedback gains K_{si} , Λ_{si} , $i = 1, \dots, N$). On the other hand, conditions (2.41) -

(2.43) can be satisfied by an appropriate assignment of either master gains Γ_m or force reflection gains Γ^{rb} (or simultaneous adjustment of both). Thus, stability of the cooperative teleoperation system with network-induced communication constraints can be achieved by an appropriate choice of the system's gains. It is worth noting, however, that significant decrease of Γ_m , Γ^{rb} generally leads to transparency deterioration, since low Γ_m implies high stiffness/damping of the master manipulators, while $\Gamma^{rb} < \mathbb{I}$ results in attenuation of the force reflection term. This fact represents the inherent trade-off between stability and transparency in bilateral teleoperation. Resolving this contradiction would require further developments, such as application of the projection-based force reflection principle [21], and is a topic for future research.

Remark 2. In the design process described above, we addressed the case of the direct force reflection where the interaction forces between the environment and a slave are reflected over the communication channel to the motors of the corresponding master device, according to (2.34). It is worth to mention that the small gain approach itself does not impose restrictions on the particular form of the force reflecting term; specifically, any function of the slave/environment state/output can be chosen as a force reflection signal within the small-gain framework. On the contrary, the passivity-based approaches generally impose severe restrictions on the choice of the force reflection signal, because these approaches require the force reflecting signal to be a passive output of the slave/environment interconnection. In particular, the last requirement can frequently be in contradiction with the transparency considerations. Such a flexibility in terms of the choice of the force reflection signal may be one of the advantages of the small-gain framework addressed in our work in comparison with the passivity-based one.

•

2.4 Experimental Results

In this section, we present examples of the experimental results that were achieved in support of the theoretical developments presented above. The experimental setup is shown schematically in Figure 2.2. It consists of two-master-two-slave cooperative force reflection teleoperator system, where two PHANTOM Omni devices are used as master manipulators, while the slaves are represented by two simulated models of PHANTOM Premium 1.5A devices implemented

in a virtual environment. The PHANTOM Omni devices have 6 DOF position sensing and 3 DOF force feedback, and are manufactured by SensAble Technologies Inc. The OpenHaptics Toolkit is used for programming of the haptic devices. The virtual environment is rendered using OpenGL. The host computers are connected over network using TCP/IP network protocol. The simulation is run at a sampling frequency 1000Hz.

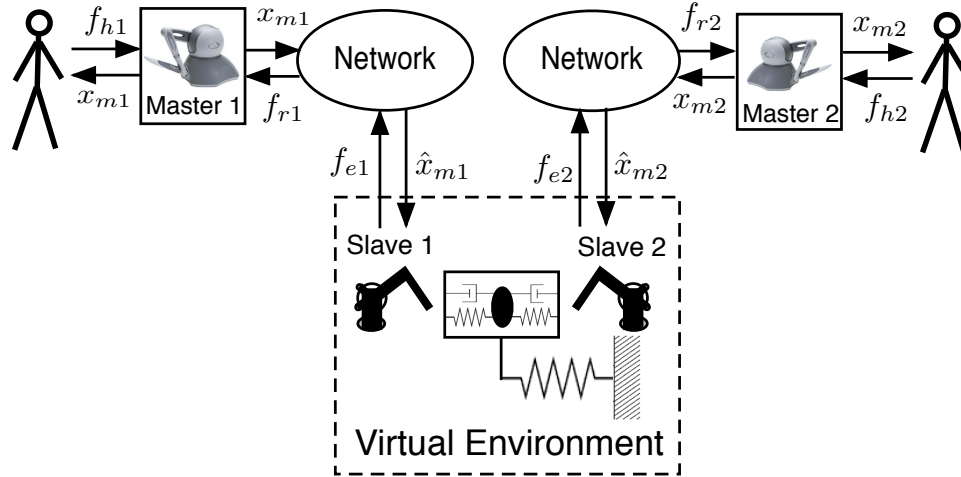


Figure 2.2: Experimental setup scheme

The virtual environment renders two mathematical models of the PHANTOM Premium 1.5A slave devices as well as the environment in the form of a rectangular object with which the slave devices interact. The implementation of the virtual object used in our experiments is shown in Figure 2.3; it consists of a mass m attached to the base using a spring with stiffness K ; the sidewalls of the object are connected to the mass using springs and dampers; the stiffness of the springs is denoted by k and the damping coefficients are denoted by d . The goal pursued by the human operators in our experiments is to cooperatively stabilize the object at the origin by pressing against its sides. The execution of this task clearly involves the interaction and consequently the energy exchange between the slave devices through the object.

In the experiments presented in below, the virtual object is initially located at the origin and has the initial velocity of 0.04 m/s in the positive direction of the x -axis. The virtual object is characterized by the mass $m = 1$ kg, width $l = 0.1$ m, the (inner) stiffness of the object $k = 1000$ N/m, and the stiffness of the spring at the base is $K = 10$ N/m. In order to avoid

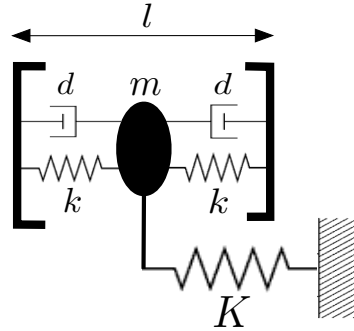


Figure 2.3: Implementation of the object in virtual environment

the oscillations of the mass between the sidewalls, the (inner) damping of the implementation has to be chosen sufficiently high to keep the overall system critically damped or over damped. In our experiments, we chose the mass to be critically damped inside the object, which corresponds to the value of damping coefficient $d = 2000 \text{ N}\cdot\text{s}/\text{m}$. Please note that such a high value of the damping is just a consequence of the simplified lumped implementation of the virtual object used in our experiments. If one uses a more advanced implementation of the virtual object, such as based on the finite-elements methods, high damping is not required; however, these methods cannot be used in our case because of the strict real-time requirements that the experimental setup must satisfy.

According to the theoretical results presented at the end of Section 2.3, the stability of the cooperative force-reflecting teleoperator system with arbitrary prescribed restriction and offset is guaranteed if the gain $\Gamma_f^s \in \mathcal{K}_{lin}^{N \times N}$ is sufficiently small and, at the same time, the combination of gains $\Gamma_m \circ \Gamma^{rb} \in \mathcal{G}^{N \times N}$ is also “sufficiently small”. It was mentioned above that the gain $\Gamma_f^s \in \mathcal{K}^{N \times N}$ can be assigned arbitrarily small if the slave’s feedback gains $K_{si}, \Lambda_{si}, i = 1, \dots, N$ are sufficiently large. The latter is confirmed by our experimental results, where we have found that the slave-environment interaction is more stable for larger $K_{si}, \Lambda_{si}, i = 1, \dots, N$. In particular, in the experimental results presented below, the slave’s feedback gains are chosen as follows: $\Lambda_{si} = \text{diag}\{100, 100, 100\}$, $K_{si} = \text{diag}\{1, 1, 1\}$, $i = 1, \dots, N$; this choice of gains guarantees satisfactory stability characteristics of the slave-environment contact. As for the condition that the combination of gains $\Gamma_m \circ \Gamma^{rb} \in \mathcal{G}^{N \times N}$ must be “sufficiently small”, our experimental results indicate that this condition may be overly conservative from practical point of view. The explanation to this fact is straightforward: the conditions (2.41) -(2.43) that in-

volve the combination of gains $\Gamma_m \circ \Gamma^{rb}$ are essentially the “worst-case” stability conditions that guarantee stability in the case where the human operators release the master devices. In most practical situations, including the one considered in our experiments, the slaves-environment contact takes place when the human operators hold the master devices. In this case, the human operators essentially play the role of stabilizing controllers for their corresponding master devices; as a result, the actual gain of the human-master interconnections appears to be significantly lower comparing to the gain of the master devices alone, which results in the overall stability even if the conditions (2.41) -(2.43) are not directly satisfied. In actual fact, we have found that the teleoperator system in our experiments have good stability properties for unit force reflection gain and for negligibly small damping and stiffness coefficients of the master’s control laws. Other parameters of the control algorithm in our experimental results discussed below are as follows: $g_i = 10$, $\alpha_{1i} = 4$, $\alpha_{0i} = 4$, where $i = 1, 2$.

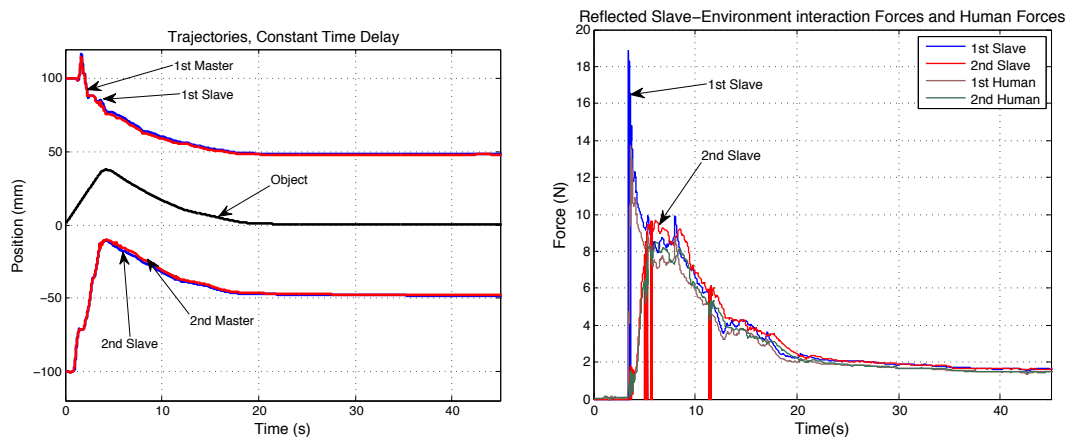


Figure 2.4: Case of negligible communication delays (RTT delay ≈ 0): x -trajectories of the masters, slaves, and the object (left); Interaction x -forces (right)

Examples of the experimental results for different types of communication constraints are shown in Figures 2.4-2.6. In all these figures, the left plots represent the x -components of the position trajectories of the two masters and two slaves as well as the x -component of the trajectory of the object. The right plots, on the other hand, represent the forces applied by the human operators to the master devices as well as the contact forces between the slaves and the object; the latter are also the forces that are reflected back to the motors of the corresponding

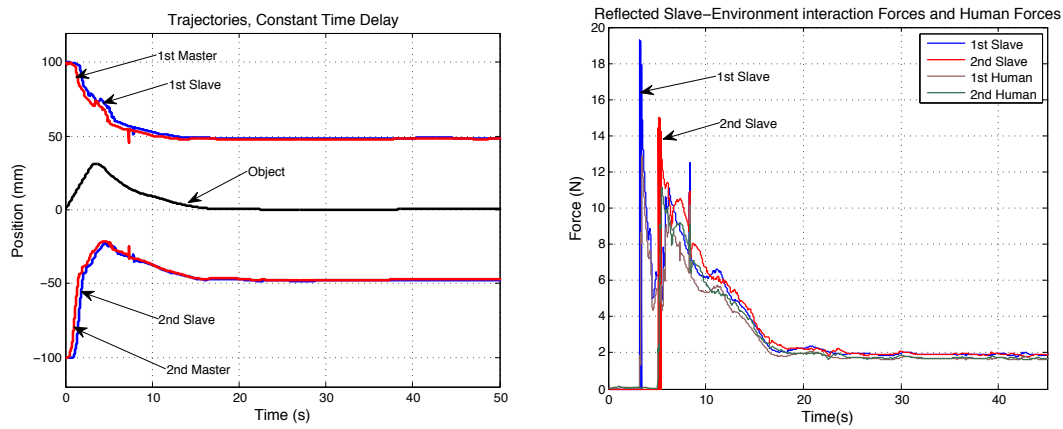


Figure 2.5: Case of sufficiently large constant communication delays (RTT delay ≈ 1 s): x -trajectories of the masters, slaves, and the object (left); Interaction x -forces (right)

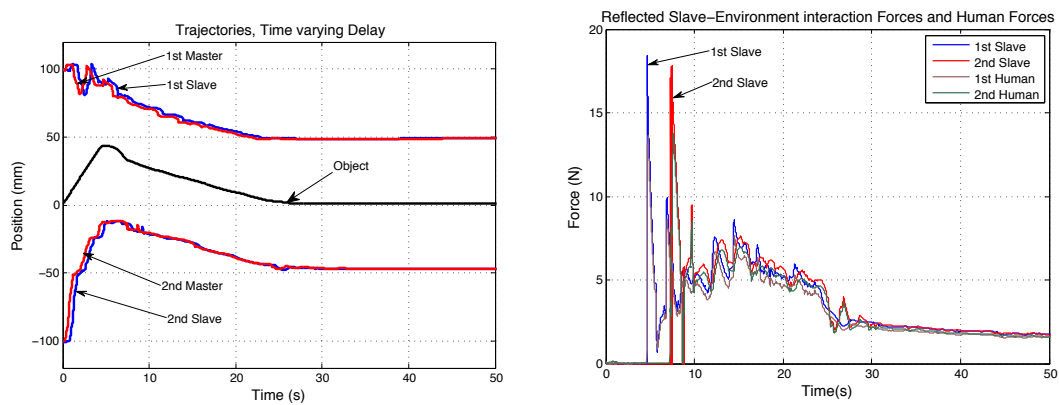


Figure 2.6: Case of time-varying communication delays with random packet dropouts: x -trajectories of the masters, slaves, and the object (left); Interaction x -forces (right)

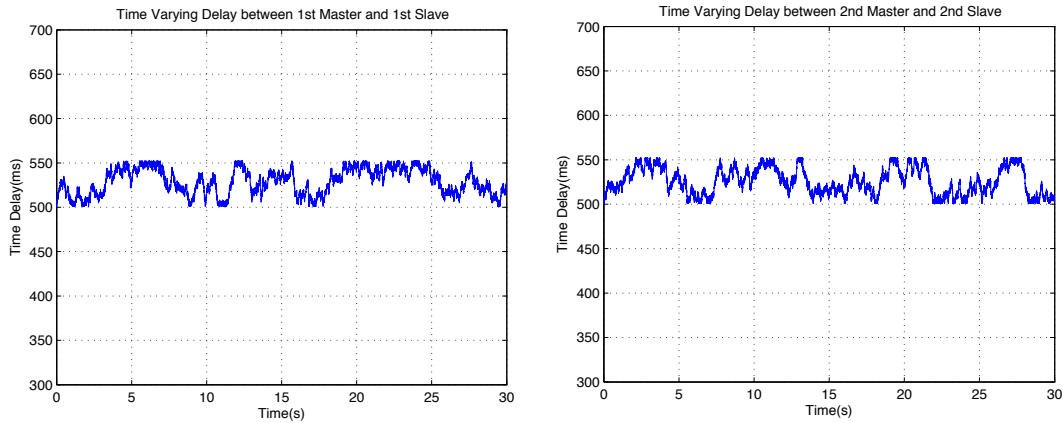


Figure 2.7: Examples of time-varying communication delays for experiments in Figure 2.6: Network 1 (left); Network 2 (right)

master devices. In particular, Figure 2.4 corresponds to the case of negligible communication delays. In Figure 2.5, the case of sufficiently large approximately constant communication delays is shown; specifically, the round-trip-time (RTT) communication delay in this figure is approximately equal to 1 s (0.5 s in each direction). The communication delay here is created using internal buffers. Also, in Figure 2.6 the case of time-varying communication delay with random packet dropouts is addressed; the corresponding profiles of the communication delays in the network communication channels in this case are shown in Figure 2.7. As these figures demonstrate, in all these cases the stabilization is achieved successfully, although the transient performance is the best for negligible communication delays and the worst for time-varying communication delay with packet dropouts. The major reason for such a performance deterioration is probably that the presence of irregular communication delays makes it less intuitive for the human operator to control the closed-loop system, as delays destroy the natural causality feeling for the human operator. Overall, the experimental results confirm the validity of the proposed approach.

2.5 Conclusions

In this work, we present a design framework for networked force-reflecting cooperative tele-operator systems which is based on the small-gain methodology. Using a new version of the

WIOPS nonlinear small gain theorem, we've designed a cooperative force-reflecting teleoperator system which is guaranteed to be stable in the presence of multiple network-induced communication constraints by appropriate adjustment of the system's parameters. To the best of our knowledge, this paper is the first work where the small gain approach is applied to analyze stability of a cooperative force reflecting teleoperator system; moreover, this is probably the first work which contains a rigorous stability analysis of a cooperative force reflecting teleoperator system in the presence of irregular communication delays and communication errors. It is worth noting that the generalization of more conventional passivity-based approaches to bilateral teleoperation to the case of cooperative teleoperator systems is probably a viable alternative to the small-gain approach developed in our paper. However, there are several aspects where the small-gain approach may eventually have an advantage over the the passivity-based ones. First, the passivity-based approaches are not directly applicable to the case where the slave manipulators are different in size. In this case, the scaled passivity can be violated in cooperative teleoperator systems due to physical interaction between slaves of different sizes through the common environment. Second, the passivity approaches have some well-known problems with achieving the trajectory tracking. Third, extension of passivity-based approaches to the case of irregular communication delays meets significant difficulties, as irregular communication delays may generate energy (although some partial extensions exist [17, 5, 24, 15]). Also, the small-gain approach allows significant flexibility in the choice of the force reflection signal, while in the passivity-based approaches, the force reflection signal must be a passive output of the slave-environment interconnection. The later requirement, in particular, may significantly limit the transparency of the teleoperator system. In all these aspects, the small-gain approach developed in our work seems to be advantageous in comparison to the passivity-based approaches that can potentially be applied to the cooperative force-reflecting teleoperator systems with communication constraints.

Bibliography

- [1] Robert J. Anderson and Mark W. Spong. Bilateral control of teleoperators with time delay. *IEEE Transactions on Automatic Control*, AC-34(5):494–501, May 1989.

- [2] David Angeli. Input-to-state stability of PD-controlled robotic systems. *Automatica*, 35:1285–1290, 1999.
- [3] Murat Arcak and Eduardo D. Sontag. Diagonal stability of a class of cyclic systems and its connection with the secant criterion. *Automatica*, 42(9):1531–1537, 2006.
- [4] R. Bacocco and C. Melchiorri. LQ control design of cooperative teleoperation systems. In *IEEE International Conference on Advanced Robotics*, pages 1 – 6, Munich, 2009.
- [5] N. Chopra, M. W. Spong, S. Hirche, and M. Buss. Bilateral teleoperation over the internet: the time varying delay problem. In *American Control Conference*, pages 155 – 160, Denver, CO, June 2003.
- [6] Sergey Dashkovskiy, Björn Rüffer, and Fabian R. Wirth. An ISS small gain theorem for general networks. *Mathematics of Control, Signals, and Systems*, 19(2):93–122, 2007.
- [7] Sergey Dashkovskiy, Björn Rüffer, and Fabian R. Wirth. Small gain theorems for large scale systems and construction of ISS Lyapunov functions. *SIAM Journal of Control and Optimization*, 48(6):4089–4118, 2010.
- [8] Denis Efimov, Antonio Loria, and Elena Panteley. Robust output stabilization: Improving performance via supervisory control. *International Journal of Robust and Nonlinear Control*, 21:1219–1236, 2011.
- [9] Manuel Ferre, Martin Buss, Rafael Aracil, Claudio Melchiorri, and Carlos Balaguer, editors. *Advances in Telerobotics*, volume 31 of *Springer Tracts in Advanced Robotics*. Springer, 2007.
- [10] Ken Goldberg and Roland Siegwart, editors. *Beyond Webcams: An Introduction to Online Robots*. MIT Press, 2002.
- [11] David J. Hill and Peter J. Moylan. Stability results for nonlinear feedback systems. *Automatica*, 13(4):377–382, July 1977.
- [12] Peter F. Hokayem and Mark W. Spong. Bilateral teleoperation: A historical survey. *Automatica*, 42(12):2035–2057, 2006.

- [13] Zhong-Ping Jiang. Control of interconnected nonlinear systems: a small gain viewpoint. In M. de Queiroz, M. Malisoff, and P. Wolenski, editors, *Optimal Control, Stabilization, and Nonsmooth Analysis*, pages 183–195. Springer-Verlag, Heidelberg, 2004.
- [14] Iasson Karafyllis and Zhong-Ping Jiang. A vector small-gain theorem for general nonlinear systems. In *48th IEEE Conference on Decision and Control and 28th Chinese Control Conference*, pages 7996–8001, Shanghai, P. R. China, December 2009.
- [15] Dongjun Lee and Ke Huang. Passive position feedback over packet-switching communication network with varying-delay and packet-loss. In *Symposium on Haptic Interfaces for Virtual Environments and Teleoperator Systems 2008*, Reno, NV, March 2008.
- [16] Dongjun Lee and Mark W. Spong. Passive bilateral control of teleoperators under constant time delay. *IEEE Transactions on Robotics*, 22(2):269–281, 2006.
- [17] Gunter Niemeyer and Jean-Jacques E. Slotine. Towards force reflecting teleoperation over the Internet. In *International Conference on Robotics and Automation*, pages 1909–1915, Leuven, Belgium, 1998.
- [18] Gunter Niemeyer and Jean-Jacques E. Slotine. Telemanipulation with time delays. *International Journal of Robotics Research*, 23(9):873–890, September 2004.
- [19] Emmanuel Nuño, Luis Basañez, and Romeo Ortega. Passivity-based control for bilateral teleoperation: A tutorial. *Automatica*, pages 485–495, January 2011.
- [20] Ilia G. Polushin, Peter X. Liu, and Chung-Horng Lung. A control scheme for stable force-reflecting teleoperation over IP networks. *IEEE Transactions on Systems, Man, and Cybernetics, Part B: Cybernetics*, 36(4):930–939, 2006.
- [21] Ilia G. Polushin, Peter X. Liu, and Chung-Horng Lung. A force-reflection algorithm for improved transparency in bilateral teleoperation with communication delay. *IEEE/ASME Transactions on Mechatronics*, 12(3):361–374, 2007.
- [22] Ilia G. Polushin, Horacio J. Marquez, Abdelhamid Tayebi, and Peter X. Liu. A multi-channel IOS small gain theorem for systems with multiple time-varying communication delays. *IEEE Transactions on Automatic Control*, 54(2):404–409, 2009.

- [23] Björn Ruffer, Rudolf Sailer, and Fabian R. Wirth. Comments on “A multichannel IOS small gain theorem for systems with multiple time-varying communication delays”. *IEEE Transactions on Automatic Control*, 55(7):1722–1725, July 2010.
- [24] Jee-Hwan Ryu and Carsten Preusche. Stable bilateral control of teleoperators under time-varying communication delay: Time domain passivity approach. In *2007 IEEE International Conference on Robotics and Automation*, pages 3508–3513, 2007.
- [25] Peyman Setoodeh, Shahin Sirouspour, and Ali Shahdi. Discrete-time multi-model control for cooperative teleoperation under time delay. In *2006 IEEE International Conference on Robotics and Automation*, pages 2921–2926, Orlando, FL, May 2006.
- [26] Shahin Sirouspour. Modeling and control of cooperative teleoperation systems. *IEEE Transactions on Robotics*, 21(6):1220–1225, December 2005.
- [27] Eduardo D. Sontag. Input-to-state stability: Basic concepts and results. In P. Nistri and G. Stefani, editors, *Nonlinear and Optimal Control Theory*, pages 163–220. Springer-Verlag, Berlin, 2006.
- [28] Mark W. Spong. Motion control of robot manipulators. In W. Levine, editor, *Handbook of Control*, pages 1339–1350. CRC Press, 1996.
- [29] Andrew R. Teel. A nonlinear small gain theorem for the analysis of control systems with saturation. *IEEE Transactions on Automatic Control*, AC-41(9):1256–1270, September 1996.
- [30] Andrew R. Teel. Connections between Razumikhin-type theorems and the ISS nonlinear small gain theorem. *IEEE Transactions on Automatic Control*, AC-43(7):960–964, July 1998.
- [31] Shanaz Tiwari, Yuan Wang, and Zhong-Ping Jiang. A nonlinear small-gain theorem for large-scale time-delay systems. In *48th IEEE Conference on Decision and Control and 28th Chinese Control Conference*, pages 7204–7209, Shanghai, P. R. China, December 2009.

- [32] Xiao-Gang Wang, Mehrdad Moallem, and Rajni V. Patel. An Internet-based distributed multiple-telerobot system. *IEEE Transactions on Systems, Man, and Cybernetics, Part A: Systems and Humans*, 33(5):627–633, September 2003.

Chapter 3

Small Gain Design of Cooperative Teleoperator Systems with PBFR

An abridged version of this work has been published in the *Proceedings of the IEEE International Conference on Intelligent Robots and Systems (IROS)*, pp. 653 – 658, San Francisco, 2011.

3.1 Introduction

A cooperative force-reflecting teleoperator system consists of multiple master-slave pairs, where the slaves execute task on a common environment, while the interaction forces between the environment and the slaves are transferred back to the corresponding master devices where they used for haptic feedback. There exists a significant number of practical applications where collaboration between several geographically separated human operators through the use of a networked cooperative teleoperator system may lead to fundamental improvement in manipulation capabilities, functionality, and performance of the teleoperation. The design of cooperative networked force reflecting teleoperator systems, however, brings additional challenges that come from existence of communication constraints generated by multiple networked channels, as well as possibility of mechanical interaction between slaves through the common environment. These limit applicability of the passivity based approaches to the design of cooperative

force-reflecting teleoperator systems; in particular, scaled passivity approach is generally not applicable, as in this case the energy can be generated during direct physical contact between slaves. Several approaches to the design of cooperative force-reflecting teleoperation were recently discussed in the literature [27, 34, 26, 2, 10, 11]; however, these works either skip the stability analysis entirely or address special cases such as linear systems with zero or constant communication delays. The input-to-output stability (IOS) small-gain framework for design of networked cooperative force reflecting teleoperators was recently introduced in [12, 23]. This framework allows for the analysis and design in general nonlinear setting and under extremely mild assumptions on communication process; however, it suffers from a drawback typical for any direct application of the small-gain arguments to the design of force-reflecting teleoperators. Specifically, the small-gain design leads to conservative results in that it generally requires the master subsystems to have sufficiently low admittance to guarantee the stability of the overall system. Low admittance (high impedance) of the master devices, however, is highly undesirable in the impedance controlled teleoperator systems; in particular, it contradicts the performance requirements.

In this work, we present developments to the small gain framework for networked cooperative force-reflecting teleoperator system. The main topic addressed in this work is how exactly the above mentioned conservatism of the small gain design can be overcome. More specifically, we start from formulating the small gain condition for stability of networked cooperative force-reflecting teleoperator system, and we demonstrate that the bottleneck of the small gain approach is essentially the requirement that the master subsystems must have sufficiently low input-output gains. The main question, therefore, is how this requirement can be satisfied without increasing the impedance of the master devices. We seek an answer to this question through combination of the two main ideas. The first one is based on reformulation of a traditional passivity assumption of the human dynamics in a form suitable for the small gain stability analysis. In our previous works on the small-gain framework for cooperative teleoperation [12, 23], a somewhat simplified approach was taken in that the human operators were considered external sources of uniformly bounded forces. Although such a simplified approach can be justified (see, for example [24, p. 752]), it doesn't allow description of how the human dynamics can affect the behaviour of the master devices in the presence of external forces. In

this work, following the ideas of [20], we reformulate the traditional passivity assumption imposed on the human dynamics in terms of the input-to-state stability (ISS) Lyapunov function of the closed-loop master subsystem. This new formulation, in particular, allows for explicit description of the effect of the human dynamics on the closed-loop gain of the master subsystems with respect to force reflection signals. Second, we address the conservativeness issue of the small-gain design by incorporating the projection-based force reflection principle into the above described framework. The projection-based force reflection principle was introduced in [16] as a means to resolve the stability vs. high force reflection gain trade-off in bilateral teleoperators. In this work, we apply this principle to the design of cooperative force reflecting teleoperators in combination with the assumptions on the human dynamics mentioned above. In particular, we derive explicit formulas for the masters gains that take into account the properties of the human dynamics as well as specific type of the force reflection algorithm. Applying these formulas to the small gain framework described above, we derive conditions for stability of the cooperative force reflecting teleoperator systems in the presence of network induced communication constraints.

In particular, the analysis presented in this paper shows that, even if one rejects the consideration of decreasing the force reflection gain or of increasing the damping and stiffness of the master manipulators, there still exist at least two possibilities to fulfill the small-gain condition and therefore guarantee the overall stability. The first possibility lies in the assumption that the human operators are able to stabilize the master manipulators in the sense that can be explicitly defined by considering the corresponding ISS-Lyapunov functions (see Section 3.4). In this case, if the impedance of the human hand is sufficiently high, the small gain condition can be fulfilled and the stability of the overall system is guaranteed. This theoretical result reflects a very well known fact that a firm grasp of the human operator helps to stabilize the teleoperator system [5, 8]. From the practical point of view, however, the obvious drawback of this result is that it relies on the human operators to stabilize the dynamics of the cooperative teleoperator system. If some of the human operators loosen their grasps or, even further, release the masters, the system's stability is no longer guaranteed. This potential instability can, however, be ruled out by using the projection-based force reflection principle. Specifically, we show that using projection-based FR, the cooperative teleoperator system can be made stable regardless of the

stiffness of the human hand. In particular, the stability remains when the human operators release the master devices. Experimental results are presented that, in particular, show that the improvement of stability is achieved largely without transparency deterioration. Preliminary simplified versions of some of the results of this work were presented without proofs in the conference paper [21].

The structure of this paper is as follows. Notation and basic definitions are described in Section 3.2. In Section 3.3, we formulate a general stability result for networked cooperative teleoperator systems that is based on multi-channel small gain approach. The result is generally similar to the one presented in [22], although the details are adjusted to better serve the subsequent developments. In Section 3.4, we describe assumptions imposed on the dynamics of the human operator and present a stability result that takes into account the human dynamics. Furthermore, in Section 3.5 we incorporate projection-based force reflection principle and show that in this case the stability can be guaranteed regardless of the human hand impedances. Experimental results are briefly described in Section 3.6, and concluding remarks are given in Section 3.7.

3.2 Notation and Definitions

In this section, we establish notation and give basic definitions that will be used throughout the paper. The small gain approach addressed in this work allows for the stability analysis of an interconnected system based on the individual subsystems' gains. Many different definitions of gain functions are possible; however, the existence of irregular communication delays makes the use of the uniform gains (or “ \mathcal{L}_∞ to \mathcal{L}_∞ ” type of gains [29]) more appropriate. In this work, we utilize the notions of input-to-state stability (ISS) and input-to-output stability (IOS), and all the gain functions are understood to be ISS and/or IOS gains. For further details related to these notions, and for extensive bibliography, the reader is referred to [29]. Denote $\mathbb{R}_+ := [0, +\infty)$. Following the terminology used in nonlinear control literature, we will say that a function $\alpha: \mathbb{R}_+ \rightarrow \mathbb{R}_+$ belongs to a class \mathcal{K} ($\alpha \in \mathcal{K}$) if and only if $\alpha(0) = 0$ and is strictly increasing; also, $\alpha \in \mathcal{K}$ belongs to a class \mathcal{K}_∞ ($\alpha \in \mathcal{K}_\infty$) if and only if it is unbounded ($\lim_{s \rightarrow +\infty} \alpha(s) = +\infty$). In our derivations below, the arguments of \mathcal{K} -class functions will occasionally take negative

values; in this case we assume without loss of generality that, for any $\alpha \in \mathcal{K}$, $\alpha(r) \equiv 0$ for $r \leq 0$. The Euclidean norm of a finite-dimensional vector x is denoted by $|x|$.

Definition [29] A system of the form

$$\dot{x} = F(x, u), \quad (3.1)$$

where $x \in \mathbb{R}^n$ is a state and $u \in \mathbb{R}^m$ is an input, is said to be input-to-state stable (ISS) if there exists $\beta \in \mathcal{K}_\infty$ and $\gamma \in \mathcal{K}$ such that the following two properties are satisfied along the trajectories of the system:

i) *uniform boundedness*: the inequality

$$|x(t)| \leq \max \left\{ \beta(|x(t_0)|), \gamma \left(\sup_{s \in [t_0, t]} |u(s)| \right) \right\}$$

holds for all $t_0, t \in \mathbb{R}, t \geq t_0$,

ii) *asymptotic gain*:

$$\limsup_{t \rightarrow +\infty} |x(t)| \leq \gamma \left(\limsup_{t \rightarrow +\infty} |u(t)| \right). \bullet$$

The function $\gamma \in \mathcal{K}$ in the above definition is called the ISS gain. For a system with an output

$$\begin{aligned} \dot{x} &= F(x, u), \\ y &= H(x, u), \end{aligned} \quad (3.2)$$

where $y \in \mathbb{R}^l$ is the output, the above defined ISS property implies the so-called input-to-output stability (IOS) which is represented by the following inequalities

$$\begin{aligned} |x(t)| &\leq \max \left\{ \beta^y(|x(t_0)|), \gamma^y \left(\sup_{s \in [t_0, t]} |u(s)| \right) \right\}, \\ \limsup_{t \rightarrow +\infty} |y(t)| &\leq \gamma^y \left(\limsup_{t \rightarrow +\infty} |u(t)| \right), \end{aligned}$$

where the first inequality holds for all $t_0, t \in \mathbb{R}, t \geq t_0$, and where $\beta^y \in \mathcal{K}_\infty$ and $\gamma^y \in \mathcal{K}$, the latter is called the IOS gain.

Below, we will frequently deal with MIMO (multi-input-multi-output) systems. For a MIMO system, the ISS (IOS) property can be characterized by a set of gains rather than individual gain functions; in such a case, the corresponding ISS (IOS) gains will be understood in the ‘‘maximum’’ sense. Specifically, consider a system

$$\dot{x} = F(x, u_1, \dots, u_p), \quad (3.3)$$

where x is a state, and u_1, \dots, u_p are inputs. The system (3.3) is input-to-state stable with ISS gains $\gamma_1, \dots, \gamma_p \in \mathcal{K}$ if and only if there exists $\beta \in \mathcal{K}_\infty$ such that

$$|x(t)| \leq \max \left\{ \begin{array}{l} \beta(|x(t_0)|), \gamma_1 \left(\sup_{s \in [t_0, t]} |u_1(s)| \right), \\ \dots, \gamma_p \left(\sup_{s \in [t_0, t]} |u_p(s)| \right) \end{array} \right\}$$

holds for all $t_0, t \in \mathbb{R}, t \geq t_0$, and

$$\limsup_{t \rightarrow +\infty} |x(t)| \leq \max \left\{ \begin{array}{l} \gamma_1 \left(\limsup_{t \rightarrow +\infty} |u_1(s)| \right), \\ \dots, \gamma_p \left(\limsup_{t \rightarrow +\infty} |u_p(s)| \right) \end{array} \right\}.$$

Similarly, for a MIMO system with outputs of the form

$$\begin{aligned} \dot{x} &= F(x, u_1, \dots, u_p), \\ y_1 &= H_1(x, u_1, \dots, u_p), \\ &\vdots \\ y_q &= H_q(x, u_1, \dots, u_p), \end{aligned} \tag{3.4}$$

where y_1, \dots, y_q are the outputs, the ISS implies IOS property; the latter is equivalent to the existence of $\beta_i^y \in \mathcal{K}_\infty, \gamma_{ij}^y \in \mathcal{K}, i \in \{1, \dots, q\}, j \in \{1, \dots, p\}$, such that

$$|y_i(t)| \leq \max \left\{ \begin{array}{l} \beta_i^y(|x(t_0)|), \gamma_{i1}^y \left(\sup_{s \in [t_0, t]} |u_1(s)| \right), \\ \dots, \gamma_{ip}^y \left(\sup_{s \in [t_0, t]} |u_p(s)| \right) \end{array} \right\}$$

holds for all $t_0, t \in \mathbb{R}, t \geq t_0$, and

$$\limsup_{t \rightarrow +\infty} |y_i(t)| \leq \max \left\{ \begin{array}{l} \gamma_{i1}^y \left(\limsup_{t \rightarrow +\infty} |u_1(s)| \right), \\ \dots, \gamma_{ip}^y \left(\limsup_{t \rightarrow +\infty} |u_p(s)| \right) \end{array} \right\}.$$

In this case, $\gamma_{ij}^y \in \mathcal{K}$ is the IOS gain from j -th input to i -output. The overall system's IOS gain can be conveniently represented in the matrix form $\Gamma^y := \left\{ \gamma_{ij}^y \right\}_{\substack{i=1, \dots, q \\ j=1, \dots, p}}$; in this case, we will write $\Gamma^y \in \mathcal{K}^{q \times p}$ if all $\gamma_{ij}^y \in \mathcal{K}$. The class $\mathcal{K}_\infty^{q \times p}$ is defined analogously. Formally, $\Gamma \in \mathcal{K}^{q \times p}$ is a map $\Gamma: \mathbb{R}_+^p \rightarrow \mathbb{R}_+^q$, where \mathbb{R}_+^p be the positive orthant in \mathbb{R}^p , *i.e.*, $\mathbb{R}_+^p := \{x \in \mathbb{R}^p, x_i \geq 0 \text{ for all } i = 1, \dots, p\}$; it is defined by the formula $\Gamma(s) = [(\Gamma(s))_1, \dots, (\Gamma(s))_q]$, where

$$(\Gamma(s))_i := \max_{j \in \{1, \dots, p\}} \gamma_{ij}(s_j). \tag{3.5}$$

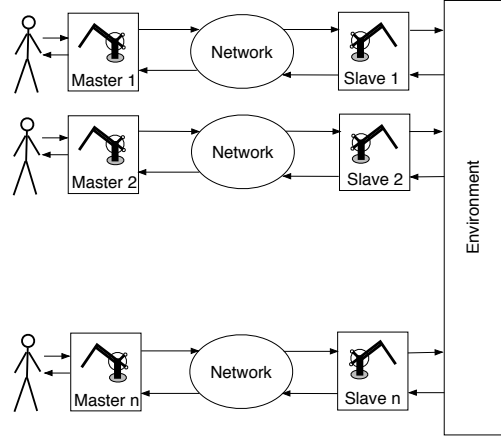


Figure 3.1: Cooperative network-based teleoperator system [12]

Some further notation is as follows. Given two maps Γ_1, Γ_2 of appropriate dimensions, their composition is denoted by $\Gamma_1 \circ \Gamma_2$ (*i.e.*, $\Gamma_1 \circ \Gamma_2(s) := \Gamma_1(\Gamma_2(s))$). Furthermore, given $x, y \in \mathbb{R}_+^n$, we write $x \geq y$ iff $x_i \geq y_i$ for all $i \in \{1, \dots, n\}$, and $x \not\geq y$ otherwise. Relations $>$ and $\not>$ are defined analogously. Also, the maximum of two or more vectors is calculated componentwise.

3.3 Small gain analysis of networked cooperative teleoperators

In this section, we present a general mathematical description of a cooperative networked teleoperator system and formulate stability conditions for such a system in terms of the small-gain approach. The cooperative teleoperator system under consideration consists of N master-slave pairs, where the i -th master communicates with the i -th slave over a bidirectional networked communication channel, and where the slave robots interact with each other through a common environment. The structure of the cooperative teleoperator system is illustrated in Figure 3.1. The dynamics of the i -th closed-loop human-master subsystem, which includes a human operator that interacts with the master manipulator possibly controlled by some local control algorithm, are described in general form as follows

$$\begin{aligned} \dot{x}_{hmi} &= F_{hmi}(x_{hmi}, \hat{f}_{si}^m), \\ y_{mi}^s &= H_{hmi}(x_{hmi}, \hat{f}_{si}^m), \end{aligned} \quad i = 1, \dots, N, \quad (3.6)$$

where x_{hmi} is the state of i -th human-master subsystem, \hat{f}_{si}^m is the force reflection signal that contains information about slave-environment interaction, and y_{mi}^s is an output signal that is sent over the i -th communication channel to the corresponding slave robot. The communication process in the i -th channel is described according to the formula

$$\hat{y}_{mi}^s(t) := y_{mi}^s(t - \tau_{fi}(t)) + \delta_{fi}(t), \quad i = 1, \dots, N, \quad (3.7)$$

where \hat{y}_{mi}^s is the signal that arrives at i -th slave, $\tau_{fi}(t)$ is communication delay in the i -th channel, and $\delta_{fi}(\cdot)$ is the communication error in the channel that is assumed to be uniformly essentially bounded. Delays $\tau_{fi}(t)$ are allowed to be time-varying, discontinuous and possibly unbounded; the exact assumption imposed on communication delays is formulated below (Assumption 4). Each closed-loop slave manipulator is described as a nonlinear system of the form

$$\begin{aligned} \dot{x}_{si} &= f_{si}(x_{si}, \hat{y}_{mi}^s, f_{ei}), \\ f_{si}^m &= h_{si}^m(x_{si}, \hat{y}_{mi}^s, f_{ei}), \quad i = 1, \dots, N, \\ y_{si}^e &= h_{si}^e(x_{si}, \hat{y}_{mi}^s, f_{ei}), \end{aligned} \quad (3.8)$$

where x_{si} is the state of the i -th slave, \hat{y}_{mi}^s is the signal that arrives from the i -th master (described by (3.7)), and f_{ei} is the environmental force that acts on the i -th slave. Also, the output signal y_{si}^e is applied to the environment, while the output f_{si}^m is transmitted over the communication channel to the corresponding master manipulator where it plays a role of the force reflection signal. The environment is described as a nonlinear model of the following general form,

$$\begin{aligned} \dot{x}_e &= f_e(x_e, y_{s1}^e, \dots, y_{sN}^e), \\ f_{e1} &= g_{e1}(x_e, y_{s1}^e, \dots, y_{sN}^e), \\ &\vdots \\ f_{eN} &= g_{eN}(x_e, y_{s1}^e, \dots, y_{sN}^e), \end{aligned} \quad (3.9)$$

where x_e is the state of the environment, y_{si}^e are the inputs from the corresponding slave manipulators, and f_{ei} are environmental forces that act on the slaves. Finally, the signal f_{si}^m (that, in particular, may depend on the i -th slave state as well as interaction forces between the environment and the i -th slave) is sent over the communication channel to the i -th master site where it is used for force reflection. The communication process is described by the following equation

$$\hat{f}_{si}^m(t) := f_{si}^m(t - \tau_{bi}(t)) + \delta_{bi}(t), \quad i = 1, \dots, N, \quad (3.10)$$

where \hat{f}_{si}^m is the signal that arrives to i -th master, $\tau_{bi}(t)$ is communication delay in the i -th channel in the backward direction (from the slave to the master), and $\delta_{bi}(\cdot)$ is the communication error in the i -th channel; each $\delta_{bi}(\cdot)$, $i \in \{1, \dots, N\}$ is assumed to be uniformly essentially bounded.

Assumption 1. The closed-loop human-master subsystems (3.6) are input-to-state stable (ISS). •

Conditions under which the Assumption 1 holds will be addressed in detail below in Sections 3.4 and 3.5. The input-to-state stability property of the systems (3.6) implies in particular that, for i -th human-master subsystem $i \in \{1, \dots, N\}$, there exists a well defined input-to-output (IOS) gain $\gamma_{mi} \in \mathcal{K}$ that provides an estimate of the norm of the output y_{mi}^s in terms of the norm of f_{ei} . For our purposes, it is convenient to group all these gains together and consider a matrix gain function $\Gamma_m \in \mathcal{K}^{N \times N}$ which is defined according to the formula $\Gamma_m := \text{diag}\{\gamma_{m1}, \dots, \gamma_{mN}\}$. The stability assumption imposed on the slave subsystems is formulated as follows.

Assumption 2. The slave manipulators (3.8) are input-to-state stable. Moreover, the IOS gains from f_{ei} to y_{si}^e , $i \in \{1, \dots, N\}$, can be assigned arbitrarily. •

Examples of control algorithms that make the slave robots input-to-state stable can be found, for example, in [15, 14]; in particular, the mentioned IOS gains can be assigned arbitrarily by an appropriate choice of the slave's feedback gains. Since each slave subsystem (3.8) has two inputs and two outputs, the ISS of (3.8) implies the existence of four well-defined IOS gains. We denote them as follows: let $\gamma_{si}^{mm}, \gamma_{si}^{me}, \gamma_{ei}^{em}, \gamma_{si}^{ee} \in \mathcal{K}$ be the IOS gains of the i -th slave subsystem from \hat{y}_{mi}^s to f_{si}^m , from \hat{y}_{mi}^s to y_{si}^e , from f_{ei} to f_{si}^m , and from f_{ei} to y_{si}^e , respectively. Again, for our purposes, it is convenient to represent these gains in the matrix form, according to the formulas $\Gamma_s^{mm} := \text{diag}\{\gamma_{s1}^{mm}, \dots, \gamma_{sN}^{mm}\} \in \mathcal{K}^{N \times N}$, $\Gamma_s^{me} := \text{diag}\{\gamma_{s1}^{me}, \dots, \gamma_{sN}^{me}\} \in \mathcal{K}^{N \times N}$, $\Gamma_s^{em} := \text{diag}\{\gamma_{s1}^{em}, \dots, \gamma_{sN}^{em}\} \in \mathcal{K}^{N \times N}$, and $\Gamma_s^{ee} := \text{diag}\{\gamma_{s1}^{ee}, \dots, \gamma_{sN}^{ee}\} \in \mathcal{K}^{N \times N}$.

Assumption 3. The environment (3.9) is input-to-state stable. •

The input-to-state stability property of the environment also implies the existence of N^2 well-defined nonlinear IOS gain functions that can be conveniently represented in the matrix

form, as follows:

$$\Gamma_e = \begin{bmatrix} \gamma_{11}^e & \cdots & \gamma_{1N}^e \\ \vdots & \ddots & \vdots \\ \gamma_{N1}^e & \cdots & \gamma_{NN}^e \end{bmatrix} \in \mathcal{K}^{N \times N}, \quad (3.11)$$

where $\gamma_{ij}^e \in \mathcal{K}$ represents an IOS gain from $y_{s_j}^e$ to f_{ei} . These IOS gains depend on the mechanical properties of the environment (stiffness, damping, geometry, etc.) and generally cannot be adjusted.

It is also worth mentioning that one of the advantages of the small-gain approach is that it allows us to guarantee stability under extremely mild assumptions imposed on communication delays. In particular, all the communication delays $\tau_{fi}(t)$, $\tau_{bi}(t)$, $i \in \{1, \dots, N\}$, in the communication channels (3.7), (3.10) are allowed to be time-varying, discontinuous and even unbounded. Specifically, all the delays satisfy the following assumption.

Assumption 4. The communication delays $\tau_{fi}, \tau_{bi}: \mathbb{R}_+ \rightarrow \mathbb{R}_+$, $i \in \{1, \dots, N\}$, are Lebesgue measurable functions with the following properties:

- i) there exists a piecewise continuous function $\tau^*: \mathbb{R}_+ \rightarrow \mathbb{R}_+$ satisfying $\tau^*(t_2) - \tau^*(t_1) \leq t_2 - t_1$, such that $\max_{i \in \{1, \dots, N\}} \{\tau_{fi}(t), \tau_{bi}(t)\} \leq \tau^*(t)$ holds for all $t \geq 0$;
- ii) $t - \max_{i \in \{1, \dots, N\}} \{\tau_{fi}, \tau_{bi}\} \rightarrow +\infty$ as $t \rightarrow +\infty$. •

The assumption imposed on the communication process is similar to the one used in [14, 19]. The fulfilment of this assumption does not depend on the characteristics of the communication channel (such as bandwidth, packet loss percentage, etc.) and can always be satisfied in a communication network unless the communication is completely lost on a semi-infinite time interval. For details, see [14, 19].

The gain structure of the above described cooperative teleoperator system is illustrated in Figure 3.2. Using the small-gain theorem presented in [12, 22] and following the same lines of reasoning, one can establish a small gain stability result in terms of the above defined gain matrices $\Gamma_m, \Gamma_s^{mm}, \Gamma_s^{me}, \Gamma_s^{em}, \Gamma_s^{ee}$, and Γ_e , as follows:

Theorem 3.3.1 *Consider a cooperative networked force reflecting teleoperator system (3.6) – (3.10). Suppose Assumptions 1 – 4 hold. Then the system is input-to-state stable with respect*

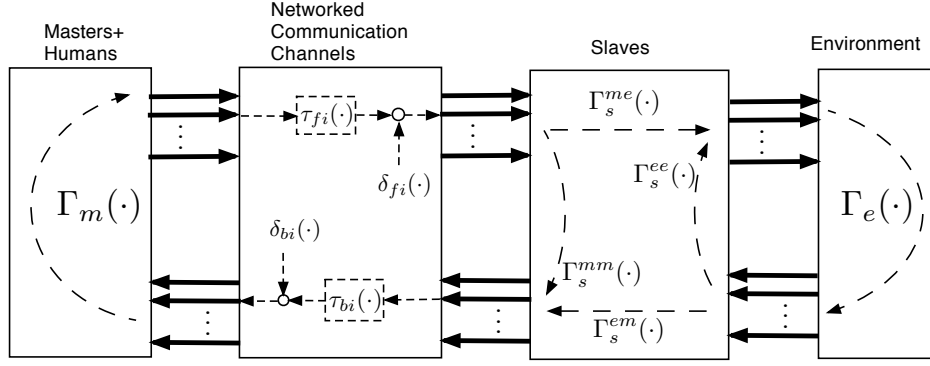


Figure 3.2: Gain structure of the cooperative teleoperator systems

to communication errors δ_{fi} , δ_{bi} , $i = 1, \dots, N$, if the following small-gain condition holds:

$$\begin{bmatrix} \circ & \Gamma_m & \circ & \circ \\ \Gamma_s^{mm} & \circ & \circ & \Gamma_s^{em} \\ \Gamma_s^{me} & \circ & \circ & \Gamma_s^{ee} \\ \circ & \circ & \Gamma_e & \circ \end{bmatrix} (s) \not\geq s, \quad \forall s \in \mathbb{R}_+^{4N} \setminus \{0\}, \quad (3.12)$$

where \circ is the zero map of the appropriate dimension. •

Since the closed-loop cooperative teleoperator system contains multiple delayed communication channels, the input-to-state stability in Theorem 3.3.1 should be understood in the sense of its version for functional-differential equations discussed for example in [33, 14]. The small-gain condition (3.12) is equivalent to the fact that the following three inequalities are satisfied:

$$\Gamma_m \circ \Gamma_s^{mm}(s) \not\geq s, \quad \forall s \in \mathbb{R}_+^N \setminus \{0\}; \quad (3.13)$$

$$\Gamma_m \circ \Gamma_s^{em} \circ \Gamma_e \circ \Gamma_s^{me}(s) \not\geq s, \quad \forall s \in \mathbb{R}_+^N \setminus \{0\}; \quad (3.14)$$

$$\Gamma_s^{ee} \circ \Gamma_e(s) \not\geq s, \quad \forall s \in \mathbb{R}_+^N \setminus \{0\}. \quad \bullet \quad (3.15)$$

Conditions (3.13)-(3.15) can be constructively checked using their equivalence to a set of minimal cycle conditions described as follows. It is well known (see for example [3]) that, for “maximum” definitions of matrix gains as in (3.5), the condition “ $\Gamma(s) \not\geq s$ for all $s \in \mathbb{R}_+^n$ ” is equivalent to the fact that every minimal cycle of the matrix $\Gamma(s) := \{\gamma_{ij}\}_{i,j \in \{1, \dots, n\}} \in \mathcal{K}^{n \times n}$ (i.e., every composition of the form $\gamma_{k_1 k_2} \circ \gamma_{k_2 k_3} \circ \dots \circ \gamma_{k_p k_1}$, where $p \in \{1, \dots, n\}$, $k_1, \dots, k_p \in \{1, \dots, n\}$,

$k_1 \neq k_2 \neq k_p$) satisfy the inequality

$$\gamma_{k_1 k_2} \circ \gamma_{k_2 k_3} \circ \dots \circ \gamma_{k_p k_1}(s) < s \text{ for all } s > 0.$$

It is straightforward to see that every nonzero minimal cycle for (3.13), (3.14) contains at least one diagonal element of Γ_m , and every nonzero minimal cycle for (3.15) contains at least one diagonal element of Γ_s^{ee} . Thus, one can conclude that the cooperative force reflecting teleoperator system (3.6) – (3.10) is stable if all master gains $\gamma_{mi} \in \mathcal{K}$ are “sufficiently low” and all gains $\gamma_{si}^{ee} \in \mathcal{K}$ are also “sufficiently low”. According to Assumption 2, however, the gains $\gamma_{si}^{ee} \in \mathcal{K}$ can be assigned arbitrarily low by an appropriate choice of the slave feedback gains. In particular, this implies that under Assumption 2 the condition (3.15) can always be met. The rest of this paper addresses the question of how the master gains $\gamma_{mi} \in \mathcal{K}$ can be assigned sufficiently low without negative effect on the transparency of the system.

3.4 Dynamics of the human operators and stability of the cooperative teleoperator system

In this section, we take a closer look at the structure of the human-master interconnections (3.6) and, in particular, formulate stability conditions for networked cooperative teleoperator system based on the properties of the human dynamics as well as the local master control algorithms. Let the i -th closed-loop master manipulator (*i.e.*, the master manipulator together with the corresponding local master control algorithm) be described as an affine nonlinear system of the form

$$\begin{aligned} \dot{x}_{mi} &= f_{mi}(x_{mi}) + g_{mi}(x_{mi})u_{mi}, & i = 1, \dots, N, \\ y_{mi}^s &= h_{mi}(x_{mi}), \end{aligned} \quad (3.16)$$

where

$$u_{mi} = [f_{hi} - f_{ri}], \quad i = 1, \dots, N, \quad (3.17)$$

and where f_{hi} is the force/torque applied by the i -th human operator and f_{ri} is i -th force reflection term. We assume that each master manipulator is equipped with a local control algorithm that makes it input-to-state stable (see Definition 3.2) with respect to external forces. It was

demonstrated in [30] that for an affine system of the form

$$\begin{aligned} \dot{x} &= f(x) + g(x)u \\ y &= h(x), \end{aligned} \quad (3.18)$$

where $x \in \mathbb{R}^n$, $u \in \mathbb{R}^m$, $y \in \mathbb{R}^l$, $f(\cdot)$, $g(\cdot)$, $h(\cdot)$ are locally Lipschitz functions of the corresponding dimensions, $f(0) = 0$, $h(0) = 0$, the ISS property is equivalent to the existence of a so called ISS Lyapunov function (strictly speaking, this result is also valid for nonaffine systems of the more general form (3.1), but we don't need this). More specifically, the input-to-state stability property of the system (3.18) is equivalent to the existence of a smooth (continuously differentiable) function $V: \mathbb{R}^n \rightarrow \mathbb{R}_+$ satisfying

$$\sigma_1(|x|) \leq V(x) \leq \sigma_2(|x|) \quad (3.19)$$

for some $\sigma_1, \sigma_2 \in \mathcal{K}_\infty$, such that $\frac{\partial V}{\partial x} [f(x) + g(x)u] \leq -\sigma_0(V(x))$ holds whenever $|x| \geq \chi(|u|)$, where $\sigma_0(\cdot)$, $\chi(\cdot)$ are some \mathcal{K} -class functions. In particular, the ISS gain γ of (3.18) can be calculated in terms of the functions σ_1 , σ_2 and $\chi(\cdot)$ according to the formula

$$\gamma := \sigma_{1i}^{-1} \circ \sigma_{2i} \circ \chi \in \mathcal{K}. \quad (3.20)$$

Moreover, the IOS gain of the above system can be calculated according to the formula

$$\gamma^y := \sigma_h \circ \gamma \in \mathcal{K},$$

where $\sigma_h \in \mathcal{K}$ is defined as $\sigma_h(s) := \sup_{|x| \leq s} |h(x)|$. Using the above described equivalence, the input-to-state stability assumption on the closed-loop master subsystems can be formulated as follows.

Assumption 5. The closed-loop master manipulators (3.16) are input-to-state stable with respect to their respective force (torque) inputs (3.17). Specifically, there exist a smooth ISS Lyapunov functions $V_i(x_{mi}) \in \mathbb{R}_+$ and functions $\sigma_{1i} \in \mathcal{K}_\infty$, $\sigma_{2i} \in \mathcal{K}_\infty$, $\sigma_{0i} \in \mathcal{K}$, and $\chi_i \in \mathcal{K}_\infty$, $i \in \{1, \dots, N\}$, such that

$$\sigma_{1i}(|x_{mi}|) \leq V_i(x_{mi}) \leq \sigma_{2i}(|x_{mi}|) \quad (3.21)$$

and

$$\frac{\partial V_i}{\partial x_{mi}} [f_{mi}(x_{mi}) + g_{mi}(x_{mi})u_{mi}] \leq -\sigma_{0i}(V_i(x_{mi})) \quad (3.22)$$

whenever $|x_{mi}| \geq \chi_i(|u_{mi}|)$. •

Assumption 5 implies in particular that

$$\gamma_{mi}^0 := \sigma_{1i}^{-1} \circ \sigma_{2i} \circ \chi_i \in \mathcal{K}_\infty \quad (3.23)$$

is the ISS gain of the i -th master subsystem (3.16).

Remark 1. There are several points worth mentioning regarding the above Assumption 5. First, for master manipulators described by Euler-Lagrange equations, the ISS property with respect to the force input can be achieved using simple local controllers, such as PD; the corresponding results can be found in [1, 14]. Second, although each master is assumed to be input-to-state stable, no restrictions are imposed on the corresponding ISS gains; in particular, these gains can be arbitrarily high. Since the gain from force input to position-velocity state provides an upper bound for admissible master compliance, high admissible ISS gain results in high admissible compliance of the master manipulator or, equivalently, low admissible impedance. In practice, this implies that Assumption 5 does not impose restrictions on the damping and the stiffness of master manipulators; in particular, both can be made arbitrarily low. Low damping and stiffness of the master manipulators are very important for teleoperator's performance, as high damping-stiffness lead to transparency deterioration and require the human operator to apply significant forces when moving the master. Also, Assumption 5 can be generalized to the case of the input-to-state stability with respect to compact sets [31], as it was done for example in [20]. The latter version of the ISS assumption may be more suitable for teleoperator systems as it allows for statically balanced master manipulators. We do not follow this path in this work for the sake of simplicity of presentation, although the corresponding extension is probably possible. •

Remark 2. In the formulation of Assumption 5, the inequality (3.22) can be equivalently replaced with the following

$$\frac{\partial V_i}{\partial x_{mi}} f_{mi}(x_{mi}) + \left| \frac{\partial V_i}{\partial x_{mi}} g_{mi}(x_{mi}) \right| \cdot |u_{mi}| \leq -\sigma_{0i}(V_i(x_{mi})). \quad (3.24)$$

Indeed, (3.24) clearly implies (3.22). To show the converse, denote $\xi_i := \frac{\partial V_i}{\partial x_{mi}} g_{mi}(x_{mi})$. If $\xi_i = 0$, the inequalities (3.22) and (3.24) are equivalent. Suppose $\xi \neq 0$. According to Assumption 5, (3.22) holds for an arbitrary u_{mi} such that $|x_{mi}| \geq \chi_i(|u_{mi}|)$. Then, it also holds for $u_{mi}^* = |u_{mi}| \cdot \frac{\xi_i^T}{|\xi_i|}$, which implies (3.24). •

The ISS Lyapunov functions $V_i(x_{mi})$ provide a tool that, in particular, allows us to classify the external forces in terms of their effect on the system's stability; specifically, an external force can be considered destabilizing (stabilizing) if its contribution to the time-derivative of V_i is positive (negative). The time derivative of V_i along the trajectories of the i -th master subsystem (3.16), (3.17) is expressed by the formula

$$\dot{V}_i = \frac{\partial V_i}{\partial x_{mi}} f_{mi}(x_{mi}) + \frac{\partial V_i}{\partial x_{mi}} g_{mi}(x_{mi}) [f_{hi} - f_{ri}].$$

In particular, the contribution of the i -th human operator force/torque f_{hi} to the time-derivative of the ISS Lyapunov function V_i is $\frac{\partial V_i}{\partial x_{mi}} g_{mi}(x_{mi}) f_{hi}$; the positivity of this contribution corresponds to destabilizing actions of the human operator. Our basic assumption imposed on the human dynamics is that the human operator does not perform such destabilizing actions. Specifically, the assumption is as follows.

Assumption 6. The force/torque of i -th human operator satisfies

$$\frac{\partial V_{mi}}{\partial x_{mi}} g_{mi}(x_{mi}) f_{hi} \leq 0. \quad (3.25)$$

Assumption 6 implies that the contribution of the human force to the time-derivative of the corresponding ISS Lyapunov function V_{mi} is nonpositive. This precisely means that the human operator does not destabilize the system in the sense determined by the ISS Lyapunov function V_{mi} . If V_{mi} is considered as a storage function and, therefore, represents the amount of energy stored in the system, Assumption 6 says that the actions of i -th human operator do not add energy to the system and therefore are passive. In the following, we will also need a stronger assumption which corresponds to strict passivity of the human operator, as follows.

Assumption 7. There exists $0 < \epsilon_0 \leq 1$ such that the force/torque of i -th human operator satisfies

$$\frac{\partial V_{mi}}{\partial x_{mi}} g_{mi}(x_{mi}) f_{hi} \leq -\epsilon_0 \cdot \left| \frac{\partial V_{mi}}{\partial x_{mi}} g_{mi}(x_{mi}) \right| \cdot |f_{hi}|. \quad (3.26)$$

Remark 3. Regarding Assumption 7, it is worth mentioning that $u = -\frac{\partial V_{mi}}{\partial x_{mi}} g_{mi}(x_{mi})$ represents the so-called “speed-gradient” [4] or “passivity-based” [25] stabilization algorithms; it also represents the “universal stabilizer” for affine nonlinear systems [28]. Assumption 7 essentially says that actions of the human operator (if nonzero) form an acute angle with the “speed-gradient” or “universally stabilizing” control (if nonzero), and this angle is less or equal

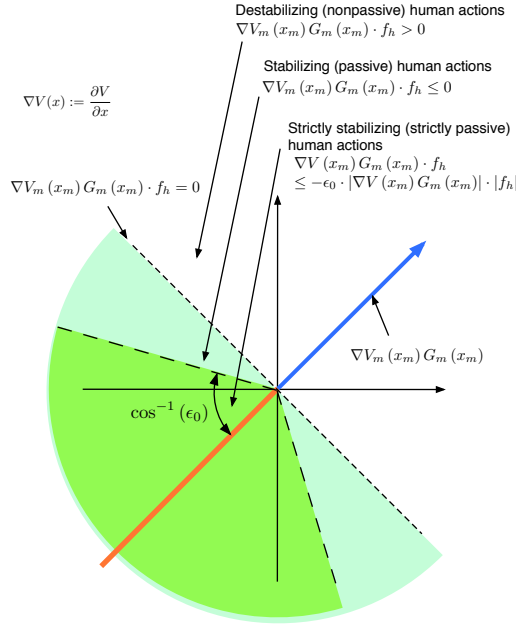


Figure 3.3: Dynamics of the human operator

than $\cos^{-1}(\epsilon_0)$. This means that the actions of the human operator, if nonzero, stabilize the master subsystem. Also, if one considers V_{mi} to be a storage function representing the amount of energy stored in the system, then Assumption 7 implies that the actions of the human operator are strictly passive. Assumptions 6 and 7 are illustrated in Figure 3.3. •

For the developments below, we also need to introduce a measure of the magnitude of the human hand impedance. We do this by way of the following assumption.

Assumption 8. The magnitude of the force of i -th human operator satisfies

$$|f_{hi}| \geq \mu_{i0}(|x_{mi}|), \quad (3.27)$$

for some $\mu_{i0} \in \mathcal{K} \cup \{0\}$.

Remark 4. As the state x_{mi} typically consists of positions and velocities of the i -th master, we see that the function $\mu_{i0}(\cdot)$ describes the minimum admissible impedance of the i -th human hand. In particular, assumption 8 makes it possible that $\mu_{i0}(\cdot) \equiv 0$. This allows us to consider a case of zero human hand impedance, *i.e.*, the situation where the human effectively releases the master. •

At this point, we address stability properties of the networked cooperative teleoperator

system with direct force reflection described by the formula

$$f_{ri} = \hat{f}_{si}^m, \quad i = 1, \dots, N, \quad (3.28)$$

under the above described assumptions on human dynamics. We start from the following proposition which described how does the ISS gain of the master-human interconnection depend on the properties of the human operator dynamics.

Proposition 3.4.1 *Consider the i -th master device (3.16), (3.17). Suppose Assumption 5 holds for this master device with ISS gain $\gamma_{mi}^0 \in \mathcal{K}_\infty$. Then the following statements are valid.*

i) If the i -th human operator dynamics satisfy Assumption 6, the closed-loop master device is ISS with ISS gain $\bar{\gamma}_{mi} := \gamma_{mi}^0 \in \mathcal{K}_\infty$.

ii) If the i -th human operator dynamics satisfy Assumptions 7, 8, the closed-loop master device is ISS with ISS gain

$$\bar{\gamma}_{mi} := \sigma_{1i}^{-1} \circ \sigma_{2i} \circ \left[\left[\gamma_{mi}^0 \right]^{-1} \circ \sigma_{1i}^{-1} \circ \sigma_{2i} + \epsilon_0 \cdot \mu_{i0} \right]^{-1} \in \mathcal{K}_\infty. \quad (3.29)$$

Proof. Assumption 5 in combination with Remark 2 imply that, for each $i \in \{1, \dots, N\}$, there exists an ISS Lyapunov function $V_i(x_{mi}) \in \mathbb{R}_+$ such that $\sigma_{1mi}(|x_{mi}|) \leq V_{mi}(x_{mi}) \leq \sigma_{2mi}(|x_{mi}|)$, and

$$\frac{\partial V_{mi}}{\partial x_{mi}} f_{mi}(x_{mi}) + \left| \frac{\partial V_{mi}}{\partial x_{mi}} g_{mi}(x_{mi}) \right| \cdot |u| \leq -\sigma_0(V_{mi}) \quad (3.30)$$

whenever $|x_{mi}| \geq \chi_{mi}(|u|)$, where $\chi_{mi} := \sigma_{2i}^{-1} \circ \sigma_{1i} \circ \gamma_{mi}^0 \in \mathcal{K}$. To prove i), assume that the dynamics of the human operator satisfy Assumption 6. Calculating the time derivative of V_{mi} along the trajectories of (3.16), and taking into account Assumption 6, we have

$$\begin{aligned} \dot{V}_{mi} &= \frac{\partial V_{mi}}{\partial x_{mi}} f_{mi}(x_{mi}) + \frac{\partial V_{mi}}{\partial x_{mi}} g_{mi}(x_{mi}) [f_{hi} - f_{ri}] \\ &\leq \frac{\partial V_{mi}}{\partial x_{mi}} f_{mi}(x_{mi}) - \frac{\partial V_{mi}}{\partial x_{mi}} g_{mi}(x_{mi}) f_{ri} \\ &\leq \frac{\partial V_{mi}}{\partial x_{mi}} f_{mi}(x_{mi}) + \left| \frac{\partial V_{mi}}{\partial x_{mi}} g_{mi}(x_{mi}) \right| \cdot |f_{ri}|. \end{aligned} \quad (3.31)$$

Thus, $|x_{mi}| \geq \chi_{mi}(|f_{ri}|)$ implies $\dot{V}_{mi} \leq -\sigma_0(V_{mi})$, where $\chi_{mi} := \sigma_{2i}^{-1} \circ \sigma_{1i} \circ \gamma_{mi}^0 \in \mathcal{K}$, and the system is ISS with gain $\bar{\gamma}_{mi} := \gamma_{mi}^0 \in \mathcal{K}_\infty$. On the other hand, If the i -th human operator

dynamics satisfy Assumptions 7, 8 then, combining (3.26) and (3.27), we have

$$\begin{aligned} \frac{\partial V_{mi}}{\partial x_{mi}} g_{mi}(x_{mi}) f_{hi} &\leq -\epsilon_0 \cdot \left| \frac{\partial V_{mi}}{\partial x_{mi}} g_{mi}(x_{mi}) \right| \cdot |f_{hi}| \\ &\leq -\epsilon_0 \cdot \left| \frac{\partial V_{mi}}{\partial x_{mi}} g_{mi}(x_{mi}) \right| \mu_{i0}(|x_{mi}|), \end{aligned} \quad (3.32)$$

Calculating the time derivative of V_{mi} along the trajectories of (3.16) while taking (3.32) into account, we see that

$$\begin{aligned} \dot{V}_{mi} &= \frac{\partial V_{mi}}{\partial x_{mi}} f_{mi}(x_{mi}) + \frac{\partial V_{mi}}{\partial x_{mi}} g_{mi}(x_{mi}) [f_{hi} - f_{ri}] \\ &\leq \frac{\partial V_{mi}}{\partial x_{mi}} f_{mi}(x_{mi}) \\ &\quad + \left| \frac{\partial V_{mi}}{\partial x_{mi}} g_{mi}(x_{mi}) \right| \cdot (-\epsilon_0 \cdot \mu_{i0}(|x_{mi}|) + |f_{ri}|). \end{aligned} \quad (3.33)$$

Using (3.30), we see that the condition

$$\chi_{mi}^{-1}(|x_{mi}|) \geq -\epsilon_0 \cdot \mu_{i0}(|x_{mi}|) + |f_{ri}| \quad (3.34)$$

guarantees that $\dot{V}_{mi} \leq -\sigma_0(V_{mi})$. The inequality (3.34) is equivalent to

$$|x_{mi}| \geq \bar{\gamma}_{mi}(|f_{ri}|),$$

where $\bar{\gamma}_{mi} \in \mathcal{K}_\infty$ is defined by (3.29). Thus, the system is ISS with ISS gain $\bar{\gamma}_{mi}$. •

Remark 5. Proposition 3.4.1 describes how the interaction between a master device and a human operator affects the master ISS gain. Part i) states that if the operator does not perform destabilizing actions (*i.e.*, the dynamics of the human operator satisfy Assumption 6), then such an interaction preserves the original ISS gain. On the other hand, if the human operator is able to perform stabilizing actions (*i.e.*, the dynamics of the human operator satisfy Assumption 7), then the master ISS gain also depends on the impedance of the human operator hand. More specifically, part ii) of Proposition 3.4.1 implies that the ISS gain of the master-human interconnection can be made arbitrarily small if the impedance of the human hand is sufficiently high. Indeed, given an i -th master ISS gain $\gamma_{mi}^0 \in \mathcal{K}_\infty$ and a desired i -th master ISS gain $\gamma_{mi}^* \in \mathcal{K}_\infty$, denote

$$\mu_i^*(s) := \frac{1}{\epsilon_0} \left[[\gamma_{mi}^*]^{-1} - [\gamma_{mi}^0]^{-1} \right] \circ \sigma_{1i}^{-1} \circ \sigma_{2i}(s). \quad (3.35)$$

From (3.29) it is easy to derive that if

$$\mu_{i0}(s) \geq \mu_i^*(s) \quad (3.36)$$

for all $s \geq 0$, then the i -th master-human interconnection is ISS with ISS gain $\bar{\gamma}_{mi} \in \mathcal{K}_\infty$ satisfying $\bar{\gamma}_{mi}(s) \leq \gamma_{mi}^*(s)$ for all $s > 0$. •

Remark 6. In the “linear” case (*i.e.*, where all the involved \mathcal{K}_∞ -functions are linear), formula (3.29) becomes

$$\bar{\gamma}_{mi} := \frac{\gamma_{mi}^0}{1 + \frac{\sigma_{1i}}{\sigma_{2i}} \cdot \epsilon_0 \cdot \mu_{i0} \cdot \gamma_{mi}^0}.$$

We see that $\gamma_{mi}^* > 0$ can be assigned arbitrarily small if $\mu_{i0} > 0$ is sufficiently large. •

The following theorem describes stability properties of the networked teleoperator system under the above described assumptions on the human dynamics. In this theorem (as well as in Theorem 3.5.2 in the following section), the input-to-state stability of the networked cooperative teleoperator system is understood in the sense of [13, Definition 1], where the input disturbances are the communication errors $\delta_{fi}, \delta_{bi}, i = 1, \dots, N$.

Theorem 3.4.2 *Consider a cooperative networked force reflecting teleoperator system (3.7)–(3.10), (3.16), (3.17). Suppose Assumptions 2, 3, 4, 5 are satisfied. Then there exist $\gamma_{mi}^* \in \mathcal{K}_\infty, i \in \{1, \dots, N\}$, such that the teleoperator system is input-to-state stable if, for each $i \in \{1, \dots, N\}$, at least one of the following statements are valid:*

i) The dynamics of i -th human operator satisfy Assumption 6, and $\gamma_{mi}^0(s) \leq \gamma_{mi}^(s)$ for all $s \geq 0$, where $\gamma_{mi}^0(\cdot)$ is defined by (3.23).*

ii) The dynamics of i -th human operator satisfy Assumptions 7, 8, and $\mu_{i0}(s) \geq \mu_i^(s)$ for all $s \geq 0$, where $\mu_i^*(\cdot)$ is defined by (3.35). •*

Proof. The results of Theorem 3.4.2 follow directly from Proposition 3.4.1, Remark 5, and the small-gain arguments presented in Section 3.3. •

Remark 7. Theorem 3.4.2 essentially states that the stability of a cooperative force reflecting teleoperator system can be guaranteed in the presence of irregular communication delays if, for each master subsystem, at least one of the conditions i), ii) is satisfied. Condition i) requires that the human operator does not destabilize the master device, and that the ISS gain of the master device is sufficiently low. The latter is essentially equivalent to the requirement of

sufficiently high impedance of the master. This condition may be conservative in some cases as high impedance of a master device in the impedance controlled teleoperator systems may lead to poor transparency. On the other hand, condition ii) requires the human operator to apply stabilizing actions to the corresponding master device, and also requires that the impedance of the human operator's hand is sufficiently high. This part of Theorem 3.4.2 can be linked to a fact which is practically well-known for single-master-single slave teleoperator systems: a firm grasp of the master is likely to stabilize the system while a loose grasp or the release of the master tends to make the system unstable [6, 9]. Obviously, the main shortcoming of condition ii) is that it relies on the dynamical properties of the human operator to guarantee stability of the system. If some of the human operators loosen their grasps or release the corresponding master(s), the system's stability is no longer guaranteed. As we are going to demonstrate in the following section, these shortcomings can be avoided using the projection-based force reflection principle. •

3.5 Stability of cooperative teleoperator system with projection-based force reflection

The main idea behind the projection-based force reflection principle is to decompose the force reflection signal into the “interaction” and “momentum-generating” components and attenuate the latter while applying the former in full. For details, motivation, and additional explanations, see [17, 18]. A force-reflection scheme is described by the following formula

$$f_{ri} = \frac{\alpha_i(|\hat{f}_{si}^m|)}{|\hat{f}_{si}^m|} \hat{f}_{si}^m + \frac{[\mathbb{I} - \alpha_i](|\hat{\phi}_i|)}{|\hat{\phi}_i|} \hat{\phi}_i, \quad i = 1, \dots, N, \quad (3.37)$$

where f_{ri} is the force reflection signal applied to the motors of the i -th master, \hat{f}_{si}^m is the force signal that is received directly from the remote slave-environment subsystem, $\hat{\phi}_i$ is the estimate of the interaction component described below, and $\alpha_i \in \mathcal{K}_\infty$ is the corresponding weighting function such that $[\mathbb{I} - \alpha_i] \in \mathcal{K}_\infty$, where $\mathbb{I} : \mathbb{R}_+ \rightarrow \mathbb{R}_+$ is the identity function, $\mathbb{I}(r) = r$ for all $r \geq 0$. The term $\hat{\phi}_i$ is calculated according to the formula

$$\hat{\phi}_i := \text{Sat}_{[0,1]} \left\{ \frac{(\hat{f}_{si}^m)^T f_{hi}}{\max\{|f_{hi}|^2, \epsilon_1\}} \right\} f_{hi}, \quad (3.38)$$

where f_{hi} is the human force applied to the master manipulator, $\epsilon_1 > 0$ is a sufficiently small constant, and $\text{Sat}\{x\}_{[a,b]} := \max\{a, \min\{x, b\}\}$. Algorithm (3.38) estimates the interaction component of the environmental force as the component that is directed against the human force with magnitude bounded by the magnitude of the human force; specifically, it calculates $\hat{\phi}_i$ as the projection of \hat{f}_{si}^m onto the subspace spanned by the human force estimate f_{hi} .

The following proposition can be considered as an extension of Proposition 3.4.1 to the case of projection-based force reflection.

Proposition 3.5.1 *Consider the i -th master device (3.16), (3.17) equipped with the projection-based force reflection algorithm (3.37), (3.38). Suppose Assumption 5 holds for this master device with ISS gain $\gamma_{mi}^0 \in \mathcal{K}_\infty$. Then the following statements are valid.*

i) If the i -th human operator dynamics satisfy Assumption 6, the closed-loop master device is ISS with ISS gain

$$\bar{\gamma}_{mi} := \gamma_{mi}^0 \circ \alpha_i. \quad (3.39)$$

ii) If the i -th human operator dynamics satisfy Assumptions 7, 8, the closed-loop master device is ISS with ISS gain

$$\bar{\gamma}_{mi} := \sigma_{1i}^{-1} \circ \sigma_{2i} \circ \left[\left[\gamma_{mi}^0 \right]^{-1} \circ \sigma_{1i}^{-1} \circ \sigma_{2i} + \epsilon_0 \cdot \alpha_i \circ \mu_{i0} \right]^{-1} \circ \alpha_i. \quad (3.40)$$

Proof. First, (3.38) implies that, if $\hat{\phi}_i \neq 0$, then $\hat{\phi}_i$ is collinear to f_{hi} , i.e.,

$$\frac{\hat{\phi}_i}{|\hat{\phi}_i|} = \frac{f_{hi}}{|f_{hi}|}.$$

Therefore,

$$\begin{aligned} f_{hi} - \frac{[\mathbb{I} - \alpha_i](|\hat{\phi}_i|)}{|\hat{\phi}_i|} \hat{\phi}_i &= f_{hi} - \frac{[\mathbb{I} - \alpha_i](|\hat{\phi}_i|)}{|f_{hi}|} f_{hi} \\ &= f_{hi} \left(1 - \frac{[\mathbb{I} - \alpha_i](|\hat{\phi}_i|)}{|f_{hi}|} \right) = f_{hi} \left(\frac{|f_{hi}| - [\mathbb{I} - \alpha_i](|\hat{\phi}_i|)}{|f_{hi}|} \right). \end{aligned} \quad (3.41)$$

Note also, that (3.38) implies $|\hat{\phi}_i| \leq |f_{hi}|$, which implies

$$\frac{|f_{hi}| - [\mathbb{I} - \alpha_i](|\hat{\phi}_i|)}{|f_{hi}|} \geq \frac{|f_{hi}| - [\mathbb{I} - \alpha_i](|f_{hi}|)}{|f_{hi}|} = \frac{\alpha_i(|f_{hi}|)}{|f_{hi}|} \geq 0. \quad (3.42)$$

Now, suppose the dynamics of i -th human operator satisfy Assumption 6. Calculating the time derivative of V_{mi} along the trajectories of (3.16), (3.37), (3.38), and using (3.41), (3.42), we have

$$\begin{aligned}
\dot{V}_{mi} &= \frac{\partial V_{mi}}{\partial x_{mi}} f_{mi}(x_{mi}) + \frac{\partial V_{mi}}{\partial x_{mi}} g_{mi}(x_{mi}) \left[f_{hi} - \frac{\alpha_i(|\hat{f}_{si}^m|)}{|\hat{f}_{si}^m|} \hat{f}_{si}^m - \frac{[\mathbb{I}-\alpha_i](|\hat{\phi}_i|)}{|\hat{\phi}_i|} \hat{\phi}_i \right] \\
&\leq \frac{\partial V_{mi}}{\partial x_{mi}} f_{mi}(x_{mi}) + \frac{\partial V_{mi}}{\partial x_{mi}} g_{mi}(x_{mi}) \left[f_{hi} \left(\frac{|\hat{f}_{si}^m| - [\mathbb{I}-\alpha_i](|\hat{\phi}_i|)}{|\hat{f}_{si}^m|} \right) - \frac{\alpha_i(|\hat{f}_{si}^m|)}{|\hat{f}_{si}^m|} \hat{f}_{si}^m \right] \\
&\leq \frac{\partial V_{mi}}{\partial x_{mi}} f_{mi}(x_{mi}) - \frac{\partial V_{mi}}{\partial x_{mi}} g_{mi}(x_{mi}) \frac{\alpha_i(|\hat{f}_{si}^m|)}{|\hat{f}_{si}^m|} \hat{f}_{si}^m \\
&\leq \frac{\partial V_{mi}}{\partial x_{mi}} f_{mi}(x_{mi}) + \left| \frac{\partial V_{mi}}{\partial x_{mi}} g_{mi}(x_{mi}) \right| \cdot \alpha_i(|\hat{f}_{si}^m|).
\end{aligned} \tag{3.43}$$

Remark 2 then implies that $\dot{V}_{mi} \leq -\sigma_0(V_{mi})$ if $|x_{mi}| \geq \sigma_{2i}^{-1} \circ \sigma_{1i} \circ \gamma_{mi}^0 \circ \alpha_i(|\hat{f}_{si}^m|)$, which implies that the system is ISS with ISS gain $\bar{\gamma}_{mi} \in \mathcal{K}_\infty$ defined by (3.39). On the other hand, suppose the i -th human operator dynamics satisfy Assumptions 7, 8. In this case, the inequalities for time derivative of V_{mi} along the trajectories of (3.16), (3.37), (3.38), have a form

$$\begin{aligned}
\dot{V}_{mi} &= \frac{\partial V_{mi}}{\partial x_{mi}} f_{mi}(x_{mi}) + \frac{\partial V_{mi}}{\partial x_{mi}} g_{mi}(x_{mi}) \left[f_{hi} - \frac{\alpha_i(|\hat{f}_{si}^m|)}{|\hat{f}_{si}^m|} \hat{f}_{si}^m - \frac{[\mathbb{I}-\alpha_i](|\hat{\phi}_i|)}{|\hat{\phi}_i|} \hat{\phi}_i \right] \\
&\leq \frac{\partial V_{mi}}{\partial x_{mi}} f_{mi}(x_{mi}) + \frac{\partial V_{mi}}{\partial x_{mi}} g_{mi}(x_{mi}) \left[f_{hi} \left(\frac{|\hat{f}_{si}^m| - [\mathbb{I}-\alpha_i](|\hat{\phi}_i|)}{|\hat{f}_{si}^m|} \right) - \frac{\alpha_i(|\hat{f}_{si}^m|)}{|\hat{f}_{si}^m|} \hat{f}_{si}^m \right] \\
&\leq \frac{\partial V_{mi}}{\partial x_{mi}} f_{mi}(x_{mi}) - \epsilon_0 \cdot \left| \frac{\partial V_{mi}}{\partial x_{mi}} g_{mi}(x_{mi}) \right| \cdot |f_{hi}| \left(\frac{|\hat{f}_{si}^m| - [\mathbb{I}-\alpha_i](|\hat{\phi}_i|)}{|\hat{f}_{si}^m|} \right) - \frac{\partial V_{mi}}{\partial x_{mi}} g_{mi}(x_{mi}) \frac{\alpha_i(|\hat{f}_{si}^m|)}{|\hat{f}_{si}^m|} \hat{f}_{si}^m \\
&\leq \frac{\partial V_{mi}}{\partial x_{mi}} f_{mi}(x_{mi}) - \epsilon_0 \cdot \left| \frac{\partial V_{mi}}{\partial x_{mi}} g_{mi}(x_{mi}) \right| \cdot |f_{hi}| \cdot \frac{\alpha_i(|\hat{f}_{si}^m|)}{|\hat{f}_{si}^m|} + \left| \frac{\partial V_{mi}}{\partial x_{mi}} g_{mi}(x_{mi}) \right| \cdot \alpha_i(|\hat{f}_{si}^m|) \\
&\leq \frac{\partial V_{mi}}{\partial x_{mi}} f_{mi}(x_{mi}) - \epsilon_0 \cdot \left| \frac{\partial V_{mi}}{\partial x_{mi}} g_{mi}(x_{mi}) \right| \cdot \alpha_i(|f_{ri}|) + \left| \frac{\partial V_{mi}}{\partial x_{mi}} g_{mi}(x_{mi}) \right| \cdot \alpha_i(|\hat{f}_{si}^m|) \\
&\leq \frac{\partial V_{mi}}{\partial x_{mi}} f_{mi}(x_{mi}) + \left| \frac{\partial V_{mi}}{\partial x_{mi}} g_{mi}(x_{mi}) \right| \cdot \left[-\epsilon_0 \cdot \alpha_i \circ \mu_{i0}(|x_{mi}|) + \alpha_i(|\hat{f}_{si}^m|) \right].
\end{aligned} \tag{3.44}$$

Using (3.30), we see that $\dot{V}_{mi} \leq -\sigma_0(V_{mi})$ is guaranteed if the following condition holds

$$\chi_{mi}^{-1}(|x_{mi}|) \geq -\epsilon_0 \cdot \alpha_i \circ \mu_{i0}(|x_{mi}|) + \alpha_i(|\hat{f}_{si}^m|), \tag{3.45}$$

where $\chi_{mi} := \sigma_{2i}^{-1} \circ \sigma_{1i} \circ \gamma_{mi}^0 \in \mathcal{K}$. The inequality (3.45) is equivalent to

$$|x_{mi}| \geq \left[\left[\gamma_{mi}^0 \right]^{-1} \circ \sigma_{1i}^{-1} \circ \sigma_{2i} + \epsilon_0 \cdot \alpha_i \circ \mu_{i0} \right]^{-1} \circ \alpha_i(|\hat{f}_{si}^m|).$$

This implies that the system is ISS with ISS gain defined by (3.40). The proof is complete. •

Remark 8. Proposition 3.5.1 presents formulas for calculation of the ISS gain of a master subsystem in the presence of interaction with a human hand for the case where the force reflection algorithm is built upon the projection-based principle. It is straightforward to see that,

in both cases (3.39) and (3.40), an arbitrarily low ISS gain $\gamma_{mi}^* \in \mathcal{K}_\infty$ can be guaranteed by an appropriate choice of the weighting function $\alpha_i \in \mathcal{K}_\infty$. In addition, an arbitrarily low $\gamma_{mi}^* \in \mathcal{K}_\infty$ can be achieved in (3.40) if the human hand impedance function $\mu_{i0} \in \mathcal{K}_\infty$ is sufficiently large. Specifically, denote

$$\mu_i^\sharp(s) := \alpha_i^{-1} \circ \frac{1}{\epsilon_0} \left[\alpha_i \circ [\gamma_{mi}^*]^{-1} - [\gamma_{mi}^0]^{-1} \right] \circ \sigma_{1i}^{-1} \circ \sigma_{2i}(s). \quad (3.46)$$

From (3.40), it is easy to derive that $\mu_{i0}(s) \geq \mu_i^\sharp(s)$ implies $\bar{\gamma}_{mi}(s) \leq \gamma_{mi}^*$. Also, in the linear case, formulas (3.39) and (3.40) become

$$\bar{\gamma}_{mi} := \gamma_{mi}^0 \cdot \alpha_i \quad \text{and} \quad \bar{\gamma}_{mi} := \frac{\alpha_i \cdot \gamma_{mi}^0}{1 + \alpha_i \cdot \frac{\sigma_{1i}}{\sigma_{2i}} \cdot \epsilon_0 \cdot \mu_{i0} \cdot \gamma_{mi}^0},$$

respectively. •

The theorem below presents stability results for the networked cooperative teleoperator system with projection-based force reflection. Similarly to the case of Theorem 3.4.2 from the previous section, the input-to-state stability here is understood in the sense of [13, Definition 1], where again the input disturbances are the communication errors $\delta_{fi}, \delta_{bi}, i = 1, \dots, N$.

Theorem 3.5.2 *Consider a cooperative networked force reflecting teleoperator system (3.7)–(3.10), (3.16), (3.17) equipped with a projection-based force reflection algorithm (3.37), (3.38). Suppose Assumptions 2, 3, 4, 5 hold. Then there exist $\alpha_i^* \in \mathcal{K}_\infty, i \in \{1, \dots, N\}$ such that the cooperative teleoperator system is input-to-state stable if for each $i \in \{1, \dots, N\}$, at least one of the following conditions holds:*

- i) the dynamics of the i -th human operator satisfy Assumption 6, and the corresponding weighting coefficient $\alpha_i(\cdot)$ in (3.37) satisfies $\alpha_i(s) \leq \alpha_i^*(s)$ for all $s \geq 0$;*
- ii) the dynamics of the i -th human operator satisfy Assumptions 7, 8, and the function $\mu_{i0}(\cdot)$ is (3.27) satisfies*

$$\mu_{i0}(s) \geq \alpha_i^{-1} \circ \frac{1}{\epsilon_0} \cdot \left[\alpha_i \circ [\alpha_i^*]^{-1} - \mathbb{I} \right] \circ [\gamma_{mi}^0]^{-1} \circ \sigma_{1i}^{-1} \circ \sigma_{2i}(s)$$

for all $s \geq 0$. •

Proof. *The results of Theorem 3.5.2 can be obtained by combination of Proposition 3.5.1 and the small-gain arguments in Section 3.3. •*

Remark 9. Theorem 3.5.2 presents conditions for stability of networked cooperative teleoperator systems with projection-based force reflection. The fundamental difference with the case of direct force reflection (described by Theorem 3.4.2) is that in the case of projection-based force reflection the stability does not require low master ISS gains and/or does not necessarily rely on the properties of the human operators' dynamic responses. Instead, part i) of Theorem 3.5.2 demonstrates that stability can be achieved by an appropriate assignment of the weighting coefficients in the projection-based force reflection algorithms. This results holds irrespective of the human operators' behaviour as long as the human operators do not perform destabilizing actions (*i.e.*, as long as the dynamics of the human operators satisfy Assumption 6). On the other hand, part ii) demonstrates that if the weighting coefficients are not assigned properly, the stability of the overall system can still be guaranteed if the corresponding human operators apply additional stabilizing actions. •

3.6 Experimental results

In this section, we briefly discuss the results of the experimental investigation that was performed to validate the theory presented above. The experimental setup is shown schematically in Figure 3.4. It consists of a two-master-two-slave cooperative force reflection teleoperator system, where two PHANTOM Omni devices are used as the master manipulators, while the slaves are represented by two simulated models of the PHANTOM Premium 1.5A devices implemented in a virtual environment. The PHANTOM Omni devices have 6 DOF position sensing and 3 DOF force feedback, and are manufactured by SensAble Technologies Inc. The simulation is run at a sampling frequency 1000Hz. The OpenHaptics Toolkit is used for programming of the haptic devices. The virtual objects are rendered using OpenGL. The host computers are connected over the network using the TCP/IP network protocol. On top of the time-varying component generated by communication over TCP/IP, the communication delay also has a constant component which is created using internal buffers.

The implementation of the projection-based force reflection principle requires information about human forces applied to the master devices. For our experiments, a high-gain force observer was designed that provides an estimate of the human forces applied to the master

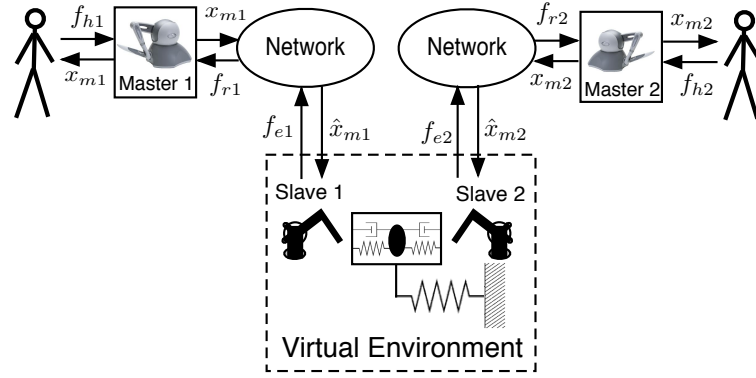


Figure 3.4: Experimental setup scheme

devices. The observer design follows the guidelines outlined in [32], and is based on a model of the PHANTOM Omni device that was developed and validated as a part of this research project; all the details, however, are skipped due to space constraints, and will be published elsewhere.

We have completed several experiments that target different aspects of the teleoperator system performance. In the first experiment, a rectangular object with mass $m = 1$ kg, width $l = 0.1$ m, and stiffness $k = 1000$ N/m was implemented in the virtual environment. The object is connected to the ground at the origin using a spring with stiffness $K = 10$ N/m. The object has an initial velocity of 0.04 m/s in the positive direction of x -axis. The goal pursued by the human operators is to cooperatively stabilize the object at the origin by pressing against its sides. This experiment was performed in the presence of negligible communication delays as well as significantly large irregular communication delays, and for different values of weighting coefficients α_i , $i = 1, 2$ in (3.37). Typical examples of experimental results for large irregular communication delays are presented in Figures 3.6-3.8. In these experiments, the delay in each direction is a sum of a constant component of 0.5 s and an additional random component with maximum magnitude of 0.05 s; an example of the resulting one-way delay is presented in Figure 3.5. The total round trip communication delay in this experiment, therefore, varies randomly between 1s and 1.1 s. Overall, this experiment demonstrates that stable telemanipulation can be achieved in the case of direct force reflection as well as in the case of projection-based force reflection for a wide range of coefficients α_i in (3.37). However, it appears that in the case of projection-based FR, the teleoperation process is generally more

stable and the interaction forces are generally lower. These facts are in agreement with our theoretical considerations presented above. Indeed, stable cooperative teleoperation is guaranteed in the case of projection-based force reflection with sufficiently low weighting functions α_i ; however, stable teleoperation can also be achieved in the case of direct force reflection ($\alpha_i = 1$) at will by appropriate actions of the human operators which, in particular, may include increasing of the human hand impedance. In the latter case, therefore, the stabilization process can reasonably be expected to appear less regular, and increased human hand impedance would typically result in higher interaction forces. To demonstrate the stability improvement

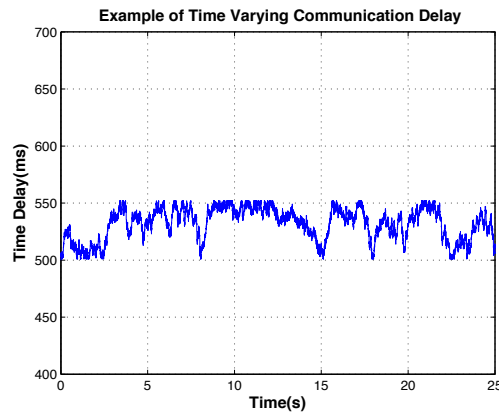


Figure 3.5: Example of communication delay

brought in by using the projection-based FR principle, we need to address a situation where the human operator is prevented from stabilizing the teleoperator system. The ultimate case of such a situation is when the human operators release the master devices. In the second experiment, we address a situation where one of the master devices is released by the human operator. We simulate a pulse of interaction forces between slaves and subsequently measure the corresponding induced master motion of the released master, for different values of α_i . The results of this experiment are shown in Figure 3.9. It is clear that the same interaction between slaves creates different amounts of movement of the released master; specifically, the amount of induced master motion [7] is the highest for direct force reflection ($\alpha_i = 1$) and decreases to zero as α_i decreases to zero. This effect can be easily understood by considering the formula in (3.37). Since in this experiment, there is no interaction between the human operator and the master (i.e., the human force is zero), the projection-based component is zero, and

the interaction forces between slaves is therefore transferred to the motors of the master with gains α_i . This is also clearly seen in Figure 3.9, left, where the reflected forces are shown, and these forces decrease to zero as α_i decreases to zero. Overall, this experiment demonstrates the mechanism of stability improvement brought in by using the projection-based force reflection principle, which is described theoretically in Theorem 3.5.2.

In the third experiment, a pulse of interaction forces between slaves is simulated as in the second experiment, however, in this case the human operator holds the master device firmly. The purpose of this experiment is to compare slave interaction forces with the forces reflected to the master devices when the latter is held by the operator, and thus evaluate the transparency deterioration introduced by using the projection based force reflection. Samples of this experiment are shown in Figure 3.10, which demonstrate that in steady state these forces are identical. This implies that in steady state there is no transparency loss. There is, however, some transparency loss during the transient process, which is partially attributed to the use of a human force estimator instead of direct human force measurement. This issue will be addressed in future research.

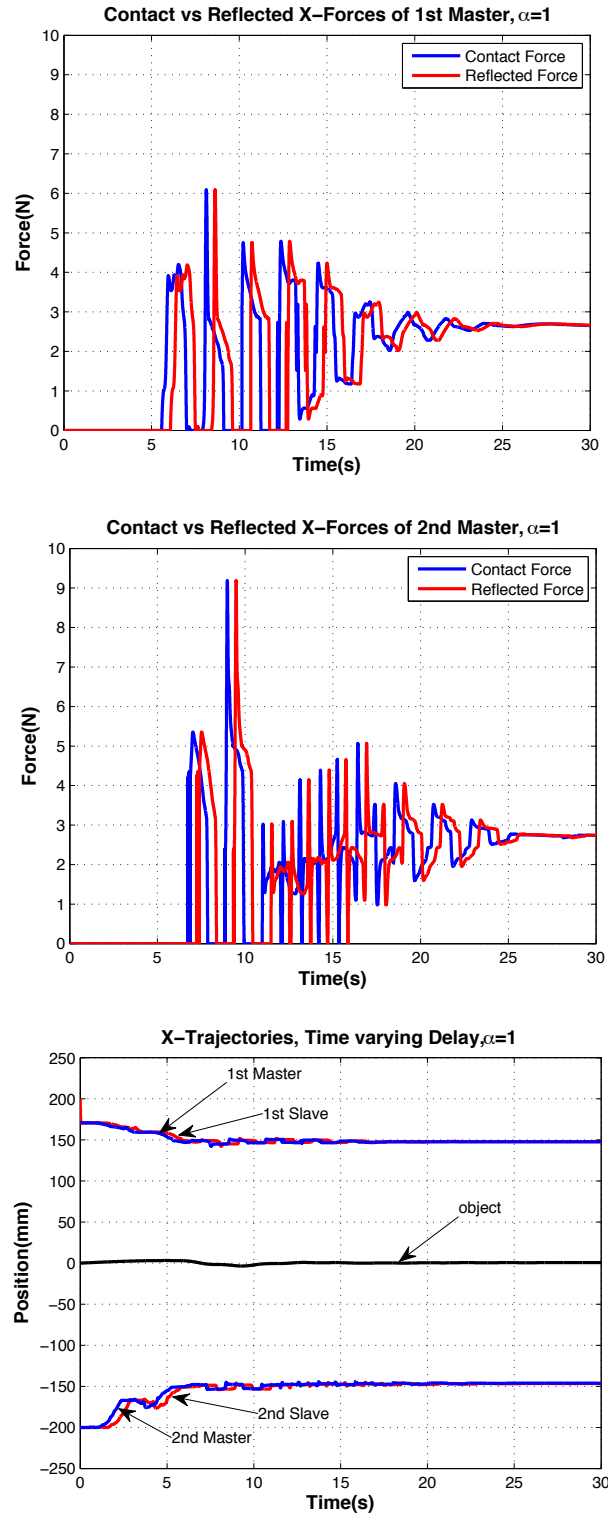


Figure 3.6: Experiment I, irregular communication delays, direct force reflection ($\alpha = 1$). Contact X-Force experienced by Slave 1 and X-Force reflected to Master 1 (top); contact X-Force experienced by Slave 2 and X-Force reflected to Master 2 (middle); X-Trajectories of masters, slaves and object (bottom)

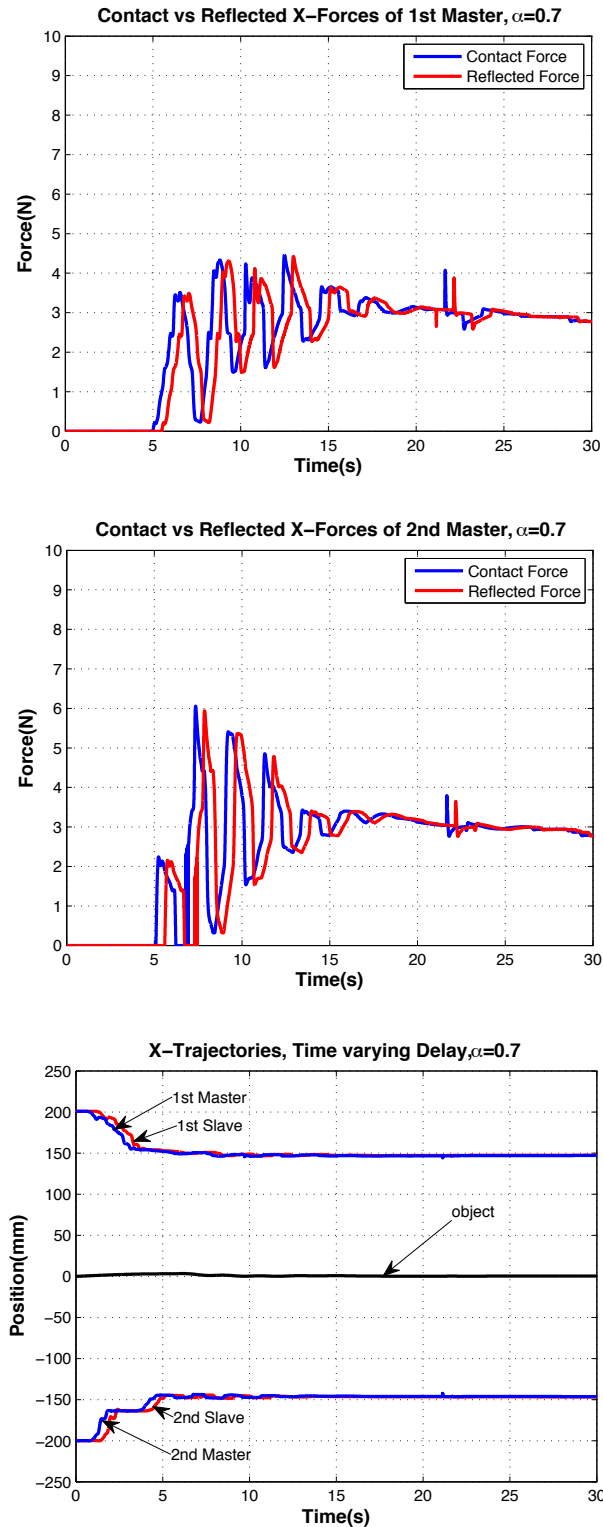


Figure 3.7: Experiment I, irregular communication delays, projection-based force reflection ($\alpha = 0.7$). Contact X-Force experienced by Slave 1 and X-Force reflected to Master 1 (top); contact X-Force experienced by Slave 2 and X-Force reflected to Master 2 (middle); X-Trajectories of masters, slaves and object (bottom)

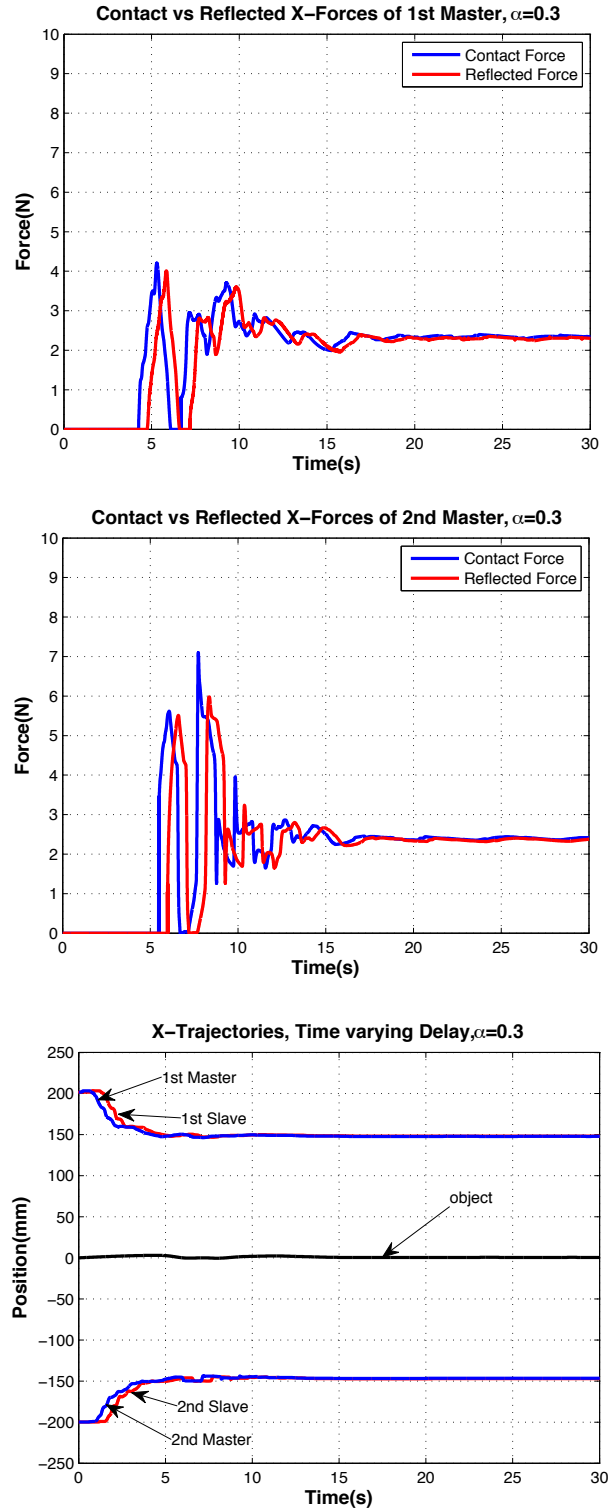


Figure 3.8: Experiment I, irregular communication delays, projection-based force reflection ($\alpha = 0.3$). Contact X-Force experienced by Slave 1 and X-Force reflected to Master 1 (top); contact X-Force experienced by Slave 2 and X-Force reflected to Master 2 (middle); X-Trajectories of masters, slaves and object (bottom)

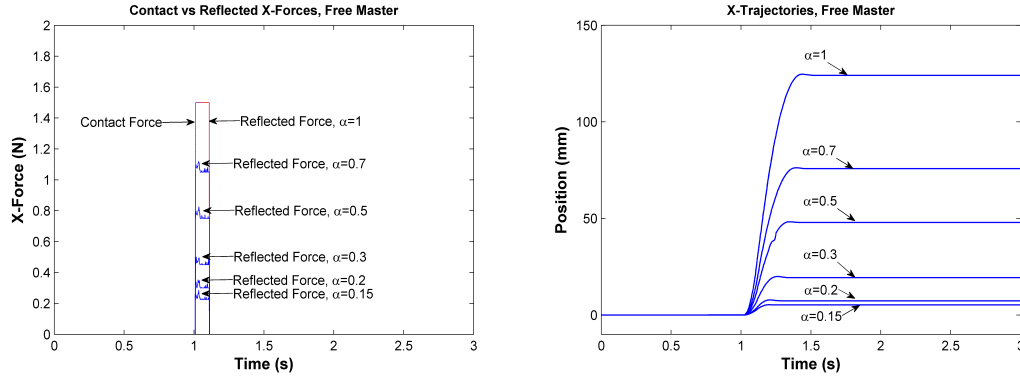


Figure 3.9: Experiment II: A pulse of interaction forces between slaves, operator releases the master. Left: Contact force and reflected forces for different $\alpha \in (0, 1]$; Right: the corresponding induced master motions

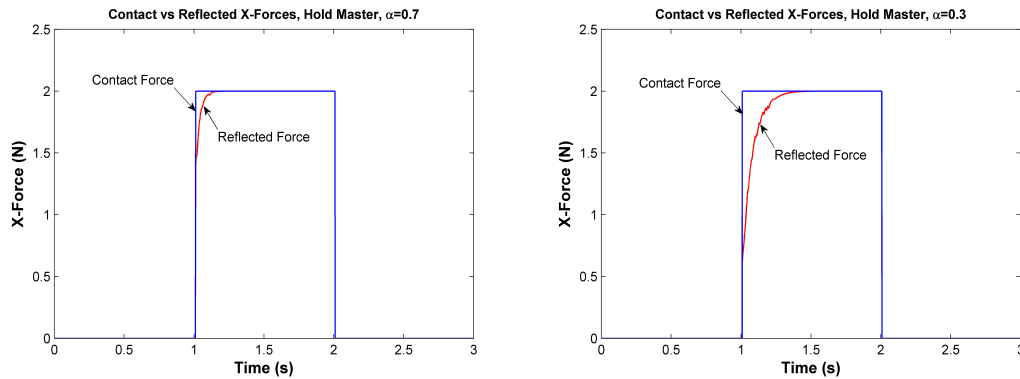


Figure 3.10: Experiment III: A pulse of interaction forces between slaves, operator holds the master. Left: Contact force vs. reflected force for $\alpha = 0.7$; Right: contact force vs. reflected force for $\alpha = 0.3$

3.7 Conclusions

In this work, we presented developments for the small gain approach to the design of cooperative force reflecting teleoperators in the presence of network-induced communication constraints. We demonstrated that the small gain conditions for stability of the cooperative teleoperator system can be reduced to the requirement that the master devices have sufficiently low

input-to-output gains in the admittance configuration. Furthermore, using appropriately specified versions of the passivity assumption imposed on the human dynamics, we derived explicit formulas that demonstrate how the IOS gains of the master devices depend on the properties of human dynamics and the type of force reflection algorithm. In particular, we showed that the use of projection-based force reflection algorithms allows us to guarantee stability of the force reflecting teleoperator system in the presence of irregular communication delays regardless of the dynamical properties (in particular, damping and stiffness) of the operator's hands. Experimental results were presented to confirm the theoretical developments.

Bibliography

- [1] David Angeli. Input-to-state stability of pd-controlled robotic systems. *Automatica*, 35(7):1285–1290, 1999.
- [2] Rita Bacocco and Claudio Melchiorri. Lq control design of cooperative teleoperation systems. In *Proceedings of the 2009 International Conference on Advanced Robotics*, pages 1–6. IEEE, 2009.
- [3] Sergey Dashkovskiy, Björn S Ruffer, and Fabian R Wirth. An iss small gain theorem for general networks. *Mathematics of Control, Signals, and Systems*, 19(2):93–122, 2007.
- [4] Aleksandr Lvovich Fradkov, Ilija Vasilevich Miroshnik, and Vladimir Olegovič Nikiforov. *Nonlinear and Adaptive Control of Complex Systems*, volume 491. Springer, 1999.
- [5] Blake Hannaford. Stability and performance tradeoffs in bi-lateral telemanipulation. In *Proceedings of the 1989 IEEE International Conference on Robotics and Automation*, pages 1764–1767. IEEE, 1989.
- [6] Blake Hannaford. Stability and performance tradeoffs in bi-lateral telemanipulation. In *Proceedings of the 1989 IEEE International Conference on Robotics and Automation*, pages 1764–1767, 1989.

- [7] Katherine J. Kuchenbecker and Gunter Niemeyer. Induced master motion in force-reflecting teleoperation. *Transactions-American Society of Mechanical Engineers Journal of Dynamic Systems Measurement and Control*, 128(4):800–810, 2006.
- [8] Dale A Lawrence. Stability and transparency in bilateral teleoperation. *IEEE Transactions on Robotics and Automation*, 9(5):624–637, 1993.
- [9] Dale A. Lawrence. Stability and transparency in bilateral teleoperation. *IEEE Transactions on Robotics and Automation*, 9:624–637, October 1993.
- [10] Pawel Malysz and Shahin Sirouspour. Cooperative teleoperation control with projective force mappings. In *Proceedings of the 2010 IEEE Haptics Symposium*, pages 301–308. IEEE, 2010.
- [11] Carolina Passenberg, Angelika Peer, and Martin Buss. Model-mediated teleoperation for multi-operator multi-robot systems. In *Proceedings of the 2010 IEEE/RSJ International Conference on Intelligent Robots and Systems*, pages 4263–4268. IEEE, 2010.
- [12] Iliia G. Polushin and Sergey N. Dashkovskiy. A small gain framework for networked cooperative teleoperation. In *Proceedings of the 8th IFAC Symposium on Nonlinear Control Systems*, pages 90–95, 2010.
- [13] Iliia G. Polushin, Peter X. Liu, and Chung-Horng Lung. A control scheme for stable force-reflecting teleoperation over IP networks. *IEEE Transactions on Systems, Man, and Cybernetics, Part B: Cybernetics*, 36(4):930–939, 2006.
- [14] Iliia G. Polushin, Peter Xiaoping Liu, and Chung-Horng Lung. A control scheme for stable force-reflecting teleoperation over ip networks. *IEEE Transactions on Systems, Man, and Cybernetics, Part B: Cybernetics*, 36(4):930–939, 2006.
- [15] Iliia G. Polushin, Abdelhamid Tayebi, and Horacio J. Marquez. Control schemes for stable teleoperation with communication delay based on ios small gain theorem. *Automatica*, 42(6):905–915, 2006.

- [16] Ilia G. Polushin, Peter Xiaoping Liu, and Chung-Horng Lung. A force-reflection algorithm for improved transparency in bilateral teleoperation with communication delay. *IEEE/ASME Transactions on Mechatronics*, 12(3):361–374, 2007.
- [17] Ilia G. Polushin, Peter Xiaoping Liu, and Chung-Horng Lung. A force-reflection algorithm for improved transparency in bilateral teleoperation with communication delay. *IEEE/ASME Transactions on Mechatronics*, 12(3):361–374, 2007.
- [18] Ilia G. Polushin, Peter Xiaoping Liu, and Chung-Horng Lung. Stability of bilateral teleoperators with projection-based force reflection algorithms. In *Proceedings of the 2008 IEEE International Conference on Robotics and Automation*, pages 677–682. IEEE, 2008.
- [19] Ilia G. Polushin, Horacio J. Marquez, Abdelhamid Tayebi, and Peter Xiaoping Liu. A multichannel ios small gain theorem for systems with multiple time-varying communication delays. *IEEE Transactions on Automatic Control*, 54(2):404–409, 2009.
- [20] Ilia G. Polushin, Peter X. Liu, and Chung-Horng Lung. Human dynamics and stability of teleoperator systems with generalized projection-based force reflection algorithms. In *18th IFAC World Congress*, pages 338–343, Milan, Italy, 2011.
- [21] Ilia G. Polushin, Amir Takhmar, and Rajni V. Patel. Small gain design of cooperative teleoperator system with projection-based force reflection. In *Proceedings of the 2011 IEEE/RSJ International Conference on Intelligent Robots and Systems*, pages 653–658. IEEE, 2011.
- [22] Ilia G. Polushin, Amir Takhmar, and Rajni V. Patel. Small-gain design of networked cooperative bilateral teleoperators. In *Proceedings of the 2011 IEEE International Conference on Robotics and Automation*, pages 892–897. IEEE, 2011.
- [23] Ilia G. Polushin, Sergey N. Dashkovskiy, Amir Takhmar, and Rajni V. Patel. A small gain framework for networked cooperative force-reflecting teleoperation. *Automatica*, 49(2): 338 – 348, 2013.

- [24] Carsten Preusche. Telerobotics. In *Springer Handbook of Robotics*, pages 741–757. Springer, 2008.
- [25] Arjan van der Schaft and AJ Schaft. *L2-Gain and Passivity in Nonlinear Control*. Springer-Verlag New York, Inc., 1999.
- [26] Peyman Setoodeh, Shahin Sirouspour, and Ali Shahdi. Discrete-time multi-model control for cooperative teleoperation under time delay. In *Proceedings of the 2006 IEEE International Conference on Robotics and Automation*, pages 2921–2926. IEEE, 2006.
- [27] Shahin Sirouspour. Modeling and control of cooperative teleoperation systems. *IEEE Transactions on Robotics*, 21(6):1220–1225, 2005.
- [28] Eduardo D. Sontag. Smooth stabilization implies coprime factorization. *IEEE Transactions on Automatic Control*, 34(4):435–443, 1989.
- [29] Eduardo D. Sontag. Input to state stability: Basic concepts and results. In *Nonlinear and Optimal Control Theory*, pages 163–220. Springer, 2006.
- [30] Eduardo D. Sontag and Yuan Wang. On characterizations of the input-to-state stability property. *Systems & Control Letters*, 24(5):351–359, 1995.
- [31] Eduardo D. Sontag and Yuan Wang. On characterizations of input-to-state stability with respect to compact sets. In *Proceedings of IFAC Non-Linear Control Systems Design Symposium NOLCOS'95*, pages 226–231, Tahoe City, CA, June 1995.
- [32] Alexander Stotsky and Ilya Kolmanovsky. Application of input estimation techniques to charge estimation and control in automotive engines. *Control Engineering Practice*, 10(12):1371–1383, 2002.
- [33] Andrew R. Teel. Connections between razumikhin-type theorems and the iss nonlinear small gain theorem. *IEEE Transactions on Automatic Control*, 43(7):960–964, 1998.
- [34] Xiao-Gang Wang, Mehrdad Moallem, and Rajnikant V. Patel. An internet-based distributed multiple-telerobot system. *IEEE Transactions on Systems, Man and Cybernetics, Part A: Systems and Humans*, 33(5):627–634, 2003.

Chapter 4

Experimental Evaluation of PBFR

Algorithm on MIS Setup

The material presented in this chapter is submitted to *IEEE Transactions on Control System Technology*.

4.1 Introduction

Robot-assisted minimally invasive surgery (RAMIS) is a particular type of minimally invasive surgery (MIS) which aims to provide surgeons with better vision, maneuverability and control in comparison with the conventional laparoscopy, through the use of specialized robotic devices. Typically, RAMIS systems have the structure of a teleoperation system, where the master device is controlled by the surgeon while the slave robot executes specific surgical tasks. Implementation of haptic feedback in RAMIS has recently received great interest in the medical robotics community [26, 12, 27]. When combined with visual feedback, haptic feedback provides surgeons with an enhanced feeling of tool/tissue interaction, which may lead to faster, more accurate, and overall more effective execution of some common surgical tasks. Although it was previously demonstrated that implementation of haptic feedback may lead to higher performance in some surgical procedures, currently available commercial telerobotic MIS systems do not provide force feedback. One of the main reasons is the stability issue that is inherent in force reflecting teleoperator systems. Such instability can be a result of different factors such

as the phase shift due to time delay in the communication channel between the master(s) and the slave(s), or because of the existence of uncompensated dynamics of the master and/or the slave robots (which occurs, for example, due to modeling uncertainty). To avoid instability while at the same time provide the surgeon with information about contact forces, sensory substitution force feedback such as graphical force displays can be used [28, 10, 24]. Substantial research has been published where the performance of a teleoperated MIS system with direct force feedback is compared with other scenarios such as a system with no force feedback or with graphical force feedback [28, 6, 25, 1, 19, 24]; however, only a few papers have evaluated the effect of a specific control scheme on the performance of the surgical tasks [5, 18, 9].

In this work, we investigate and compare the effect of two different types of force reflection algorithms on the stability and performance of a dual-arm haptic teleoperator system for MIS applications. More precisely, the major objective of this paper is to compare the performance of an MIS cooperative teleoperator system with projection-based force reflection (PBFR) with that of the same system with more conventional direct force reflection (DFR), in several typical MIS tasks. The projection-based force reflection principle was introduced for force-reflecting teleoperators in [13] and further developed in [16, 22]. The main idea behind this principle is to decompose the contact force into the interaction and the motion-generating components, and attenuate the latter while applying the former in full. This essentially allows for attenuation of the induced master motion [7] and consequently stability improvement. This is achieved without altering the interaction forces between the human operator's hand and the haptic device. In this work, for the first time, the effect of the PBFR on the performance of surgical teleoperation is evaluated both theoretically and experimentally. The surgical dual-arm MIS teleoperator system used in this work consists of two Haptic Wand Devices manufactured by Quanser Consulting Inc. and two Mitsubishi PA10-7C slave robots with daVinci tools mounted at the end-effectors of the robots. After describing the mathematical model and the controller design, we present stability analysis of the overall teleoperation system which is based on the small-gain arguments. We formulate stability conditions and discuss the effect of the PBFR on the gain of the master subsystem and, consequently, on the overall stability. Experimentally, we investigate and compare the performance of the PBFR and the DFR algorithms implemented on the above mentioned dual-arm MIS teleoperation setup in three simple surgical tasks, which

are knot tightening, pegboard transfer, and object manipulation. Nine subjects participated in these experiments; all the experiments have been performed in the presence of negligible as well as non-negligible communication delays. In each case, the performance of different algorithms was compared, in particular, by evaluating the average forces applied by the slaves and the average induced accelerations of the master devices. The experimental results obtained indicate that, in virtually all cases, the PBFR algorithms demonstrated statistically significant improvement in performance compared to the DFR algorithms.

The paper is organized as follows. In Section 4.2, the dual-arm MIS teleoperator setup used in this paper is described. The mathematical model of the MIS teleoperator system and the control design are presented in Section 4.3. The projection-based force reflection algorithms are described in Section 4.4. In Section 4.5, small gain conditions for stability of the dual-arm MIS teleoperator system used in the experiments are formulated and discussed. The experimental results are discussed in detail in Section 4.6, while the conclusions are given in Section 4.7. Appendix A contains a rigorous stability analysis of the dual-arm MIS teleoperator system with projection-based force reflection.

4.2 Experimental Setup

The two-master-two-slave teleoperator system for MIS used in our experiments is shown in Figure 4.1. The setup was developed and integrated by several past researchers at CSTAR in a project on haptics-enabled teleoperation for minimally invasive surgery [23]. The Master subsystem includes two Haptic Wand Devices manufactured by Quanser Consulting Inc. enhanced to 7-DOF at CSTAR. The slave subsystem consists of two Mitsubishi PA10-7C robots and two daVinci laparoscopic tools which are mounted as end-effectors of the robots. The visualization on the slave side is provided by an endoscopic camera and is displayed to the operator on a 17-inch monitor. Two Windows-based PCs are used as host computers, one for the master devices and one for the slave robots. The computers communicate with each other over a local area network using the UDP protocol. The control algorithms are implemented using the Quanser QuaRC real-time software integrated with Simulink.

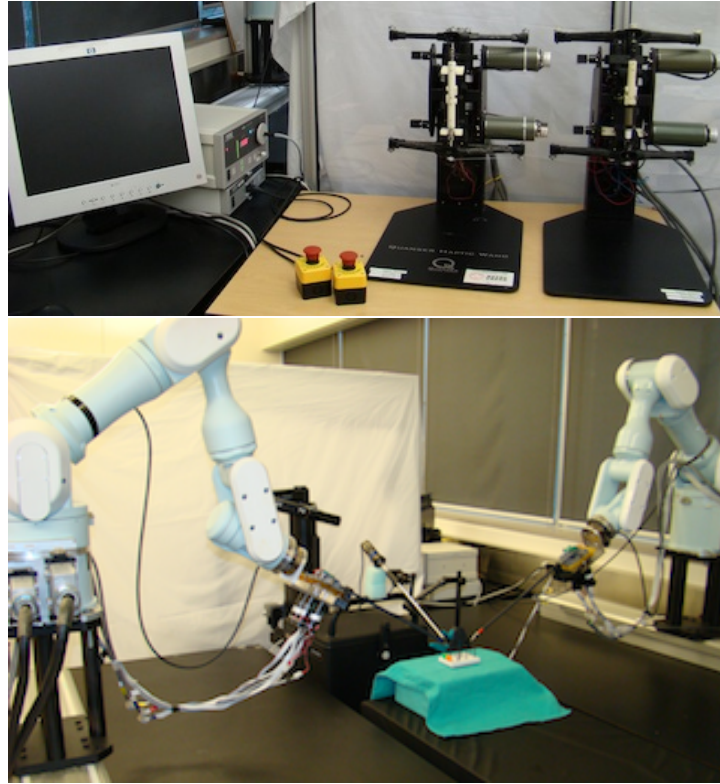


Figure 4.1: Experimental MIS setup: the master subsystem (top); the slave subsystem (bottom).

4.2.1 Haptic Wand devices

The original Quanser Haptic Wand device consisted of two 5-bar linkage mechanisms which are connected to each other with a handle through two Cardan joints. Each 5-bar linkage mechanism is actuated by use of three motors which give 3 degrees of freedom (DOFs) to each mechanism. However, addition of the Cardan joints to connect two 5-bar linkage mechanisms to each other decreases one DOF about the handle. Therefore, the original haptic device is capable of encoding and force reflection in 5 DOFs; three translational DOFs, roll, and pitch. The Haptic Wand devices which are used in our experiments were customized in CSTAR to add yaw and grasping DOFs to the original device [2, 23]. In the new design, the handle of the device is divided into two parts (upper and lower), and each part is independently actuated through additional motors. The modified Haptic Wands therefore have 7 DOFs of motion which include 3 translational DOFs, 2 rotational DOFs (roll and pitch), and 2 DOFs dedicated for grasping (yaw of the upper part of the handle and yaw of the lower part of the handle). As

shown in Figure 4.2, the robot can be represented in joint space by $q_m = \{q_{m1}, q_{m2}, \dots, q_{m8}\}$, and in Cartesian space by $x_m = \{x, y, z, \theta, \phi, \psi_l, \psi_u\}$.

4.2.2 PA10-7C Robots

The Mitsubishi PA10-7C manipulator is a 7 DOFs redundant manipulator. Figure 4.2 (b) (borrowed from [11]) shows all the DOFs, joint structure, and axis designation of the robot. The control architecture of the Mitsubishi PA10-7C robot is composed of four layers: operation control section, motion control, servo controller, and the robotic arm mechanism. The top layer is the operation control section, in which the operator can program the robot to perform a desired task. This is done by a real-time application developed in C++ or MATLAB on a personal computer. The next layer is motion control in which based on the information from level 4, a smooth joint velocity command for the servo-drives level is calculated. The communication between the personal computer and the motion control level is done using the ARCNET protocol. The servo drive level is a box which contains seven drives of the PA10 servomotors. The servo drives of the PA10 robot work both in torque and velocity modes. In both velocity and torque modes, the drives have an internal PI controller [4]. The first level of the PA10 system is the robot manipulator itself.

4.2.3 daVinci Tools

In our experiments, the PA10-7C manipulators are also equipped with da Vinci instruments, which have been modified at CSTAR to measure the interaction forces at the tips of the instruments [24, 23]. The original daVinci tool has 4 DOFs includes roll, pitch, yaw of gripper one and yaw of gripper two. In the customized tool the roll DOF is removed from the instrument to avoid the tangling of the added strain gauges inside of the robot. Therefore, the modified da Vinci tool is capable of motion and torque measurement in 3 DOFs (pitch, yaw of gripper 1, and yaw of gripper 2). To measure translational forces and the torque in roll direction applied by the end-effectors to the environment, an ATI Gamma 6-DOFs force/torque sensor is placed between the PA10-7C arm and the daVinci instrument. The calibration has been done to remove errors on the measurement such as the initial offsets and gravity effect of the daVinci tool

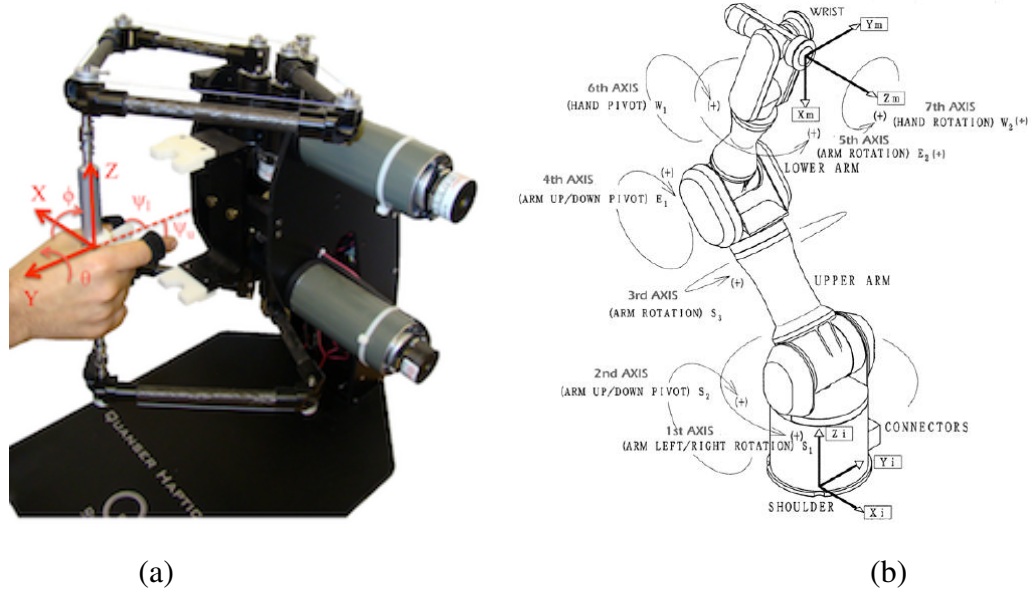


Figure 4.2: (a) Task space coordinates of the Haptic Wand device [23]; (b) Structure of the Mitsubishi PA10-7C manipulator [11].

on the force measurements [23].

4.3 Mathematical Models and Controller Design

The overall structure of the system is shown in Figure 4.3. The block diagram of the control system for each master-slave pair is shown in Figure 4.4. This control structure is the modified version of the one presented in [23]; the difference between the two is essentially that the current structure includes the projection-based force reflection algorithm. As described in the previous section, the master and the slave manipulators in each master-slave pair have dissimilar kinematics and different number of DOFs (each master has 7 Cartesian DOFs while each slave has 6 Cartesian DOFs of the Mitsubishi PA10-7C manipulator and 3 additional DOFs provided by the daVinci instrument). The mapping between the master and the slave coordinates are organized as follows. For each i -th ($i = 1, 2$) master device, the three translational degrees of freedom x_{mi} , y_{mi} , z_{mi} as well as the roll coordinate θ_{mi} serve as the reference trajectories for the corresponding DOFs of the Mitsubishi PA10-7C slave manipulator. The remaining Cartesian coordinates of the i -th master, *i.e.*, the pitch ϕ_{mi} and the two yaw angles ψ_{mli} and ψ_{mui} , serve as

the reference trajectories for the corresponding DOFs of the daVinci instrument. The reference trajectories for the pitch and the yaw of the the Mitsubishi PA10-7C slave manipulators are constantly set equal to zero.

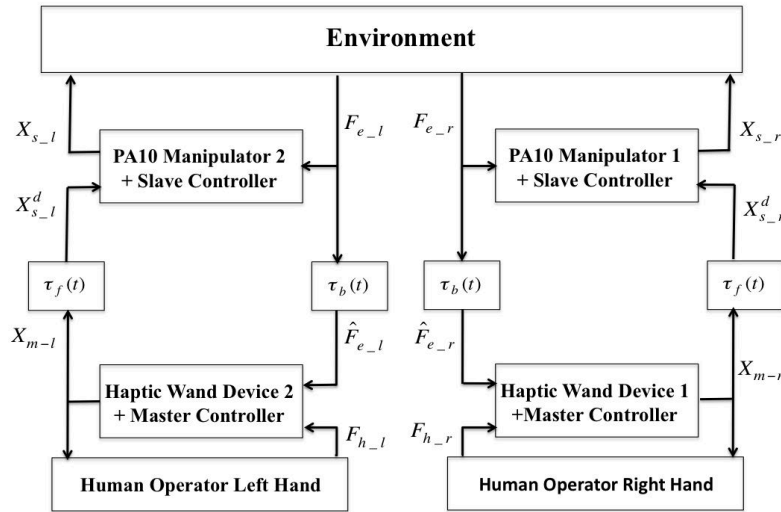


Figure 4.3: The structure of the teleoperation system

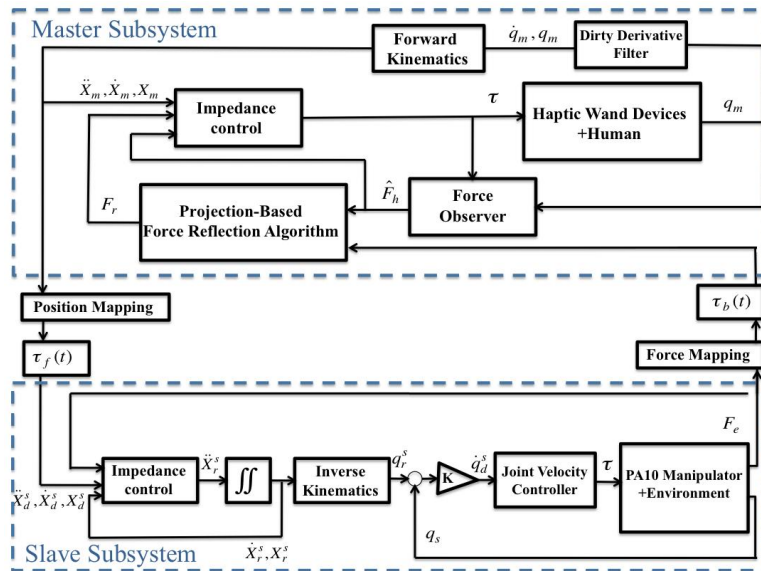


Figure 4.4: Block diagram of each master/slave system

4.3.1 Master Subsystems

The mathematical model of the modified Haptic Wands was developed in [2, 23]. The dynamics of the modified Haptic Wand can be described by two separate equations, which describe the dynamic of the original manipulator itself and the dynamics of the additional two DOFs, respectively; these dynamical equations are decoupled from each other. The dynamics of the original device are described by the Euler-Lagrange equation

$$\mathcal{H}_m(q_{mo})\ddot{q}_{mo} + C_m(q_{mo}, \dot{q}_{mo})\dot{q}_{mo} + \mathcal{G}_m(q_{mo}) = \tau_{mo}, \quad (4.1)$$

where $q_{mo} := [q_{m1}, q_{m2}, \dots, q_{m6}]^T \in \mathbb{R}^6$ represents the joint angles of the original master device, $H_m(q_{mo})$, $C_m(q_{mo}, \dot{q}_{mo})$ are the matrices of inertia and Coriolis/centrifugal forces, respectively; $\mathcal{G}_m(q_{mo})$ is the vector of gravitational forces, and τ_{mo} is the vector of control torques. The dynamics of the two additional DOFs are described according to the formulas

$$J_m\ddot{q}_{mi} + \frac{K_m^2}{R_m}\dot{q}_{mi} = \tau_{mi} \quad i = 7, 8, \quad (4.2)$$

where q_{mi} , $i = 7, 8$ are the angular positions, J_m is the moment of inertia of the motor, while K_m and R_m are the torque constant and armature resistance of the additional motors, respectively. The full dynamics of the modified Haptic Wand device can be represented by the following equation

$$H_m(q_m)\ddot{q}_m + C_m(q_m, \dot{q}_m)\dot{q}_m + G_m(q_m) + \tau_f = \tau_m + J^T(q_m)(F_h - F_r) \quad (4.3)$$

where

$$H_m(q_m) := \begin{bmatrix} \mathcal{H}_m(q_{mo}) & 0 \\ 0 & J_m I_{2 \times 2} \end{bmatrix}, \quad C_m(q_m, \dot{q}_m) := \begin{bmatrix} C_m(q_{mo}, \dot{q}_{mo}) & 0 \\ 0 & \frac{K_m^2}{R_m} I_{2 \times 2} \end{bmatrix}, \quad G_m(q_m) := \begin{bmatrix} \mathcal{G}_m(q_{mo}) \\ 0 \end{bmatrix}, \quad (4.4)$$

and where τ_f is the vector of the estimated friction forces at the device, F_h is the force applied to the master by the human operator, F_r is the force reflected back to the master device, and $J(q_m) \in \mathbb{R}^{7 \times 8}$ is the analytic Jacobian of the 7-DOF haptic device which relates the Cartesian velocity $\dot{X}_m := [\dot{x}, \dot{y}, \dot{z}, \dot{\theta}, \dot{\phi}, \dot{\psi}_l, \dot{\psi}_u]^T$ to the joint angle velocity $\dot{q}_m := [\dot{q}_{m1}, \dot{q}_{m2}, \dots, \dot{q}_{m8}]^T$. In this work, the case of 3-DOF force reflection is addressed; specifically, the force reflection term in

(4.3) has the following structure

$$F_r := \begin{bmatrix} F_r^t \\ \mathbb{O}_4 \end{bmatrix}, \quad F_r^t := [f_{rx}, f_{ry}, f_{rz}]^T, \quad (4.5)$$

where f_{rx} , f_{ry} , f_{rz} are the translational forces reflected along the X , Y , and Z directions of the master's coordinate system, respectively, and $\mathbb{O}_4 := [0, 0, 0, 0]^T$. The design of the force reflection term F_r^t is addressed in detail in Section 4.4 below. The dynamics of the Haptic Wand (4.3) can also be represented in Cartesian space as follows:

$$H_{mx}\ddot{X}_m + C_{mx}\dot{X}_m + G_{mx} + F_f = u_m + F_h - F_r, \quad (4.6)$$

where $X_m := [x, y, z, \theta, \phi, \psi_l, \psi_u]^T$ is the Cartesian position of the end-effector of the master robot, \dot{X}_m , and \ddot{X}_m are the first and second time derivative of X_m , respectively, $H_{mx}(\cdot) := J^{-T}(\cdot)H_m(\cdot)J^{-1}(\cdot)$, $C_{mx}(\cdot) := J^{-T}(\cdot)C_m(\cdot)J^{-1}(\cdot) - H_{mx}(\cdot)\dot{J}(\cdot)J^{-1}(\cdot)$, $G_{mx}(\cdot) := J^{-T}(\cdot)G_m(\cdot)$, $u_m := J^{-T}(\cdot)\tau_m$, and $F_f(\cdot) := J^{-T}(\cdot)\tau_f$; here and below, all the arguments are omitted to save space. The exact expressions for all the nonlinear functions in (4.3), (4.6) are exceedingly lengthy and therefore omitted here because of space constraints; they can be found in [23].

In this work, following [23], the impedance control approach is utilized to render the dynamics of the master manipulator. The target (desired) dynamics of the closed-loop master subsystem are described by the following equation

$$M_d^m\ddot{X}_m + B_d^m\dot{X}_m + K_d^mX_m = F_h - F_r \quad (4.7)$$

where $M_d^m, B_d^m, K_d^m \in \mathbb{R}^{7 \times 7}$ are positive definite matrices of the desired inertia, desired damping and desired stiffness of the master manipulator, respectively. The corresponding impedance control algorithm has a form

$$\tau_m = J^T \left(H_{mx}M_d^{m-1} \left(\hat{F}_h - F_r - B_d^m\hat{X}_m - K_d^mX_m \right) + C_{mx}\hat{X}_m + G_{mx} + F_f - \hat{F}_h + F_r \right), \quad (4.8)$$

where \hat{F}_h and \hat{X}_m are estimates of the human force applied to the master device and the master velocity, respectively. The impedance control algorithm (4.8) allows for rendering the master dynamics (4.6) into the form (4.7) provided that $\hat{F}_h \equiv F_h$ and $\hat{X}_m \equiv \dot{X}_m$. An estimate of the Cartesian velocity \hat{X}_m is obtained according to the formula

$$\hat{X}_m := J(q_m)\xi_2, \quad (4.9)$$

where ξ_2 is an estimate of the joint velocity \dot{q}_m generated by the following "dirty derivative" filter [13]

$$\begin{aligned}\dot{\xi}_1 &= \xi_2 + g\alpha_1(q_m - \xi_1), \\ \dot{\xi}_2 &= g^2\alpha_0(q_m - \xi_1).\end{aligned}\tag{4.10}$$

In the above equation (4.10), $g > 0$ is the filter gain, and $\alpha_0, \alpha_1 > 0$ are chosen such that the roots of $p(s) = s^2 + \alpha_1 s + \alpha_0$ have negative real parts. On the other hand, an estimate \hat{F}_h of the human forces applied to the master device is obtained in our experiments using a high gain input observer of the form [14]

$$\begin{aligned}\dot{\omega} &= -\gamma\omega + \gamma^2 H_m \xi_2 + \gamma \left(\dot{H}_m \xi_2 - C_m \xi_2 - G_m - \tau_f - J^T F_r + \tau_m \right), \\ \hat{F}_h &= J^{-T} (\gamma H_m \xi_2 - \omega),\end{aligned}\tag{4.11}$$

where $\omega \in \mathbb{R}^8$ is the observer state and $\gamma > 0$ is the observer gain. In addition, an estimate of the Cartesian acceleration $\hat{\ddot{X}}_m$ is obtained according to the formula

$$\hat{\ddot{X}}_m := \dot{J}(q_m)\xi_2 + J(q_m)\dot{\xi}_2.\tag{4.12}$$

Finally, for each master-slave pair, the information about the position of the haptic wand X_m as well as estimates of its velocity $\hat{\dot{X}}_m$ and acceleration $\hat{\ddot{X}}_m$ are transmitted to the slave site, where they are used as reference signals for the slave manipulator's trajectory.

4.3.2 Slave Subsystems

As explained above in Section 4.2.2, the Mitsubishi PA10-7C robot has a built-in internal joint velocity controller. To implement an impedance control scheme, therefore, an outer control loop can be designed, as follows. Suppose the target impedance for the slave manipulator is described according to the following equation

$$M_d^s (\ddot{X}_s - \ddot{X}_d^s) + B_d^s (\dot{X}_s - \dot{X}_d^s) + K_d^s (X_s - X_d^s) = -F_e,\tag{4.13}$$

where $X_s, \dot{X}_s, \ddot{X}_s \in \mathbb{R}^6$ are Cartesian position, velocity, and acceleration of the Mitsubishi PA10-7C slave robot, respectively, $X_d^s, \dot{X}_d^s, \ddot{X}_d^s$ represent the desired position, desired velocity, and desired acceleration of the slave robot, $M_d^s, B_d^s,$ and K_d^s are positive definite matrices of the desired inertia, desired damping, and desired stiffness of the slave, and F_e is the contact force

due to interaction with environment. A possible way to render the target impedance (4.13) is to generate a slave's reference trajectory $X_r^s(t)$ as an output of the following filter

$$\ddot{X}_r^s = \ddot{X}_d^s + M_d^{s-1} \left(-F_e - B_d^s (\dot{X}_r^s - \dot{X}_d^s) - K_d^s (X_r^s - X_d^s) \right). \quad (4.14)$$

Based on $X_r^s(t)$ generated by (4.14), the reference joint trajectory for the slave's internal controller is calculated using the inverse kinematic of the PA10-7C [23]. The desired trajectory $X_d^s, \dot{X}_d^s, \ddot{X}_d^s$ for each slave robot is defined as follows. Denote

$$X_{mi}^*(t) = X_{mi} \left(t - \theta_{fi}^x(t) \right), \quad (4.15)$$

$$\hat{X}_{mi}^*(t) = \hat{X}_{mi} \left(t - \theta_{fi}^v(t) \right), \quad (4.16)$$

$$\hat{\hat{X}}_{mi}^*(t) = \hat{\hat{X}}_{mi} \left(t - \theta_{fi}^a(t) \right), \quad (4.17)$$

where $\theta_{fi}^x(t), \theta_{fi}^v(t), \theta_{fi}^a(t)$ are the communication delay functions between the master and the slave in the position, velocity, and acceleration channels, respectively. Thus, $X_{mi}^*(t), \hat{X}_{mi}^*(t), \hat{\hat{X}}_{mi}^*(t)$ are signals that represents the delayed position, velocity, and acceleration of the i -th master available at time t on the corresponding slave's side. Then the desired position for the slave robot is defined as follows,

$$X_{id}^s(t) := \begin{bmatrix} [X_{mi}^*(t)]_{1,\dots,4} \\ 0 \\ 0 \end{bmatrix}, \quad (4.18)$$

where $[X_{mi}^*(t)]_{1,\dots,4} \in \mathbb{R}^4$ is the vector that consists of the first four components of $X_{mi}^*(t)$. Similarly,

$$\dot{X}_{id}^s(t) := \begin{bmatrix} [\hat{X}_{mi}^*(t)]_{1,\dots,4} \\ 0 \\ 0 \end{bmatrix}, \quad \ddot{X}_{id}^s(t) := \begin{bmatrix} [\hat{\hat{X}}_{mi}^*(t)]_{1,\dots,4} \\ 0 \\ 0 \end{bmatrix}. \quad (4.19)$$

The desired trajectory for the i -th da Vinci instrument is defined according to the formulas

$$\begin{bmatrix} \phi_{id}^s(t) \\ \psi_{id}^{s1}(t) \\ \psi_{id}^{s2}(t) \end{bmatrix} := [X_{mi}^*(t)]_{5,\dots,7}, \quad \begin{bmatrix} \dot{\phi}_{id}^s(t) \\ \dot{\psi}_{id}^{s1}(t) \\ \dot{\psi}_{id}^{s2}(t) \end{bmatrix} := [\hat{X}_{mi}^*(t)]_{5,\dots,7}, \quad \begin{bmatrix} \ddot{\phi}_{id}^s(t) \\ \ddot{\psi}_{id}^{s1}(t) \\ \ddot{\psi}_{id}^{s2}(t) \end{bmatrix} := [\hat{\hat{X}}_{mi}^*(t)]_{5,\dots,7}, \quad (4.20)$$

where $\phi_{id}^s(t), \psi_{id}^{s1}(t), \psi_{id}^{s2}(t)$ are the desired pitch, the desired yaw of gripper one, and the desired yaw of gripper two of the i -th da Vinci instrument, respectively. The desired trajectory of the da Vinci instrument is then executed using a conventional PID controller.

4.4 Force Reflection Algorithms

The goal of implementing force reflection in the MIS teleoperator system is to provide the surgeon with the haptic feel of interaction between the surgical tool and the tissue on the slave side. Force feedback, however, can potentially make the closed-loop system unstable, particularly in the presence of communication delays between the master and the slave sites. The force reflection scheme used in our work is organized as follows. For each slave manipulator, the interaction forces/torques between the tool and the environment are measured using ATI Gamma 6-DOFs force/torque sensors. The vector of translational interaction forces $F_e^t := [f_{ex}, f_{ey}, f_{ez}]^T$ represented in the end-effector coordinates are consequently transmitted back to the corresponding master site; this communication process is described by the formula

$$\hat{F}_e^t(t) := F_e^t(t - \theta_b(t)), \quad (4.21)$$

where \hat{F}_e^t is the contact force signal received on the corresponding master site, and $\theta_b(t)$ is the corresponding communication delay function. The signal \hat{F}_e^t is then used for haptic feedback. One problem which is of special interest for this particular work is to evaluate the stability and performance of the MIS teleoperator system where the force reflection is implemented following the projection-based principle. The projection-based force reflection algorithms for bilateral teleoperation were introduced in [13] and further developed in [14, 16]. The idea behind the projection-based force reflection is to separate the interaction and the momentum-generating components in the reflected force and attenuate the latter. Specifically, by interaction component we understand the component of the reflected force that is compensated by the interaction with the human operator's hand. One possible method to calculate the interaction component is by using the following formula [16]

$$\phi_e := \text{Sat}_{[0,1]} \left\{ \frac{(\hat{F}_e^t)^T \hat{F}_h^t}{\max\{|\hat{F}_h^t|^2, \epsilon\}} \right\} \hat{F}_h^t, \quad (4.22)$$

where $\epsilon > 0$ is a small constant which removes the singularity at $|\hat{F}_h^t| = 0$. Thus, the interaction component is the component of the reflected that is directed against the human force (notice that the reflected force comes with negative sign in (4.7)) and has a magnitude bounded by the magnitude of the human force. The projection-based principle suggests to reflect the interaction component without alteration (with gain 1) and to attenuate the residual motion-inducing

component $\hat{F}_e^t - \phi_e$ with gain $\alpha \in (0, 1]$, which gives a force reflection algorithm of the form

$$F_r^t := \phi_e + \alpha \cdot (\hat{F}_e^t - \phi_e) = \alpha \cdot \hat{F}_e^t + (1 - \alpha) \cdot \phi_e \quad (4.23)$$

The idea behind the projection-based algorithm is to allow the human operator to feel the interaction with the remote environment to the full extent, while at the same time improving stability by attenuating the motion-inducing component.

4.5 Stability Analysis

In this section, stability of the MIS teleoperator system with projection-based force reflection described above is analysed. In particular, we are interested in establishing the relationship between the stability properties of the MIS teleoperator system and the value of the weighting parameter $\alpha \in (0, 1]$ in (4.23). To simplify the analysis, we assume that the dynamics of both the dirty derivative filter (4.10) and the force observer (4.11) are sufficiently fast such that the corresponding estimation/observation errors can be neglected; in other words, it is assumed that $\hat{F}_h \approx F_h$, $\hat{X}_m \approx \dot{X}_m$, and $\hat{\dot{X}}_m \approx \ddot{X}_m$. This assumption can be justified by referring to the fact that the movements in a surgical teleoperator system are normally performed with relatively low velocity and acceleration, and the system itself is sufficiently damped for safety reasons which results in relatively low bandwidth. Also, the dynamics of the da Vinci instruments are ignored in the stability analysis below. Under these assumptions, the closed-loop MIS cooperative teleoperator system can be described by the following set of equations,

$$M_{di}^m \ddot{X}_{mi} + B_{di}^m \dot{X}_{mi} + K_{di}^m X_{mi} = F_{hi} - \begin{bmatrix} F_{ri}^t \\ \mathbb{O}_4 \end{bmatrix}, \quad i = 1, 2, \quad (4.24)$$

$$M_{di}^s (\ddot{X}_{si} - \ddot{X}_{si}^d) + B_{di}^s (\dot{X}_{si} - \dot{X}_{si}^d) + K_{di}^s (X_{si} - X_{si}^d) = -F_{ei}, \quad i = 1, 2, \quad (4.25)$$

which describe the closed-loop masters (4.24) and the closed-loop slaves (4.25), respectively. The communication channels between the masters and the slaves manipulators are described

by the following equations

$$X_{si}^d(t) = \left[\left[X_{mi}(t - \theta_{fi}^x(t)) \right]_{1,\dots,4}, 0, 0 \right]^T, \quad i = 1, 2, \quad (4.26)$$

$$\dot{X}_{si}^d(t) = \left[\left[\dot{X}_{mi}(t - \theta_{fi}^y(t)) \right]_{1,\dots,4}, 0, 0 \right]^T, \quad i = 1, 2, \quad (4.27)$$

$$\ddot{X}_{si}^d(t) = \left[\left[\ddot{X}_{mi}(t - \theta_{fi}^a(t)) \right]_{1,\dots,4}, 0, 0 \right]^T, \quad i = 1, 2, \quad (4.28)$$

$$\hat{F}_{ei}^t(t) = F_{ei}^t(t - \theta_{bi}(t)), \quad i = 1, 2, \quad (4.29)$$

while F_{ri}^t are obtained using the projection-based force reflection algorithms of the form

$$F_{ri}^t := \phi_{ei} + \alpha \cdot (\hat{F}_{ei}^t - \phi_{ei}) = \alpha_i \cdot \hat{F}_{ei}^t + (1 - \alpha_i) \cdot \phi_{ei}, \quad i = 1, 2, \quad (4.30)$$

where

$$\phi_{ei} := \text{Sat}_{[0,1]} \left\{ \frac{(\hat{F}_{ei}^t)^T \hat{F}_{hi}^t}{\max\{|\hat{F}_{hi}^t|^2, \epsilon_i\}} \right\} \hat{F}_{hi}^t, \quad i = 1, 2. \quad (4.31)$$

The stability analysis of the teleoperator system (4.24)-(4.31) is performed in our paper under a set of assumptions imposed on the environmental dynamics, on the human operators' dynamics, and on the communication process. First, the assumption imposed on the environmental dynamics is as follows.

Assumption 1. The environmental dynamics have a form

$$M_e \ddot{X}_e + B_e \dot{X}_e + K_e X_e = F_{e1} + F_{e2}, \quad (4.32)$$

where $M_e = M_e^T > 0$, $B_e = B_e^T \geq 0$, $K_e = K_e^T \geq 0$ are 6×6 matrices of the environmental inertia, damping, and stiffness, respectively, $X_e \in \mathbb{R}^6$ is the spatial coordinate that describes the position of the environment, while F_{e1} , F_{e2} are the contact forces due to interaction with Slave 1 and Slave 2, respectively. •

Furthermore, following [21], the behaviour of the i -th human operator, $i = 1, 2$, is described according to the formula

$$F_{hi} = F_{hi}^* - B_{hi} \dot{X}_{mi} - K_{hi} X_{mi}, \quad (4.33)$$

where B_{hi} , K_{hi} are positive semidefinite 7×7 matrices of i -th operator's hand damping and stiffness, respectively, and F_{hi}^* is an arbitrary uniformly essentially bounded force. The term F_{hi}^* in (4.33) represents the active forces voluntary applied by the human operator, while the other two terms represent passive reaction of the human hand to movement of the master device. Our

basic assumption regarding the dynamics of i -th human operator is that the passive reaction does not destabilize the closed loop master subsystem. This assumption can be formulated in more rigorous terms, as follows. Consider the target dynamics of the master subsystem (4.24). Since this system is stable, there exists a unique solution $\mathbb{P}_i = \mathbb{P}_i^T \in \mathbb{R}^{14 \times 14}$ of the Lyapunov equation

$$A_{mi}^T \mathbb{P} + \mathbb{P} A_{mi} = -\mathbb{I}, \quad (4.34)$$

where

$$A_{mi} := \begin{bmatrix} \mathbb{O} & \mathbb{I} \\ -(M_{di}^m)^{-1} K_{di}^m & -(M_{di}^m)^{-1} B_{di}^m \end{bmatrix} \in \mathbb{R}^{14 \times 14}. \quad (4.35)$$

Now, denote

$$B_{hi}^\rho := \begin{bmatrix} \rho \cdot \mathbb{I}_{3 \times 3} & \mathbb{O}_{3 \times 4} \\ \mathbb{O}_{4 \times 3} & \mathbb{I}_{4 \times 4} \end{bmatrix} B_{hi}, \quad K_{hi}^\rho := \begin{bmatrix} \rho \cdot \mathbb{I}_{3 \times 3} & \mathbb{O}_{3 \times 4} \\ \mathbb{O}_{4 \times 3} & \mathbb{I}_{4 \times 4} \end{bmatrix} K_{hi}, \quad \rho \in [0, 1], \quad (4.36)$$

and

$$A_{hi}^\rho := \begin{bmatrix} \mathbb{O} & \mathbb{O} \\ -(M_{di}^m)^{-1} K_{hi}^\rho & -(M_{di}^m)^{-1} B_{hi}^\rho \end{bmatrix}, \quad \rho \in [0, 1]. \quad (4.37)$$

In particular,

$$A_{hi} := A_{hi}^1 = \begin{bmatrix} \mathbb{O} & \mathbb{O} \\ -(M_{di}^m)^{-1} K_{hi} & -(M_{di}^m)^{-1} B_{hi} \end{bmatrix}.$$

Assumption 2. The inequalities

$$A_{hi}^T \mathbb{P} + \mathbb{P} A_{hi} \leq 0, \quad (A_{hi}^0)^T \mathbb{P} + \mathbb{P} A_{hi}^0 \leq 0 \quad (4.38)$$

are valid, where $\mathbb{P}_i = \mathbb{P}_i^T > 0$ is the solution of (4.34). •

Remark 1. Since A_{hi}^ρ is convex (more precisely, linear) in $\rho \in [0, 1]$, one sees that Assumption 2 actually implies that $(A_{hi}^\rho)^T \mathbb{P} + \mathbb{P} A_{hi}^\rho \leq 0$ for all $\rho \in [0, 1]$. •

Now, let us formulate the assumptions on the communication delays $\theta_{fi}^x(t)$, $\theta_{fi}^v(t)$, $\theta_{fi}^a(t)$, $\theta_{bi}(t)$ in (4.26) - (4.29). Similarly to the previous works on the small-gain approach to teleoperation [15, 17], the assumption imposed on the communication delays in this work allows for time-varying, discontinuous, and even unbounded communication delays. The assumption is formulated as follows.

Assumption 3. The communication delays $\theta_{fi}^x(t), \theta_{fi}^v(t), \theta_{fi}^a(t), \theta_{bi}(t), i = 1, 2$, are Lebesgue measurable functions of time that satisfy

$$\max_{i \in \{1,2\}} \left\{ \theta_{fi}^x(t), \theta_{fi}^v(t), \theta_{fi}^a(t), \theta_{bi}(t) \right\} \leq \theta^*(t), \quad \forall t \geq 0, \quad (4.39)$$

where $\theta^*: \mathbb{R}_+ \rightarrow \mathbb{R}_+$ is an arbitrary piecewise continuous function of time with the following properties:

- i) $\theta^*(t_2) - \theta^*(t_1) \leq t_2 - t_1$ holds for all $0 \leq t_1 \leq t_2$, and
- ii) $t - \theta^*(t) \rightarrow +\infty$ as $t \rightarrow +\infty$. •

The above Assumption 3 imposed on the communication process essentially implies that the communication delays are bounded by a function of time that does not grow faster than the time itself. This assumption is extremely mild and can always be satisfied in real-life communication networks unless the communication is completely lost on a semi-infinite time interval. For details, see [15, 17].

Under the above described Assumptions 1-3, the small gain stability condition for the closed-loop MIS teleoperator system with projection based force reflection (4.24)-(4.31) can be represented in terms of the following three inequalities,

$$\alpha_1 \cdot G_1 < 1, \quad (4.40)$$

$$\alpha_2 \cdot G_2 < 1, \quad (4.41)$$

$$\alpha_1 \cdot \alpha_2 \cdot G_3 < 1, \quad (4.42)$$

where $\alpha_i \in (0, 1], i = 1, 2$ are the weighting coefficient in the projection-based force reflection algorithm (4.30), and $G_1, G_2, G_3 > 0$ are gains that may depend on the parameters of the MIS teleoperator system but are independent on α_1 and α_2 . The corresponding small-gain analysis that results in stability conditions of the form (4.40) - (4.42) is presented in Appendix A. The conditions (4.40) - (4.42) essentially imply that the stability of the MIS teleoperator system with projection based force reflection can be achieved with arbitrary large stability margin by picking $\alpha_i \in (0, 1], i = 1, 2$ sufficiently small. In particular, this result implies that the MIS force reflecting teleoperator system with projection-based force reflection ($\alpha_i < 1$) is expected to be more robustly stable in comparison with the same system with direct force reflection ($\alpha_i = 1$). The performance of the system with projection-based force reflection during typical surgical tasks is experimentally evaluated in the following section.

4.6 Experimental Results

In this section, results of experimental investigations of the MIS teleoperator system described above are presented. Specifically, our major goal was to evaluate the stability and performance of the teleoperator system with projection-based force reflection (PBFR) in comparison with the stability/performance of the same system with more conventional direct force reflection (DFR, which corresponds to $\alpha = 1$ in the algorithm (4.23)), during different surgical tasks. The surgical tasks which were evaluated included Knot Tightening, Pegboard Transfer, and Object Manipulation. Pegboard Transfer is a standard task which is adopted from laparoscopic surgeon's skills evaluation [8]. Knot Tightening is another typical task which is widely used for the purpose of performance evaluation of robotic surgical applications [24]. Finally, Object Manipulation is a general purpose task which appears in many applications of cooperative teleoperation including different surgical scenarios. These three tasks are described below in some detail.

Experiment A: Knot Tightening

The first task to be experimentally evaluated in this work is Knot Tightening, which is one of the stages of the suturing. In our experiments, three knots have been created on an artificial tissue (see Figure 4.5); the tissue is made of silicone rubber and the threads are made from Ethicon 3 – 0 silk. The goal of the operator is to tight the knot by grasping the two ends of the thread and consequently applying pulling forces.

Experiment B: Pegboard Transfer

The experimental test-bed for the pegboard transfer task is illustrated in Figure 4.6. The pegboard transfer task consists of three stages. During the first stage, the operator grasps a peg and lifts it above the board using one the slave manipulators. During the second stage, the peg is transferred from one slave manipulator to the other without touching the board. Finally, during the third stage, the peg is placed on the side of the board opposite to its original location. The second stage of this experiment, in particular, includes interaction between the slaves which is the essential feature of the cooperative manipulation.

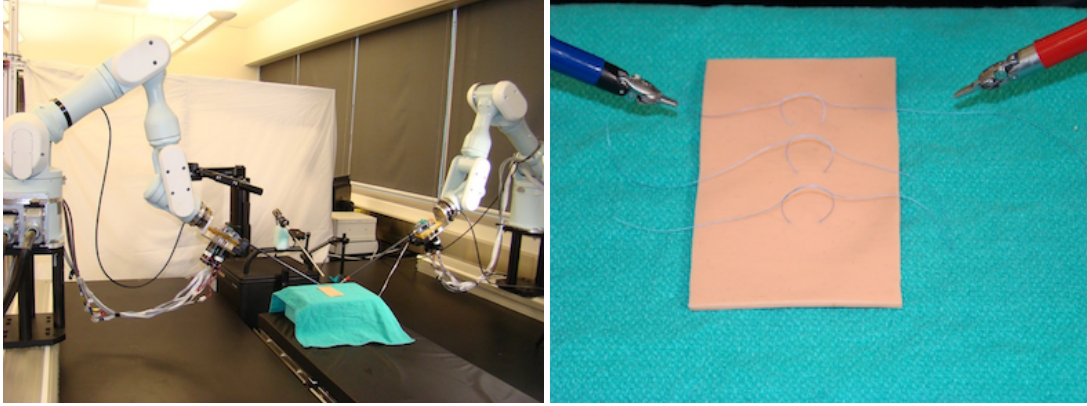


Figure 4.5: Experimental setup for the Knot Tightening task

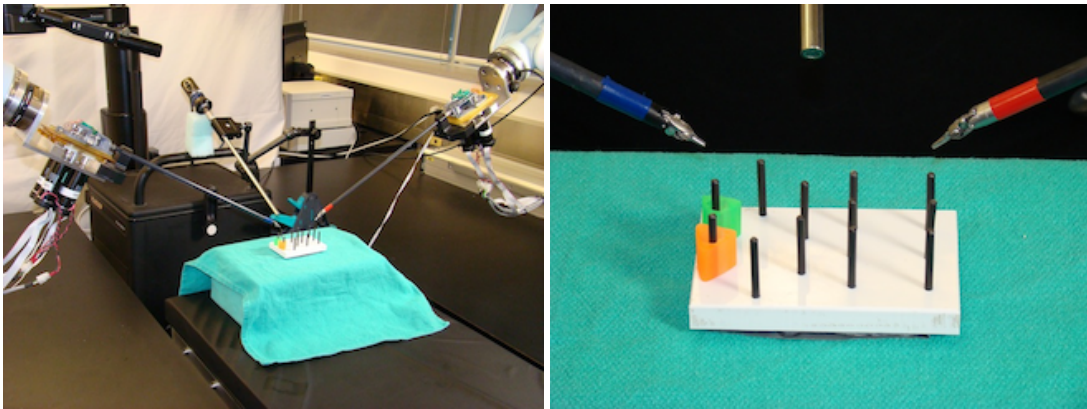


Figure 4.6: Experimental Setup for the Pegboard Transfer task

Experiment C: Object Manipulation

The third task consists of handling a soft object cooperatively using two slave manipulators (see Figure 4.7). The object is a $10\text{ cm} \times 5\text{ cm} \times 5\text{ cm}$ foam cube covered by a thin layer of a silicone rubber. During the course of the experiment, the operator lifts an object without using a grasper by applying pushing forces on the opposite sides of the object. The operator subsequently moves the object from left to right (8 cm distance) and back twice before putting it back on the surface. The stiffness of the object handled during this experiment is $K_{obj} \approx 0.3\text{ N} \cdot \text{mm}^{-1}$.

In the experiments described above, the performance of DFR and PBFR algorithms was compared in the absence of significant communication delays (*i.e.*, with Round Trip Time (RTT) delay $\approx 0\text{ s}$), as well as in the presence of time-varying communication delays with RTT

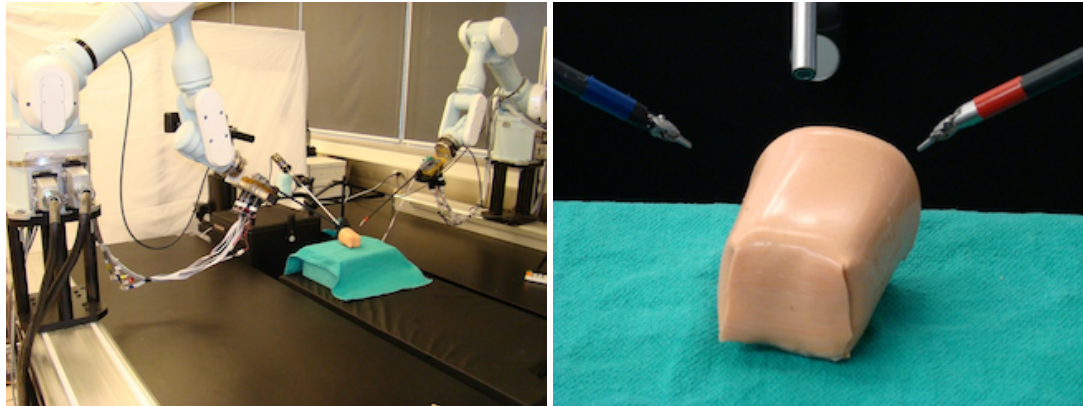


Figure 4.7: Experimental Setup for the Object Manipulation task

≈ 0.5 s (500 milliseconds). Nine adult subjects (1 female, 8 males, all right handed) with little to no experience of working with haptic devices participated in these experiments. Each subject performed 12 trials, (i.e., 3 tasks \times 2 FR algorithms \times 2 delays) and, therefore, 108 trials were performed in total, (i.e., 9 subjects \times 12 trials). After completing each task using both PBFR and DFR algorithms, each subject was asked if (s)he felt any differences between the two, and if (s)he preferred one of them. The performance of the PBFR and the DFR algorithms was also compared objectively by evaluating the average forces applied by the slaves and the average induced accelerations of the master devices. In order to determine the statistical significance of the difference between the measured values (average forces and average accelerations) for the PBFR and for the DFR algorithms, the two-sample t-test was used. The p-value calculated by this test gives the probability that the null hypothesis is true. If the calculated p-value is less than predetermined significance level (typically $p = 0.05$), the null hypothesis is to be rejected. In our experiments, the hypothesis is that the PBFR algorithm has effect on measured values (such as the interaction forces and the induced accelerations) of the system. Therefore, if the p-value becomes less than $p = 0.05$ then the null hypothesis will be rejected and will indicate that the PBFR algorithm has a significant effect on the measured values.

Throughout the experimental results presented below, the following control parameters are chosen. The matrices M_d^m, B_d^m, K_d^m of the master's target dynamics (4.7) are chosen as follows: $M_d^m := \text{diag}\{1.2 \cdot \mathbb{I}_{3 \times 3}, 10 \cdot \mathbb{I}_{4 \times 4}\}$, $B_d^m := \text{diag}\{0.6 \cdot \mathbb{I}_{3 \times 3}, 5 \cdot \mathbb{I}_{4 \times 4}\}$, and $K_d^m := 0.001 \cdot \mathbb{I}_{7 \times 7}$. (Increasing the controller stiffness would make the system more stable, however in this case the

human operator would feel extra force during the free motion which results in transparency deterioration. In our experiments, the stiffness coefficient is set low in order to show the effect of PBFR algorithms on stabilization of the system without losing the transparency.) The parameters of the filter (4.10) are $g = 12$, $\alpha_1 = 4$, and $\alpha_0 = 4$, while the gain of the force observer (4.11) is $\gamma = 10$. The parameters of the slave's target dynamics (4.13) are chosen as follows: $M_d = 8.6 \cdot \mathbb{I}_{6 \times 6}$, $B_d = 172 \cdot \mathbb{I}_{6 \times 6}$, and $K_d = 860 \cdot \mathbb{I}_{6 \times 6}$; this choice of parameters makes the target slave's dynamics critically damped (*i.e.*, damping ratio $\zeta = 1$) with natural frequency $\omega_0 = 10$ Hz. In the beginning of each experiments, the initial conditions for each slave's reference trajectory are set to $X_r^s(0) := X_s(0)$, and $\dot{X}_r^s(0) := 0$

4.6.1 Results of the Knot Tightening Experiment

During the Knot Tightening experiment, the pulling forces applied by the slaves to the thread as well as the induced accelerations of the master devices were recorded, and mean values and standard deviations (SDs) of their magnitudes were calculated; the results were compared for both DFR and PBFR algorithms for different communication delays. These means and SDs were calculated only during the part of the task when the subject completely grasps the ends of the thread and applied pulling forces to close the knot; in other words, forces and accelerations during free motion were not taken into account. The results of these experiment are summarized in Tables 4.1-4.3 and Figures 4.8, 4.9. Specifically, Table 4.1 presents the averages and corresponding SDs of the pulling forces applied by the slaves to the thread, while Table 4.2 summarizes the average and the corresponding SDs of the induced accelerations of the master devices. By induced accelerations, we mean the accelerations of the master devices generated by the reflected forces from the corresponding slaves; higher induced accelerations is an indication of performance deterioration and lower stability properties. The same information is represented graphically in Figures 4.8 and 4.9. The statistical significance (p-values) of the differences between PBFR and DFR algorithms are summarized in Table 4.3. These results indicate that, although there is no statistically significant difference in the mean forces, however, it is clear that the mean accelerations are substantially lower in the case of RBFR in comparison with the DFR, for both zero and ≈ 0.5 s communication delays. Examples of the force and the

Table 4.1: Knot Tightening experiment: mean values and SDs of magnitudes of the pulling forces applied by the slaves to the thread

		RTT Delay ≈ 0 s		RTT Delay ≈ 0.5 s	
		Mean (N)	SD (N)	Mean (N)	SD (N)
DFR ($\alpha = 1$)	Slave-2	0.3493	0.1579	0.3719	0.1759
	Slave-1	0.3645	0.1344	0.4299	0.1965
PBFR ($\alpha = 0.3$)	Slave-2	0.3174	0.1515	0.3316	0.1793
	Slave-1	0.3349	0.1570	0.3998	0.1967

Table 4.2: Knot Tightening experiment: mean values and SDs of magnitudes of the induced masters' accelerations

		RTT Delay ≈ 0 s		RTT Delay ≈ 0.5 s	
		Mean (m/s^2)	SD (m/s^2)	Mean (m/s^2)	SD (m/s^2)
DFR	Master-2	0.0197	0.0070	0.0266	0.0091
	Master-1	0.0146	0.0045	0.0231	0.0079
PBFR	Master-2	0.0156	0.0072	0.0152	0.0045
	Master-1	0.0120	0.0055	0.0147	0.0060

Table 4.3: Knot Tightening experiment: statistical significance (p-values) of the differences (mean forces and mean accelerations) between PBFR and DFR.

	Accelerations	Forces
	PBFR vs DFR	PBFR vs DFR
RTT Delay ≈ 0 s	9.94e-04	0.0994
RTT Delay ≈ 0.5 s	4.26e-06	0.0558

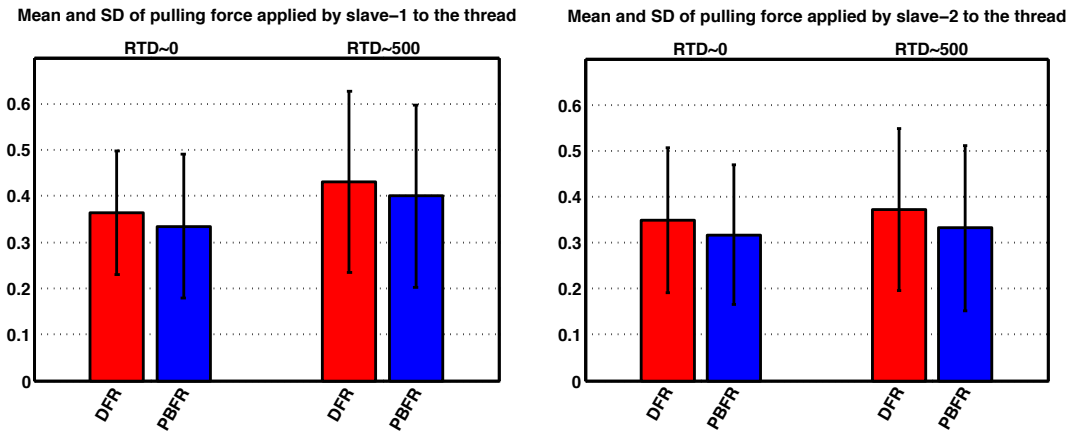


Figure 4.8: Knot Tightening experiment: mean values and SDs of magnitudes of the pulling forces applied by the slaves to the thread for RTT Delays ≈ 0 s and ≈ 0.5 s; DFR (red bars) vs. PBFR (blue bars). Left plot: Slave 1; right plot: Slave 2.

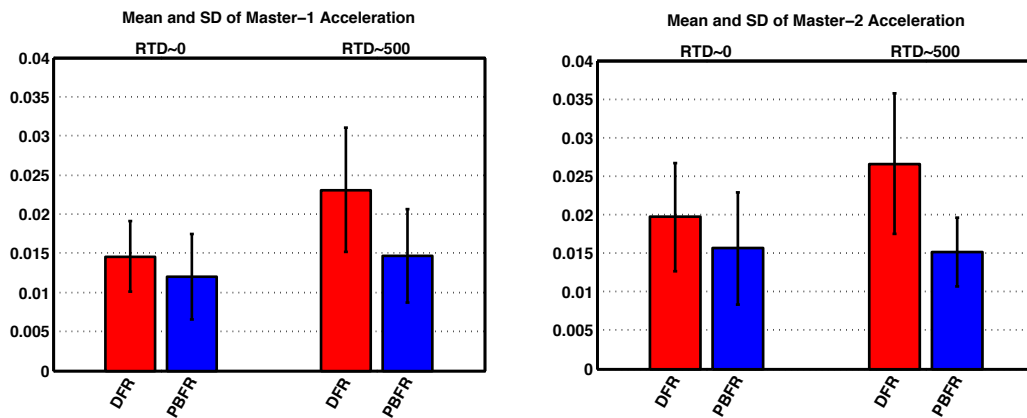


Figure 4.9: Knot Tightening experiment: mean values and SDs of magnitudes of the Masters' accelerations for RTT Delays ≈ 0 s and ≈ 0.5 s; DFR (red bars) vs. PBFR (blue bars). Left plot: Master 1; right plot: Master 2.

acceleration profiles during the Knot Tightening experiment are shown in Figures 4.10, 4.11. In particular, Figure 4.10 presents samples of the force profiles in the case of time-varying communication delay with $RTT \approx 0.5$ s for both DFR ($\alpha = 1$) and PBFR ($\alpha = 0.3$) algorithms; specifically, plots of pulling forces applied by each slave to the thread together with the human forces and the forces reflected on the motors of the master devices are shown. It can be clearly seen from this plots that all the forces have higher peak values and fluctuate more intensively in the case of DFR in comparison with the PBFR case. The Figure 4.11, on the other hand, presents an example of acceleration profiles for both DFR and PBFR cases. These acceleration profiles were recorded during the pulling phase of the knot tightening where the goal of the operator was to apply a constant pulling forces at the two ends of the thread to ensure that the knot is tightened completely. The acceleration of the master devices during this phase is induced by the force reflection term; higher induced accelerations are undesirable during this phase. It can be clearly seen that, in the case of DFR, the induced accelerations of the master devices are greater in comparison with the PBFR case.

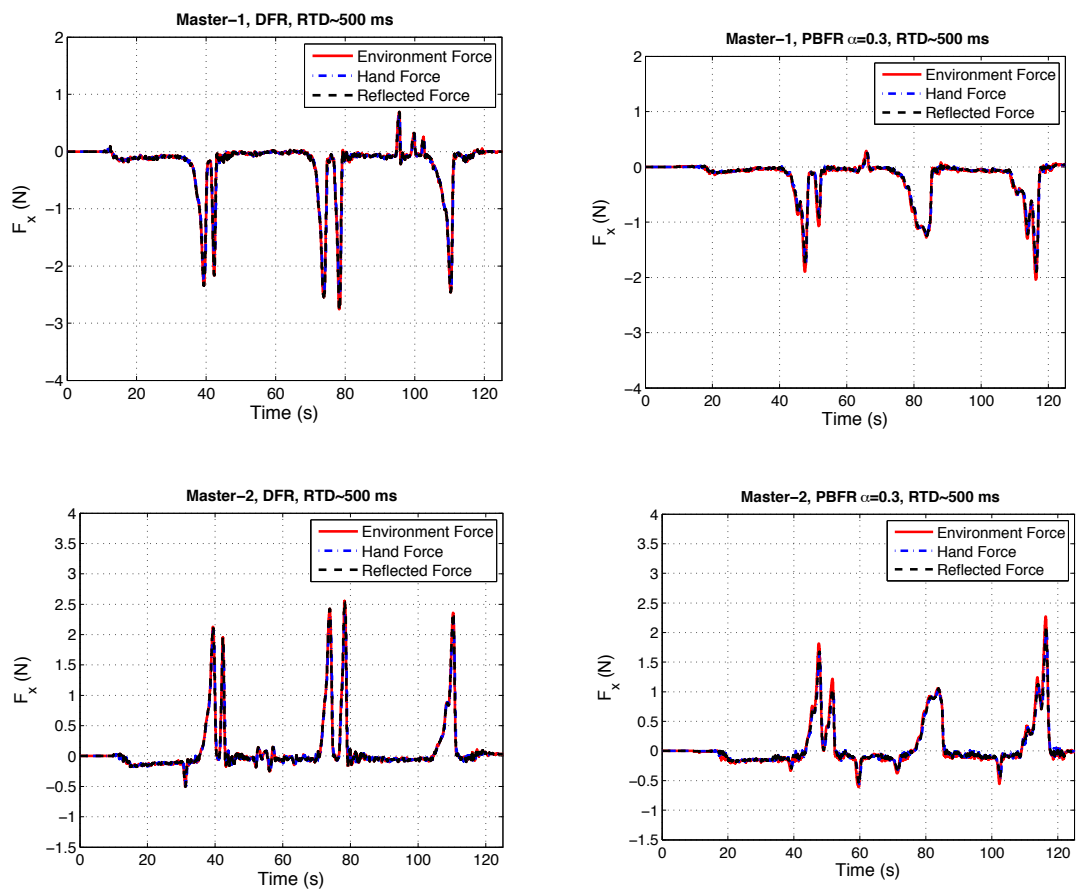


Figure 4.10: Samples of Knot Tightening experiment, RTT delay ≈ 0.5 s. Left column: DFR ($\alpha = 1$). Right column: PBFR ($\alpha = 0.3$). Top plots: contact forces, human forces, and reflected forces of the Master 1. Bottom plots: contact forces, human forces, and reflected forces of the Master 2.

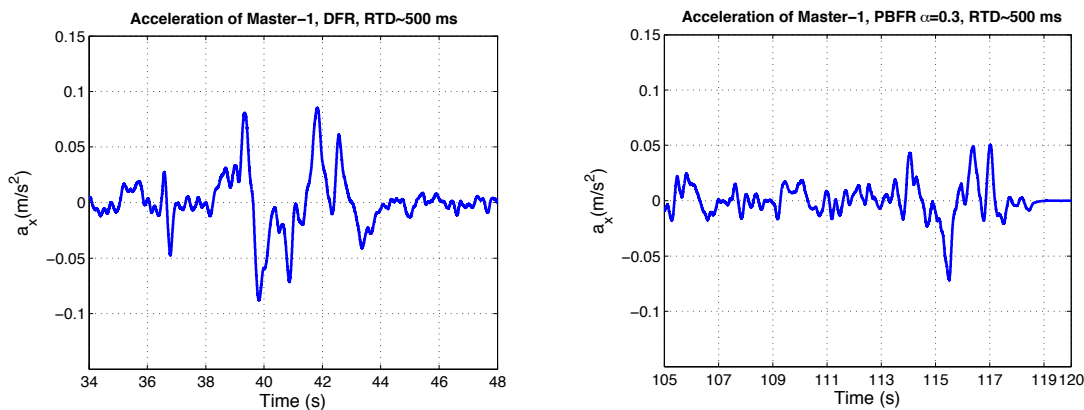


Figure 4.11: Samples of Knot Tightening experiment, RTT delay ≈ 0.5 s. Magnified view of the induced acceleration of the Master 1 during the knot tightening phase. Left plot: DFR ($\alpha = 1$), Right plot: PBFR ($\alpha = 0.3$).

4.6.2 Results of the Pegboard Transfer Experiment

The results of the Pegboard Transfer experiment are summarized in Tables 4.4-4.8 and Figures 4.12, 4.13. In particular, in Tables 4.4,4.5, the mean values and the standard deviations of the magnitudes of the slaves' forces in x- and z-directions, respectively, are presented. In Tables 4.6, 4.7, the mean values and the standard deviations of the masters' accelerations in x- and z-directions are given. The same information is represented graphically in Figures 4.12 and 4.13. It can be seen that the average of the contact forces for PBFR algorithm is clearly lower in comparison with the DFR algorithm, for both 0 s and 0.5 RTT delays. It can also be seen that the averages of masters' accelerations are lower in the case of PBFR in comparison with DFR, for all values of communication delays. The results of t-test analysis presented in Table 4.8 confirm that the PBFR algorithm has significant effect on decreasing both induced master accelerations and the interaction forces for both zero and 0.5s RTT delays.

Some examples of the experimental results obtained during the pegboard transfer experiment are shown in Figures 4.14-4.16. In particular, in Figure 4.14, experimentally obtained profiles of the contact forces, the human operator forces, and the reflected forces are shown for both DFR and PBFR algorithms. It can be seen from these plots that not only the DFR algorithm has higher peak values of the forces in comparison with the PBFR algorithm but

Table 4.4: Peg Transfer experiment: mean values and SDs of the slaves' forces in x-direction

		RTT Delay 0 s		RTT Delay 0.5 s	
		Mean (N)	SD (N)	Mean (N)	SD (N)
DFR	Slave-2	0.0792	0.0110	0.1119	0.0194
	Slave-1	0.1022	0.0232	0.1228	0.0382
PBFR	Slave-2	0.0691	0.0571	0.0847	0.0355
	Slave-1	0.0878	0.0287	0.1047	0.0415

Table 4.5: Peg Transfer experiment: mean values and SDs of the slaves' forces in z-direction

		RTT Delay \approx 0 s		RTT Delay \approx 0.5 s	
		Mean (N)	SD (N)	Mean (N)	SD (N)
DFR	Slave-2	0.0763	0.0316	0.0803	0.0382
	Slave-1	0.0785	0.0244	0.0697	0.0190
PBFR	Slave-2	0.0606	0.0226	0.0757	0.0133
	Slave-1	0.0663	0.0239	0.0647	0.0246

Table 4.6: Peg Transfer experiment: mean values and SDs of the Masters' accelerations in x-direction

		RTT Delay \approx 0 s		RTT Delay \approx 0.5 s	
		Mean (m/s^2)	SD (m/s^2)	Mean (m/s^2)	SD (m/s^2)
DFR	Master-2	0.0250	0.0099	0.0264	0.0137
	Master-1	0.0201	0.0062	0.0213	0.0078
PBFR	Master-2	0.0172	0.0086	0.0181	0.0054
	Master-1	0.0149	0.0056	0.0142	0.0051

Table 4.7: Peg Transfer experiment: mean values and SDs of the Masters' accelerations in z-direction

		RTT Delay ≈ 0 s		RTT Delay ≈ 0.5 s	
		Mean (m/s^2)	SD (m/s^2)	Mean (m/s^2)	SD (m/s^2)
DFR	Master-2	0.0207	0.0081	0.0213	0.0152
	Master-1	0.0101	0.0036	0.0099	0.0039
PBFR	Master-2	0.0108	0.0040	0.0135	0.0030
	Master-1	0.0091	0.0038	0.0075	0.0032

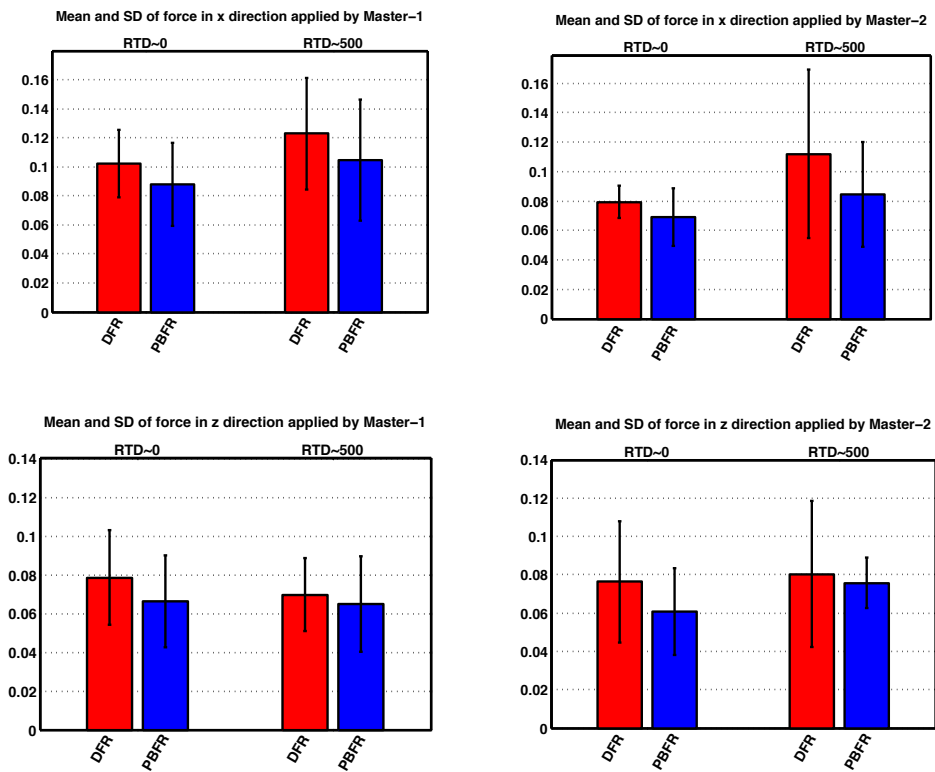


Figure 4.12: Peg Transfer experiment: mean values and corresponding SDs of the slaves' forces in x- and z-directions, DFR (red bars) vs. PBFR (blue bars). Top plots: x-forces; bottom plots: z-forces. Left plots: Slave 1; right plots: Slave 2.

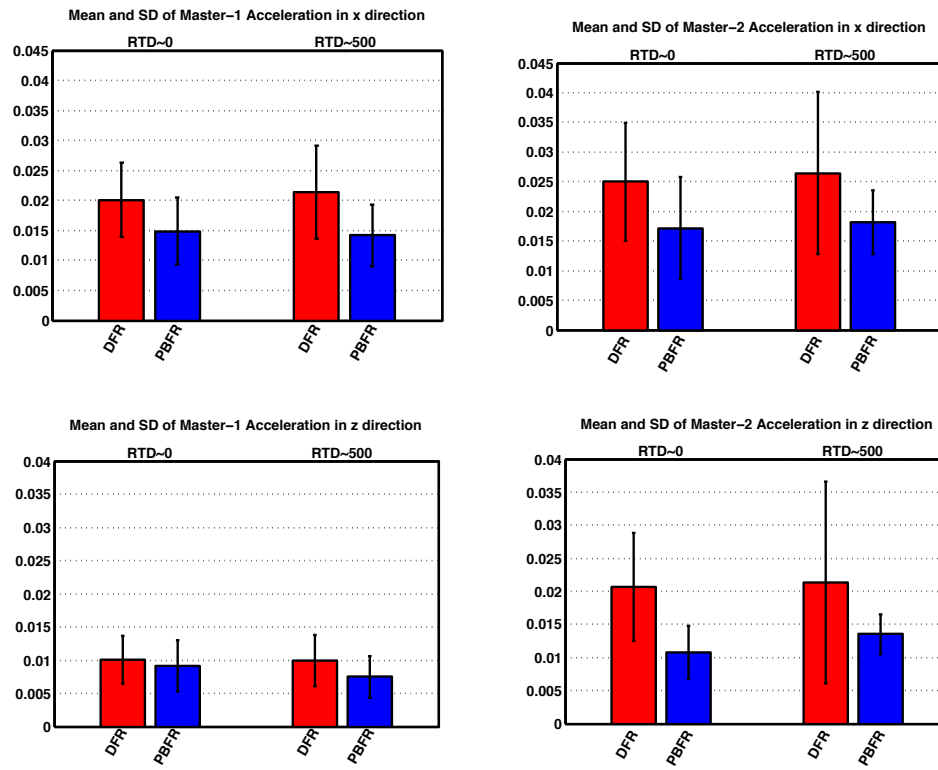


Figure 4.13: Peg Transfer experiment: mean values and corresponding SDs of the Masters' accelerations in x- and z-directions, DFR (red bars) vs. PBFR (blue bars). Top plots: x-accelerations; bottom plots: z-accelerations. Left plots: Master 1; right plots: Master 2.

Table 4.8: Peg Transfer experiment: statistical significance (p-values) of the average forces and the average accelerations between PBFR and DFR algorithms

	Acceleration	Force
	PBFR vs DFR	PBFR vs DFR
RTT Delay ≈ 0 s	7.6e-06	2.64e-02
RTT Delay ≈ 0.5 s	1.8e-03	4.35e-02

also, in the case of DFR, the user has to make a higher number of attempts in order to complete the task. Figure 4.15 shows examples of acceleration profiles during the initial phase of the pegboard transfer experiment. It can be seen that PBFR algorithm demonstrates substantially lower accelerations in comparison with the DFR. Finally, in Figure 4.16, examples of x-z trajectories of the first master-slave pair during the pegboard transfer experiment are shown, for both DFR and PBFR algorithms. It can be seen that the trajectories of the master device during the periods of time when the force reflection is nonzero (indicated by the green lines in Figure 4.16) are visibly smoother and have less jerky motion in the case of PBFR in comparison with the DFR case.

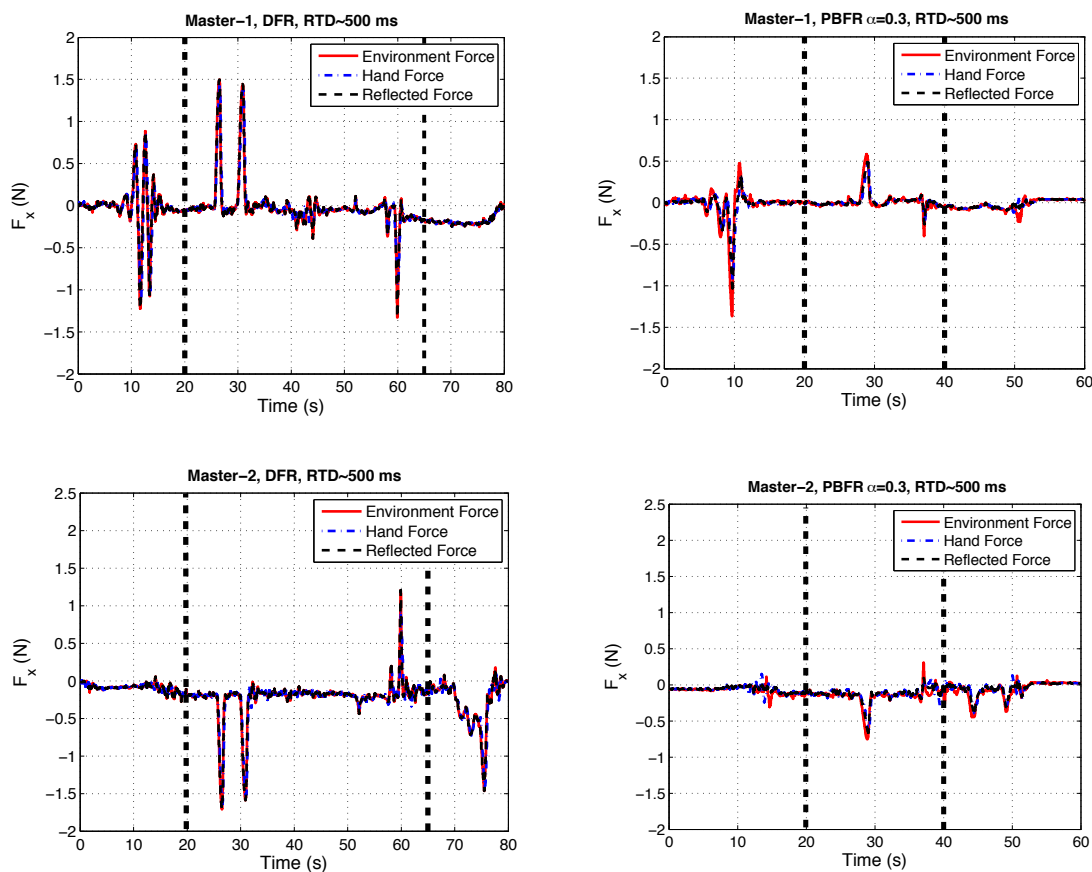


Figure 4.14: Samples of Peg Transfer experiment, RTT delay ≈ 0.5 s. Left column: DFR ($\alpha = 1$). Right column: PBFR algorithm ($\alpha = 0.3$). Top plots: contact forces, human forces, and reflected forces of the Master 1 in x direction. Bottom plots: contact forces, human forces, and reflected forces of the Master 2 in x direction.

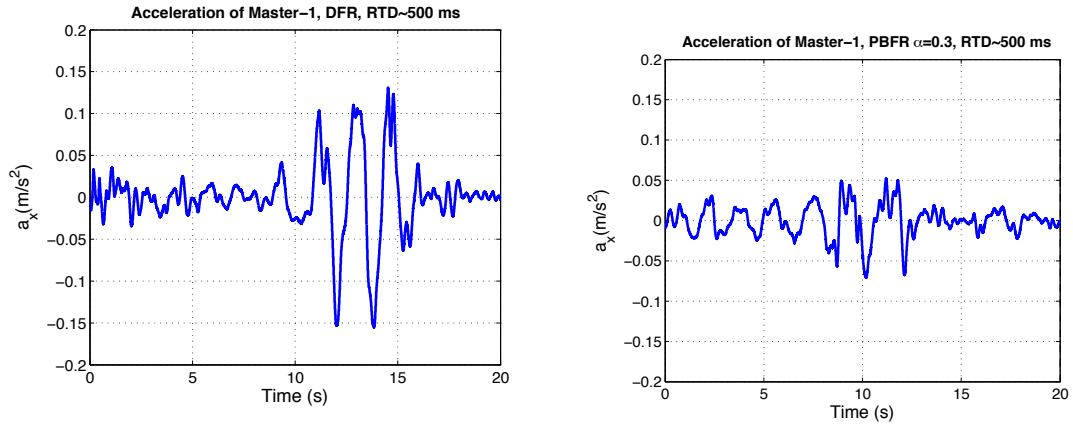


Figure 4.15: Samples of Peg Transfer experiment, RTT delay ≈ 0.5 s. Magnified view of the induced accelerations of the Master 1 in x direction during the initial phase of the experiment. Left plot: DFR ($\alpha = 1$). Right plot: PBFR algorithm ($\alpha = 0.3$).

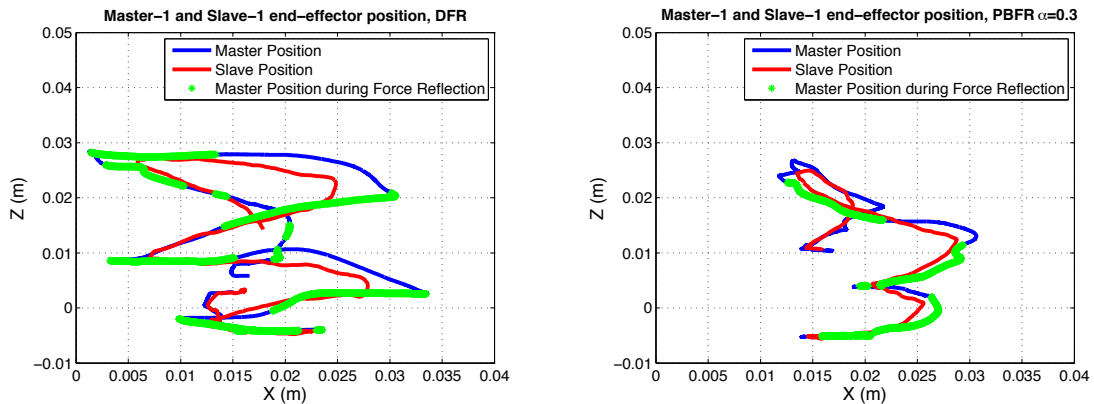


Figure 4.16: Samples of Peg Transfer experiment, RTT delay ≈ 0.5 s. Left column: Slave 1 and induced Master 1 position with DFR ($\alpha = 1$). Right column: Slave 1 and induced Master 1 position with PBFR ($\alpha = 0.3$)

4.6.3 Results of the Object Manipulation Experiment

The results of the object manipulation experiment are summarized in Tables 4.9 and 4.10, and Figures 4.17 and 4.19. In particular, Figure 4.20 graphically demonstrates the success rates of

the object manipulation experiment for DFR and PBFR algorithms in the absence as well as in the presence of communication delays (RTT delays ≈ 0 s and ≈ 0.5 s, respectively). This figure demonstrates that the success rate in the case of the DFR algorithm is substantially lower in comparison with the PBFR algorithm, particularly in the presence of communication delays. In particular, in the case of the DFR algorithm, only 4 out of 9 subjects were able to complete the task in the presence of communication delay. In contrast, when using the PBFR algorithm, 8 out of 9 subjects were able to successfully complete the task. Since more than half of the

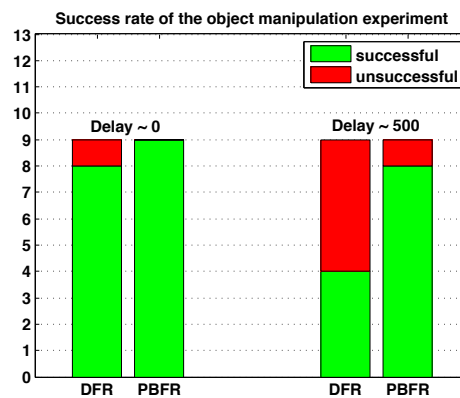


Figure 4.17: Object Manipulation experiment, Success rate of the object manipulation for $RTT \approx 0$ s and ≈ 0.5 s.

subjects were not able to complete the task using the DFR algorithm in the presence of communication delay, the comparison between the DFR and the PBFR is made below only for the case of RTT delay ≈ 0 s. Tables 4.9 and 4.10 summarize the average and the standard deviations of the slave's forces and the induced master's accelerations, respectively. The same information is represented graphically in Figure 4.18. It can be clearly seen from these tables and the figure that the averages of the slaves' interaction forces and induced masters' accelerations are clearly lower in the case of PBFR in comparison with DFR. The results of t-test analyses are summarized in Table 4.11; these results confirm that the PBFR algorithm has significant effect in decreasing both the interaction forces and induced masters' accelerations.

Examples of the force plots during the object manipulation experiment are shown in Figures 4.19 and 4.20, which correspond to the case of RTT delay ≈ 0 s and RTT delay ≈ 0.5

Table 4.9: Object Manipulation experiment, mean values and corresponding standard deviations of the forces applied by slaves in x and z direction, with zero delay

		F_x		F_z	
		Mean (N)	SD (N)	Mean (N)	SD (N)
DFR	Slave-2	1.0535	0.2596	0.3256	0.1962
	Slave-1	1.0097	0.2490	0.3159	0.1376
PBFR	Slave-2	0.8482	0.2100	0.3134	0.1991
	Slave-1	0.8312	0.2436	0.2719	0.1456

Table 4.10: Object Manipulation experiment, mean values and corresponding standard deviations of Master's acceleration in x and z direction, with zero delay

		a_x		a_z	
		Mean (m/s^2)	SD (m/s^2)	Mean (m/s^2)	SD (m/s^2)
DFR	Master-2	0.0264	0.0185	0.0086	0.0054
	Master-1	0.0200	0.0101	0.0048	0.0039
PBFR	Master-2	0.0214	0.0124	0.0073	0.0054
	Master-1	0.0153	0.0053	0.0041	0.0026

Table 4.11: Object Manipulation experiment, statistical significance (p-values) of forces and accelerations between PBFR and DFR algorithms in zero delay

	Acceleration	Force
	PBFR vs DFR	PBFR vs DFR
Delay ≈ 0	1.79e-02	2.00e-02

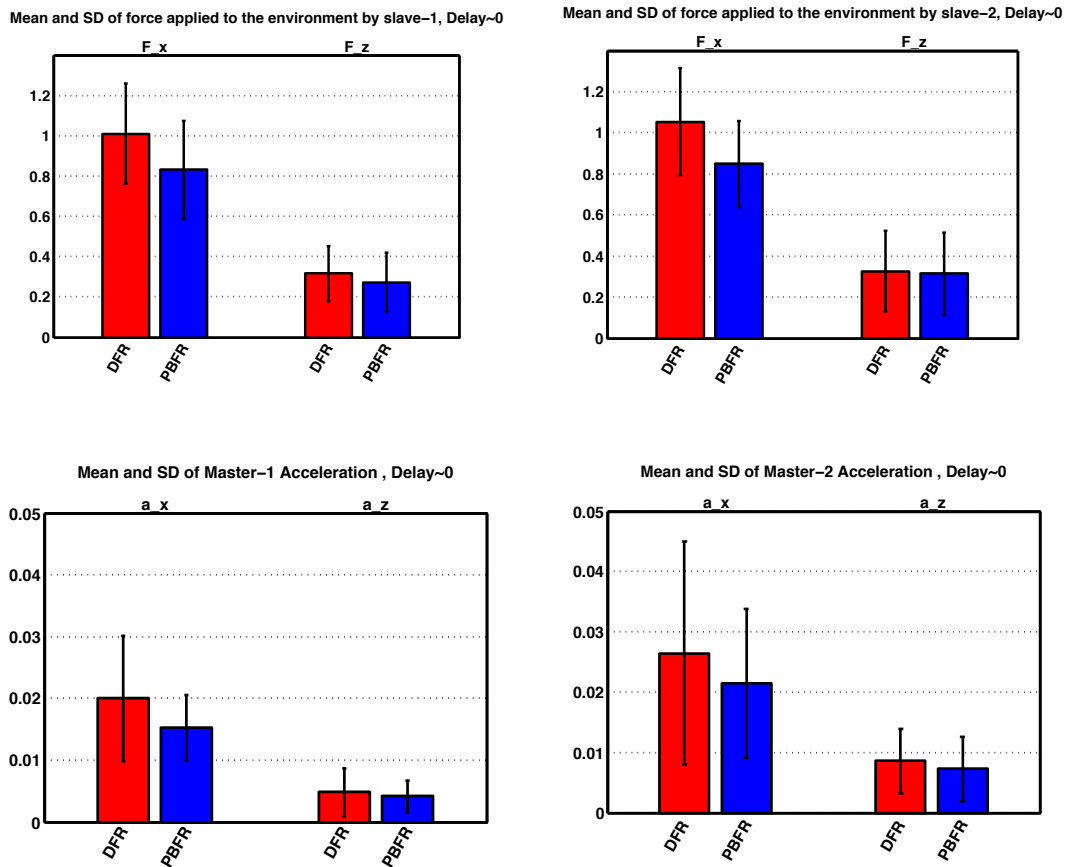


Figure 4.18: Object Manipulation experiment: mean values and corresponding standard deviations of the forces and Master's acceleration for RTT delays ≈ 0 s. Left diagram: master/slave 1; Right diagram: master/slave 2. DFR (red bars) vs. PBFR (blue bars).

s, respectively. As can be seen in Figure 4.19, the PBFR algorithm results in more consistent forces with lower maximal magnitude in comparison with DFR in the case of zero delay. Figure 4.20, on the other hand, shows examples of the corresponding plots in the case of RTT delay ≈ 0.5 s. These plots illustrate a typical situation where DFR algorithm results in instability which prevents the user from completion of the task; in the case of PBFR algorithm, on the other hand, the forces are lower and the task is completed successfully. Finally, examples of histograms of the reflected forces for both DFR and PBFR are given in Figure 4.21. A force histogram is a graphical representation of how frequently different force levels occur. It can be seen that, in the case of DFR algorithm, there is substantially higher concentration of forces around zero magnitude in comparison with the PBFR algorithm. Such a frequent occurrence of zero forces demonstrates the inability of the user to hold and move the object steadily; indeed, frequent oscillation between zero forces and relatively high forces is an indication of instability. In the case of PBFR, fewer occurrences of zero forces indicate the better ability of the user to hold the object steadily between the two end-effectors.

4.6.4 Discussion

In the experiments discussed above, the performance of the dual-arm MIS teleoperator system with PBFR was compared with that of the same system with DFR, for the following three simple surgical tasks: knot tightening, pegboard transfer, and object manipulation. The experimental results obtained demonstrate that the PBFR algorithm has a statistically significant effect on decreasing the induced master motion (specifically, induced acceleration) in comparison with the DFR algorithm for all three tasks. The lower induced acceleration obtained by using PBFR algorithm not only indicates improvement of the system's stability, but also makes the force reflection less disruptive for the human operator, which results in higher overall performance. In particular, most of the participants expressed the opinion that the system with the PBFR algorithm is easier to use and the force reflection is less disruptive (especially in the presence of delays) in comparison with the DFR algorithm. The experimental results also demonstrate that the PBFR algorithm has significant effect on decreasing the average forces applied by the slave robots during the peg transfer task, as well as during the object manipula-

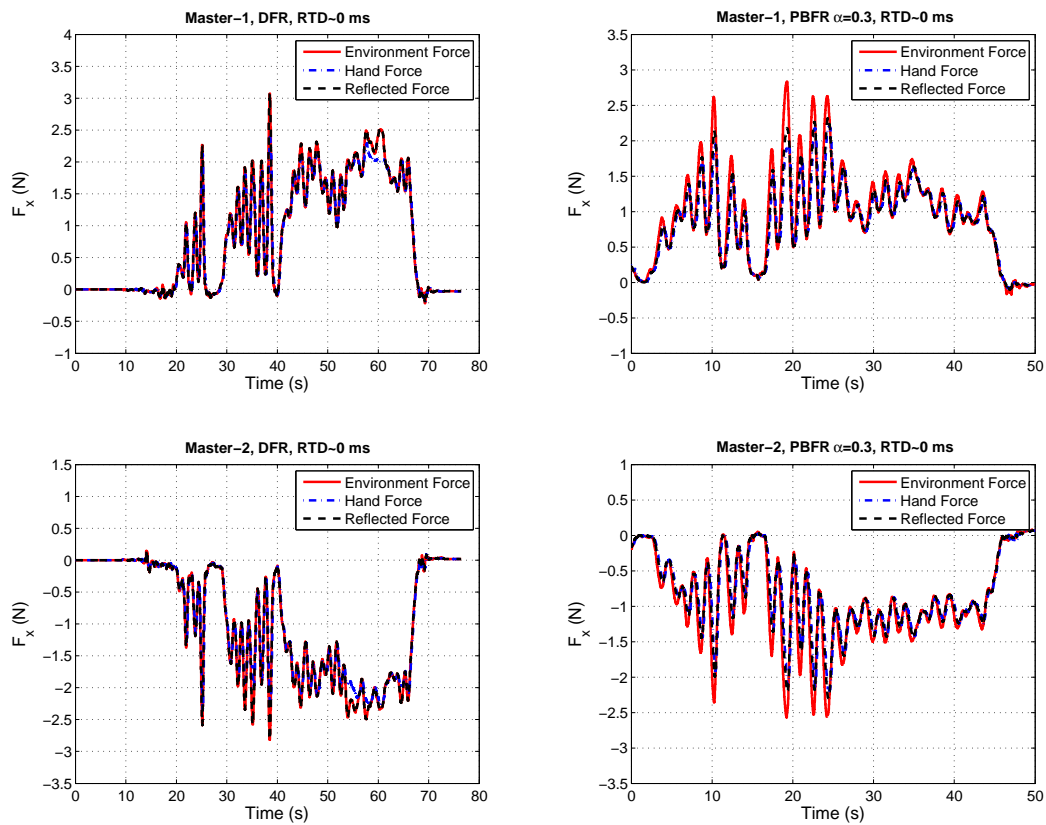


Figure 4.19: Samples of Object Manipulation experiment, RTT delay ≈ 0 s. Left column: DFR ($\alpha = 1$). Right column: PBFR algorithm ($\alpha = 0.3$). Top plots: contact forces, human forces, and reflected forces of the Master 1 in x direction. Bottom plots: contact forces, human forces, and reflected forces of the Master 2 in x direction.

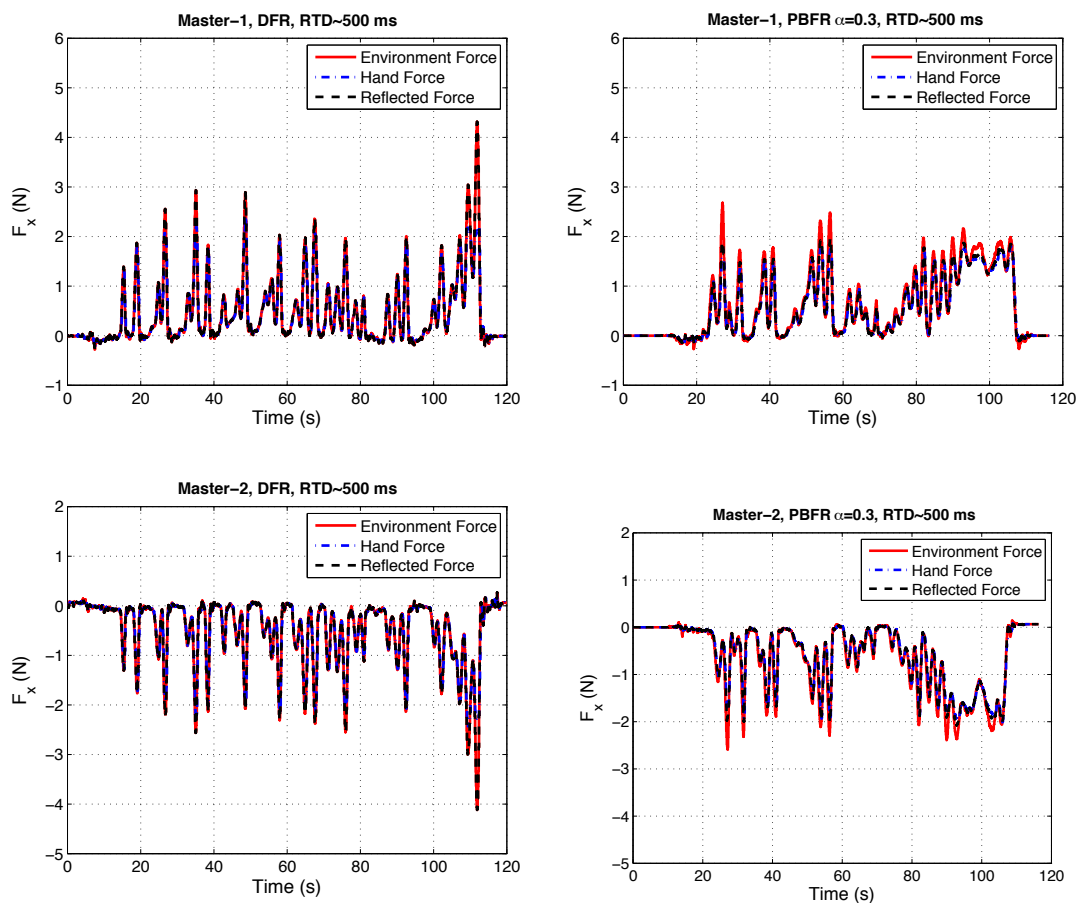


Figure 4.20: Samples of Object Manipulation experiment, RTT delay ≈ 0.5 s. Left column: DFR ($\alpha = 1$). Right column: PBFR algorithm ($\alpha = 0.3$). Top plots: contact forces, human forces, and reflected forces of the Master 1 in x direction. Bottom plots: contact forces, human forces, and reflected forces of the Master 2 in x direction.

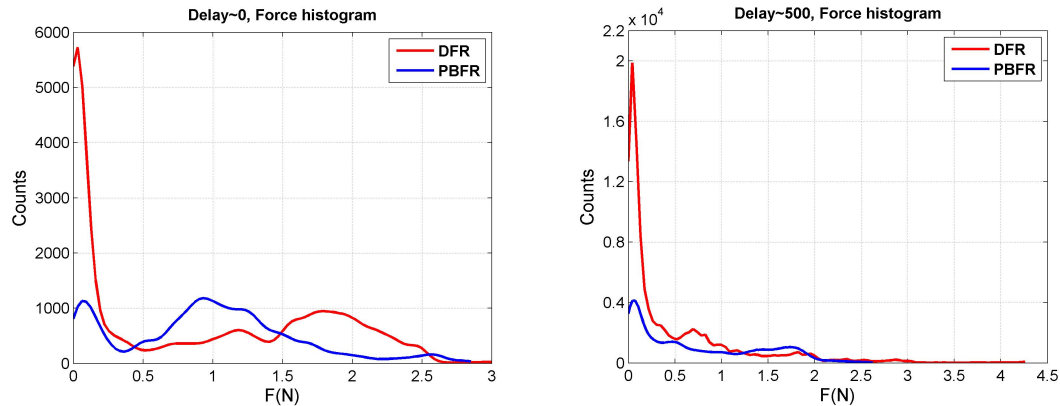


Figure 4.21: Samples of Object Manipulation experiment. Left plot: force histogram of master 1 in x direction, RTT delay ≈ 0 s. Right plot: force histogram of master 1 in x direction, RTT delay ≈ 0.5 s

tion task with zero delay. Also, the system with the PBFR algorithm allows for substantially higher success rate of completing the object manipulation task in the presence of 0.5 s RTT delay, in comparison with the DFR case. For the knot tightening task, it was also demonstrated that the average forces applied by the slaves were somewhat lower in the case of PBFR in comparison with DFR; however, the decrease was found to be not statistically significant. It should be taken into account that, in the case of knot tightening task, lower interaction forces is generally not an indication of higher performance. Indeed, in contrast with the other two tasks where applying excessive forces is undesirable, successful completion of the knot tightening task requires substantial forces to be applied to the thread to ensure that the knot is tightened completely.

4.7 Conclusions

In this paper, stability and performance of a dual-arm haptic teleoperator system with projection based force reflection (PBFR) for minimally invasive surgical applications have been studied. Specifically, we have compared, both theoretically and experimentally, the stability and performance characteristics of the system with PBFR algorithm and the same system with the direct force reflection (DFR). In particular, we have experimentally evaluated the performance

of the system in three simple surgical tasks, which are knot tightening, pegboard transfer, and object manipulation. It was demonstrated that, in the absolute majority of the cases, the PBFR algorithms lead to statistically significant improvement of performance in comparison with conventional direct force feedback.

Bibliography

- [1] Takintope Akinbiyi, Carol E Reiley, Sunipa Saha, Darius Burschka, Christopher J Hasser, David D Yuh, and Allison M Okamura. Dynamic augmented reality for sensory substitution in robot-assisted surgical systems. In *Proceedings of the 28th Annual International Conference of Engineering in Medicine and Biology Society*, pages 567–570. IEEE, 2006.
- [2] Harmanpreet Bassan, Ali Talasaz, and Rajni V. Patel. Design and characterization of a 7-DOF haptic interface for a minimally invasive surgery test-bed. In *Proceedings of the 2009 IEEE/RSJ International Conference on Intelligent Robots and Systems*, pages 4098–4103, St. Louis, MI, October 2009.
- [3] Dennis J. Bernstein and S. P. Bhat. Lyapunov stability, semistability, and asymptotic stability of matrix second-order systems. *Transactions of the ASME, Journal of Vibration and Acoustics*, 117:145–153, 1995.
- [4] Ricardo Campa, César Ramírez, Karla Camarillo, Víctor Santibáñez, and Israel Soto. Motion control of industrial robots in operational space: Analysis and experiments with the pa10 arm. *Advances in Robot Manipulators*.
- [5] Arif Kazi. Operator performance in surgical telemanipulation. *Presence: Teleoperators and Virtual Environments*, 10(5):495–510, 2001.
- [6] Masaya Kitagawa, Daniell Dokko, Allison M Okamura, Brian T Bethea, and David D Yuh. Effect of sensory substitution on suture manipulation forces for surgical teleoperation. *Studies in Health Technology and Informatics*, pages 157–163, 2004.

- [7] Katherine J. Kuchenbecker and Gunter Niemeyer. Induced master motion in force-reflecting teleoperation. *ASME Journal of Dynamic Systems, Measurement, and Control*, 128(4):800–810, 2006.
- [8] Mitchell J. H. Lum, Jacob Rosen, Thomas S. Lendvay, Mika N. Sinanan, and Blake Hannaford. Effect of time delay on telesurgical performance. In *Proceedings of the 2009 IEEE International Conference on Robotics and Automation*, pages 4246–4252, Kobe, Japan, May 2009.
- [9] Mohsen Mahvash and Allison M. Okamura. Enhancing transparency of a position-exchange teleoperator. In *Proceedings of the 2007 Second Joint EuroHaptics Conference, and Symposium on Haptic Interfaces for Virtual Environment and Teleoperator Systems*, pages 470–475, 2007.
- [10] Mohsen Mahvash, Jim Gwilliam, Rahul Agarwal, Balazs Vagvolgyi, Li-Ming Su, DD Yuh, and AM Okamura. Force-feedback surgical teleoperator: Controller design and palpation experiments. In *Proceedings of the 2008 Symposium on Haptic Interfaces for Virtual Environment and Teleoperator Systems*, pages 465–471. IEEE, 2008.
- [11] MitsubishiHeavyIndustries. General purpose robot pa10 series, programming manual. document SKC-GC20002, Rev. 0.
- [12] Allison M. Okamura. Haptic feedback in robot-assisted minimally invasive surgery. *Current Opinion in Urology*, 19:102–107, 2009.
- [13] Ilia G. Polushin, Peter X. Liu, and Chung-Horng Lung. A force-reflection algorithm for improved transparency in bilateral teleoperation with communication delay. *IEEE/ASME Transactions on Mechatronics*, 12(3):361–374, 2007.
- [14] Ilia G. Polushin, Peter X. Liu, and Chung-Horng Lung. Projection-based force reflection algorithm for stable bilateral teleoperation over networks. *IEEE Transactions on Instrumentation and Measurement*, 57(9):1854–1865, 2008.

- [15] Ilia G. Polushin, Horacio J. Marquez, Abdelhamid Tayebi, and Peter X. Liu. A multi-channel IOS small gain theorem for systems with multiple time-varying communication delays. *IEEE Transactions on Automatic Control*, 54(2):404–409, 2009.
- [16] Ilia G. Polushin, Peter X. Liu, and Chung-Horng Lung. Stability of bilateral teleoperators with generalized projection-based force reflection algorithms. *Automatica*, 48(6):1005–1016, 2012.
- [17] Ilia G. Polushin, Sergey N. Dashkovskiy, Amir Takhmar, and Rajni V. Patel. A small gain framework for networked cooperative force-reflecting teleoperation. *Automatica*, 49(2): 338 – 348, 2013.
- [18] Carsten Preusche, Tobias Ortmaier, and Gerd Hirzinger. Teleoperation concepts in minimal invasive surgery. *Control Engineering Practice*, 10(11):1245–1250, 2002.
- [19] Carol E Reiley, Takintope Akinbiyi, Darius Burschka, David C Chang, Allison M Okamura, and David D Yuh. Effects of visual force feedback on robot-assisted surgical task performance. *The Journal of Thoracic and Cardiovascular Surgery*, 135(1):196–202, 2008.
- [20] Eduardo D. Sontag. Input-to-state stability: Basic concepts and results. In P. Nistri and G. Stefani, editors, *Nonlinear and Optimal Control Theory*, pages 163–220. Springer-Verlag, Berlin, 2008.
- [21] John E. Speich, Liang Shao, and Michael Goldfarb. Modeling the human hand as it interacts with a telemanipulation system. *Mechatronics*, 15:1127–1142, 2005.
- [22] Amir Takhmar, Ilia G Polushin, and Rajni V Patel. Frequency separation in projection-based force reflection algorithms for bilateral teleoperators. In *Proceedings of the 2013 IEEE International Conference on Robotics and Automation*, pages 1492–1497. IEEE, 2013.
- [23] Ali Talasaz. "Haptics-Enabled Teleoperation for Robotics-Assisted Minimally Invasive Surgery". PhD thesis, The University of Western Ontario, 2012.

- [24] Ali Talasaz, Ana Luisa Trejos, and Rajnikant V Patel. Effect of force feedback on performance of robotics-assisted suturing. In *The Fourth IEEE RAS/EMBS International Conference on Biomedical Robotics and Biomechatronics*, pages 823–828, Roma, Italy, 2012.
- [25] M Tavakoli, RV Patel, and M Moallem. Robotic suturing forces in the presence of haptic feedback and sensory substitution. In *Proceedings of the 2005 IEEE Conference on Control Applications*, pages 1–6. IEEE, 2005.
- [26] Russell H. Taylor and Dan Stoianovici. Medical robotics in computer-integrated surgery. *IEEE Transactions on Robotics and Automation*, 19(5):765–781, October 2003.
- [27] EP Westebring-van der Putten, RHM Goossens, JJ Jakimowicz, and J Dankelman. Haptics in minimally invasive surgery—a review. *Minimally Invasive Therapy & Allied Technologies*, 17(1):3–16, 2008.
- [28] Michael C Yip, Mahdi Tavakoli, and Robert D Howe. Performance analysis of a haptic telemanipulation task under time delay. *Advanced Robotics*, 25(5):651–673, 2011.

Appendix A. Stability analysis of the dual-arm MIS teleoperator system with projection-based force reflection

In this Appendix, we present a rigorous stability analysis of the dual-arm MIS teleoperator system with projection-based force reflection. The analysis is based on the notions of the input-to-state stability (ISS) [20], (weak) input-to-output stability (WIOS), and the multi-dimensional WIOS small gain theorem for systems with communication constraints which can be found in [17]. Let us start from considering an i -th master subsystem (4.24), $i \in \{1, 2\}$, where the reflected force F_{ri}^t is an output of the projection based-force reflection algorithm (4.30), (4.31). Denote

$$F_{hi} := \begin{bmatrix} F_{hi}^t \\ F_{hi}^r \end{bmatrix}, \quad i \in \{1, 2\}, \quad (4.43)$$

where $F_{hi}^t \in \mathbb{R}^3$ are translational forces while $F_{hi}^r \in \mathbb{R}^4$ are the torques applied to the haptic wand by i -th human operator. We have

$$F_{hi} - \begin{bmatrix} F_{ri}^t \\ \mathbb{O}_4 \end{bmatrix} = \begin{bmatrix} \mathbb{O}_3 \\ F_{hi}^r \end{bmatrix} + \begin{bmatrix} F_{hi}^t - F_{ri}^t \\ \mathbb{O}_4 \end{bmatrix}. \quad (4.44)$$

Taking into account that

$$F_{hi}^t - F_{ri}^t = F_{hi}^t - \alpha_i \cdot \hat{F}_{ei}^t + (1 - \alpha_i) \cdot \text{Sat}_{[0,1]} \left\{ \frac{(\hat{F}_{ei}^t)^T \hat{F}_{hi}^t}{\max\{\|\hat{F}_{hi}^t\|^2, \epsilon_i\}} \right\} \hat{F}_{hi}^t = \varrho_i \cdot F_{hi}^t - \alpha_i \cdot \hat{F}_{ei}^t, \quad (4.45)$$

where

$$\varrho_i := 1 - (1 - \alpha_i) \cdot \text{Sat}_{[0,1]} \left\{ \frac{(\hat{F}_{ei}^t)^T \hat{F}_{hi}^t}{\max\{\|\hat{F}_{hi}^t\|^2, \epsilon_i\}} \right\} \in [\alpha_i, 1], \quad (4.46)$$

the equations of the i -th master subsystem with projection based-force reflection (4.24), (4.30), (4.31) $i \in \{1, 2\}$, can be rewritten in the form

$$M_{di}^m \ddot{X}_{mi} + B_{di}^m \dot{X}_{mi} + K_{di}^m X_{mi} = \begin{bmatrix} \varrho_i \cdot F_{hi}^t \\ F_{hi}^r \end{bmatrix} - \alpha_i \cdot \begin{bmatrix} \hat{F}_{ei}^t \\ \mathbb{O}_4 \end{bmatrix}, \quad (4.47)$$

where $\varrho_i \in [\alpha_i, 1]$ is defined by (4.46). Taking into account the human dynamics (4.33) and using notation (4.36), the equation (4.47) can be rewritten as follows

$$M_{di}^m \ddot{X}_{mi} + [B_{di}^m + B_{hi}^{\varrho_i}] \dot{X}_{mi} + [K_{di}^m + K_{hi}^{\varrho_i}] X_{mi} = \begin{bmatrix} \varrho_i \cdot \mathbb{I}_{3 \times 3} & \mathbb{O}_{3 \times 4} \\ \mathbb{O}_{4 \times 3} & \mathbb{I}_{4 \times 4} \end{bmatrix} F_{hi}^* - \alpha_i \cdot \begin{bmatrix} \hat{F}_{ei}^t \\ \mathbb{O}_4 \end{bmatrix}. \quad (4.48)$$

Now, denote

$$\mathbf{x}_{mi} := \begin{bmatrix} X_{mi} \\ \dot{X}_{mi} \end{bmatrix}, \quad B_{mi} := \begin{bmatrix} \mathbb{O}_{7 \times 7} \\ (M_{di}^m)^{-1} \end{bmatrix}.$$

Using notation (4.37), the equation of the i -th master subsystem with projection based-force reflection (4.48) can be rewritten in the form

$$\dot{\mathbf{x}}_{mi} = [A_{mi} + A_{hi}^{\varrho_i}] \mathbf{x}_{mi} + B_{mi} \left(\begin{bmatrix} \varrho_i \cdot \mathbb{I}_{3 \times 3} & \mathbb{O}_{3 \times 4} \\ \mathbb{O}_{4 \times 3} & \mathbb{I}_{4 \times 4} \end{bmatrix} F_{hi}^* - \alpha_i \cdot \begin{bmatrix} \hat{F}_{ei}^t \\ \mathbb{O}_4 \end{bmatrix} \right). \quad (4.49)$$

The following proposition plays an important role in the stability analysis.

Proposition 4.7.1 *The i -th master subsystem ($i \in \{1, 2\}$) with projection based-force reflection (4.49) is input-to-state stable. Moreover, the ISS gain of (4.49) with respect to input \hat{F}_{ei}^t can be made arbitrarily small by choosing $\alpha_i \in (0, 1]$ sufficiently small.*

Proof. Consider an ISS Lyapunov function candidate of the form

$$V_{mi} := \mathbf{x}_{mi}^T \mathbb{P}_i \mathbf{x}_{mi}, \quad (4.50)$$

where $\mathbb{P}_i = \mathbb{P}_i^T > 0$ is the solution of (4.34). Taking into account Assumption 2, the following estimate of the time derivative of V_{mi} along the trajectories of the system (4.49) can be obtained

$$\begin{aligned} \dot{V}_{mi} &= 2 \cdot \mathbf{x}_{mi}^T \mathbb{P}_i \left(\left[A_{mi} + A_{hi}^{e_i} \right] \mathbf{x}_{mi} + B_{mi} \left(\begin{bmatrix} \mathcal{Q}_i \cdot \mathbb{I}_{3 \times 3} & \mathbb{O}_{3 \times 4} \\ \mathbb{O}_{4 \times 3} & \mathbb{I}_{4 \times 4} \end{bmatrix} F_{hi}^* - \alpha_i \cdot \begin{bmatrix} \hat{F}_{ei}^t \\ \mathbb{O}_4 \end{bmatrix} \right) \right) \\ &\leq -|\mathbf{x}_{mi}|^2 + 2|\mathbf{x}_{mi}| |\mathbb{P}_i B_{mi}| |F_{hi}^*| + 2\alpha_i |\mathbf{x}_{mi}| |\mathbb{P}_i B_{mi}| |\hat{F}_{ei}^t| \\ &= -|\mathbf{x}_{mi}| \left(|\mathbf{x}_{mi}| - 2|\mathbb{P}_i B_{mi}| |F_{hi}^*| - 2\alpha_i |\mathbb{P}_i B_{mi}| |\hat{F}_{ei}^t| \right). \end{aligned}$$

From the above inequalities, one can see that if $|\mathbf{x}_{mi}| > 2|\mathbb{P}_i B_{mi}| |F_{hi}^*| + 2\alpha_i |\mathbb{P}_i B_{mi}| |\hat{F}_{ei}^t|$ then $\dot{V}_{mi} < 0$. The latter, in particular, implies [20] that the ISS gain with respect to input \hat{F}_{ei}^t is less than or equal to $2 \cdot \alpha_i \sqrt{\lambda_{\max}(\mathbb{P}_i) / \lambda_{\min}(\mathbb{P}_i)} |\mathbb{P}_i B_{mi}|$. The statement of Proposition 4.7.1 follows. •

Corollary 4.7.2 Consider the system (4.49) with an output

$$\mathbf{y}_{mi} := \left[X_{mi}^T, \dot{X}_{mi}^T, \ddot{X}_{mi}^T \right]^T. \quad (4.51)$$

The system (4.49), (4.51) is weakly input-to-output stable [17]; moreover, the IOS gain of (4.49), (4.51) with respect to input \hat{F}_{ei}^t can be made arbitrarily small by choosing $\alpha_i \in (0, 1]$ sufficiently small.

Proof: follows directly by combination of Proposition 4.7.1 and the fact that

$$|\ddot{X}_{mi}| \leq |M_{di}^m|^{-1} \left(\Upsilon_{mi} \cdot |\mathbf{x}_{mi}| + |F_{hi}^*| + \alpha_i \cdot |\hat{F}_{ei}^t| \right), \quad (4.52)$$

where $\Upsilon_{mi} := |B_{di}^m| + |B_{hi}^{e_i}| + |K_{di}^m| + |K_{hi}^{e_i}|$. •

Now, let us address the stability properties of the “Slave 1 + Environment + Slave 2” interconnection described by equations (4.25), (4.32). When the slave manipulators are in contact with the environment, we have $X_e(t) \equiv X_{s1}(t) \equiv X_{s2}(t)$, $\dot{X}_e(t) \equiv \dot{X}_{s1}(t) \equiv \dot{X}_{s2}(t)$, and $\ddot{X}_e(t) \equiv \ddot{X}_{s1}(t) \equiv \ddot{X}_{s2}(t)$. Combining (4.25), (4.32), and taking the above constraints into account, one obtains that the “Slave 1 + Environment + Slave 2” interconnection is described according to the formula

$$\hat{M} \ddot{X}_e + \hat{B} \dot{X}_e + \hat{K} X_e = \sum_{i=1}^2 \begin{bmatrix} K_{di}^s & B_{di}^s & M_{di}^s \end{bmatrix} \mathbf{u}_{ei}, \quad (4.53)$$

where $\hat{M} := M_{d1}^s + M_{d2}^s + M_e$, $\hat{B} := B_{d1}^s + B_{d2}^s + B_e$, $\hat{K} := K_{d1}^s + K_{d2}^s + K_e$, and where

$$\mathbf{u}_{ei} := \left[(X_{si}^d)^T, (\dot{X}_{si}^d)^T, (\ddot{X}_{si}^d)^T \right]^T, \quad i = 1, 2, \quad (4.54)$$

are the inputs of the ‘‘Slave 1 + Environment + Slave 2’’ interconnection. Also, taking into account the above constraints, the interaction forces F_{ei} become

$$F_{ei} = M_{di}^s (\ddot{X}_{si}^d - \ddot{X}_e) + B_{di}^s (\dot{X}_{si}^d - \dot{X}_e) + K_{di}^s (X_{si}^d - X_e), \quad i = 1, 2. \quad (4.55)$$

Let F_{ei} $i = 1, 2$, defined by (4.55) be the outputs of the ‘‘Slave 1 + Environment + Slave 2’’ interconnection (4.53). The following statement is valid.

Proposition 4.7.3 *The ‘‘Slave 1 + Environment + Slave 2’’ interconnection (4.53) is input-to-state stable. The same interconnection (4.53) with outputs (4.55) is weakly input-to-output stable.*

Proof: It follows directly from the assumptions imposed on the subsystems that \hat{M} , \hat{B} , \hat{K} are all positive definite, which implies that the system (4.53) with zero inputs $X_{si}^d(t) \equiv \dot{X}_{si}^d(t) \equiv \ddot{X}_{si}^d(t) = 0$, $i = 1, 2$, is asymptotically stable [3]. Input-to-state stability and the input-to-output stability follow immediately since the system is linear [20]. •

Now consider the overall teleoperator system which consists of the ‘‘Master+Human’’ dynamics (4.49), (4.51) and the ‘‘Slave 1 + Environment + Slave 2’’ subsystem (4.53), (4.55) interconnected through the communication channels (4.26)-(4.29), where the communication delays satisfy Assumption 3. The stability properties of this system can be analyzed using the WIOS small gain theorem for systems with communication constraints presented in [17]. Specifically, Proposition 4.7.1 together with the Corollary 4.7.2 imply that, for each $i \in \{1, 2\}$, the i -th ‘‘master+human’’ subsystem with inputs F_{hi}^* , \hat{F}_{ei}^t and output \mathbf{y}_{mi} defined by (4.51) is weakly input-to-output stable, and the corresponding IOS gain with respect to the input \hat{F}_{ei}^t is proportional to $\alpha_i \in (0, 1]$. For each $i \in \{1, 2\}$, let $\alpha_i \cdot \gamma_i^{mh} \geq 0$ denote the corresponding IOS gain from the input \hat{F}_{ei}^t to the output \mathbf{y}_{mi} . Furthermore, according to Proposition 4.7.3, the ‘‘Slave 1 + Environment + Slave 2’’ interconnection with inputs \mathbf{u}_{ei} , $i = 1, 2$ defined by (4.54) and outputs F_{ej} , $j = 1, 2$ defined by (4.55) is weakly input-to-output stable. For each $i, j = 1, 2$, let $\gamma_{ij}^{se} \geq 0$ denote the IOS gain from input \mathbf{u}_{ei} to output F_{ej} . Applying the WIOS small gain

theorem [17, Theorem 1], one can conclude that the trajectories of the closed-loop system are bounded and convergent if the following small-gain condition holds,

$$\rho \left(\begin{bmatrix} 0 & 0 & \gamma_{11}^{se} & \gamma_{21}^{se} \\ 0 & 0 & \gamma_{12}^{se} & \gamma_{22}^{se} \\ \alpha_1 \cdot \gamma_1^{mh} & 0 & 0 & 0 \\ 0 & \alpha_2 \cdot \gamma_2^{mh} & 0 & 0 \end{bmatrix} \right) < 1, \quad (4.56)$$

where $\rho(A)$ denotes the spectral radius of matrix A . The condition (4.56) can be equivalently written in terms of inequalities for minimal cycles of the above matrix, as follows,

$$\alpha_1 \cdot \gamma_1^{mh} \cdot \gamma_{11}^{se} < 1, \quad (4.57)$$

$$\alpha_2 \cdot \gamma_2^{mh} \cdot \gamma_{22}^{se} < 1, \quad (4.58)$$

$$\alpha_1 \cdot \gamma_1^{mh} \cdot \gamma_{12}^{se} \cdot \alpha_2 \cdot \gamma_2^{mh} \cdot \gamma_{21}^{se} < 1. \quad (4.59)$$

The latter conditions, in particular, demonstrate that the stability of the dual-arm MIS teleoperator system with projection based force reflection can be achieved with arbitrary large stability margin by picking $\alpha_i \in (0, 1]$ $i = 1, 2$ sufficiently small.

Chapter 5

Projection-Based Force Reflection

Algorithms with Frequency Separation

The material presented in this chapter has been accepted in *IEEE/ASME Transactions on Mechatronics*. A part of this work has also been published in the *Proceedings of IEEE International Conference of Robotics and Automation (ICRA)*, pp. 1484 – 1489, Karlsruhe, Germany 2013.

5.1 Introduction

Force reflecting teleoperation has been an extremely active research area over the last two decades. One of the major issues in the design of the force-reflecting teleoperators is the improvement of transparency while keeping the overall system stable under widest possible conditions imposed on the behaviour of the human operator as well as on the environmental dynamics. The stability, which is a notion that describes safe and predictable behaviour, is the requirement of paramount importance for any telerobotic system. Transparency, on the other hand, is a performance characteristics that describes the amount of distortion introduced by the teleoperator system in comparison with the direct execution of the task. In particular, an ideally transparent teleoperator system enables exact correspondence between the movements and forces on the master and slave sides of the system without introducing system's own dynam-

ics. The stability problems in force reflecting teleoperator systems arise due to the closed-loop structure of such a system. The strong force feedback creates destabilizing effect which manifests itself in the phenomenon known as the induced master motion (IMM, [11]). The IMM introduces perturbation in the closed-loop system, which calls for application of the design methods that make the closed-loop system robustly stable. In the case of networked teleoperators, additional stability problems arise because of communication constraints (in particular, delays) within the loop. Although there exists an enormous literature that deals with the design of stable feedback systems, direct application of most of the existing control design methods would result in unacceptably poor transparency. This constitutes the major challenge of the design of the force reflecting teleoperators.

A number of design methods for force reflecting teleoperators in the presence of communication delays has been developed, including scattering & wave-variable based methods [1, 13], time-domain passivity methods [23, 7], methods based on absolute stability [8], integral quadratic constraints (IQC [15]), linear matrix inequalities (LMIs [27, 10]), frequency-domain methods [6, 5], among many others. The input-to-output stability (IOS) small-gain approach to force reflecting teleoperators in the presence of communication delays was developed in [17, 22], among other works. Major advantages of the IOS small-gain approach are that it is applicable regardless of the specific choice of the force reflection signal and is robust with respect to communication constraints, such as irregular communication delays and packets drops. Direct application of the small-gain approach, however, imposes constraints on the force reflection gain. These constraints (which essentially reflect the requirement of the closed loop gain to be less than one) in many practical cases may severely limit the applicability of the teleoperator system. For example, in the impedance controlled teleoperator system that has position-force structure with no position or force scaling, the small gain condition essentially requires that the human-master interconnection must be more stiff than the slave-environment interconnection. To eliminate the conservatism of the small-gain approach, projection-based force reflection (PBFR) algorithms were introduced [18]. Our previous theoretical as well as experimental results indicate that the use of PBFR algorithms allows for drastic improvement in stability properties of the force reflecting teleoperator systems which, in particular, is achieved without increasing the impedance of the master manipulator and/or scaling down the

force reflection term. In particular, the approach guarantees that the steady-state error between the contact force on the slave side and the force reflected to the motors of the master is zero.

Despite of all the advantages described above, the PBFR algorithms developed so far have one substantial shortcoming. Specifically, the high-frequency component of the contact forces generated during initial phase of the contact with environment was typically filtered out from the force reflection term. This high-frequency component, however, is known to be very important for the haptic perception of stiff environments, in particular, they hardness and texture [4]; a high performance teleoperator system should therefore reflect the high-frequency component of the environmental forces with little to no distortion. In this work, we solve the above described problem by developing a new type of PBFR algorithms. The idea of these developments is to separate different frequency bands in the force reflection signal and use different algorithms to reflect these to the motors of the haptic device. In the simplest case, the force reflection signal is decomposed into its low- and high-frequency components; the high-frequency component is then applied to the master device directly, while the low-frequency force is reflected using the projection-based principle. It is interesting to notice that a somewhat similar idea of reflecting high frequency component of the contact force directly, although within a fundamentally different framework of wave variables, was used in [26]. We present a detailed stability analysis of a force reflecting teleoperator system with new type of PBFR algorithms in the presence of irregular communication delays. Using the small gain methods, we show that the stability of the force reflecting teleoperator system can always be achieved by implementing projection-based force reflection with the frequency separation scheme described above, by adjusting certain design parameters of the algorithm. Our experimental results demonstrate fundamental improvement of fidelity of the transient force response in comparison with the PBFR algorithm studied previously in [18, 21], which is achieved without any negative effect on stability of the system.

The paper is organized as follows. The teleoperator system under consideration is described in Section 5.2, including assumptions imposed on the stability properties of the controlled master and slave subsystems as well as assumptions on the human dynamics. In Section 5.3, the projection-based force reflection algorithms with frequency separation are described. The main theoretical result is presented in Section 5.4. In Section 5.5, the experimental results are

described in some detail. Conclusions are given in Section 5.6. Appendix 5.6 contains a proof of the main theoretical result as well as some necessary background materials.

5.2 Teleoperator system and human dynamics

We consider a force reflecting teleoperator system that consists of one master and one slave manipulator communicating over a networked channel. A linear model of the controlled master manipulator is addressed as follows:

$$\begin{aligned} M_m \ddot{x}_m &= -D_m \dot{x}_m - K_m x_m + f_h - f_r, \\ y_m &= C_{m1} x_m + C_{m2} \dot{x}_m, \end{aligned} \quad (5.1)$$

where $x_m, \dot{x}_m, \ddot{x}_m \in \mathbb{R}^n$ are the master position, velocity, and acceleration, respectively, $M_m, D_m, K_m \in \mathbb{R}^{n \times n}$ are symmetric nonnegative definite matrices of the master's equivalent inertia, damping, and stiffness, respectively, and $C_{m1}, C_{m2} \in \mathbb{R}^{p \times n}$ are some matrices. Also, $f_h \in \mathbb{R}^n$ is the human force and $f_r \in \mathbb{R}^n$ is the force reflected to the motors of the master. The closed-loop linear model (5.1) can be obtained as a result of linearization of the corresponding nonlinear Euler-Lagrange equations and/or by means of active control algorithms, such as impedance control. Below, we use the notation

$$A_m := \begin{bmatrix} \mathbb{O} & \mathbb{I} \\ -M_m^{-1} K_m & -M_m^{-1} D_m \end{bmatrix} \in \mathbb{R}^{2n \times 2n}. \quad (5.2)$$

where $\mathbb{O}, \mathbb{I} \in \mathbb{R}^{n \times n}$ are zero and unit matrices, respectively. The following stability condition is imposed on the controlled master device (5.1).

Assumption 1. The matrix A_m is Hurwitz, *i.e.*, $\Re \lambda_i < 0$, where $\lambda_i, i = 1, \dots, 2n$ are the eigenvalues of A_m . •

Remark 1. Assumption 1 is satisfied, in particular, if the matrices M_m, D_m, K_m are all positive definite. A detailed treatment of the stability problem of n-DOF linear second-order systems can be found in [2].

Remark 2. Assumption 1 is equivalent to the fact that A_m satisfies the following Lyapunov equation

$$A_m^T P + P A_m = -I, \quad (5.3)$$

where $\mathbb{P} = \mathbb{P}^T \in \mathbb{R}^{2n \times 2n}$ is a positive definite matrix defined as

$$\mathbb{P} := \int_0^{+\infty} e^{A_m^T t} e^{A_m t} dt. \quad (5.4)$$

This simple fact will be used frequently throughout the paper. •

The purpose of the slave manipulator is to execute task while interacting with the environment. In this work, we assume that the slave-environment interconnection is described by a linear time-invariant system of the following form

$$\begin{aligned} \dot{x}_{se} &= A_{se} x_{se} + B_{se} u_{se} + F_{se} w_{se}, \\ y_{se} &= C_{se} x_{se} + D_{se} u_{se} + G_{se} w_{se}, \end{aligned} \quad (5.5)$$

where $x_{se} \in \mathbb{R}^{n_{se}}$ is the state of the slave environment interconnection, which is typically a combination of the slave's and the environment's states, $u_{se} \in \mathbb{R}^{m_{se}}$ is the reference input that arrives from the master site, $w_{se} \in \mathbb{R}^{q_{se}}$ are the external disturbances acting on the slave environment interconnection, $y_{se} \in \mathbb{R}^n$ is the output of the slave-environment interconnection, and A_{se} , B_{se} , C_{se} , D_{se} , F_{se} , G_{se} are matrices of the corresponding dimensions. The assumption of linearity of the slave-environment interconnection is not essential for our work and is made entirely for the purpose of simplifying the presentation. However, the essential assumption is that the system (5.5) is stable, which means that the slave local control system is designed in such a way that the coupled stability problem for the slave-environment interconnection is solved. For details and some basic results on coupled stability, see for example [3].

Assumption 2. The matrix A_{se} in (5.5) is Hurwitz. •

The communication between the master and the slave is described according to the formulae

$$u_{se}(t) := y_m(t - \tau_f(t)) + \delta_f(t), \quad (5.6)$$

$$f_{env}(t) := y_{se}(t - \tau_b(t)) + \delta_b(t), \quad (5.7)$$

where $\tau_f, \tau_b: \mathbb{R}_+ \rightarrow \mathbb{R}_+$ are forward and backward communication delay functions which, in general, can be time-varying, discontinuous and unbounded, $\delta_f(t)$, $\delta_b(t)$ are communication errors in the forward and backward communication channels, and f_{env} is the force feedback signal from the slave site. The communication process is assumed to satisfy the following assumption.

Assumption 3. The communication delays $\tau_f, \tau_b: \mathbb{R}_+ \rightarrow \mathbb{R}_+$ are Lebesgue measurable functions satisfying

$$\max \{ \tau_b(t), \tau_f(t) \} \leq \tau_*(t) \quad \text{for all } t \in \mathbb{R}_+, \quad (5.8)$$

where $\tau_*: \mathbb{R}_+ \rightarrow \mathbb{R}_+$ is such that $\tau_*(t_2) - \tau_*(t_1) \leq t_2 - t_1$ and $t - \tau_*(t) \rightarrow +\infty$ as $t \rightarrow +\infty$. The communication errors $\delta_f(t), \delta_b(t)$ are arbitrary Lebesgue measurable uniformly essentially bounded signals. •

Assumption 3 imposes extremely mild constraints on the communication process and can always be satisfied in any real-life communication networks unless the communication is totally lost on a semi-infinite time interval. See also [19].

The dynamics of the human operator are described by the following simplified linear model [25]:

$$f_h = -D_h \dot{x}_m - K_h x_m + f_h^*, \quad (5.9)$$

where $D_h, K_h \in \mathbb{R}^{n \times n}$ are symmetric nonnegative definite matrices that represent damping and stiffness of the human operator hand, and $f_h^*(\cdot)$ is an uniformly essentially bounded force. The first two terms in the right-hand side of (5.9) represent a passive reaction of the human operator hand to the movement of the master device, while f_h^* represents an active component of the human hand force which is voluntary generated by the human operator, typically for the purpose of moving the master device along a desired trajectory. While there are no assumptions imposed on the active component f_h^* (except the mentioned uniform essential boundedness), the assumption regarding the reactive component of the human dynamics (5.9) is that it does not destabilize the master device (5.1). A rigorous formulation of this assumption is as follows.

Assumption 4. The inequality

$$A_h^T \mathbb{P} + \mathbb{P} A_h \leq 0 \quad (5.10)$$

is valid, where $\mathbb{P} = \mathbb{P}^T$ is defined by (5.4), and

$$A_h := \begin{bmatrix} \mathbb{O} & \mathbb{O} \\ -M_m^{-1} K_h & -M_m^{-1} D_h \end{bmatrix} \in \mathbb{R}^{2n \times 2n}. \bullet$$

Remark 3. Assumption 4 can be given the following interpretation. As Remark 2 above indicates, $V_m := \begin{bmatrix} x_m^T & \dot{x}_m^T \end{bmatrix} \mathbb{P} \begin{bmatrix} x_m^T & \dot{x}_m^T \end{bmatrix}^T$ is a Lyapunov function for the controlled master subsystem (5.1). Inequality (5.10) then implies that the contribution of the reactive component

of the human operator forces to the time derivative of V is nonpositive, which implies that the natural reaction of the human hand to the movement of the master device is such that it does not destabilize the master subsystem. This assumption is in accordance with the conclusions made by Hogan in [9] that “... this experimental result strongly suggests that neural feedback in the human arm is carefully tuned to preserve stability under the widest possible set of conditions.”

•

Remark 4. The assumptions imposed on the human dynamics, in particular, allow for the case where $D_h = K_h = \mathbb{O}$, and $f_h^*(t) \equiv 0$, which essentially corresponds to the situation where the human operator releases the master device. Therefore, under the above assumptions, the case where the human operator holds the master and the case where (s)he releases the master can be considered simultaneously. •

5.3 Projection-based force reflection algorithms with frequency separation

The force feedback may be useful as it enables the interaction between the operator’s hand and the remote environment; it can also be harmful as it may generate the momentum which potentially results in instability. Which of these two effects dominates in fact depends on the behaviour of the human operator. More specifically, the component of the reflected force that is explicitly compensated by the counter-force of the human hand creates a feeling of interaction for the human operator; the residual component of the reflected force may, in particular, generate momentum potentially leading to instability. The projection-based force reflection principle [18, 21] suggests to identify these two complementary components, apply the former in full and attenuate the latter to a level which is not dangerous for the stability of the overall system. Since the former component is the one that creates the haptic feeling of the interaction while the latter is the one that may generate instability, the projection-based force reflection principle essentially aims to improve stability without compromising the feeling of interaction with the environment. One possible rule of a thumb to define the “interaction” component ϕ_{env}

is described by the formula

$$\phi_{env} := \text{Sat}_{[0,1]} \left\{ \frac{f_{env}^T \bar{f}_h}{\|\bar{f}_h\|^2 + \epsilon} \right\} \bar{f}_h, \quad (5.11)$$

where f_{env} is the force feedback from the slave site, \bar{f}_h is the estimate of the human force applied to the haptic device, $\epsilon > 0$ is a small constant introduced to avoid singularity at $\bar{f}_h = 0$, and $\|\cdot\|$ denotes the 2-norm. Essentially, the algorithm (5.11) calculates the interaction component as the projection of the force feedback onto the direction against human force with magnitude bounded by the magnitude of the human force. The projection-based force reflection principle then suggests to generate the force reflection signal as a weighted combination of the direct force feedback f_{env} and the projection based component ϕ_{env} , according to the formula

$$f_r = \alpha \cdot f_{env} + (1 - \alpha) \cdot \phi_{env}, \quad (5.12)$$

where f_r is the force reflected to the motors of the master device, and $\alpha \in [0, 1)$ is the weighting coefficient. The above formula may become easier to interpret if one introduces a notation $\chi := f_{env} - \phi_{env}$. Thus, χ represents the momentum-generating component which is residual to ϕ_{env} . In this notation, the formula (5.12) becomes

$$f_r = \phi_{env} + \alpha \cdot \chi, \quad (5.13)$$

which implies that the force reflection algorithm (5.12) directly reflects the projection-based component ϕ_{env} while attenuating the residual momentum-generating component χ .

It was previously demonstrated [18, 21] that the use of PBFR algorithms allows for drastic improvement in stability properties of the force reflecting teleoperator systems and haptic interfaces for interaction with virtual environment (VE). Moreover, experiments with force-reflecting teleoperator systems [21] and haptic interfaces for interaction with VE [20] demonstrate that the PBFR algorithms guarantee perfect force convergence in the steady state. However, these experiments also reveal that, although the reflected forces converge to the contact forces, this convergence becomes somewhat slower for low values of α . The reason for this is that, in the case of PBFR algorithms, the force reflection depends on the interaction between the human hand and the haptic device. For small α , only a small fraction of the reflected force is applied to the haptic device in the very beginning of the contact. If the counter force applied by the human operator is detected, the force reflected increases by the amount which is not

greater than the human counterforce. In the situation where the estimate of the human force is obtained using an observer with its own relatively slow dynamics, it typically takes certain amount of time to build up the reflected force. As a result, the high-frequency component of the reflected force is filtered out in the beginning of the contact, which results in loss of important haptic information and contributes to transparency deterioration.

In this work, we propose a solution to the above described problem. The solution is based on the idea to separate different frequency bands in the force reflection signal and use different algorithms to reflect these to the motors of the haptic device. In the simplest case considered in this paper, the force reflection signal is decomposed into its low- and high-frequency components; the high-frequency component is then applied to the master device directly, while the low-frequency force is reflected using the projection-based algorithm. Mathematically, we propose a modification of the force reflection algorithm (5.11), (5.12), which is based on a decomposition of the force feedback signal into the sum of high- and low-frequency components, as follows,

$$f_{env} = f_{env}^l + f_{env}^h, \quad (5.14)$$

where f_{env}^l and f_{env}^h are low- and high-frequency components of the force feedback signal, respectively, that are obtained using complimentary low- and high-pass filters described in Laplace domain as follows,

$$f_{env}^l(s) := \frac{\omega_c}{s + \omega_c} \cdot f_{env}(s), \quad (5.15)$$

$$f_{env}^h(s) := \frac{s}{s + \omega_c} \cdot f_{env}(s), \quad (5.16)$$

where $\omega_c > 0$ is the cut-off frequency of the filters. We propose to consider the following force reflecting scheme,

$$f_r := f_{env}^h + \alpha \cdot f_{env}^l + (1 - \alpha) \cdot \phi_{env}^l, \quad (5.17)$$

where ϕ_{env}^l is the projection-based component of the low-frequency signal f_{env}^l which is calculated according to the formula

$$\phi_{env}^l := \text{Sat}_{[0,1]} \left\{ \frac{\bar{f}_h^T \cdot f_{env}^l}{|\bar{f}_h|^2 + \epsilon} \right\} \bar{f}_h, \quad (5.18)$$

and $\alpha \in [0, 1]$ is a weighting coefficient that represents the relative weight of the direct component in the force reflection algorithm; the relative weight of the projection-based force reflection

tion component is therefore equal to $1 - \alpha \in [0, 1]$. In (5.18), \bar{f}_h is the measurement/estimate of the human force f_h which is performed with an error Δf_h , *i.e.*,

$$\Delta f_h := \bar{f}_h - f_h, \quad (5.19)$$

and $\epsilon > 0$ is a small constant. The overall structure of the teleoperation system with PBFR algorithms and frequency separation is shown in Figure 5.1.

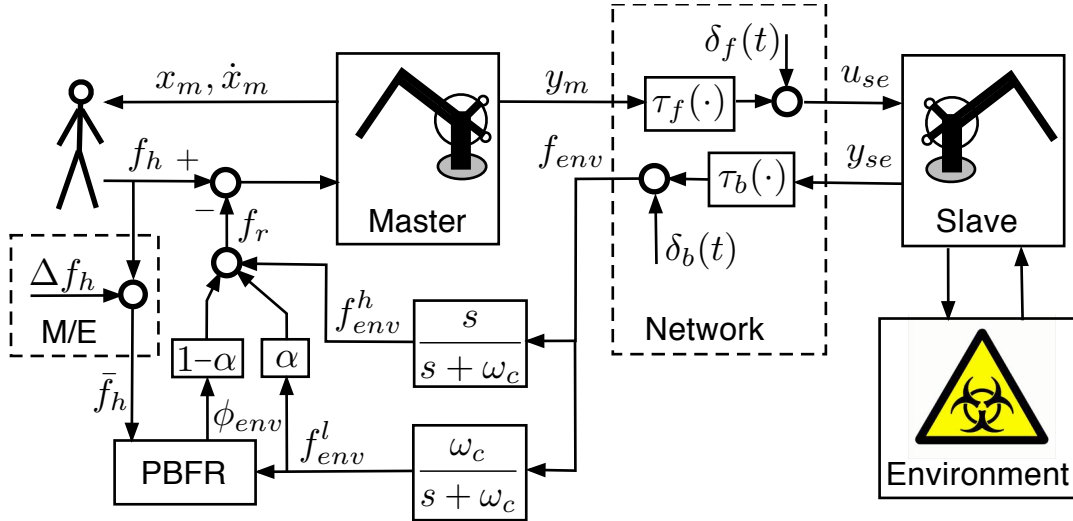


Figure 5.1: General structure of the teleoperator system with projection-based force reflection and frequency separation. Acronyms: PBFR - projection-based force reflection algorithm; M/E - measurement/estimation of the human force.

5.4 Theoretical Results

In this section, we establish the main theoretical result of this work. The result states that stability of the teleoperator system described above can be achieved by choosing the cut-off frequency $\omega_c \geq 0$ of the filters (5.15), (5.16) sufficiently large and the weighting coefficient $\alpha \in (0, 1]$ in the algorithm (5.17) sufficiently small. To formulate this result in a rigorous manner, let us introduce the following notation. For a transfer matrix $H(s) \in \mathbb{C}^{p \times m}$, its 1-norm is defined according to the formula

$$\|H(s)\|_1 := \int_{t=0}^{+\infty} |h(\tau)| d\tau,$$

where $h(t) := \mathcal{L}^{-1} [H(s)]$ the impulse response matrix corresponding to $H(s)$. Denote

$$\gamma_{u_{se}}^{y_{se}} := \left\| C_{se} [s\mathbb{I} - A_{se}]^{-1} B_{se} + D_{se} \right\|_1, \quad (5.20)$$

$$\gamma_{w_{se}}^{y_{se}} := \left\| C_{se} [s\mathbb{I} - A_{se}]^{-1} F_{se} + G_{se} \right\|_1, \quad (5.21)$$

$$\gamma_{hy} := \left\| \left[C_m [s\mathbb{I} - A_{mh}]^{-1} B_m \right] \cdot \left[\frac{s}{s + \omega_c} \right] \right\|_1, \quad (5.22)$$

$$\gamma_{hf} := \left\| \left[C_h [s\mathbb{I} - A_{mh}]^{-1} B_m \right] \cdot \left[\frac{s}{s + \omega_c} \right] \right\|_1, \quad (5.23)$$

where

$$A_{mh} := \begin{bmatrix} \mathbb{O} & \mathbb{I} \\ -M_m^{-1} (K_m + K_h) & -M_m^{-1} (D_m + D_h) \end{bmatrix},$$

$$B_m := \begin{bmatrix} \mathbb{O} \\ M_m^{-1} \end{bmatrix}, \quad C_m := \begin{bmatrix} C_{m1} & \mathbb{O} \\ \mathbb{O} & C_{m2} \end{bmatrix}, \quad C_h := \begin{bmatrix} K_h & \mathbb{O} \\ \mathbb{O} & D_h \end{bmatrix},$$

Also, denote

$$\gamma_{f_h}^{y_m} := 2 \bar{\sigma}(C_m) \cdot \bar{\sigma}(\mathbb{P} B_m) \cdot \sqrt{\lambda_{\max}(\mathbb{P}) / \lambda_{\min}(\mathbb{P})}, \quad (5.24)$$

$$\gamma_{f_e}^{y_m} := \gamma_{hy} + \gamma_{hf} \cdot \gamma_{f_h}^{y_m} + \gamma_{f_h}^{y_m} \cdot \alpha, \quad (5.25)$$

where $\lambda_{\max}(\mathbb{P})$, $\lambda_{\min}(\mathbb{P})$ are maximum and minimum eigenvalues, respectively, of a symmetric matrix \mathbb{P} defined by (5.4), and $\bar{\sigma}(\cdot)$ denotes the largest singular value. The main theoretical result of this paper can now be formulated as follows.

Theorem 5.4.1 *Consider the teleoperator system (5.1), (5.5), (5.6), (5.7), (5.9), (5.15), (5.16), (5.17), (5.18), (5.19). Suppose Assumptions 1, 2, 3, and 4 hold. If*

$$\gamma_{f_e}^{y_m} \cdot \gamma_{u_{se}}^{y_{se}} < 1, \quad (5.26)$$

then the trajectories of the closed-loop teleoperator system are bounded and convergent; specifically, the following estimates are valid

$$\begin{aligned} \sup_{t \geq 0} |y_m(t)| &\leq |C_m| \cdot \sqrt{|x_m(0)|^2 + |\dot{x}_m(0)|^2} \\ &+ \gamma_{f_e}^{y_m} \cdot |C_{se}| \cdot |x_{se}(0)| + \gamma_{f_e}^{y_m} \cdot \gamma_{w_{se}}^{y_{se}} \cdot \sup_{t \geq 0} |w_{se}(t)| \\ &+ \gamma_{f_h}^{y_m} \cdot \sup_{t \geq 0} |f_h^*(t)| + \gamma_{f_h}^{y_m} \cdot (1 - \alpha) \cdot \sup_{t \geq 0} |\Delta f_h(t)| \\ &+ \gamma_{f_e}^{y_m} \cdot \sup_{t \geq 0} |\delta_b(t)| + \gamma_{f_e}^{y_m} \cdot \gamma_{u_{se}}^{y_{se}} \cdot \sup_{t \geq 0} |\delta_f(t)|, \end{aligned} \quad (5.27)$$

$$\begin{aligned}
\sup_{t \geq 0} |y_{se}(t)| &\leq |C_{se}| \cdot |x_{se}(0)| \\
&+ \gamma_{u_{se}}^{y_{se}} \cdot |C_m| \cdot \sqrt{|x_m(0)|^2 + |\dot{x}_m(0)|^2} \\
&+ \gamma_{u_{se}}^{y_{se}} \cdot \gamma_{f_h}^{y_m} \cdot \sup_{t \geq 0} |f_h^*(t)| + \gamma_{w_{se}}^{y_{se}} \cdot \sup_{t \geq 0} |w_{se}(t)| \\
&+ \gamma_{u_{se}}^{y_{se}} \cdot \gamma_{f_h}^{y_m} \cdot (1 - \alpha) \cdot \sup_{t \geq 0} |\Delta f_h(t)| \\
&+ \gamma_{u_{se}}^{y_{se}} \cdot \sup_{t \geq 0} |\delta_f(t)| + \gamma_{u_{se}}^{y_{se}} \cdot \gamma_{f_e}^{y_m} \cdot \sup_{t \geq 0} |\delta_b(t)|,
\end{aligned} \tag{5.28}$$

$$\begin{aligned}
\limsup_{t \rightarrow +\infty} |y_m(t)| &\leq \gamma_{f_e}^{y_m} \cdot \gamma_{w_{se}}^{y_{se}} \cdot \limsup_{t \rightarrow +\infty} |w_{se}(t)| \\
&+ \gamma_{f_h}^{y_m} \limsup_{t \rightarrow +\infty} |f_h^*(t)| + \gamma_{f_h}^{y_m} (1 - \alpha) \limsup_{t \rightarrow +\infty} |\Delta f_h(t)| \\
&+ \gamma_{f_e}^{y_m} \limsup_{t \rightarrow +\infty} |\delta_b(t)| + \gamma_{f_e}^{y_m} \gamma_{u_{se}}^{y_{se}} \limsup_{t \rightarrow +\infty} |\delta_f(t)|,
\end{aligned} \tag{5.29}$$

$$\begin{aligned}
\limsup_{t \rightarrow +\infty} |y_{se}(t)| &\leq \gamma_{w_{se}}^{y_{se}} \cdot \limsup_{t \rightarrow +\infty} |w_{se}(t)| \\
&+ \gamma_{u_{se}}^{y_{se}} \cdot \gamma_{f_h}^{y_m} \cdot \limsup_{t \rightarrow +\infty} |f_h^*(t)| \\
&+ \gamma_{u_{se}}^{y_{se}} \gamma_{f_h}^{y_m} (1 - \alpha) \limsup_{t \rightarrow +\infty} |\Delta f_h(t)| \\
&+ \gamma_{u_{se}}^{y_{se}} \limsup_{t \rightarrow +\infty} |\delta_f(t)| + \gamma_{u_{se}}^{y_{se}} \gamma_{f_e}^{y_m} \limsup_{t \rightarrow +\infty} |\delta_b(t)|.
\end{aligned} \tag{5.30}$$

In addition, the gain $\gamma_{f_e}^{y_m} > 0$ defined by (5.25) can be assigned arbitrarily small and, therefore, the small gain condition (5.26) can always be met by choosing $\omega_c \geq 0$ sufficiently large and $\alpha \in (0, 1]$ sufficiently small. •

Proof of Theorem 5.4.1 is given in Appendix 5.6.

Remark 5. The gain $\gamma_{f_e}^{y_m} > 0$ defined by (5.25) quantifies the relationship between the force reflected from the slave side and the resulting amount of the induced master motion (IMM [11]); thus, $\gamma_{f_e}^{y_m}$ can reasonably be called the IMM gain of the teleoperator system. The small-gain condition (5.26) implies that the teleoperator system is stable if its IMM gain is sufficiently low. This result is in complete accordance with the considerations presented in [11], where it was demonstrated that the IMM, if sufficiently strong, triggers the mechanism of instability in the force reflecting teleoperators. •

Remark 6. Formula (5.25) implies that the IMM gain can be represented as a sum $\gamma_{f_e}^{y_m} = \gamma_h^\# + \gamma_l^\#$, where $\gamma_h^\# := \gamma_{hy} + \gamma_{hf} \cdot \gamma_{f_h}^{y_m}$ and $\gamma_l^\# := \gamma_{f_h}^{y_m} \cdot \alpha$ correspond to the high- and the low-frequency components of the reflected force, respectively. Gains $\gamma_h^\#, \gamma_l^\#$ can be made arbitrarily

low by choosing $\omega_c > 0$ sufficiently large and $\alpha > 0$ sufficiently small, respectively. To derive the minimum value of $\omega_c > 0$ and the maximum value of $\alpha > 0$ such that the stability condition (5.26) is satisfied, one can use the following procedure. First, $\gamma_{u_{se}}^{y_{se}}$ and $\gamma_{f_h}^{y_m}$ are to be calculated using formulas (5.20) and (5.24), respectively. Next, the maximum admissible values of γ_{hy} , γ_{hf} , and α can be found from (5.25) and (5.26). An appropriately small $\alpha > 0$ can then be directly assigned by the designer. On the other hand, it is demonstrated in the proof of Theorem 5.4.1 that $\gamma_{hy} > 0$ and $\gamma_{hf} > 0$ can be made arbitrarily small by choosing $\omega_c > 0$ sufficiently large. For given maximal admissible values of $\gamma_{hy} > 0$ and $\gamma_{hf} > 0$, the lower bound for $\omega_c > 0$ can be found from (5.22), (5.23) using partial fraction expansion. •

Remark 7. An important feature of our approach is that decreasing the IMM gain does not affect the gain $\gamma_{f_h}^{y_m}$ defined by (5.24), which represents the gain between the human force and the resulting motion of the master manipulator. Indeed, $\gamma_{f_h}^{y_m}$ is determined entirely by the mechanical parameters of the master manipulator and the local master control algorithm and does not depend on ω_c and α . From practical point of view, this implies that the stability of the system can be achieved (with an arbitrarily large margin if necessary), while the master manipulator remains compliant with respect to the forces applied by the human operator. This is an important and, to the best of our knowledge, unique feature of the projection-based force reflection algorithms. •

5.5 Experimental Results

In this section, we present some results of experimental evaluation of the effect on the stability and force convergence of a force-reflecting teleoperator system brought in by the PBFR algorithms with frequency separation.

Experimental setup. The experimental setup is shown in Figure 5.2; it consists of a single-master single-slave force reflecting telerobotic system, where the master is controlled by the human operator and the slave interacts with a virtual wall. The Phantom Omni™ haptic devices manufactured by SensAble Technologies Inc. were used as the master and the slave devices in these experiments. Phantom Omni™ devices have 6 DOF position sensing and 3 DOF force feedback, and they were programmed using the OpenHaptics toolkit. The mas-

ter and the slave devices were controlled from two different PCs connected over a local area network. The time-varying communication delays between the master and the slave devices were artificially created using internal buffers and an algorithm that generates random delays and packet dropouts with prescribed characteristics. All the experiments were run at the sampling frequency of 1000 Hz. The estimates of the human force which are used in the PBFR algorithms are obtained using the high-gain force observer designed in [20].

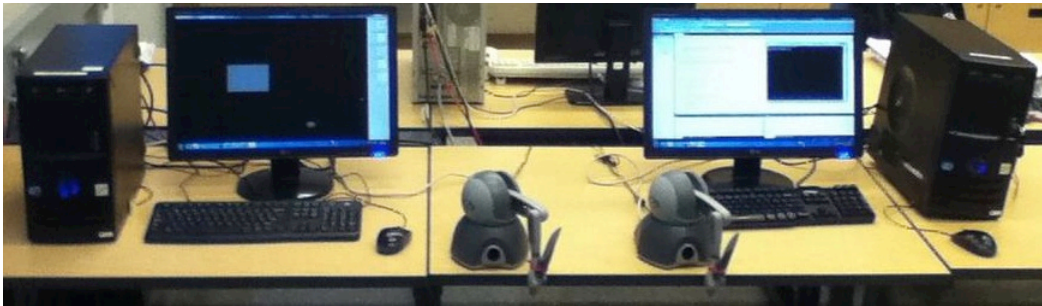


Figure 5.2: Experimental Setup

Control algorithm. The slave device is controlled in joint space using the following model based control algorithm [16]:

$$u_s = M_s(q_s)(\dot{\xi}_2 + \Lambda_s(\dot{\xi}_1 - \dot{q}_s)) + C_s(q_s, \dot{q}_s)(\xi_2 + \Lambda_s(\xi_1 - q_s)) + G_s(q_s) - K_{vs}(\dot{q}_s - \xi_2) - K_{ps}\Lambda_s(q_s - \xi_1),$$

where $M_s(q_s) \in \mathbb{R}^{3 \times 3}$, $C_s(q_s, \dot{q}_s) \in \mathbb{R}^{3 \times 3}$, and $G_s(q_s) \in \mathbb{R}^3$ are the matrices of inertia and of Coriolis/centrifugal forces/torques and the vector of gravitational forces/torques, respectively, of the mathematical model of the Phantom OmniTM haptic device identified in [20]. Also, K_{ps} , K_{vs} , $\Lambda_s \in \mathbb{R}^{3 \times 3}$ are symmetric positive definite gain matrices; in the experiments discussed below, $K_{psi} = \text{diag}\{4, 4, 4\}$, $K_{vsi} = \text{diag}\{0.01, 0.01, 0.01\}$, and $\Lambda_{si} = \text{diag}\{1, 1, 1\}$. Furthermore, ξ_1 , ξ_2 are estimates generated by a filter of the form

$$\begin{aligned} \dot{\xi}_1 &= \xi_2 + g\alpha_1(\hat{q}_m - \xi_1), \\ \dot{\xi}_2 &= g^2\alpha_0(\hat{q}_m - \xi_1), \end{aligned} \tag{5.31}$$

where \hat{q}_m is the vector of master joint coordinates as received on the slave side, α_0 , $\alpha_1 > 0$ are such that the roots of $p(s) = s^2 + \alpha_1 s + \alpha_0$ have negative real parts, and $g > 0$ is the gain of the

filter. In the presence of time-varying discontinuous communication delays $\tau(t)$, the reference trajectory $\hat{q}_m(t) = q_m(t - \tau(t))$ may become discontinuous; the main purpose of the filter (5.31) is to generate a smooth approximation of a possibly discontinuous reference signal $\hat{q}_m(t)$. In the experiments presented below, $g = 10$, $\alpha_1 = 1$, and $\alpha_0 = 1$.

Experimental results: free motion. The above designed teleoperator system demonstrates excellent trajectory tracking properties in free motion; the results of a free motion test are shown in Figure 5.3.

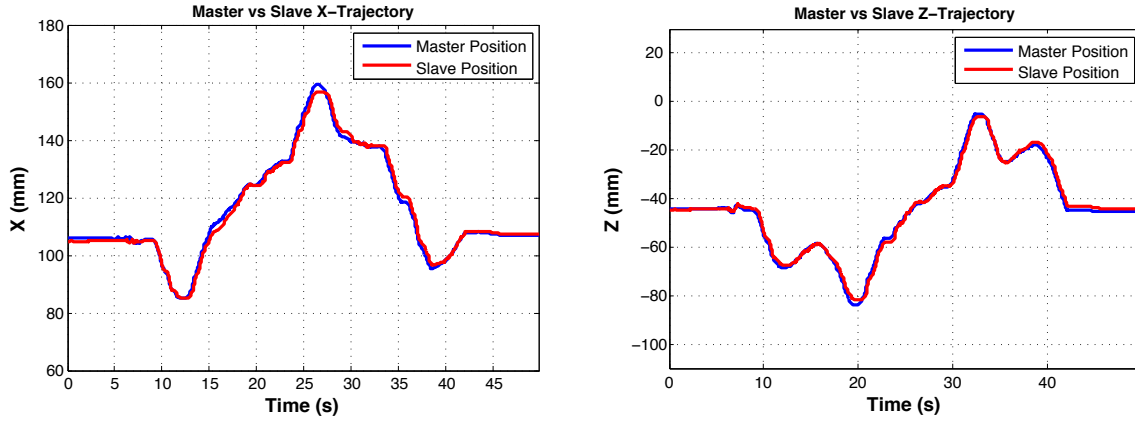


Figure 5.3: Tracking performance of the teleoperator system during free motion test: X-trajectories of the master and slave vs. time (left); Z-trajectories of the master and slave vs. time (right).

Experimental results: contact with an obstacle. In this set of experiments, we evaluate stability and force convergence of the proposed method in the situation where the slave contacts an obstacle in virtual environment. Specifically, the human operator moves the master device, and the slave follows the motion of the master and contacts the virtual wall. The contact force is then transferred back to the master site where it is reflected to the motors of the master using PBFR algorithms, with or without frequency separation. The virtual wall is positioned perpendicular to the x -direction of the spatial coordinate system and is located at $x = 0$. In order to realistically display a hard contact with the environment, we use the method for rendering of a virtual wall developed in [14] (see also [12]). In this approach, the contact force is generated according to the formula

$$f_{env} = -Kx - A \cdot v_0 \cdot \exp(-Bt) \cdot \sin(2\pi\omega t), \quad (5.32)$$

where x is the depth of penetration of the end-effector avatar into the surface of the wall, $K \geq 0$ is the wall stiffness, v_0 is the impact velocity, A is the amplitude slope parameter, B is the decay rate of the sinusoid, and ω is the frequency of the sinusoidal signal. The second term in the right-hand side of (5.32) is the temporal impact vibration which is produced at the start of the contact and has a form of exponentially decaying sinusoid. In the experiments presented below, the following parameters are chosen: $\omega = 300$ Hz, $A = 0.3$ N·s/m, and $B = 90$ s⁻¹.

In Figures 5.4 – 5.9, the results of experiments are shown for $K = 1000$ N/m and the time-varying communication delay with minimum round-trip time (RTT) equal to 0.4 s; the profile of (one direction) communication delay is shown in Figure 5.4 (left plot). Results shown in Figure 5.5 correspond to the case of PBFR algorithm without frequency separation (PBFR without FS), while Figures 5.6, 5.7, and 5.8 correspond to PBFR with frequency separation (PBFR FS) with $\omega_c = 30$ Hz, $\omega_c = 20$ Hz, and $\omega_c = 10$ Hz, respectively; in each case, the X-trajectories of the master and the slave devices as well as the contact X-forces as received at the master site and the X-forces reflected to the master device are shown. In all these experiments, $\alpha = 0.1$. It can be seen that the teleoperator system demonstrates stable behaviour in all these cases; however, the force convergence during initial phase of the contact is fundamentally improved when using PBFR FS. More specifically, the force convergence improves as ω_c decreases; in particular, PBFR without FS (which can be considered as a “limit case” of PBFR FS with $\omega_c = +\infty$) demonstrates the worst force convergence, while PBFR FS with $\omega_c = 10$ Hz performs the best. For the purpose of comparison, the magnified view of the force responses during the initial phase of the contact are shown in Figure 5.9 for PBFR without FS (top plot) and PBFR FS with $\omega_c = 10$ Hz (bottom plot). It can be seen that, in the case of PBFR without FS, the force response convergence is slow, and the high-frequency component of the contact force during the initial phase of the contact is almost completely lost. On the other hand, in the case of PBFR FS with $\omega_c = 10$ Hz, the reflected force is virtually indistinguishable from the delayed contact force during the initial phase of the contact, and the high-frequency component of the contact force is reflected without distortion.

Samples of experimental results for longer communication delays with minimum RTT = 1 s are shown in Figures 5.10-5.12; the delay profile is shown in Figure 5.4 (right plot). Although longer communication delays result in some minor overall performance deterioration,

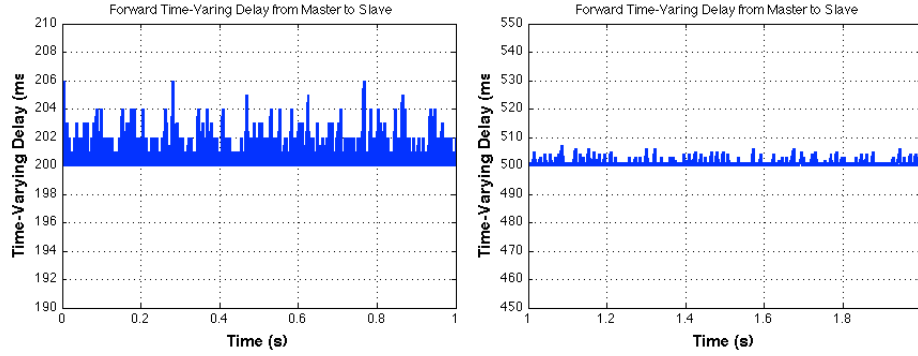


Figure 5.4: Examples of (one directional) communication delays: delay with minimum RTT= 400 ms used in the experiments shown in Figures 5.5-5.9 (left plot); delay with minimum RTT= 1000 ms used in the experiments shown in Figures 5.10-5.12 (right plot)

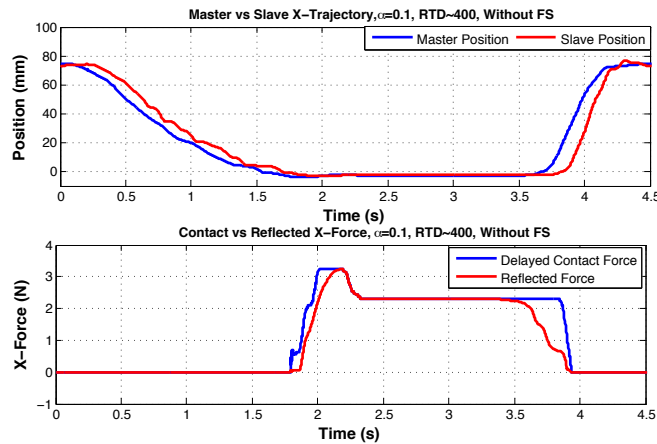


Figure 5.5: Response of the teleoperator system, min RTT= 400 ms, PBFR without FS (5.11), (5.12), $\alpha = 0.1$: X-trajectories of the master and slave (top plot); contact X-forces as received on the master site vs. reflected X-forces (bottom plot).

however, the picture remains the same in that the force convergence during the initial contact is also fundamentally improved by using PBFR FS which, in particular, can be clearly seen in Figure 5.12.

Experimental results: stability test. The above presented experimental results demonstrate fundamental improvement of the force convergence during the initial phase of contact with environment; however, these results do not allow for a clear conclusion on how the change of cut-off frequency $\omega_c > 0$ affects stability of the teleoperator system. Indeed, the teleoperator system appears to be stable for a wide range of $\omega_c > 0$; however, since the human operator

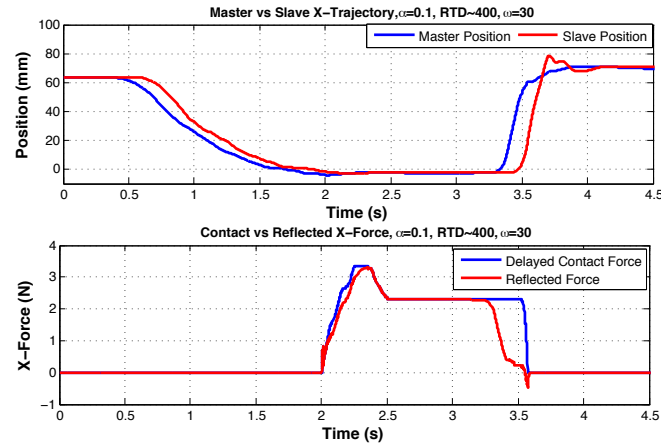


Figure 5.6: Response of the teleoperator system, min RTT= 400 ms, PBFR FS (5.15), (5.16), (5.17), (5.18), $\alpha = 0.1$, $\omega_c = 30$ Hz: X-trajectories of the master and the slave (top plot); contact X-forces as received on the master site vs. reflected X-forces (bottom plot).

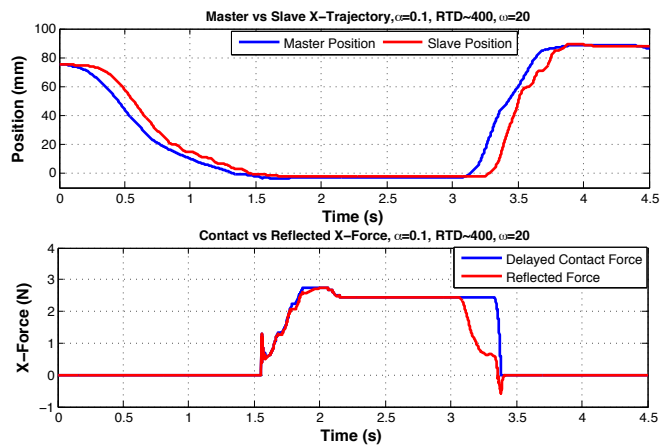


Figure 5.7: Response of the teleoperator system, min RTT= 400 ms, PBFR FS (5.15), (5.16), (5.17), (5.18), $\alpha = 0.1$, $\omega_c = 20$ Hz: X-trajectories of the master and the slave (top plot); contact X-forces as received on the master site vs. reflected X-forces (bottom plot).

holds the device throughout the experiment, the stability may be a consequence of the human operator's stabilizing actions. One possible way to evaluate stability of a teleoperator system independently on the human operator actions is to observe the amount of the induced master motion (IMM) generated by a similar profile of interaction forces, while the operator releases the master device. Indeed, as explained in Remark 5, stability of the teleoperator system is directly related to its IMM gain $\gamma_{f_e}^{y_m}$; lower IMM gain (equivalently, lower amount of IMM)

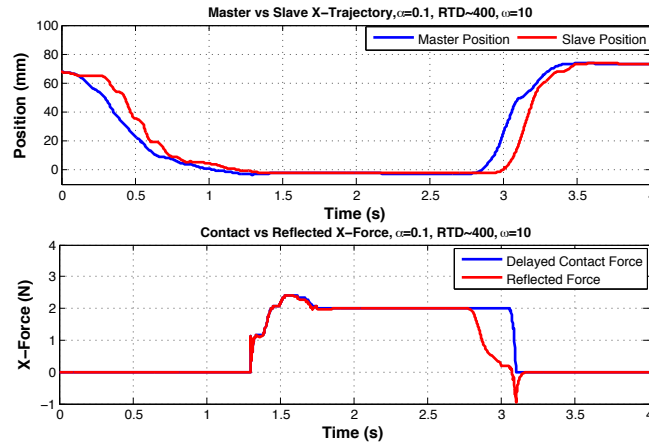


Figure 5.8: Response of the teleoperator system, min RTT= 400 ms, PBFR FS (5.15), (5.16), (5.17), (5.18), $\alpha = 0.1$, $\omega_c = 10$ Hz: X-trajectories of the master and the slave (top plot); contact X-forces as received on the master site vs. reflected X-forces (bottom plot).

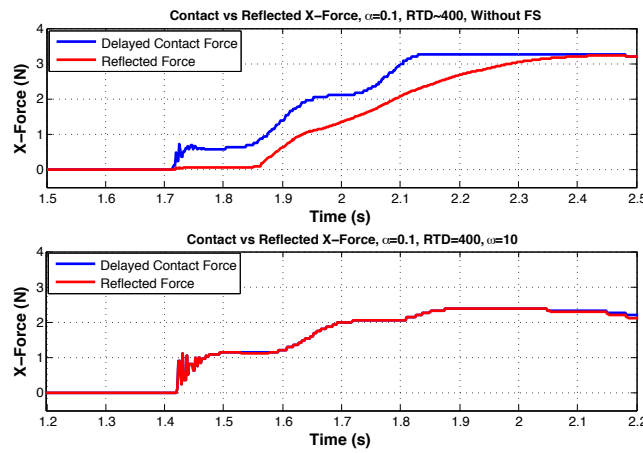


Figure 5.9: Magnified plot of the force responses during the initial phase of the contact, min RTT= 400 ms: PBFR without FS, $\alpha = 0.1$ (top plot); PBFR FS, $\alpha = 0.1$, $\omega_c = 10$ Hz (bottom plot).

corresponds to a more stable teleoperator system. One, therefore, can experimentally compare stability properties of different force reflection algorithm by observing the amount of the IMM generated by a similar profile of the interaction forces. In the next experiment, the same rectangular pulse of forces has been applied through the force reflection channel to the master device while the latter is released by the human operator; the IMM for different parameters $\alpha \in [0, 1]$ and $\omega_c > 0$ are shown in Figure 5.13. It can be clearly seen that changing $\alpha \in (0, 1]$ has

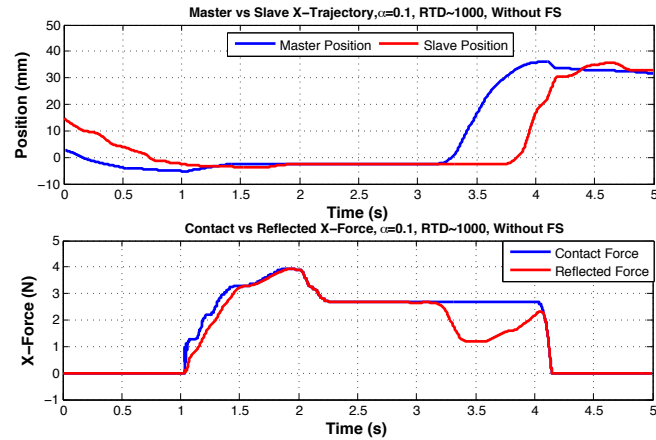


Figure 5.10: Response of the teleoperator system, min RTT= 1000 ms, PBFR without FS (5.11), (5.12), $\alpha = 0.1$: X-trajectories of the master and slave (top plot); contact X-forces as received on the master site vs. reflected X-forces (bottom plot).

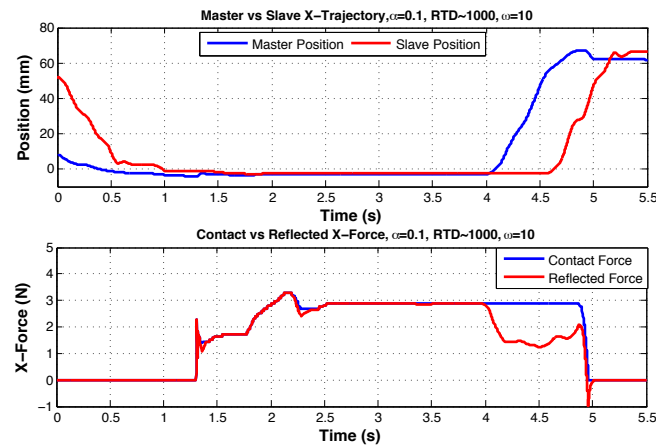


Figure 5.11: Response of the teleoperator system, min RTT= 1000 ms, PBFR FS (5.15), (5.16), (5.17), (5.18), $\alpha = 0.1$, $\omega_c = 10$ Hz: X-trajectories of the master and the slave (top plot); contact X-forces as received on the master site vs. reflected X-forces (bottom plot).

substantial effect on the amount of the IMM, with lower $\alpha \in (0, 1]$ resulting in a more stable teleoperator system, as expected. On the other hand, there is virtually no difference between the amount of IMM for the PBFR algorithms with FS in comparison with the PBFR algorithm without FS. Specifically, the curves that correspond to PBFR algorithm with FS with $\alpha = 0.1$ and $\omega_c = 10$ Hz, $\omega_c = 20$ Hz, and $\omega_c = 30$ Hz are all very close the curve that corresponds to PBFR without FS with the same $\alpha = 0.1$, which means that the level of stability of these system is approximately the same. Thus, introduction of the frequency separation into PBFR

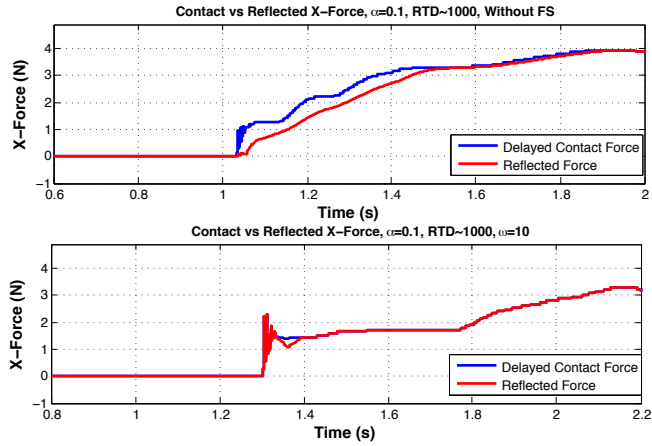


Figure 5.12: Magnified plot of the force responses during the initial phase of the contact, min $RTT = 1000$ ms: PBFR without FS, $\alpha = 0.1$ (top plot); PBFR FS, $\alpha = 0.1$, $\omega_c = 10$ Hz (bottom plot).

algorithms has negligible effect on the stability properties of the teleoperator system for cut-off frequencies of 10 Hz and higher. In particular, these results essentially confirm that the fundamental improvement in force convergence demonstrated in the previous experiments is achieved without paying the price in terms of decreased stability properties.

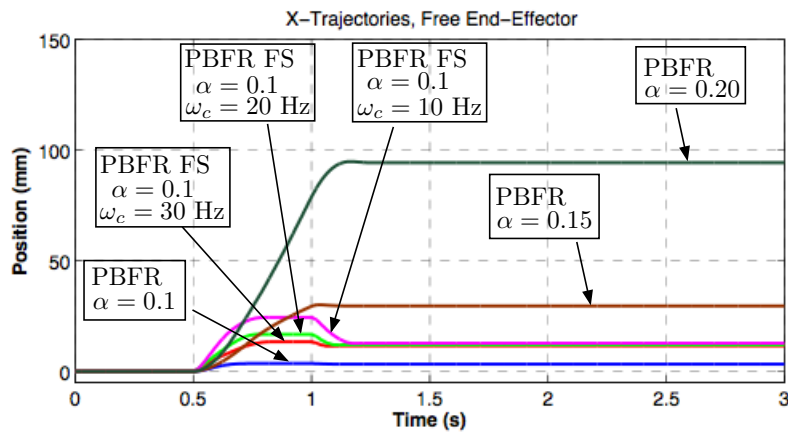


Figure 5.13: Stability test: a pulse of contact force is simulated in VE, the operator releases the haptic device; the corresponding induced master motions for different $\alpha \in [0, 1]$ and $\omega_c > 0$ are shown.

5.6 Conclusions

The projection-based force reflection algorithms were previously demonstrated to substantially improve stability characteristics of the force reflecting teleoperator systems and haptic interfaces. It was previously noted, however, that the transient response of the projection-based force reflection algorithms suffers from relatively slow force convergence; in particular, the high frequency component of the contact force during the initial contact with stiff environment is typically filtered out from the reflected force. In this work, we present developments to the projection-based force reflection principle that, in particular, solve the above mentioned problem. The new algorithms are based on the idea of separation of different frequency bands in the contact force signal and apply the projection-based force reflection algorithms to the low frequency component, while reflecting the high-frequency component directly. The main theoretical result of this work deals with stability of the force reflecting teleoperator system in the presence of irregular communication delays: it states that the stability of the teleoperator system can always be guaranteed by implementing projection-based force reflection with frequency separation. The experimental results demonstrate fundamental improvement of fidelity of the force reflection in comparison with projection-based force reflection algorithms without frequency separation.

Bibliography

- [1] Robert J. Anderson and Mark W. Spong. Bilateral control of teleoperators with time delay. *IEEE Transactions on Automatic Control*, AC-34(5):494–501, May 1989.
- [2] Dennis J. Bernstein and S. P. Bhat. Lyapunov stability, semistability, and asymptotic stability of matrix second-order systems. *Transactions of the ASME, Journal of Vibration and Acoustics*, 117:145–153, 1995.
- [3] J. Edward Colgate and Neville Hogan. Robust control of dynamically interacting systems. *International Journal of Control*, 48(1):65–88, 1988.

- [4] R. W. Daniel and P. R. McAree. Fundamental limits of performance for force reflecting teleoperation. *International Journal of Robotics Research*, 8:811–830, 1998.
- [5] E Delgado, M Diaz-Cacho, D Bustelo, and A Barreiro. Generic Approach to Stability Under Time-Varying Delay in Teleoperation: Application to the Position-Error Control of a Gantry Crane. *IEEE/ASME Transactions on Mechatronics*, 18(5):1581–1591, 2013.
- [6] Alessandro Eusebi and Claudio Melchiorri. Force reflecting telemanipulators with time-delay: Stability analysis and control design. *IEEE Transactions on Robotics and Automation*, 14:635–640, 1998.
- [7] Michel Franken, Stefano Stramigioli, Sarthak Misra, Cristian Secchi, and Alessandro Macchelli. Bilateral telemanipulation with time delays: A two-layer approach combining passivity and transparency. *IEEE Transactions on Robotics*, 27(4):741–756, 2011.
- [8] Amir Haddadi and Keyvan Hashtrudi-Zaad. Robust stability of teleoperation systems with time delay: A new approach. *IEEE Transactions on Haptics*, 2013, to appear, available online at <http://ieeexplore.ieee.org>, article 6287509.
- [9] Neville Hogan. Controlling impedance at the man/machine interface. In *Proceedings of the IEEE Conference on Robotics and Automation*, volume 3, pages 1626–1631, Scottsdale, AZ, 1989.
- [10] Chang-Chun Hua and X.P. Liu. A new coordinated slave torque feedback control algorithm for network-based teleoperation systems. *IEEE/ASME Transactions on Mechatronics*, 18(2):764–774, 2013.
- [11] Katherine J. Kuchenbecker and Gunter Niemeyer. Induced master motion in force-reflecting teleoperation. *ASME Journal of Dynamic Systems, Measurement, and Control*, 128(4):800–810, 2006.
- [12] Katherine J. Kuchenbecker, Jonathan Fiene, and Gunter Niemeyer. Improving contact realism through event-based haptic feedback. *IEEE Transactions on Visualization and Computer Graphics*, 12(2):219–230, 2006.

- [13] Gunter Niemeyer and Jean-Jacques E. Slotine. Telem Manipulation with time delays. *International Journal of Robotics Research*, 23(9):873–890, September 2004.
- [14] Allison M. Okamura, Mark R. Cutkosky, and Jack Tigh Dennerlein. Reality-based models for vibration feedback in virtual environments. *IEEE/ASME Transactions on Mechatronics*, 6(3):245 – 252, 2001.
- [15] Ilhan Polat and Carsten W. Scherer. Stability analysis for bilateral teleoperation: An IQC formulation. *IEEE Transactions on Robotics*, 28(6):1294 –1308, 2012.
- [16] Ilia G. Polushin, Peter X. Liu, and Chung-Horng Lung. A control scheme for stable force-reflecting teleoperation over IP networks. *IEEE Transactions on Systems, Man, and Cybernetics, Part B: Cybernetics*, 36(4):930–939, 2006.
- [17] Ilia G. Polushin, Abdelhamid Tayebi, and Horacio J. Marquez. Control schemes for stable teleoperation with communication delay based on IOS small gain theorem. *Automatica*, 42(6):905–915, 2006.
- [18] Ilia G. Polushin, Peter X. Liu, and Chung-Horng Lung. A force-reflection algorithm for improved transparency in bilateral teleoperation with communication delay. *IEEE/ASME Transactions on Mechatronics*, 12(3):361–374, 2007.
- [19] Ilia G. Polushin, Horacio J. Marquez, Abdelhamid Tayebi, and Peter X. Liu. A multi-channel IOS small gain theorem for systems with multiple time-varying communication delays. *IEEE Transactions on Automatic Control*, 54(2):404–409, 2009.
- [20] Ilia G. Polushin, M. Zayed Hasan, and Amir Takhmar. Experimental evaluation of a projection-based force reflection algorithm for haptic interfaces. In *Proceedings of IEEE Haptics Symposium 2012*, pages 503–508, Vancouver, BC, March 2012.
- [21] Ilia G. Polushin, Peter X. Liu, and Chung-Horng Lung. Stability of bilateral teleoperators with generalized projection-based force reflection algorithms. *Automatica*, 48(6):1005–1016, 2012.

- [22] Ilia G. Polushin, Sergey N. Dashkovskiy, Amir Takhmar, and Rajni V. Patel. A small gain framework for networked cooperative force-reflecting teleoperation. *Automatica*, 49(2): 338 – 348, 2013.
- [23] Jee-Hwan Ryu, Dong-Soo Kwon, and Blake Hannaford. Stable teleoperation with time-domain passivity control. *IEEE Transactions on Robotics and Automation*, 20(2):365–373, April 2004.
- [24] Eduardo D. Sontag. Input-to-state stability: Basic concepts and results. In P. Nistri and G. Stefani, editors, *Nonlinear and Optimal Control Theory*, pages 163–220. Springer-Verlag, Berlin, 2008.
- [25] John E. Speich, Liang Shao, and Michael Goldfarb. Modeling the human hand as it interacts with a telemanipulation system. *Mechatronics*, 15:1127–1142, 2005.
- [26] Neal A. Tanner and Gunter Niemeyer. Improving perception in time-delayed telerobotics. *The International Journal of Robotics Research*, 24(8):631–644, aug 2005.
- [27] Kevin C Walker, Ya-Jun Pan, and Jason Gu. Bilateral teleoperation over networks based on stochastic switching approach. *Mechatronics, IEEE/ASME Transactions on*, 14(5): 539–554, 2009.

Appendix: Proof of Theorems and related materials

This Appendix presents the proof of Theorem 5.4.1 together with some necessary technical preliminaries. Section 5.6 contains some technical notions and results that are used in the proof of Theorem 5.4.1; the proof itself is presented in Section 5.6.

Weak input-to-output stability with linear gains and the small-gain theorem

Consider a system

$$\begin{aligned}\dot{x} &= F(x, u_1, \dots, u_p), \\ y &= H(x, u_1, \dots, u_p),\end{aligned}\tag{5.33}$$

where x is a state, $u_1 \in \mathbb{R}^{m_1}, \dots, u_p \in \mathbb{R}^{m_p}$ are inputs, $y \in \mathbb{R}^q$, and $F(x, u_1, \dots, u_p), H(x, u_1, \dots, u_p)$ are Lipschitz continuous function of their arguments. A continuous function $\gamma: \mathbb{R}_+ \rightarrow \mathbb{R}_+$ is said to belong to class \mathcal{K}_∞ ($\gamma \in \mathcal{K}_\infty$) if it is strictly increasing, unbounded, and satisfies $\gamma(0) = 0$. The following notion is a relaxed version of the input-to-output stability notion [24].

Definition A system (5.33) is said to be *weakly input-to-output stable (WIOS) with linear IOS gains* $\gamma_i^y \geq 0, i \in \{1, \dots, p\}$, if there exists $\beta^y \in \mathcal{K}_\infty$ such that for any Lebesgue measurable uniformly essentially bounded inputs u_1, \dots, u_p , the following inequalities hold along the trajectories of (5.33):

i) *uniform boundedness*: the inequality

$$|y(t)| \leq \beta^y(|x(t_0)|) + \sum_{i=1}^p \gamma_i^y \sup_{s \in [t_0, t]} |u_i(s)|$$

holds for all $t_0, t \in \mathbb{R}, t \geq t_0$;

ii) *asymptotic gain*:

$$\limsup_{t \rightarrow +\infty} |y(t)| \leq \sum_{i=1}^p \gamma_i^y \limsup_{t \rightarrow +\infty} |u_i(t)|.$$

The following small gain theorem, which is a special case of the more general stability result [19, Theorem 1], is used as a basic stability tool in our paper.

Theorem 5.6.1 *Consider two systems of the form*

$$\begin{aligned}\dot{x}_i &= F_i(x_i, u_i, w_i) \\ y_i &= H_i(x_i, u_i, w_i),\end{aligned}\quad i = 1, 2,\tag{5.34}$$

whose inputs and outputs are interconnected according to the following formulas: $u_1(t) \equiv 0$, $u_2(t) \equiv 0$ for $t < 0$, and $u_2(t) = y_1^*(t - \tau_f(t)) + \delta_2(t)$, $u_1(t) = y_2^*(t - \tau_b(t)) + \delta_1(t)$ for $t \geq 0$, where $y_i^*(t) \equiv 0$ for $t < 0$ and $y_i^*(t) \equiv y_i(t)$ for $t \geq 0$, $i = 1, 2$, δ_1, δ_2 are uniformly essentially bounded perturbations, and $\tau_f(\cdot), \tau_b(\cdot)$ are the time delay functions that satisfy Assumption 3 of this paper. Suppose both the systems (5.34) are WIOS with linear IOS gains; specifically, let $\gamma_{iu}^y \geq 0, \gamma_{iw}^y \geq 0$ be the linear IOS gains of the i -th subsystem with respect to inputs u_i, w_i , respectively, where $i = 1, 2$. If the following small-gain condition

$$\gamma_{1u}^y \cdot \gamma_{2u}^y < 1 \quad (5.35)$$

holds, then the interconnected system is WIOS; specifically, the following inequalities

$$\begin{aligned} \sup_{t \geq 0} |y_1(t)| &\leq \beta_1(|x_1(0)|) + \gamma_{1u}^y \cdot \beta_2(|x_2(0)|) \\ &\quad + \gamma_{1u}^y \cdot \gamma_{2w}^y \cdot \sup_{t \geq 0} |w_2(t)| + \gamma_{1w}^y \cdot \sup_{t \geq 0} |w_1(t)| \\ &\quad + \gamma_{1u}^y \cdot \sup_{t \geq 0} |\delta_1(t)| + \gamma_{1u}^y \cdot \gamma_{2u}^y \cdot \sup_{t \geq 0} |\delta_2(t)|, \\ \sup_{t \geq 0^+} |y_2(t)| &\leq \beta_2(|x_2(0)|) + \gamma_{2u}^y \cdot \beta_1(|x_1(0)|) \\ &\quad + \gamma_{2u}^y \cdot \gamma_{1w}^y \cdot \sup_{t \geq 0} |w_1(t)| + \gamma_{2w}^y \cdot \sup_{t \geq 0} |w_2(t)| \\ &\quad + \gamma_{2u}^y \cdot \sup_{t \geq 0} |\delta_2(t)| + \gamma_{2u}^y \cdot \gamma_{1u}^y \cdot \sup_{t \geq 0} |\delta_1(t)|, \\ \limsup_{t \rightarrow +\infty} |y_1(t)| &\leq \gamma_{1u}^y \gamma_{2w}^y \limsup_{t \rightarrow +\infty} |w_2(t)| + \gamma_{1w}^y \limsup_{t \rightarrow +\infty} |w_1(t)| \\ &\quad + \gamma_{1u}^y \limsup_{t \rightarrow +\infty} |\delta_1(t)| + \gamma_{1u}^y \gamma_{2u}^y \cdot \limsup_{t \rightarrow +\infty} |\delta_2(t)|, \\ \limsup_{t \rightarrow +\infty} |y_2(t)| &\leq \gamma_{2u}^y \cdot \gamma_{1w}^y \cdot \limsup_{t \rightarrow +\infty} |w_1(t)| + \gamma_{2w}^y \cdot \limsup_{t \rightarrow +\infty} |w_2(t)| \\ &\quad + \gamma_{2u}^y \cdot \limsup_{t \rightarrow +\infty} |\delta_2(t)| + \gamma_{2u}^y \cdot \gamma_{1u}^y \cdot \limsup_{t \rightarrow +\infty} |\delta_1(t)|, \end{aligned}$$

hold along the trajectories of the closed-loop interconnected system. •

Proof of Theorem 5.4.1

The proof of Theorem 5.4.1 is based on the small-gain arguments. Consider an interconnection which consists of the master device (5.1), the human operator (5.9), and the force reflection al-

gorithm (5.15), (5.16), (5.17), (5.18). Our goal is to analyze the input-to-output stability properties of this interconnection, in particular, calculate the IOS gains from the inputs f_{env} , f_h^* , and Δf_h to the output y_m . The structure of this interconnection is shown in Figure 5.14. Applying the superposition principle to the interconnection of the master and the passive human reaction subsystems, the above structure can be transformed into the form shown in Figure 5.15, which is more convenient for our analysis.

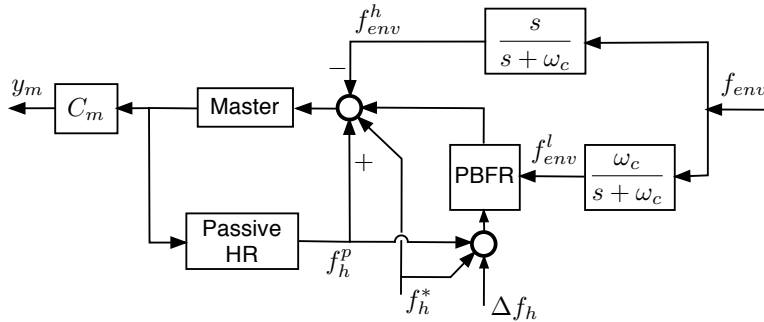


Figure 5.14: Structure of the master interconnection. Acronyms: PBFR - projection-based force reflection; Passive HR - passive reaction of the human operator hand to movement of the master device.

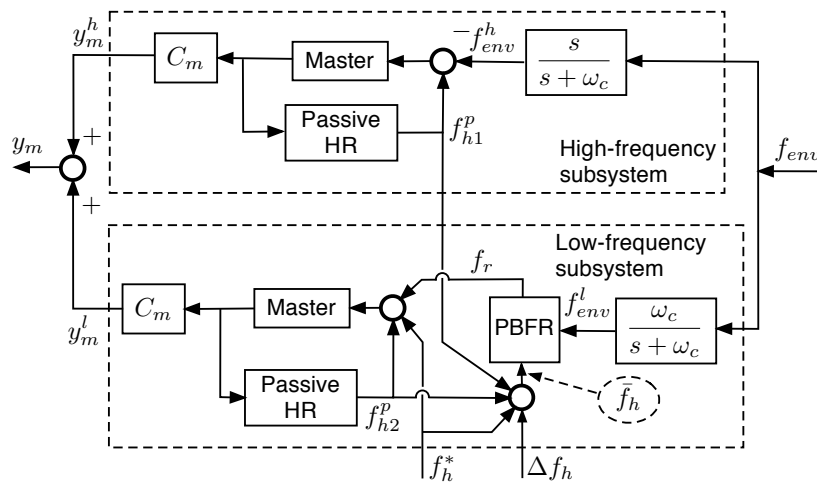


Figure 5.15: Transformed structure of the master interconnection.

The structure shown in Figure 5.15 is an interconnection of two subsystems which we loosely call the “high-frequency” subsystem and the “low-frequency” one. Below, we analyze the input-to-output stability properties of these subsystems separately.

IOS Gains of the high-frequency subsystem

Let us first consider the “high-frequency” subsystem. This subsystem has one input f_{env} and two outputs y_m^h and f_{h1}^p . The transfer functions from f_{env} to y_m^h , f_{h1}^p are

$$H_{hy}(s) := \left[C_m [s\mathbb{I} - A_{mh}]^{-1} B_m \right] \cdot \left[\frac{s}{s + \omega_c} \right], \quad (5.36)$$

$$H_{hf}(s) := \left[C_h [s\mathbb{I} - A_{mh}]^{-1} B_m \right] \cdot \left[\frac{s}{s + \omega_c} \right], \quad (5.37)$$

respectively. Since the IOS gain of a system described by a stable proper transfer function is equal to its 1-norm, we see that the IOS gains from f_{env} to y_m^h and f_{h1}^p are defined by expressions (5.22), (5.23), respectively. The following proposition states that these gains can be assigned arbitrarily small by choosing the cut-off frequency $\omega_c > 0$ sufficiently large. Specifically, the following result is valid.

Proposition 5.6.2 *Given $\gamma_{hy}^* > 0$, $\gamma_{hf}^* > 0$, there exists $\omega^* \in [0, +\infty)$ such that $\omega_c \geq \omega^*$ implies that the gains γ_{hy} , γ_{hf} defined by (5.22), (5.23), satisfy $\gamma_{hy} \in (0, \gamma_{hy}^*]$, $\gamma_{hf} \in (0, \gamma_{hf}^*]$, respectively.*

Proof. Denote

$$H_{my}(s) := C_m [s\mathbb{I} - A_{mh}]^{-1} B_m = \frac{C_m \operatorname{adj}(s\mathbb{I} - A_{mh}) B_m}{\det(s\mathbb{I} - A_{mh})},$$

$$H_{mf}(s) := C_h [s\mathbb{I} - A_{mh}]^{-1} B_m = \frac{C_h \operatorname{adj}(s\mathbb{I} - A_{mh}) B_m}{\det(s\mathbb{I} - A_{mh})},$$

are the transfer matrices from f_{env}^h to the outputs y_m^h and f_{h1}^p , respectively. We, therefore, have

$$H_{hy}(s) = H_{my}(s) \cdot \left[\frac{s}{s + \omega_c} \right], \quad H_{hf}(s) = H_{mf}(s) \cdot \left[\frac{s}{s + \omega_c} \right].$$

Consider, for example, $H_{hy}(s)$. Note that $\operatorname{adj}(s\mathbb{I} - A_{mh})$ is a matrix whose elements are polynomials with degree strictly less than the degree of $\det(s\mathbb{I} - A_{mh})$, we see that the elements of $H_{my}(s)$ are strictly proper rational transfer functions (degree of numerator < degree of denominator). Then, partial fraction expansion of every element of $H_{hy}(s)$ indicates that 1 norm of every element of $H_{hy}(s)$ can be made arbitrarily small by choosing $\omega_c > 0$ sufficiently large. Since 1 norm of a system described by a stable proper transfer function is also an IOS gain of the system, this implies that the IOS gain from the input f_{env} to the output y_m^h can be made arbitrarily small by choosing $\omega_c > 0$ sufficiently large. Similar analysis can be performed for $H_{hf}(s)$. The proof of Proposition 5.6.2 is complete. •

IOS gains of the low-frequency subsystem

Now, consider the “low-frequency” subsystem. This subsystem has four inputs, which are f_{env} , f_h^* , Δf_h , and f_{h1}^p , and one output y_m^l . The next Proposition 5.6.3 describes the input-to-output properties of the low-frequency subsystem. Let $\gamma_{f_h}^{y_m}$ be defined by (5.24). The following proposition gives an estimate of the IOS gain of the low frequency path.

Proposition 5.6.3 *The low-frequency subsystem is stable, and the IOS gains from inputs f_{env} , f_h^* , Δf_h , and f_{h1}^p to output y_m^l are less than or equal to $\gamma_{f_h}^{y_m} \cdot \alpha$, $\gamma_{f_h}^{y_m}$, $\gamma_{f_h}^{y_m} \cdot (1 - \alpha)$, and $\gamma_{f_h}^{y_m}$, respectively, regardless of the cut-off frequency $\omega_c \in (0, +\infty)$. •*

Proof The input to the low-frequency master subsystem is

$$\begin{aligned} u_{lf} &:= f_h - f_{h1}^p - (1 - \alpha) \text{Sat}_{[0,1]} \left\{ \frac{f_h^T \cdot f_{env}^l}{|f_h|^2 + \epsilon} \right\} (f_h + \Delta f_h) \\ -\alpha f_{env}^l &= -f_{h1}^p - \alpha f_{env}^l + \theta f_h - (1 - \theta) \Delta f_h, \end{aligned} \quad (5.38)$$

where $\theta(\cdot) := 1 - (1 - \alpha) \text{Sat}_{[0,1]} \left\{ \frac{f_h^T \cdot f_{env}^l}{|f_h|^2 + \epsilon} \right\} \in [\alpha, 1]$. Denote $\mathbf{x}_m = \begin{bmatrix} x_m & \dot{x}_m \end{bmatrix}^T \in \mathbb{R}^{2n}$, and consider an ISS-Lyapunov function candidate of the form $V_m := \mathbf{x}_m^T \mathbb{P} \mathbf{x}_m$, where $\mathbb{P} \in \mathbb{R}^{2n \times 2n}$ is defined by (5.4). The time derivative of V_m along the trajectories of the controlled master subsystem with input (5.38) admits the following estimate

$$\begin{aligned} \dot{V} &= \left(u_{lf}^T B_m^T + \mathbf{x}_m^T A_m^T \right) \mathbb{P} \mathbf{x}_m + \mathbf{x}_m^T \mathbb{P} (A_m \mathbf{x}_m + B_m u_{lf}) \\ &= \mathbf{x}_m^T \left[\left(\theta A_h^T + A_m^T \right) \mathbb{P} + \mathbb{P} (A_m + \theta A_h) \right] \mathbf{x}_m \\ &\quad + 2 \mathbf{x}_m^T \mathbb{P} B_m \left(\theta \cdot f_h^* - (1 - \theta) \cdot \Delta f_h - \alpha \cdot f_{env}^l - f_{h1}^p \right) \\ &\leq -|\mathbf{x}_m|^2 + 2 |\mathbf{x}_m| \bar{\sigma}(\mathbb{P} B_m) \times \\ &\quad \times \left(|f_h^*| + (1 - \alpha) \cdot |\Delta f_h| + \alpha \cdot |f_{env}^l| + |f_{h1}^p| \right). \end{aligned}$$

In particular, we see that $\dot{V} < 0$ whenever $|\mathbf{x}_m| > 2 \bar{\sigma}(\mathbb{P} B_m) \left[|f_h^*| + (1 - \alpha) |\Delta f_h| + \alpha |f_{env}^l| + |f_{h1}^p| \right]$, which implies [24] that

$$\gamma_{f_h}^{x_m} := 2 \bar{\sigma}(\mathbb{P} B_m) \sqrt{\lambda_{\max}(\mathbb{P}) / \lambda_{\min}(\mathbb{P})}, \quad (5.39)$$

is an ISS gain with respect to the “input” $|f_h^*| + \alpha |f_{env}^l| + (1 - \alpha) |\Delta f_h| + |f_{h1}^p|$. By linearity of the gain functions, we see that $\gamma_{f_h}^{x_m}$, $\gamma_{f_h}^{x_m} \cdot \alpha$, $\gamma_{f_h}^{x_m} \cdot (1 - \alpha)$, and $\gamma_{f_h}^{x_m}$ are the ISS gains with respect to the inputs f_h^* , f_{env}^l , Δf_h , and f_{h1}^p , respectively. The corresponding IOS gains, therefore, are

less than or equal to $\gamma_{f_h}^{y_m}$, $\gamma_{f_h}^{y_m} \cdot \alpha$, $\gamma_{f_h}^{y_m} \cdot (1 - \alpha)$, and $\gamma_{f_h}^{y_m}$, respectively. Finally, consider the filter (5.15). The filter is a stable LTI system with one input f_{env} and one output f_{env}^l ; its IOS gain, therefore, is equal to the 1-norm of the transfer function, which is $\left\| \frac{\omega_c}{s + \omega_c} \right\|_1 := \int_{t=0}^{+\infty} \omega_c e^{-\omega_c t} dt = 1$, regardless of the cut-off frequency $\omega_c > 0$. Taking into account that the IOS gain of a cascade interconnection of two IOS subsystems is equal to the product of the subsystems' gains, the statement of Proposition 5.6.3 follows. •

Now, let $\gamma_{f_e}^{y_m}$ be defined by (5.25). Combining the Proposition 5.6.2 and 5.6.3, and performing some direct calculations, the following result can be obtained.

Proposition 5.6.4 *The master interconnection (5.1), (5.9), (5.15), (5.16), (5.17), (5.18) is stable, and the corresponding IOS gains from inputs f_{env} , f_h^* , Δf_h to output y_m are less than or equal to $\gamma_{f_e}^{y_m}$, $\gamma_{f_h}^{y_m}$, and $\gamma_{f_h}^{y_m} \cdot (1 - \alpha)$, respectively. In particular, the gain $\gamma_{f_e}^{y_m} > 0$ can be made arbitrarily small by choosing $\alpha \in (0, 1]$ sufficiently small and $\omega_c > 0$ sufficiently large. •*

The proof of Theorem 5.4.1 can now be completed using the small-gain result given by Theorem 5.6.1. Specifically, applying Theorem 5.6.1 to the teleoperator system under consideration (5.1), (5.5), (5.6), (5.7), (5.9), (5.15) – (5.19), and using Proposition 5.6.4, one concludes that the small gain condition (5.26) implies that the trajectories of the closed-loop teleoperator system are bounded and convergent, and the estimates (5.27)–(5.30) are valid. Proposition 5.6.4 also implies that the gain $\gamma_{f_e}^{y_m} > 0$ can be assigned arbitrarily small and the small gain condition (5.26) can always be met by choosing $\omega_c \geq 0$ sufficiently large and $\alpha \in (0, 1]$ sufficiently small. This concludes the proof of Theorem 5.4.1. •

Chapter 6

Conclusions and Future Work

In this chapter, the contributions of this thesis are summarized, and some possible directions for future work are discussed.

6.1 Conclusions

The results presented in this thesis can be summarized as follows.

In Chapter 2, a multi-dimensional WIOPS small gain approach is utilized for stability analysis of the cooperative force reflecting teleoperator system in the presence of multiple time-varying communication delays. The small gain framework is subsequently used for the controller design. The theoretical results show that the stability of the cooperative teleoperator system can always be achieved by appropriate tuning of the local master and slave controllers. The experimental results presented confirm the validity of the theoretical analysis. The proposed approach may have several advantages over more conventional passivity-based approaches. For example, one advantage of the proposed approach is its flexibility with respect to the choice of the force reflection signal. In passivity-based approaches, on the contrary, the reflected signal must be a passive output of the slave-environment interconnection which limits possible choices of the force reflection signal and usually results in transparency deterioration. The other advantages of the developed small-gain approach are simplicity of its extension to the case of time-varying communication delays and better trajectory tracking properties of the system.

In Chapter 3, the PBFR algorithms are incorporated into the design of cooperative force-reflecting teleoperator system to overcome the conservatism of the small gain design. Specifically, it has been shown in Chapter 2 that the small gain stability conditions essentially require the gain of the human/master subsystem to be sufficiently small. The latter requires the impedance of the master subsystem to be sufficiently high, which makes the whole design conservative. In Chapter 3, based on the assumption that the human operator does not destabilize the master subsystem, we demonstrate that the gain of the human/master subsystem depends on the human hand dynamics and the type of the force reflection algorithm. It is shown that, in the case of direct force reflection, the human/master system has low gain if either the gain of the master device is low (which implies high damping and stiffness of the device) or the human operator applies stabilizing actions and the stiffness of the human hand is high. On the other hand, in the case of PBFR algorithm, the gain of the human/master subsystem can be assigned arbitrarily low by an appropriate assignment of the weighing coefficient in the PBFR algorithm, regardless of the human hand dynamics as long as the latter do not destabilize the master subsystem. Therefore, PBFR algorithms allow for stability improvement without increasing the impedance of the master device or scaling down the force reflection gain. The experimental results confirm the theoretical analysis.

In Chapter 4, the stability and performance of a dual-arm haptic teleoperator system with the PBFR algorithm for minimally invasive surgical applications have been studied. Specifically, the stability and performance characteristics of the system with PBFR algorithm and the same system with direct force feedback have been compared both theoretically and experimentally. In particular, we have experimentally evaluated the performance of the system in three simple surgical tasks-knot tightening, pegboard transfer, and object manipulation. It was demonstrated that, in the majority of the cases, the PBFR algorithms lead to statistically significant improvement of performance in comparison with conventional direct force feedback (DFR algorithm).

Chapter 5 presents a new PBFR algorithm that aims to improve the transient fidelity of the force reflection. It is well-known that the high frequency force component of the contact force generated during the initial phase of the contact with an environment is very important for haptic perception. However, the experimental investigation of the previously developed

PBFR algorithms show that the high frequency component is typically filtered out from the force reflection signal. In the new PBFR algorithm, the force reflection signal is decomposed into low-frequency and high-frequency components. The high frequency component is consequently applied directly to the motors of the master device, while the low-frequency component is reflected using PBFR algorithm. The theoretical small gain stability analysis of the system shows that the stability of the proposed algorithm can always be guaranteed by appropriate adjustment of the design parameters such as cut-off frequency of the filters and the weighing coefficient of the PBFR algorithm. The experimental results confirm the improvement in the transparency and stability achieved using the proposed approach.

6.2 Future Work

In this final section, some possible extensions of the results presented are discussed and possible direction for future research are outlined.

One potential direction for future research is the extension of the small-gain design framework to the case of three channel teleoperation systems. The two-channel (bilateral) teleoperator systems that are based on the small-gain approach developed so far are not statically balanced. To overcome this problem, an additional position feedback can be sent from the slave to the master side, and an additional control component may be incorporated into the master controller that can guarantee the whole system is statically balanced.

The other important issue that requires further research is the stability of the slave subsystems. In most of the previous work, we have considered the environment to be IOS stable with a specific gain, which may be a limiting assumption. However, in real surgical applications, the gain of the environment may be unknown or may not even exist. In such cases, more advanced control algorithms (such as adaptive impedance control) can be implemented on the slave side to improve stability and performance characteristics of the system. In particular, adaptive and/or learning impedance control is used by humans to cope with unknown environments [1, 2]. Similar methods may be implemented in teleoperator system, which may lead to more human-like performance.

In Chapter 4, it has been shown that cooperative object manipulation was one of the most

difficult task to execute using a cooperative teleoperator system. Even in successful experiments, the internal forces applied to the object were substantial which may damage the object. For successful execution of similar difficult tasks, a control scheme that coordinates all the slave manipulators may be required, in addition to separate controllers for each slave. A number of approaches have been developed in the area of the cooperative manipulation such as object impedance control [5], load distribution and internal force control [4], that could be used for control of cooperative teleoperation system.

During the experimental research, it was found that the ability of the human operator to compensate for the reflected forces from the slave side depends on the direction of the forces as well as on the position of the human arm in grasping. Hogan [3] has shown that the stiffness property of the human hand is isotropic in proximal position and more anisotropic in distal positions. It was also shown that the stiffness of the hand depends on the posture of the arm; also, it has been shown that the maximal stiffness of the hand in each position lies in the direction of the line joining the hand to the shoulder. This property could be used for development of an adaptive projection-based force reflection algorithm that is based on the posture of the hand. In the direction of the maximal hand stiffness, the human is likely able to compensate for the reflected force and, therefore, the force reflection gain could be increased. On the other hand, in the direction of low hand stiffness, the force reflection gain should be chosen sufficiently low to avoid instability.

Bibliography

- [1] Etienne Burdet, Keng Peng Tee, I Mareels, Theodore E Milner, Chee-Meng Chew, David W Franklin, Rieko Osu, and Mitsuo Kawato. Stability and motor adaptation in human arm movements. *Biological Cybernetics*, 94:20–32, 2006.
- [2] David W Franklin, Etienne Burdet, Keng Peng Tee, Rieko Osu, Chee-Meng Chew, Theodore Milner, and Mitsuo Kawato. CNS Learns Stable, Accurate, and Efficient Movements Using a Simple Algorithm. *Journal of Neuroscience*, 28(44):11165, October 2008.

- [3] Neville Hogan. The mechanics of multi-joint posture and movement control. *Biological Cybernetics*, 52(5):315–331, 1985.
- [4] Ping Hsu. Control of multimanipulator systems-trajectory tracking, load distribution, internal force control, and decentralized architecture. In *Proceedings of the 1989 IEEE International Conference on Robotics and Automation*, pages 1234–1239. IEEE, 1989.
- [5] Stanley A. Schneider and Robert H. Cannon Jr. Object impedance control for cooperative manipulation: Theory and experimental results. *IEEE Transactions on Robotics and Automation*, 8(3):383–394, 1992.

Appendix A

Reprint Permissions

ELSEVIER LICENSE
TERMS AND CONDITIONS
Jul 05, 2013

This is a License Agreement between Amir Takhmar ("You") and Elsevier ("Elsevier") provided by Copyright Clearance Center ("CCC"). The license consists of your order details, the terms and conditions provided by Elsevier, and the payment terms and conditions.

All payments must be made in full to CCC. For payment instructions, please see information listed at the bottom of this form.

Supplier	Elsevier Limited
Registered Company Number	1982084
Customer name	Amir Takhmar
Customer address	
License number	3182620258691
License date	Jul 05, 2013
Licensed content publisher	Elsevier
Licensed content publication	Automatica
Licensed content title	A small gain framework for networked cooperative force-reflecting teleoperation
Licensed content author	Ilya G. Pokushin, Sergey N. Dashkovskiy, Amir Takhmar, Rajni V. Patel
Licensed content date	February 2013
Licensed content volume number	49
Licensed content issue number	2
Number of pages	11
Start Page	338
End Page	348
Type of Use	reuse in a thesis/dissertation
Portion	full article
Format	both print and electronic
Are you the author of this Elsevier article?	Yes
Will you be translating?	No
Order reference number	
Title of your thesis/dissertation	Control Design of Cooperative Haptics-Enabled Teleoperation System for Minimally Invasive Surgery
Expected completion date	Dec 2013
Estimated size (number of pages)	200
Elsevier VAT number	GB 494 6272 12
Permissions price	0.00 USD
VAT/Local Sales Tax	0.00 USD / 0.00 GBP
Total	0.00 USD
Terms and Conditions	

INTRODUCTION

1. The publisher for this copyrighted material is Elsevier. By clicking "accept" in connection with completing this licensing transaction, you agree that the following terms and conditions apply to this transaction (along with the Billing and Payment terms and conditions established by Copyright Clearance Center, Inc. ("CCC"), at the time that you opened your Rightslink account and that are available at any time at <http://myaccount.copyright.com>).

GENERAL TERMS

2. Elsevier hereby grants you permission to reproduce the aforementioned material subject to the terms and conditions indicated.

3. Acknowledgement: If any part of the material to be used (for example, figures) has appeared in our publication with credit or acknowledgement to another source, permission must also be sought from that source. If such permission is not obtained then that material may not be included in your publication/copies. Suitable acknowledgement to the source must be made, either as a footnote or in a reference list at the end of your publication, as follows:

"Reprinted from Publication title, Vol /edition number, Author(s), Title of article / title of chapter, Pages No., Copyright (Year), with permission from Elsevier [OR APPLICABLE SOCIETY COPYRIGHT OWNER]." Also Lancet special credit - "Reprinted from The Lancet, Vol. number, Author(s), Title of article, Pages No., Copyright (Year), with permission from Elsevier."

4. Reproduction of this material is confined to the purpose and/or media for which permission is hereby given.

5. Altering/Modifying Material: Not Permitted. However figures and illustrations may be altered/adapted minimally to serve your work. Any other abbreviations, additions, deletions and/or any other alterations shall be made only with prior written authorization of Elsevier Ltd. (Please contact Elsevier at D)

6. If the permission fee for the requested use of our material is waived in this instance, please be advised that your future requests for Elsevier materials may attract a fee.

7. Reservation of Rights: Publisher reserves all rights not specifically granted in the combination of (i) the license details provided by you and accepted in the course of this licensing transaction, (ii) these terms and conditions and (iii) CCC's Billing and Payment terms and conditions.

8. License Contingent Upon Payment: While you may exercise the rights licensed immediately upon issuance of the license at the end of the licensing process for the transaction, provided that you have disclosed complete and accurate details of your proposed use, no license is finally effective unless and until full payment is received from you (either by publisher or by CCC) as provided in CCC's Billing and Payment terms and conditions. If full payment is not received on a timely basis, then any license preliminarily granted shall be deemed automatically revoked and shall be void as if never granted. Further, in the event that you breach any of these terms and conditions or any of CCC's Billing and Payment terms and conditions, the license is automatically revoked and shall be void as if never granted. Use of materials as described in a revoked license, as well as any use of the materials beyond the scope of an unrevoked license, may constitute copyright infringement and publisher reserves the right to take any and all action to protect its copyright in the materials.

9. Warranties: Publisher makes no representations or warranties with respect to the licensed material.

10. **Indemnity:** You hereby indemnify and agree to hold harmless publisher and CCC, and their respective officers, directors, employees and agents, from and against any and all claims arising out of your use of the licensed material other than as specifically authorized pursuant to this license.

11. **No Transfer of License:** This license is personal to you and may not be sublicensed, assigned, or transferred by you to any other person without publisher's written permission.

12. **No Amendment Except in Writing:** This license may not be amended except in a writing signed by both parties (or, in the case of publisher, by CCC on publisher's behalf).

13. **Objection to Contrary Terms:** Publisher hereby objects to any terms contained in any purchase order, acknowledgment, check endorsement or other writing prepared by you, which terms are inconsistent with these terms and conditions or CCC's Billing and Payment terms and conditions. These terms and conditions, together with CCC's Billing and Payment terms and conditions (which are incorporated herein), comprise the entire agreement between you and publisher (and CCC) concerning this licensing transaction. In the event of any conflict between your obligations established by these terms and conditions and those established by CCC's Billing and Payment terms and conditions, these terms and conditions shall control.

14. **Revocation:** Elsevier or Copyright Clearance Center may deny the permissions described in this License at their sole discretion, for any reason or no reason, with a full refund payable to you. Notice of such denial will be made using the contact information provided by you. Failure to receive such notice will not alter or invalidate the denial. In no event will Elsevier or Copyright Clearance Center be responsible or liable for any costs, expenses or damage incurred by you as a result of a denial of your permission request, other than a refund of the amount(s) paid by you to Elsevier and/or Copyright Clearance Center for denied permissions.

LIMITED LICENSE

The following terms and conditions apply only to specific license types:

15. **Translation:** This permission is granted for non-exclusive world **English** rights only unless your license was granted for translation rights. If you licensed translation rights you may only translate this content into the languages you requested. A professional translator must perform all translations and reproduce the content word for word preserving the integrity of the article. If this license is to re-use 1 or 2 figures then permission is granted for non-exclusive world rights in all languages.

16. **Website:** The following terms and conditions apply to electronic reserve and author websites:

Electronic reserve: If licensed material is to be posted to website, the web site is to be password-protected and made available only to bona fide students registered on a relevant course if:

This license was made in connection with a course,

This permission is granted for 1 year only. You may obtain a license for future website posting,

All content posted to the web site must maintain the copyright information line on the bottom of each image,

A hyper-text must be included to the Homepage of the journal from which you are licensing at <http://www.sciencedirect.com/science/journal/xxxxx> or the Elsevier homepage for books at <http://www.elsevier.com>, and

Central Storage: This license does not include permission for a scanned version of the material to be stored in a central repository such as that provided by Heron/XanEdu.

17. **Author website** for journals with the following additional clauses:

All content posted to the web site must maintain the copyright information line on the bottom of each image, and the permission granted is limited to the personal version of your paper. You are not allowed to download and post the published electronic version of your article (whether PDF or HTML, proof or final version), nor may you scan the printed edition to create an electronic version. A hyper-text must be included to the Homepage of the journal from which you are licensing at <http://www.sciencedirect.com/science/journal/xxxxx> . As part of our normal production process, you will receive an e-mail notice when your article appears on Elsevier's online service ScienceDirect (www.sciencedirect.com). That e-mail will include the article's Digital Object Identifier (DOI). This number provides the electronic link to the published article and should be included in the posting of your personal version. We ask that you wait until you receive this e-mail and have the DOI to do any posting.

Central Storage: This license does not include permission for a scanned version of the material to be stored in a central repository such as that provided by Heron/XanEdu.

18. **Author website** for books with the following additional clauses:

Authors are permitted to place a brief summary of their work online only.

A hyper-text must be included to the Elsevier homepage at <http://www.elsevier.com> .

All content posted to the web site must maintain the copyright information line on the bottom of each image. You are not allowed to download and post the published electronic version of your chapter, nor may you scan the printed edition to create an electronic version.

Central Storage: This license does not include permission for a scanned version of the material to be stored in a central repository such as that provided by Heron/XanEdu.

19. **Website** (regular and for author): A hyper-text must be included to the Homepage of the journal from which you are licensing at <http://www.sciencedirect.com/science/journal/xxxxx> . or for books to the Elsevier homepage at <http://www.elsevier.com>

20. **Thesis/Dissertation**: If your license is for use in a thesis/dissertation your thesis may be submitted to your institution in either print or electronic form. Should your thesis be published commercially, please reapply for permission. These requirements include permission for the Library and Archives of Canada to supply single copies, on demand, of the complete thesis and include permission for UMI to supply single copies, on demand, of the complete thesis. Should your thesis be published commercially, please reapply for permission.

21. **Other Conditions**:

v1.6

If you would like to pay for this license now, please remit this license along with your payment made payable to "COPYRIGHT CLEARANCE CENTER" otherwise you will be invoiced within 48 hours of the license date. Payment should be in the form of a check or money order referencing your account number and this invoice number RLNK501059474.

Once you receive your invoice for this order, you may pay your invoice by credit card. Please follow instructions provided at that time.



RightsLink®

[Home](#)
[Account Info](#)
[Help](#)


Title: Small-gain design of networked cooperative bilateral teleoperators

Conference Proceedings: Small-gain design of networked cooperative bilateral teleoperators

Author: Polushin, I.G.; Takhmar, A.; Patel, R.V.

Publisher: IEEE

Date: 9-13 May 2011

Copyright © 2011, IEEE

Logged in as:
Amir Takhmar
Account #:

[LOGOUT](#)

Thesis / Dissertation Reuse

The IEEE does not require individuals working on a thesis to obtain a formal reuse license, however, you may print out this statement to be used as a permission grant:

Requirements to be followed when using any portion (e.g., figure, graph, table, or textual material) of an IEEE copyrighted paper in a thesis:

- 1) In the case of textual material (e.g., using short quotes or referring to the work within these papers) users must give full credit to the original source (author, paper, publication) followed by the IEEE copyright line © 2011 IEEE.
- 2) In the case of illustrations or tabular material, we require that the copyright line © [Year of original publication] IEEE appear prominently with each reprinted figure and/or table.
- 3) If a substantial portion of the original paper is to be used, and if you are not the senior author, also obtain the senior author's approval.

Requirements to be followed when using an entire IEEE copyrighted paper in a thesis:

- 1) The following IEEE copyright/ credit notice should be placed prominently in the references: © [year of original publication] IEEE. Reprinted, with permission, from [author names, paper title, IEEE publication title, and month/year of publication]
- 2) Only the accepted version of an IEEE copyrighted paper can be used when posting the paper or your thesis on-line.
- 3) In placing the thesis on the author's university website, please display the following message in a prominent place on the website: In reference to IEEE copyrighted material which is used with permission in this thesis, the IEEE does not endorse any of [university/educational entity's name goes here]'s products or services. Internal or personal use of this material is permitted. If interested in reprinting/republishing IEEE copyrighted material for advertising or promotional purposes or for creating new collective works for resale or redistribution, please go to http://www.ieee.org/publications_standards/publications/rights/rights_link.html to learn how to obtain a License from RightsLink.

If applicable, University Microfilms and/or ProQuest Library, or the Archives of Canada may supply single copies of the dissertation.

Curriculum Vitae

Name: Amir Takhmar

Education *University of Western Ontario*, London, Ontario, Canada

- **Ph.D.**, Electrical and Computer Engineering (2009 - 2013)

- Thesis Title: Control Design of Cooperative Haptic-Enabled Teleoperation System for Robotic-Assisted Minimally Invasive Surgery.

- Supervisors: Prof. Rajni V. Patel and Prof. Ilia G. Polushin

K.N. Toosi University of Technology, Tehran, Iran

- **M.E.Sc**, Mechanical Engineering (2005-2008)

- Thesis Title: Dynamic Modeling and Control of a Biped Robot

- Supervisor: Prof. S. A. Moosavian

Ferdowsi University of Mashhad, Mashhad, Iran

- **B.Sc**, Mechanical Engineering (Sep 2001 - Sep 2005)

- Thesis Title: Optimal Positioning of Rod Head in Rack and Pinion Steering System

Honours and • NSERC CAMI Scholarship (\$15,000/y), 2011-2013

Awards: • Western Graduate Research Scholarship (WGRS, \$10,500/y), 2009-2013

- K.N.Toosi Graduate First Student award , 2008

Academic • *University of Western Ontario*

Experience • *Teaching Assistant*, 2009 - 2013

- Programming Fundamental for Engineers, Fall 2012, Winter/summer 2013.
- Digital Logic Systems, Fall 2011.
- Introduction to Signal Processing, Winter 2011.
- Electrical Instrumentation and Measurements, Winter 2010.

• *Research Assistant*, Cooperative Haptic Teleoperation, 2009-2013.

• *K. N. Toosi University of technology*

• *Teaching Assistant*, Dynamics , Fall 2007.

• *Research Assistant*, Modeling, Stability and Control of Biped Robot, 2005 - 2008.

Publications:

• *Journal Paper:*

- Polushin I.G., Dashkovskiy S.N., A. *Takhmar*, R.V. Patel., "A Small Gain Framework for Networked Cooperative Force-Reflecting Teleoperation", Vol. 49, No. 2, pp. 338-348 , 2013.
- Polushin I.G., A. *Takhmar*, R.V. Patel, "Small Gain Design of Cooperative Teleoperator System with Projection-Based Force Reflection", submitted to IEEE Transaction on Robotics, Submission number:12-0021, 2012.
- Polushin I.G., A. *Takhmar*, R.V. Patel, "Projection-Based Force Reflection Algorithms with Frequency Separation", submitted to IEEE/ASME Transactions on Mechatronics, Submission number:TMECH-09-2012-2544, 2012.
- A. Takhmar, Polushin I.G., A. Talasaz, R.V. Patel, " Cooperative Teleoperation with Projection-Based Force Reflection for MIS", submitted to IEEE Transaction on Control System Technology, Submission number: TCST-2013-0859, 2014.

- **A. Takhmar**, S. Ali A. Moosavian, M. Alghooneh, "Chattering Eliminated and Stable Motion of Biped Robots Using a Fuzzy Sliding Mode Controller", *Majlesi Journal of Electrical Engineering*, Vol. 7, No. 1, pp. 31-42, 2013.
- M. Alghooneh, **A. Takhmar**, S. Ali A. Moosavian, Monitoring the Postural Stability of Planar Bipedal Robots using the Moment-Height Stability Measure, *International Journal on Smart Sensing and Intelligent Systems*, Vol. 5, No. 2, pp. 329-346, 2012.
- S. Ali A. Moosavian, M. Alghooneh, **A. Takhmar**, "Cartesian Approach for Gait Planning and Control of Biped Robots on Irregular Surfaces", *International Journal of Humanoid Robotics*, Vol. 6, No. 4, pp. 675-697, 2009.

•*Conference Papers:*

- **A. Takhmar**, Polushin I.G., R.V. Patel , "Frequency Separation in Projection-Based Force Reflection Algorithms for Bilateral Teleoperators", *IEEE International Conference on Robotics and Automation ICRA 2013*, Karlsruhe, Germany, May 6 - 10, 2013, pp. 1492-1497.
- Polushin I.G., M.Z. Hasan, **A. Takhmar**, "Experimental evaluation of a projection-based force reflection algorithm for haptic interfaces", *Haptics Symposium 2012*, Vancouver, BC, March 4-7, 2012, pp. 503-507.
- Polushin I.G., **A. Takhmar**, R.V. Patel , "Small Gain Design of Cooperative Teleoperator System with Projection-Based Force Reflection", *2011 IEEE/RSJ International Conference on Intelligent Robots and Systems IROS 2011*, San Francisco, CA, September 25-30, 2011, pp. 653 - 658.
- Polushin I.G., **A. Takhmar**, R.V. Patel , "Small-Gain Design of Networked Cooperative Bilateral Teleoperators", *IEEE International Conference on Robotics and Automation ICRA 2011*, Shanghai, China, May 9-13, 2011, pp. 892 - 897.
- V. Sotoudehnejad, **A. Takhmar**, R.M. Kermani, I.G. Polushin, "Counteracting modeling errors for sensitive observer-based manipulator collision detection", *IEEE/RSJ Interna-*

tional Conference on Intelligent Robots and Systems IROS 2012, Vilamoura, Portugal, October 7-12, 2012, pp. 4315-4320.

- **A. Takhmar**, M. Alghooneh, K. Alipour and S. Ali A. Moosavian, "MHS Measure for Postural Stability Monitoring and Control of Biped Robots", IEEE/ASME International Conference on Advanced Intelligent Mechatronics, AIM 2008, Xian, China, July 2008.
- S. Ali A. Moosavian, M. Alghooneh, **A. Takhmar**, "Gate Planning and Motion Control of a Biped Robot", 16th Iranian Conference on Electrical Engineering ICEE 2008, Tehran, Iran, May 2008.
- S. Ali A. Moosavian, **A. Takhmar**, M. Alghooneh, "Stable Trajectory Planning, Complete Dynamics Modeling and Fuzzy Regulated Sliding Mode Control of a Biped Robot", IEEE/RAS 7th International Conference on Humanoid Robots, Pittsburgh, Pennsylvania, USA, December 2007.
- S. Ali A. Moosavian, M. Alghooneh, **A. Takhmar**, "Introducing a Cartesian Approach for Gate Planning and Control of Biped Robots and Implementing on Various Slopes", IEEE/RAS 7th International Conference on Humanoid Robots, Pittsburgh, Pennsylvania, USA, December 2007.
- S. Ali A. Moosavian, M. Alghooneh, **A. Takhmar**, "Modified Transpose Jacobian Control of a Biped Robot", IEEE/RAS 7th International Conference on Humanoid Robots, Pittsburgh, Pennsylvania, USA, December 2007.
- S. Ali A. Moosavian, **A. Takhmar**, M. Alghooneh, "Regulated Sliding Mode Control of a Biped Robot", IEEE/ICMA International Conference on Mechatronics and Automation, Harbin, China, August 2007.